EYE DEVELOPMENT IN THE CUBOZOAN JELLYFISH *CARYBDEA MARSUPIALIS*

A Thesis
by
JENNA ROSE VALLEY

Submitted to the Graduate School
Appalachian State University
in partial fulfillment of the requirements for the degree of
MASTER OF SCIENCE

August 2011
Department of Biology

EYE DEVELOPMENT IN THE CUBOZOAN JELLYFISH *CARYBDEA MARSUPIALIS*

A Thesis
by
JENNA ROSE VALLEY
August 2011

APPROVED BY:

_____
Dr. Vicki J. Martin
Chairperson, Thesis Committee

_____
Dr. Susan L. Edwards
Member, Thesis Committee

_____
Dr. Ted Zerucha
Member, Thesis Committee

_____
Dr. Steven W. Seagle
Chairperson, Department of Biology

_____
Dr. Edelma D. Huntley
Dean, Research and Graduate Studies

FOREWORD

The research described in this thesis is formatted according to the guidelines detailed in the *Publication Manual of the American Psychological Association (6th Edition).*

Abstract

EYE DEVELOPMENT IN THE CUBOZOAN JELLYFISH *CARYBDEA MARSUPIALIS*

Jenna Rose Valley, B.S., University of North Carolina Wilmington

M.S., Appalachian State University

Chairperson: Vicki J. Martin

Cnidarians are the most primitive invertebrates alive today to possess eyes. The complex eyes of the cubozoan jellyfish *Carybdea marsupialis* exhibit many similarities to the camera-type eyes of higher metazoans including the presence of a cornea, lens, and retina of ciliated photoreceptors. It is these similarities that make understanding the evolution and development of eyes in basal cnidarians important, as they may lead to a better understanding of eye evolution. During the transformation of the polyp to the eye-bearing medusa, the development and arrangement of several components were followed including the neuropeptide phenylalanine-methionine-arginine-phenylalanine-NH_2 (FMRFamide), ultraviolet (UV) opsin-like protein (indicates photoreceptor formation), J1-crystallin (indicates lens formation), and shielding pigment formation. In following the 14-day transformative process, 8 morphological stages were identified. Starting with a steady-state polyp, the main features of transformation included recession of polyp tentacles, change of symmetry from radial to tetraradial, eye development, emergence of medusa tentacles, and detachment. The first ocelli to appear were the complex eyes followed by the simple ocelli; the small complex eye was the first to exhibit pigment formation (melanin) as well as photoreceptor maturation. J1-crystallin was located in the developing lenses/lens-like material in the complex eyes and slit ocelli and also exhibited extraocular staining. Crystallin staining was present in all six ocelli in adult rhopalia. Extensive neurological rearrangement and development takes place during the transformation. In addition, it

was observed that transforming polyps producing eyes were able to regress back to the original eyeless polyp state under varying conditions. Developmental mechanisms in eye formation similar to both vertebrates and invertebrates were seen including the formation of an ocular placode, formation of an invaginated optic cup, synthesis of a crystallin lens in the optic cup, differentiation of the retina (resulting in multiple photoreceptor populations exhibiting opsin and melanin synthesis), and formation of neuropeptide-producing rhopalial nerves in close vicinity with the eyes/ocelli. This study clearly demonstrates the presence of the basic optic molecules and developmental mechanisms in the first multicellular animals possessing complex camera-type eyes.

Dedication

To my parents, Robert and Ellen Valley

Acknowledgments

First and foremost, I must acknowledge the mentorship provided by Dr. Vicki Martin who helped me expand on my interest in cnidarians and vastly add to my knowledge of jellyfish and their amazing eyes. Having only minimal research experience upon entering the graduate program, Dr. Martin helped me to learn and master a variety of techniques in histology, immunohistochemistry, and in the preparation of samples for analysis using the laser scanning confocal and scanning electron microscopes. I also wish to thank my other committee members, Drs. Sue Edwards and Ted Zerucha who both provided invaluable support and guidance through the research and writing process. Although the entire Biology department faculty are an amazing and wonderful group of professionals, my great appreciation extends to a few who also provided much useful advice and support, particularly Betsy Harris, Dr. Gary Walker, Dr. Shea Tuberty, and particularly Dr. Michael Windelspecht who was always willing to discuss current endeavors and future goals. Monique Eckard is a priceless member of Team Jellyfish and I value all time spent with her in the lab and lugging up barrels of seawater from the bottom floor. To all of my fellow grad students, I cannot even express the preservation of my sanity due to the friendships I have made. To Caroline Cochrane, Kyle Nelson, Ricky De Triquet, Sal Blair, Ciara Lockstadt, Yosuke Sakamachi, and Danny Jackson, thank you for being next door or down the hallway when I need a little social interaction. To Ashley Williams and Andrew Jenkins, your friendships in particular have greatly added to my experience at ASU. Without the aid of Dr. Guichuan Hou in the microscopy lab, the vast majority of my work would never have been accomplished and I truly value the friendship that has grown from spending so much of my time with him during the week and on weekends. For the kind gift of the J1-crystallin antibody, I thank Dr. Joram Piatigorsky. Also vital in completing my research and degree was the funding I

received including research grants from the Office of Student Research, a Graduate Teaching Assistantship, an Alumni and Provost Fellowship, and the Research Assistantship kindly obtained for me by Dr. Martin through the National Science Foundation. Having saved the most important for last, I cannot express my thanks for the love and support from my family: thank you Mom, Dad, Tess, Bev, Ron, Cam, and especially Zac for putting up with me during this exhausting but rewarding process. I also must acknowledge my furry family for being there to make me smile and alleviate my stress.

Table of Contents

Introduction

Cnidarians (including hydras, jellyfish, sea anemones, and corals) are the most primitive extant invertebrates to possess eyes (Martin, 2002). The similarities that exist between cnidarian eyes and those of higher metazoans provide an important linkage to the origin and development of the eye, as its evolution is not well understood (Arendt, 2003; Arendt & Wittbrodt, 2001; Fernald, 2000; Fernald, 2004a; Gehring, 2004; Gehring & Ikeo, 1999). The principle dichotomy in the evolutionary debate deals with whether eyes are monophyletic or polyphyletic in origin (Fernald, 2004a; Gehring, 2004; Salvini-Plawen & Mayr, 1977). Despite having a debated history, the fascinating eyes of cnidarians contain many similar morphological features (cornea, lens, retina, photoreceptors) and common ocular molecules (opsins, melanins, neurotransmitters) that exist in higher forms (Kozmik, Ruzickova, et al., 2008; Martin, 2002). In addition to acknowledging the shared presence of proteins which are elemental in the mechanics of vision in all eyed organisms, it is also important to understand how these ocular components are assembled in these basal animals as the eye forms and how these developmental mechanisms and patterns of protein establishment compare to what is already known in higher animals.

Introduction to Metazoan Eyes in General: Rhabdomeric versus Ciliary, Invertebrate versus Vertebrate

The basics of assembling a light-detecting organ involve the presence of photoreceptive elements in association with a dark shielding pigment such as melanin. The job of a photoreceptor is to convert light into an intracellular signal while the dark pigment reduces the scattering of light via absorption and helps to focus the light to the region of the cell most sensitive to the photon stream (Arendt & Wittbrodt, 2001; Gehring, 2004; Kozmik, Ruzickova, et al., 2008; Land & Nilsson, 2002). The non-visual sensing of light by animals is primarily based on the use of either cryptochromes or

opsins, whereas vision exclusively utilizes opsins (Cashmore, Jarillo, Wu, & Liu, 1999; Nilsson, 2009). The basis of a photoreceptor cell is a ciliated epidermal cell with a membrane containing photopigments which are a combination of a vitamin-A-derived chromophore and an opsin protein (Arendt, 2003; Arendt & Wittbrodt, 2001; Fernald, 2000; Goldsmith, 1990; Gould, 1994; Land & Fernald, 1992; Lythgoe & Partridge, 1989; Tsuda, 1987). Opsins, which belong to the G-protein-coupled receptor family (Arendt, 2003; Pierce, Premont, & Lefkowtiz, 2002), are the protein carriers for a light-sensitive chromophore group such as retinal (vitamin-A aldehyde), which is responsible for the conversion of light energy into neural signaling (Arendt & Wittbrodt, 2001; Lythgoe & Partridge, 1989). Retinal responds to light by changing in conformation from an 11-*cis* to an all-*trans* form (Nilsson, 2009).

There are two different branches of photoreceptors: rhabdomeric and ciliary (Arendt, 2003; Fernald, 2000). Although both forms utilize opsins in association with a chromophore, rhabdomeric and ciliated photoreceptors differ in the method of increasing membranous surface area, the types of opsins used, as well as the use of different phototransduction cascades (Arendt, 2003; Arendt & Wittbrodt, 2001) involving different physiological responses to light (Fernald, 2000). Structurally, the enlarged membranous surface of the photoreceptor is due to a folding of the ciliary membrane into internal discs or outer microvilli in ciliated photoreceptors while, for rhabdomeric photoreceptors, is due to an out-folding of the apical cell membrane into microvilli (Arendt & Wittbrodt, 2001; Eakin, 1979). According to Arendt (2003), rhabdomeric photoreceptors use rhabdomeric opsins (r-opsins), whereas ciliated photoreceptors use ciliary opsins (c-opsins). Although both forms of opsin have a conserved lysine residue to which retinal binds, the variation in the opsin structure triggers different phototransduction cascades by the binding of the opsin to different G-protein subtypes (Suga, Schmid, & Gehring, 2008; Terakita, 2005). The binding of a photopigment in a rhabdomeric photoreceptor triggers a phospholipase C cascade, whereas the binding of a photopigment in a ciliated photoreceptor triggers a phosphodiesterase cascade (Arendt, 2003; Arendt & Wittbrodt, 2001). Respectively, the end result of the phospholipase C cascade and phosphodiesterase cascade is a

depolarization of rhabdomeric photoreceptor cells and a hyperpolarization of ciliated photoreceptor cells (Fernald, 2000). Interestingly, rhabdomeric and ciliary photoreceptors have been shown to coexist in many taxonomic groups (Arendt, 2003) and even within the same organism: in addition to the rhabdomeric photoreceptors found in the marine worm *Platynereis dumerilii*, ciliary photoreceptors were found in the brain and utilized a photopigment closely related to the rod and cone opsins found in vertebrate eyes (Arendt, Tessmar-Rabile, Snyman, Dorresteijn, & Wittbrodt, 2004). In addition, the non-visual photopigment melanopsin, which is found in vertebrates, is a member of the r-opsin family (Lamb, 2009; Nilsson, 2009; Terakita, 2005).

Melanin, a good example of a shielding pigment, whose purpose is to both absorb and orient light and may be found in specialized pigment cells or in association with the photoreceptors, can be found in vertebrate eyes as the exclusive dark pigment (Kozmik, Ruzickova, et al., 2008), in cephalopod eyes (Bliss 1943; Bliss, 1948; Fox & Crane, 1942), annelid eyes (Hermans & Eakin, 1974), and has even been found in the eye spots of the cercarial/metacercarial stages of many trematodes (Nadakal, 1960). Melanin is a light-absorbing polymer derived from the amino acid tyrosine and appears dark due to its wide spectral absorbance (Riley, 1997).

All vertebrate eyes and some invertebrate eyes utilize a transparent cellular lens made of water-soluble proteins known as crystallins (Piatigorsky, Horwitz, Kuwabara, & Cutress, 1989). These crystallin proteins can be widespread as well as taxonomically specific in distribution (Piatigorsky et al., 1989) and though these proteins often differ among species, most are either related or identical to a variety of common and widely expressed stress-protective proteins and certain metabolic enzymes (Ingolia & Craig, 1982; Piatigorsky, 2008a, 2008b; Tomarev & Piatigorsky, 1996; Wistow, Mulders, & de Jong, 1987; Wistow & Piatigorsky, 1987). Invertebrate crystallins that have been examined include cephalopods, gastropods, cnidarians, and arthropods (Tomarev & Piatigorsky, 1996). Whereas vertebrate lenses are formed from modified crystallin-containing epithelial cells, invertebrate lenses are formed via the secretion of crystallin proteins by specialized cells (Fernald,

2000). Although all vertebrates possess a cornea, many invertebrates, such as some cephalopods, do not and instead have a transparent eyelid (Fernald, 2004a).

The largest variety of eye types can be found among the invertebrates (Fernald, 2004a). A good model of an advanced invertebrate eye can be found on the squid, whose camera-type eye is structurally similar to the vertebrate eye (Gehring, 2004). In both humans (who provide a good example of the vertebrate eye) and squids, light enters the eyes through the pupil and is then focused by the lens onto the photoreceptor cells making up the retina (Lane, 1960). The rhabdomeric photoreceptors of most squid utilize only one visual photopigment, rendering them color-blind (Seidou et al., 1990). Human retinas are made up of two types of photoreceptors: cones, which function best in high-light environments, and rods, which function best in low-light conditions (Carroll, 2008). Our eyes utilize four different photopigments, one type in the rod cells and 3 types in the cone cells (Carroll, 2008). Due to differences in eye development, the squid photoreceptors are located at the front of the eye and are oriented towards the light source while human photoreceptors are located at the back of the eye and are oriented away from the light source (Fernald, 2000); therefore, everted squid retinas receive light directly (Gehring, 2004) while the inverted human retinas receive indirect light that first must pass through various neuronal layers before reaching the photoreceptor cells (Svet & Khazen, 2009). Although both squid and human eyes possess a lens made up of high concentrations of crystallin proteins, the type of crystallin proteins that make up the lens differs: α, β, and γ crystallins are found in all vertebrate lenses (Piatigorsky et al., 1989) while S and Ω crystallins have been isolated in cephalopod eyes (Piatigorsky, 2008a; Tomarev & Piatigorsky, 1996). Despite both squid and human eyes using lenses, some cephalopods lack a cornea, which sits atop the iris and pupil in vertebrate eyes and contributes to the majority of the eyes' ability to focus (Kaufman, Barron, & McDonald, 1998); in aquatic animals, it is the lens which is the primary focusing structure, as there is little refraction of light crossing from the aqueous medium through the cornea due to nearly identical refractive indexes (Gregory, 2008; Greiling & Clark, 2008; Land &

Nilsson, 2002). The cephalopod cornea is simply a transparent eyelid that has evolved to permanently cover the lens and is produced by different tissue than in vertebrates (Fernald, 2004a).

Evolutionary Debate: Polyphyletic or Monophyletic?

With more than 95% of all extant animal species possessing eyes (de Queiroz, 1999; Fernald, 2004b; Land & Nilsson, 2002), it is no surprise that they come in an astounding array of morphological diversity (Land & Nilsson, 2002) and also represent significant differences in the developmental method used (Gehring, 2005). This incredible variety led scientists to propose a polyphyletic theory for eye evolution, suggesting that eyes evolved independently 40-60 times (Salvini-Plawen & Mayr, 1977). Even Darwin devoted an entire chapter to discussing the difficulty he had in applying his theory of natural selection to an "organ of extreme perfection and complication" (Darwin, 1882, p. 143). The opposing theory, based primarily on recent genetic evidence, is one which argues in favor of a monophyletic origin of eyes where all eyes arose from a common ancestor and subsequent divergent, parallel, and convergent evolution gave rise to the variety of eyes that exist today (Gehring, 2005; Gehring & Ikeo, 1999; Gehring & Seimiya, 2010; Halder, Callaerts, & Gehring, 1995b; Jacobs et al., 2007).

The polyphyletic argument of eye evolution, proposed by Salvini-Plawen and Mayr (1977), was based on the extensive morphological and developmental differences found among eye types such as the use of different opsins, retinal structure, and different modes of development. For example, the vertebrate eye utilizes ciliary opsin (Arendt, 2003; Arendt & Wittbrodt, 2001; Fernald, 2000), has an inverted retina where the photoreceptors are atypically oriented away from the source of light (Svet & Khazen, 2009), and the eye originates from the neural tube (the precursor to the brain and spinal cord; Gehring, 2004; Hyer, Kuhlman, Afif, & Mikawa, 2003). In contrast, the structurally similar camera-type eye found in squids utilizes rhabdomeric opsin, has a conventional retina where the photoreceptors are oriented towards the source of light (Gehring, 2004), and the eye is completely ectodermal in origin (Meinertzhagen, 1990). Based on these differences in eye structure and mode of development, the polyphyletic theory of eye evolution argues that eyes must have evolved

independently several times throughout history in order for such a variety to have resulted in extant species (Fernald, 1997; Nilsson, 1996; Salvini-Plawen & Mayr, 1977).

Doubt of the polyphyletic view of eye evolution has existed since Darwin, who believed that the random evolution of a prototypic eye was highly improbable and not driven by selection (Darwin, 1882), making the theory of multiple independent ocular origins very unlikely (Gehring, 2005). Gehring (2004, 2005) proposes that all eye types can be traced back to a primitive prototype eye, consisting of the close-association of photoreceptor cells (containing an opsin-based photopigment) with a nearby shielding pigment (Arendt & Wittbrodt, 2001; Darwin, 1882; Gehring, 2005; Land & Nilsson, 2002; Oakley, 2003), and that more complex eyes along with the variety of existing eye types arose via selection through divergent, parallel, and convergent evolution. One of the key arguments for the monophyletic theory of eye evolution involves the *Pax6* gene which has been demonstrated to be universally involved in eye development (Callaerts et al., 1999; Gehring & Ikeo, 1999; Kumar & Moses, 2001; Simpson & Price, 2002; Sun et al., 1997) and has, therefore, been referred to as a master control gene for eye development (Gehring, 2004; Gehring & Ikeo, 1999; Halder, Callaerts, & Gehring, 1995a). This idea has been questioned based on the significant involvement of other genes in eye development, the involvement of *Pax6* in other important extra-ocular functions (Fernald, 2000; Grindley, Davidson, & Hill, 1995; Kozmik, 2005; Piatigorsky & Kozmik, 2004; Simpson & Price, 2002), and the presence of *Pax6*-like genes in primitive eyeless organisms (Hill et al., 2010; Hoshiyama et al., 1998) which makes it difficult to argue a monophyletic evolution of eyes if the ancestral function of *Pax6* was not ocular (Gregory, 2008; Kumar, 2001). This debate aside, the similarities that exist between the vertebrate and invertebrate genetic cascade leading to eye formation cannot be denied and suggest a common evolutionary ancestry (Gehring, 2005; Gehring & Seimiya, 2010). The recent genetic evidence has even prompted Ernst Mayr (2001), one of the original propagators of the polyphyletic theory, to question his stance. Even if the same developmental regulatory genes can be found throughout animal taxa, the fact that the regulatory networks they form also appear to be conserved between distantly related organisms is a convincing

argument for these genes and networks having originated in a common ancestor (Gehring & Seimiya, 2010).

Regardless of having arisen once in evolutionary history or multiple times, hypotheses also exist to explain how a complex feature such as the eye was able to evolve in the first place (Gregory, 2008). The most basic hypothesis involves direct adaptive evolution where, through natural selection, incremental changes slightly improve an organism's ability to process visual information (Bahar, 2002; Miller, 1994; Nilsson & Pelger, 1994; Osorio, 1994; Salvini-Plawen & Mayr, 1977). A model of this, created by Nilsson & Pelger (1994), demonstrated the progression of eye evolution following this method from a rudimentary light-sensitive patch of cells to a complex camera-type eye via a series of intermediate stages. Although an abstract model, living representatives of these intermediate stages exist (Conn, 1900; Darwin, 1859; Land & Nilsson, 2002). Although one would think that this progressive improvement would take an extensive amount of time, the model indicates that sophisticated eyes would theoretically been able to evolve separately several times during evolution, thereby providing support to the polyphyletic view of eye evolution based on the elimination of potential time constraints (Nilsson & Pelger, 1994). One group of organisms in which many of the aforementioned 'intermediate stages' can be found is the Cnidaria which exhibit ocelli that are diverse both between and among species (Piatigorsky & Kozmik, 2004) and these diversities illustrate clear improvements in eye design (Nilsson, 1989; Nilsson, 1990; Nilsson & Pelger, 1994).

Introduction to Cnidarians Eyes

The eyes of cnidarians are associated with the medusa stage, with exceptions found in the pigment spot ocelli in a scyphozoan polyp (Blumer, Salvini-Plawen, Kikinger, & Büchinger, 1995) and single-celled ocelli found in a cubozoan larva (Nordström, Wallen, Seymour, & Nilsson, 2003). These eyes range in complexity and can include simple eye spots, pigment cups, complex pigment cups including a lens, and camera-type eyes that include a cornea, lens, and retina (Martin, 2002). An epithelial patch of photoreceptor cells combined with non-sensory pigment cells is referred to as a simple eyespot. These pigment cells can vary in shape and size, depending on the species, and contain

pigment granules (Singla, 1974, Singla & Weber, 1982); a study done by Weber (1981b) showed the pigment in the pigment cells of *C. radiatum* to be melanin. If the photoreceptor cells project into a cup produced by pigment cells, then this is called a pigment-cup ocellus. There are two types of pigment-cup ocelli: everted and inverted. In an everted pigment-cup ocellus, the photoreceptor cells extend into the lumen of the cup in between the pigment cells whereas in an inverted pigment-cup ocellus, the photoreceptor cells still project into the lumen of the cup but not between the pigment cells which are found below the epidermis (Martin, 2002). The opening of the pigment cup in an inverted ocellus allows the light-receptor portion of the photoreceptor cells to reach the pigment layer and also provides an exit for the tapered axons of the photoreceptor cells. In addition to having simple eyes consisting only of photoreceptors and an associated shielding pigment, certain cnidarians exhibit camera-type eyes with a retina of ciliated photoreceptors, a lens, and cornea (Martin, 2002). A complex camera-type eye is characterized by a narrowed opening of the pigment cup and the presence of a spherical, graded-index lens found in the center of the encircling concave retina (Martin, 2002).

Interestingly, the photoreceptors making up the retinas of cnidarians are ciliated and not rhabdomeric like most other invertebrates (Eakin, 1979; Eakin & Westfall, 1962); an exception can be found in the larva of the cubozoan *T. cystophora*, which has numerous single-celled ocelli utilizing rhabdomeric photoreceptors (Nordström et al., 2003). The term camera-type eye refers to the ability of an eye to focus an image on a retina by refraction of a photon stream through a lens (Martin, 2002). Soluble proteins known as crystallins make up the transparent cellular lens (Bloemendal, 1982; Mackie, 1999; Wistow & Piatigorsky, 1988) whose purpose is thought to be the collection of light as opposed to resolving an image on the retina like most vertebrate eyes (Laska & Hündgen, 1982). Sitting atop the lenses in some complex cnidarians eyes is a cornea which aids in the refraction of light (Kaufman et al., 1998). Different grades of ocellar organization and complexity are found in three of the four classes in the phylum Cnidaria: the ocelli in Hydrozoa range from simple eye spots to the inverted pigment cup found in *Tiaropsis multicirrata* (Singla, 1974). These ocelli can be found as single eyes at the base of the tentacle where it joins the bell (tentacular bulb) or can exist in large

numbers on the bell margins (Martin, 2002). The ocelli in Scyphozoa and Cubozoa are similarly organized (Hyman, 1940) although the advanced camera-type eyes are found only in cubozoans (Berger, 1898; Martin, 2004). The ocelli of these two classes are arranged on club-shaped structures called rhopalia that are either located on pedalia around the bell margin (Scyphozoa) or on the sides of the bell (Cubozoa; Hyman, 1940). The polyp forms in all four classes of Cnidaria have been shown to exhibit light-sensitive behaviors (Martin, 2002) although only the interstitial polyp stage of the scyphozoan *Stylocoronella riedli* has been shown to exhibit tangible ocelli in the form of pigment spots (Blumer et al., 1995). Cnidarian eyes in general are believed to use at least two types of opsins including an ancestral opsin class referred to as cnidops and a ciliary opsin type very similar to the c-opsins used in the ciliary photoreceptors of vertebrates (Koyanagi et al., 2008; Kozmik, Ruzickova, et al., 2008; Plachetzki, Degnan, & Oakley, 2007; Suga et al., 2008). It has been proposed that the c-opsin type found in cnidarians gave rise to all c-opsins seen today (Plachetzki et al., 2007).

Cubozoan Eye

Cubozoa is the smallest class within the phylum Cnidaria (Coates, 2003). Although the rhopalia of cubozoans can bear ocelli as simple as pigment spots, the cubozoans stand out among cnidarians for the complex camera-type eyes which are structurally complex and have similarities to the advanced eyes found in certain invertebrates such as cephalopods as well as in vertebrates (Coates, 2003); these similarities comprise the presence of a cornea, lens, and retina of ciliated photoreceptors (Martin, 2002). Cubozoans exhibit a total of 24 eyes/ocelli arranged in groups of 6 on 4 rhopalia located on each side of the bell within an exumbrellar niche that is protected by a flap of cells which acts as a rudimentary eyelid (Martin, 2002). There are four morphologically different types of eyes: two pit ocelli and the small lensed eye are directed upward through the umbrella, while two slit ocelli and the large lensed eye are directed inward/downward. At the base of the rhopalium is a statocyst which is a gravity-sensing structure that keeps the ocelli correctly oriented in relation to gravity (Berger, 1898; Garm & Ekström, 2010; Sötje et al., 2011) even when the animal is upside down (Garm, Oskarsson, & Nilsson, 2011). The animal's radial symmetry and transparent bell,

coupled with the free-moving rhopalia, allow for a nearly unobstructed view of its surroundings. The slit ocelli, located above and on either side of the large complex eye, and the pit ocelli, located on either side of the small complex eye, consist of slits and invaginated pits lined with long, slender ciliated epithelial cells. The photoreceptors in both types of simple ocelli contain pigment granules, although fewer to no pigment granules are found in cells lining the pit ocelli (Martin, 2004). The cornea, consisting of a layer of epithelial cells, covers the lenses in the complex ocelli and is continuous with the rhopalial epithelium (Martin, 2004). Although rudimentary, the slit ocelli contain elongated lenses (Martin, 2004). True lenses can be found in the large and small complex camera-type eyes along with a retina of ciliated photoreceptors and cornea (Berger, 1898; Martin, 2002; Martin & Givens, 1999; Nilsson, Coates, Gislén, Skogh, & Garm, 2005; Yamasu & Yoshida, 1976).

A study done on the box jellyfish *C. rastonii* revealed the use of a novel phototransduction cascade using a novel G-protein subtype which triggers an adenylyl cyclase cascade (Koyanagi et al., 2008). Despite using a novel cascade, similarities still exist with that used by vertebrates such as the use of ciliary photoreceptors, the use of cyclic nucleotide signaling, bleaching of the visual photopigment (Koyanagi et al., 2008; O'Connor, Garm, et al., 2010), and possibly the usage of a chromophore retinal-replacement system (Koyanagi et al., 2008). In the cubomedusan *T. cystophora*, an alternative cascade was suggested which uses ciliary opsin and the same G-protein (Gt or transducin) as in vertebrate eyes (Kozmik, Ruzickova, et al., 2008).

The retinas of the eight complex eyes of cubomedusans are made up of a sensory region, a pigmented region, and a nuclear region (Pearse & Pearse, 1978) and corresponds to the structure of the individual ciliated photoreceptors: the photoreceptor cells in the complex eyes of the cubozoan *Carybdea marsupialis* consist of a long cylindrical cell with the basal end housing the nucleus (unlike the photoreceptor cells in the simple ocelli where the nucleus is housed in the apical portion) and tapering into an axon (Martin, 2004). The middle segment contains extensive mobile pigment granules which act as a shielding pigment to absorb excess light. A study done by Kozmik, Ruzickova, et al. (2008) used a direct chemical assay to show melanin (the exclusive dark pigment

found in vertebrate eyes) to be the retinal pigment in the camera-type eyes of the cubozoan *Tripedalia cystophora*, although in vertebrates, the pigment is housed in separate non-sensory pigment cells instead of within the photoreceptor cells (Piatigorsky, 2008b) as is seen in the retinas of hydromedusae, most ocelli in scyphomedusae (Garm & Ekström, 2010), and some cubomedusae (O'Connor, Garm, & Nilsson, 2009; Yamasu & Yoshida, 1976). The apical end forms the light-receptor process and is characterized by stacks of perpendicularly-oriented membranous discs and a single cilium. The cilium extending from the apical end of the photoreceptor cell is made up of a 9 + 2 pattern of microtubules (Martin, 2002). Although similar in morphology, at least two types of photoreceptors were found in the large complex eye (Martin, 2002).

Eight of the 24 eyes found in cubozoans are complex camera-type eyes containing a spherical lens (Martin, 2002). Three crystallin proteins making up the cellular lenses of the cubomedusan *Tripedalia cystophora* have been isolated: J1-crystallins, J2-crystallin, and J3-crystallin (Kozmik, Swamynathan, et al., 2008; Piatigorsky et al., 1989; Piatigorsky, Horwitz, & Norman, 1993; Piatigorsky et al., 2001). The J1-crystallins were found in the lenses of both complex eyes while the J2- and J3-crystallins were confined to the large complex eye. At least two proteins of similar molecular weights were found in the lenses of *Carybdea marsupialis* and the lens material of this species cross-reacted with an antibody targeting J1-crystallin. The J1-crystallin is the only crystallin protein found in the lenses of both the small and large complex eyes (Piatigorsky & Kozmik, 2004). The lenses of the complex eyes of *C. marsupialis* were found to be composed of two structurally different cells, with fibrous cells comprising the outer portion of the lens and more rounded cells in the center. In addition, the central portion of the lens contains a greater concentration of proteins than does the peripheral region (Martin, 2004). A study done by Nilsson et al. (2005) on the eyes of *Tripedalia cystophora* showed that the lens of the upper eye contains a refractive index gradient that results in a visual ability comparable to that seen in higher vertebrates. Although having a graded index lens can eliminate spherical aberration (Nilsson, 1990), when considered with the geometry of the eye, Nilsson et al. (2005) also found that the image is out of focus which was attributed to the

benefit of removing fine image details, allowing visual detection of only large objects and not minute particles. The presence of a gravity-sensing statocyst and flexible rhopalial stalk enables the visual field to remain in a semi-constant orientation, a characteristic thought to be unique to cubomedusae (Garm & Ekström, 2010). This attribute simplifies the collection of visual information, as the animal does not first have to process where in the visual environment the information is originating (Wehner, 1987).

Preliminary studies have been done to test the visual abilities of these structures and their components (Arkett & Spencer, 1986; Hamner, 1994; Hartwick, 1991; Nilsson et al., 2005; Stewart, 1996; Taddei-Ferretti, Musio, Sentillo, & Cotugno, 2004). For example, Garm, O'Connor, Parkefelt, and Nilsson (2007) demonstrated visually guided obstacle avoidance in two species of box jellyfish but were unable to conclude whether this was due to color vision or simply to light contrast; regardless, these and other results indicate some degree of spatial resolution in the lensed eyes (Nilsson et al., 2005). The study of color vision in cubozoans centers around the disagreement among investigators as to how many opsins are present in cubozoan photoreceptors as it is the diversity of wavelength reactivity in different opsins which is the basis for color vision (Arendt, 2003; Dulai, von Dornum, Mollon, & Hunt, 1999; Gerl & Morris, 2008). A study done by Coates, Garm, Theobald, Thompson, and Nilsson (2006) demonstrated similar spectral sensitivities in both lensed eyes of *Tripedalia cystophora* which was attributed to the probable presence of a single receptor type and opsin. Although an immunoreactive study done by Martin (2004) indicated the presence of three different opsins (blue, green, and UV-sensing opsins in the complex ocelli) and therefore supported the possibility of color vision in cubozoans, Ekström, Garm, Pålsson, Vihtelic, and Nilsson (2008) concluded a lack of color vision in the two lensed eyes of both *Carybdea marsupialis* and *Tripedalia cystophora* based on the suggestion of a single opsin type by electroretinogram and immunohistochemistry data; this study concluded that the peak sensitivity of the large lensed eye of *C. marsupialis* is in the blue part of the color spectrum. Colorblindness was also the conclusion in a spectral sensitivity study done on *Tripedalia cystophora* (Coates et al., 2006), in an electroretinogram

study of the cubozoans *T. cystophora* and *Chiropsalamus sp*. (Garm, Coates, Gad, Seymour, & Nilsson, 2007), and in a microspectrophotometry and immunohistochemistry study done on the cubozoan *Chiropsella bronzie* (O'Connor, Garm, et al., 2010). The recent study by O'Connor, Garm, et al. (2010), like Martin (2004), used antibodies directed against the different zebrafish retinal opsins, but only the antibody directed against UV opsin labeled any photoreceptors. Studies in spectral sensitivity (Coates et al., 2006), behavior (Coates, 2005), and antibody labeling (Martin, 2004) indicated a peak sensitivity of the lensed eyes in *Tripedalia cystophora* and *Carybdea marsupialis* to both blue and green wavelengths of light and a lack of response to red light/red-sensing opsins. Interestingly, blue light has been found to initiate a swimming pattern interpreted as a feeding behavior (Gershwin & Dawes, 2008). This same study also demonstrated positive phototaxis to red light in addition to white, green, blue, and orange in juvenile *Chironex fleckerii*.

Cnidarian Nervous System

Cnidarians possess primitive nervous systems due to the low concentrations of neurons and synapses (Grimmelikhuijzen, Graff, & Spencer, 1988) and are regarded as being the first group over evolutionary time to show evidence of a functional nervous system (Mackie, 1990; Watanabe, Fujisawa, & Holstein, 2009) which is known to be strongly peptidergic (Grimmelikhuijzen, Leviev, & Carstensen, 1996). Although simple, the cnidarian nervous system exhibits many similarities to more complex systems on a cellular level (Brumwell & Martin, 2002). In general, the structure of the cnidarian nervous system is that of a diffuse nerve net with some concentrations of neurons forming neural plexuses and linear or circular nerve tracts (Grimmelikhuijzen et al., 1996). Two types of neurons can be found in cnidarians including sensory cells, which project up to the ectodermal or endodermal surface and are attached to basal ganglion cells that are located closer to the acellular mesoglea found in between the two cell layers (Hadži, 1909; Schneider, 1890). Functioning in the same fashion as higher organisms, the neurons in the cnidarian nervous system utilize action potentials mediated by the fluctuation of Na^+ (sodium) currents, and synaptic transmission is primarily chemical with the exception of electric coupling existing in hydrozoans (for a review, see

Anderson, 2004). Although the specific neurotransmitters thought to be involved in the chemical signaling in the eye have yet to be identified (Martin, 2002), immunoreactivity in the RFamide neuropeptide family has been found in the nervous systems of all cnidarians studied thus far (Grimmelikhuijzen et al., 1996; Plickert & Schneider, 2004) and neurons expressing glutamate, serotonin, GABA (gamma-aminobutyric acid), and RFamide, which are known to be involved in the visual system of vertebrates and invertebrates (Lam, Frederick, Hollyfield, Sarthy, & Marc, 1982) have also been shown to occur in close association with cnidarian photoreceptive structures (Martin, 2002). Many local functions of various cnidarians neuropeptides have yet to be determined, although RFamides have been implicated in the transmission of photic stimuli to the nervous system and subsequent light-directed locomotion (Plickert & Schneider, 2004).

The nervous system of jellyfish has been described as simple and primitive in the past but is now understood to be very complex with on-going arguments for the presence of a centralized nervous system (for a commentary, see Satterlie, 2011). The nervous system of cubomedusae is comprised of a subumbrellar motor nerve net that is connected to a central nerve ring located near the base of the bell (Satterlie, 1979); the polyp form of cubozoans also possesses a nerve ring that is located where the hypostome meets the tentacular region (Werner, Chapman, & Cutress, 1976). The medusan nerve ring connects with the alternating rhopalia and pedalia and has four sets of radial ganglia at the site branching out to the rhopalia as well as four sets of pedal ganglia where the nerve ring connects to the tentacles (Conant, 1898, Laska & Hündgen, 1982; Satterlie, Thomas, & Gray, 2005). A rhopalial ganglion, composed of nerve fibers and cell bodies, is found between the sensory organs (ocelli and statocyst) as well as in the gut extension into the rhopalium (Conant, 1898, Laska & Hündgen, 1982). A group of pacemaker neurons, which are believed to be located close to the emergence of the rhopalial stalk, can be found in each rhopalium along with a rhopalial neuropil, consisting of a tangle of neurites that is found just below the pacemaker region (Gray, Martin, & Satterlie, 2009; Satterlie, 1979, 2002; Yatsu, 1917). The pacemaker region is known to regulate swimming through control of the motor nerve net (Satterlie 1979, 2002) in response to visual input

(Garm & Bielecki, 2008; Garm & Mori, 2009) and it is in the rhopalial neuropil where visual information is thought to be integrated (Parkefelt, Skogh, Nilsson, & Ekström, 2005). Within the rhopalium, the basal regions of the photoreceptor cells of the complex eyes taper and feed into second-order nerve cells just below the retina (Martin, 2004; Singla & Weber, 1982; Toh, Yoshida, & Tateda, 1979; Yamamoto & Yoshida, 1980) and the axons of these neurons cluster together to form an ocular nerve (Martin, 2002). Some of these bipolar neurons form connections with neurons contained in the stalk of the rhopalium and subsequently with neurons located in the main nerve ring (Martin, 2004). The neuronal organization within the rhopalium of cubozoans has been shown to be bilaterally symmetric with groups of interconnected neural elements located on either side (Parkefelt et al., 2005; Plickert & Schneider, 2004; Satterlie, 2002; Skogh, Garm, Nilsson, & Ekström, 2006). The neural peptide FMRFamide has been indicated as having an important role in the functioning of many primitive nervous systems (Grimmelikhuijzen, 1983) and the similar neuropeptide RFamide has been found in neurons located in the slit ocelli, below the retina in the small and large complex eye, at the base of the rhopalial stalk, as well as up the stalk into the main nerve ring in the cubozoan *Carybdea marsupialis* (Martin, 2002, 2004; Plickert & Schneider, 2004; Skogh et al., 2006). The nerve ring has been proposed as the location of the central nervous system of the animal (Martin, 2004), although many studies have suggested that some if not most of the processing of visual information occurs within the rhopalia, which are considered part of the central nervous system and connected to the main nerve ring by neurites in the rhopalial stalk (Garm, Ekström, Boudes, & Nilsson, 2006; Garm, Poussart, Parkefelt, Ekström, & Nilsson, 2007; Parkefelt & Ekström, 2009; Parkefelt et al., 2005).

Genetic Involvement in Cnidarian Eye Development

Regulatory genes involved in sense organ development are conserved (Bebenek, Gates, Morris, Hartenstein, & Jacobs, 2004) and it is increasingly being discovered that vertebrates and cnidarians share more genes than previously thought (Kortschak, Samuel, Saint, & Miller, 2003). Several genes and gene families known to be important for ocular development have been isolated in

the Cnidaria. *Pax* (or paired-box) genes encode a family of transcription factors that play many different roles in the development of animals. Several Pax proteins have been implicated in the development of the visual system across several species (Kozmik, 2005). Pax6, in particular, has been demonstrated to have a nearly universal use in eye development (Callaerts et al., 1999; Gehring & Ikeo, 1999; Kumar & Moses, 2001; Simpson & Price, 2002; Sun et al., 1997). *Pax* genes have been isolated in all four major classes of cnidarians (Catmull et al., 1998; Kozmik et al., 2003; Miller et al., 2000; Suga et al., 2010; Sun et al., 1997). It has been suggested that *PaxB*, one of the cnidarian *Pax* genes, and not *Pax6*, represents the primordial ancestral gene during the evolution of complex eyes (Kozmik et al., 2003; Piatigorsky & Kozmik, 2004) due to its structural similarities to the two *Pax* genes primarily used in eye development (*Pax2* and *Pax6*) and to its ability to substitute for these genes (Kozmik et al., 2003) and to induce ectopic eye formation (Kozmik et al., 2003; Plaza, de Jong, Gehring, & Miller, 2003). Cnidarian *Pax* genes have been found to be expressed in the rhopalia of adult cubozoan medusae (Kozmik et al., 2003) and in adult hydrozoan rhopalia (Suga et al., 2010). In addition, *PaxB* has been shown to regulate the expression of cnidarian crystallin genes (Kozmik et al., 2003; Kozmik, Swamynathan, et al., 2008), a job that is known in vertebrates to be regulated by *Pax6* (Cvekl & Piatigorsky, 1996; Duncan, Cvekl, Kantorow, & Piatigorsky, 2004; Grindley et al., 1995; Kamachi, Uchikawa, Tanouchi, Sekido, & Kondoh, 2001), to regulate the expression of opsin regulator genes (Kozmik et al., 2003), and has also been implicated in the differentiation of the nervous system in a hydrozoan (Gröger, Callaerts, Gehring, & Schmid, 2000). Other important gene families found in cnidarians that are known to be involved in vertebrate and invertebrate eye development include the *Six* genes (Bebenek et al., 2004; Stierwald, Yanze, Bamert, Kammermeier, & Schmid, 2004), the *Eyes Absent* genes (Suga et al., 2010), the *Dachshund* gene (Stierwald, 2004), *Otd/otx* genes (Müller, Yanze, Schmid, & Spring, 1999; Nakanishi, Yuan, Hartenstein, & Jacobs, 2010; Smith, Gee, Blitz, & Bode, 1999), *BMP* genes (Reber- Müller et al., 2006), *Sox* genes (Jager, Quéinnec, Houliston, & Manuel, 2006), and *Hedgehog* genes (Matus, Pang, Daly, & Martindale, 2007).

Function of Cnidarians Eyes

The visual abilities demonstrated in cubozoans are applied in several interconnected areas of the animal's existence including the need to swim, feed, reproduce, and navigate its environment (Martin, 2004). In addition to bearing the eyes, the rhopalium has also been shown to be responsible for the initiation of swimming impulses (Satterlie, 1979, 2002), which are now known to be modulated by visual input (Garm & Bielecki, 2008). Complete removal of the rhopalia leads to a cessation of swimming (Berger, 1900). As swarms of potential prey often gather in shafts of sunlight near the surface of the water in mangrove habitats (the habitat of the cubomedusan *Tripedalia cystophora*), it is necessary for the jellyfish to be able to navigate and swim into these light shafts and such positively-phototactic behavior has been observed both in the natural habitat and in laboratory settings (Buskey, 2003; Martin, 2002; Stewart, 1996). Besides the need to navigate within the environment, it can also be important to be able to remain within an environment where a food source is located. A recent study by Garm et al., (2011) showed that *Tripedalia cystophora* can use visual cues of the mangrove canopy to remain within the mangrove lagoon; the animals were able to detect the canopy up to 8 m from outside the lagoon edge and subsequently swim back to their natural environment. An additional need for a visual system is also demonstrated in the fragility of the jellyfish body, as the animal must be able to navigate among potentially destructive obstacles such as mangrove roots and pier pilings as well as evade potential predators (Coates, 2003; Coates et al., 2006; Garm, O'Connor, et al., 2007; Hamner, 1994; Martin, 2004). Besides feeding and navigation, cubozoans also rely on a strong swimming ability (Buskey, 2003) in the reproduction process, as many cubozoans engage in copulatory behaviors involving pursuit of the female by the male (Martin, 2002).

Purpose of Study

Although many studies have followed the metamorphic process of jellyfish formation in Scyphozoa (Berrill, 1949; Calder, 1972; Gohar & Eisawy, 1960), Hydrozoa (Gröger & Schmid, 2000; Reber-Müller et al., 2006; Stierwald et al., 2004; Weber, 1981b), and Cubozoa (Stangl, Salvini-

Plawen, & Holstein, 2002; Straehler-Pohl & Jarms, 2005), few studies have followed the development of the rhopalia and eyes/ocelli. While the genetic study by Stierwald et al. (2004) centered around the presence or absence of eyes, the morphological process of eye development was not directly addressed. A handful of studies have focused on the development of the rhopalia (Spangenberg, 1991) and rhopalial nervous system in Scyphozoa, which, like in cubozoans, was found to be bilaterally symmetric (Nakanishi, Hartenstein, & Jacobs, 2009; Nakanishi et al., 2010), however, few studies have specifically focused on the morphological process of eye formation (Weber, 1981b; Yoshida & Yoshino, 1980). Due to the differences in complexity, structure, and organization of the rhopalia and eyes between Hydromedusae, Scyphomedusae, and Cubomedusae, the information obtained from these studies is vastly inconsequential in the understanding of eye development in cubozoans. The study by Stangl et al. (2002) on the metamorphosis of the cubozoan *Carybdea marsupialis* commented on the appearance of pigment spots on the fused tentacle bases and described that the invagination of the first pigment spots appear to give rise to the lensed eyes. The development of the rhopalia during the metamorphosis of *C. marsupialis*, which was identified to be a modified strobilation (Straehler-Pohl & Jarms, 2005), is described as similar to the strobilating scyphozoans with a difference in the number of tentacles involved: while only some tentacles are involved in rhopalial formation in scyphozoans, all polyp tentacles are involved in *Carybdea*.

This is the first study examining eye development in a cnidarian that specifically follows the appearance and development of the morphological components necessary for constructing the complex camera-type eyes of cubozoan jellyfish. Utilizing multiple tools, scanning electron microscopy, light histology, brightfield examination, melanin staining, laser scanning confocal microscopy, and antibodies directed against opsin proteins, crystallin proteins, and the neuropeptide FMRFamide, basic features of eye formation were identified in a cubozoan and compared to eye formation in higher animals. As opsins, melanin, crystallins, and neuropeptides are important ocular components utilized in the construction of eyes of bilaterians, it is important to determine if these molecules are also involved in eye development in this basal metazoan.

Materials and Methods

Polyp Maintenance and Usage

Carybdea marsupialis polyps were maintained in 90 mm x 20 mm Petri dishes in pH 7.9 North Carolina coastal seawater at room temperature (23°C). Polyps were induced to transform to the medusa eye-bearing form by increasing the water temperature to 25°C in a Precision 818 incubator (in the dark) and by cessation of feeding. Steady-state polyps were allowed to feed on brine shrimp weekly for approximately 2 hours followed by a water change. Animals were selected at the various stages of transformation to be fixed and prepared for observation under the scanning electron microscope or appropriately stained and fixed for observation under the confocal laser scanning electron microscope. In the case of melanin detection and hematoxylin and eosin staining, prepared samples were examined using an Olympus IX81 inverted brightfield microscope. Using a Wild Heerbrugg M3Z dissecting microscope, seven stages were established and examined including Stage 0 (the steady-state polyp), Stage 1 (rearrangement of the tentacles from a radial to tetraradial arrangement/fusion of tentacle bases), Stage 2 (appearance of initial eyespot), Stage 3 (progression of initial eyespot to all six developing ocelli), Stage 4 (completion of polyp tentacle recession/resemblance of developing rhopalia to miniature adult rhopalia), Stage 5 (withdrawal of developing rhopalia inside the developing bell), and Stage 7 (free-swimming juvenile medusa). Stage 6 animals were not directly examined as this stage represents the Stage 7 medusa prior to detachment from the polyp remnants and does not represent additional rhopalial development. Measurements of the developing animals were obtained using an eye graticule in the eyepiece of the Wild Heerbrugg M3Z dissecting microscope. Adult rhopalia and rhopalia from transforming stages were carefully dissected out using a scalpel when they were examined separately from the rest of the body.

Scanning Electron Microscopy

The procedure for the fixation and preparation of animals for scanning electron microscopy was as follows: whole animals were relaxed for 45 minutes in calcium-free seawater containing 0.2% magnesium chloride (Sigma, St. Louis, MO) plus 1 drop of 1% Lidocaine (Hospira, Lake Forest, IL) per 2 ml of the mixture before they were fixed in 2.5% glutaraldehyde (EMS, Ft. Washington, PA) in 0.2M Millonig's buffer pH 7.2 for one hour. Stock 0.4M Millonig's phosphate buffer pH 7.2 was prepared from sodium phosphate monobasic monohydrate (Fisher, Fair Lawn, NJ; 55.4g/L) and sodium hydroxide (Fisher, Fair Lawn, NJ; 14.25g/L) dissolved in distilled water. The animals were then rinsed in 0.2M Millonig's buffer pH 7.2 for three 15-minute intervals. After they were post-fixed for one hour in 2% osmium (EMS, Hatfield, PA) in a 1.25% sodium bicarbonate (Sigma, St. Louis, MO) buffer pH 7.2, the samples were rinsed in 1.25% sodium bicarbonate buffer for three 15-minute intervals. Next, the animals were rinsed in distilled water for one minute. Dehydration followed and included progressively immersing the animals in 50%, 70%, 80%, 95%, and four times in 100% ethanol for 15 minutes each. The animals were then critically point dried in a Polaron critical point dryer with a model 4850 BioRad heater and subsequently mounted on stubs with double-sticky tape. After the samples were sputter coated with gold palladium for two minutes using a Polaron SEM coating system, they were ready to be observed and imaged under varying magnifications using a Quanta 200 scanning electron microscope at a voltage of 25kV. All measurements were obtained using scale bars generated by the Quanta 200 series imaging software (FEI company, Hillsborough, OR).

Laser Scanning Confocal Microscopy

The fixation and preparation of animals for immunofluorescent labeling was as follows: whole animals from steady-state polyps (Stage 0), Stage 1, Stage 2, Stage 3, Stage 4, Stage 5, and Stage 7 animals were relaxed for 45 minutes in calcium-free seawater containing 0.2% magnesium chloride plus 1 drop of 1% Lidocaine per 2 ml of the mixture. Animals that were prepared for FMRFamide staining were fixed in Zamboni's fixative [2% paraformaldehyde (Sigma, St. Louis,

MO) + 0.2% picric acid (Fisher, Fair Lawn, NJ) in 0.1 M Millonig's phosphate buffer pH 7.2] overnight at 0°C. Animals that were prepared for opsin and crystallin protein detection were fixed in 4% paraformaldehyde in 0.2M Millonig's buffer pH 7.2 overnight at 0°C. The samples that were prepared for FMRFamide staining were progressively rinsed at room temperature in PBS-Tween (phosphate buffered saline pH 7.2 + 0.05% Tween-80; Fisher, Fair Lawn, NJ) three times for 20 minutes each, 0.4M glycine (Sigma, St. Louis, MO) pH 7.2 for 1 hour, and PBS-Triton (PBS pH 7.2 + 0.25% Triton X-100; LabChem, Pittsburgh, PA) three times for 20 minutes each. The 10X PBS pH 7.2 stock was prepared from sodium phosphate monobasic monohydrate (2.56g/L), sodium phosphate dibasic (Sigma, St. Louis, MO; 11.94g/L), and sodium chloride (Fisher, Fair Lawn, NJ; 87.66g/L) dissolved in distilled water; this stock was diluted 1:9 to obtain the working PBS solution. Animals that were prepared for opsin and crystallin protein detection were progressively rinsed at room temperature in 0.2M Millonig's buffer pH 7.2 three times for 20 minutes each, 0.4M glycine pH 7.2 for 1 hour, and 0.1M Millonig's buffer pH 7.2 + 0.25% Triton X-100 three times for 20 minutes each. All organisms were then placed in blocking serum [10 % fetal calf serum (Sigma, St Louis, MO) in PBS pH 7.2 + 0.1% sodium azide (Fisher, Fair Lawn, NJ)] overnight at 0°C. Samples were held in blocking serum at 0°C until needed. Rhopalia that were to be examined separately from the rest of the body were carefully excised using a scalpel from Stage 2, Stage 3, Stage 4, Stage 5, and Stage 7 animals in a small amount of blocking serum. Next, the primary antibody [rabbit FMRFamide antiserum directed against molluscan neurons (Bachem, Torrance, CA) diluted 1:200 in blocking serum, rabbit J1-crystallin protein antiserum directed against cubozoan crystallin proteins of the lens diluted 1:1000 in 0.1M Millonig's buffer pH 7.2 containing 0.25% Triton X-100 + 0.25% human serum albumin (Sigma, St. Louis, MO), and rabbit opsin antiserum directed against zebra fish UV opsins found in photoreceptors diluted 1:200 in 0.1M Millonig's buffer pH 7.2 containing 0.25% Triton X-100 + 0.25% human serum albumin] was added and left overnight at 0°C. All subsequent incubations were performed at room temperature. After rinsing three times for 20 minutes each in PBS-Triton for samples stained for FMRFamide and 0.1M Millonig's buffer pH 7.2 + 0.25% Triton

X-100 for samples stained for opsin and crystallin proteins, the secondary antibody [Alexa Fluor 546 goat anti-rabbit IgG (Invitrogen, Carlsbad, CA) diluted 1:800 in blocking serum] was added for an hour in total darkness (as were all subsequent incubations) followed by another rinse in PBS-Triton three times for 20 minutes each. After two 10-minute rinses each in PBS and distilled water, the samples were mounted in PBS/glycerol/n-propyl gallate [50% glycerol (Sigma, St. Louis, MO) in PBS pH 7.2 + 5% n-propyl gallate (Sigma, St. Louis, MO)] on microscope slides, coverslipped and imaged using the HeNe543 laser of a Zeiss LSM 510 laser scanning confocal microscope under varying magnifications. For many samples, simultaneous DIC (differential interference contrast) images were obtained using the same microscope and software to provide structural context. All measurements were obtained using scale bars generated by the Zeiss LSM 510 imaging software (Carl Zeiss, Oberkochen, Germany).

Brightfield Examination of Whole Rhopalia

Whole rhopalia of Stage 2, Stage 3, Stage 4, Stage 5, Stage 7, and adult animals were carefully dissected off of extra samples of transforming animals being held in blocking serum for immunohistochemisty. The rhopalia were rinsed two times for 10 minutes each in PBS before they were mounted on a coverslip in a drop of 1:1 PBS:glycerol and examined using the Olympus IX81 inverted brightfield microscope at 32X. All measurements were obtained using scale bars generated by the Olympus IX81 imaging software (Olympus, Center Valley, PA).

Melanin Staining

The fixation and preparation of animals for the detection of melanin was as follows: whole Stage 2, Stage 3, Stage 4, Stage 5, and Stage 7 animals were relaxed for 45 minutes in calcium-free seawater containing 0.2% magnesium chloride plus 1 drop of 1% Lidocaine per 2 ml of the mixture before they were fixed in 10% formalin (Sigma, St. Louis, MO) in seawater for 1 hour at room temperature. Prior to fixation, whole rhopalia were carefully removed from living adult medusae using a scalpel. After they were rinsed two times for 15 minutes each in distilled water, the samples were dehydrated in increasing levels of ethanol [50%, 70%, 80%, 90% + 0.5% eosin (Polysciences,

Warrington, PA), 95%] for 15-minute intervals. The samples were then placed in a 1:1 TBA [tertiary butanol (Fisher, Fair Lawn, NJ)]: 95% ethanol mixture for 15 minutes on top of an oven set at 80°C. The following 15-minute and overnight incubation also took place on top of the oven. Following a 15-minute rinse in TBA, the samples were left overnight in a second TBA rinse. After they were placed in a 1:1 TBA:warm paraffin slush in the paraffin oven set at 62°C for 15 minutes, the samples remained in the oven in for 15 minutes each in two 100% paraffin changes. The samples were then embedded in fresh paraffin. After the paraffin blocks were sectioned at a thickness of 10 μm using a sharpened steel knife on a Spencer Lens Company (Buffalo, New York) rotary microtome, the sections were adhered to standard glass slides using a 1:1 mixture of egg albumin and glycerol + two thymol crystals (Fisher, Fair Lawn, NJ) and by heating on a 56°C slide warmer for two to three minutes. Sections to be used for the melanin control bleaching procedure (see below) were mounted on Superfrost Plus slides (Fisher Scientific, Pittsburgh, PA). The slides were then stored in slide boxes at room temperature until needed.

The staining procedure for the detection of melanin was as follows: the paraffin section slides were dewaxed and rehydrated to distilled water using two-minute immersions in the following solutions: xylene (2; Fisher, Fair Lawn, NJ), 100% ethanol (2), 95% ethanol, 80% ethanol, 70% ethanol, 50% ethanol, and distilled water (2). The slides were then stained in filtered Working Fontana Silver Nitrate [ammonium hydroxide (Fisher, Fair Lawn, NJ) added to 10% silver nitrate (Fisher, Fair Lawn, NJ) until just clear and left overnight] in a 56°C oven for 1 hour 30 minutes (Luna, 1968; Masson, 1928). Following dehydration to distilled water, control samples were bleached for 20 minutes in 0.25% potassium permanganate (Fisher, Fair Lawn, NJ) followed by a two-minute rinse in distilled water, five minutes in 5% oxalic acid (Fisher, Fair Lawn, NJ), and a final two-minute rinse in distilled water (Prophet, Mills, Arrington, & Sobin, 1992; Sheehan & Hrapchak, 1980) before they were put into Working Fontana Silver Nitrate with non-bleached slides; non-control slides were kept in distilled water during the bleaching procedure. After coming out of the oven, the slides were rinsed in distilled water for three two-minute changes and then toned in 0.2% gold chloride (EMD

chemicals, Gibbstown, NJ) for 1 minute. Following a two-minute rinse in distilled water, the sections were placed in 5% sodium thiosulfate (Fisher, Fair Lawn, NJ) for one minute and rinsed for one minute in distilled water. The samples were then counterstained with Nuclear Fast Red (Ricca, Arlington, TX) for three minutes and rinsed in two two-minute changes of distilled water. After they were dehydrated in subsequent changes of 50%, 70%, 80%, 95%, and 100%(2) ethanol, the samples were cleared in two two-minute changes of xylene, mounted with Permount (Fisher, Fair Lawn, NJ) using glass slides and coverslips, and imaged using an Olympus IX81 inverted light microscope under varying magnifications. All measurements were obtained using scale bars generated by the Olympus IX81 imaging software (Olympus, Center Valley, PA).

Hematoxylin and Eosin Staining

Steady-state polyps, Stage 1, Stage 2, Stage 3, Stage 4, Stage 5, and Stage 7 animals were prepared, embedded, sectioned, and mounted as described for the melanin staining procedure. The paraffin section slides were first dewaxed in two 11-minute changes of Safeclear (Fisher, Kalamazoo, MI) followed by rehydration to distilled water using two 5-minute changes in 100% ethanol, two 5-minute changes in 95% ethanol, and a two-minute rinse in distilled water. The slides were then dipped multiple times and left to sit in Harris Hematoxylin (Fisher, Kalamazoo, MI) for 7 minutes before they were rinsed in running tap water for one minute. Next, the slides were placed in 0.3% acid alcohol [.3% hydrochloric acid (Fisher, Fair Lawn, NJ) in 100% ethanol] for one minute followed by 30 seconds in Scott's Tap Water [10g/L magnesium sulfate (Fisher, Fair Lawn, NJ) and .667g/L sodium bicarbonate (Sigma, St. Louis, MO) in tap water]. After they were dipped 10 times in 95% ethanol, the slides were counterstained by dipping the slides 10 times into a 1% alcoholic solution of Eosin Y (Fisher, Kalamazoo, MI). After another 7 dips in 95% ethanol, the slides were dipped 15 times each in three rinses of 100% ethanol and two rinses of Safeclear. The slides were then mounted with Permount using glass slides and coverslips and were imaged using an Olympus IX81 light microscope under varying magnifications. All measurements were obtained using scale bars generated by the Olympus IX81 imaging software (Olympus, Center Valley, PA).

Results

Staging and Morphology During Transformation

Adult: polyp and medusa forms. The steady-state polyp, which has a length of approximately 3 mm, is eyeless (Figure 1A). The body column of the animal is connected to a slender stalk and foot, which attaches the animal to the substrate, at one end, and to the hypostome, or mouth region, at the other end. The mouth opening of the animal is located in the center of the hypostome. Surrounding the base of the hypostome are roughly 13 to 16 radially-distributed tentacles which are equidistant from each other. The steady-state polyp asexually reproduces via lateral budding (Fischer & Hofmann, 2004).

Understanding the structure of adult rhopalia and ocelli is necessary to understand the development of the eyes over the course of transformation. The adult medusa of *Carybdea marsupialis* has an average bell height of approximately 30 mm and appears clear with peppered flecks (Martin, 2004; Figure 1B). A sensory structure, called a rhopalium, is located on each quadrant of the box-shaped bell and from each of the four bottom corners of the bell is a structure referred to as a pedalium, which each bears a single tentacle. The rhopalia, which are approximately 700 μm long and 500 μm in diameter, are located in indented pockets of the bell suspended by a stalk and are partially covered by a flap which functions similar to an eyelid (Martin, 2002, 2004; Figure 1C). The stalks of the rhopalia resemble the pendulum of a clock in that they are capable of swinging back and forth, twisting and turning (Martin, 2002, 2004). A statocyst is located at the base of the rhopalium and is involved in keeping the eyes correctly oriented in relation to gravity (Berger, 1898; Garm & Ekström, 2010; Garm et al., 2011; Sötje et al., 2011). Six eyes can be found on each rhopalium consisting of two complex camera-type eyes and two pairs of simple eyes (ocelli; Figure 1D). The rhopalia face inward, away from the eyelid and surrounding environment. The large complex eye,

located above the statocyst closest to the bottom of the rhopalium with a diameter of approximately 400 μm, is oriented inward towards the center of the bell. The small complex eye, located above the large complex eye with a length (perpendicular to the rhopalia length) of roughly 300 μm and a height (parallel to the rhopalial length) of roughly 250 μm, is oriented upward towards the apex of the bell. The slit ocelli, located slightly above and on either side of the large complex eye with an approximate length of 250 μm and height of 100 μm, are oriented inward along with the pit ocelli, which are located on either side of the small complex eye and have an approximate diameter of 150 μm (Table 1). Often found in between the slit and pit ocellus is a small, pigmented, and spherical structure which can range in size from roughly 25-50 μm in diameter. The distance located between the pigment boundaries of the large and small complex eye (measured from pigment boundaries at closest distance) is approximately 40 μm, the distance between the pigment boundaries of the large complex eye and each slit ocellus is approximately 50 μm, the distance between the pigment boundaries of the large complex eye and each pit ocellus is approximately 150 μm, the distance between the pigment boundaries of the small complex eye and each of the four simple ocelli is approximately 45 μm, the distance between the pigment boundaries of a pit ocellus and slit ocellus is approximately 60 μm, the distance between the pigment boundaries of the two slit ocelli is approximately 265 μm, and the distance between the pigment boundaries of the two pit ocelli is approximately 300 μm (Figure 2A).

In the adult rhopalium, the retina of the large lensed eye (also referred to as the large complex eye) appears as a raised doughnut with the lens positioned in the middle (Figure 3A). The bottom half of this doughnut, closest to the statocyst, is more defined along its edges than the top half and the topmost portion connects with the small lensed eye (also referred to as the small complex eye). A deep groove, which faces down towards the basal statocyst can be seen encircling the top half of the lens (closest to the small complex eye) while the bottom edge of the lens shows how the corneal covering, sitting on top of the lens, is continuous with cells flowing out over the encircling retina (Figure 3A). The entire rhopalial surface is ciliated, but the density of ciliation varies as the front of

the rhopalium (where the eyes are located) is much less heavily ciliated than the back. These cilia are 10-15 μm in length and 0.5 μm in diameter (Figure 3B). The base of each cilium is encircled by a ring of microvilli which are approximately 1 μm in length. Microvilli of roughly the same size also line the perimeter of most cells and are distributed across the surface of most cells, such as those covering the surface of the small complex eye lens (Figure 3B). These microvilli give the cells a "rough" appearance. The cells covering the lens of the large complex eye, which corresponds to the location of the cornea, vary in the length of their cilia. The surface of the bottom region of the retina, closest to the statocyst, has cells with shortened cilia ranging in length from approximately 5-9 μm. Just above this region of the retina, the cells covering the lens exhibit an even smaller range in cilia length and, as the upper edge of the lens is reached (closest to the small complex eye), most cilia are less than 3 μm in length (Figure 3C). Some of the cells in the lower region of the raised retina (closest to the statocyst) of the large complex eye and the majority of the cells covering the lens of the large complex eye have a smooth surface appearing to lack the microvilli surrounding the cilium, across the cell surface, and along the cell perimeter (Figure 3C). With the exception of these "smooth" cells, the cells covering the rhopalium are rough in texture like those seen covering the lens of the small complex eye (Figure 3B). The raised retina of the small lensed eye, the bulk of which is found below the lens, tapers up on either side of the lens and abruptly ends at two horizontal concave indentations (Figures 3A, D). The sheet of cells folding down over the lens of the small complex eye is continuous with the cells on the top of the rhopalium with only a very slight indentation defining the apical edge of the lens. Unlike the cells covering the lens of the large complex eye, the cilia of the cells covering the small complex eye lens are not shortened and remain at a length of 10-15 μm (Figure 3B). A much deeper indentation, which faces upward towards the top of the rhopalium, can be seen differentiating the bottom visible portion of the lens (closest to the large complex eye) from the retina below it (Figure 3D). The slit ocelli, which are positioned on either side and slightly above the large complex eye, appear as slit shaped grooves with lens-like material positioned at its surface (Figures 3A, E). This lens-like material is found on the surface of the laterally-flattened spherical

photoreceptor cells in the central slit of the ocellus and gives the surface of these photoreceptor cells a bumpy appearance. The pit ocelli appear as ciliated pits located on either side of the small lensed eye near the top of the rhopalium (Figures 3A, F). The cells covering the retinal surface of the small (Figure 3B) and large (Figure 3C) complex eyes and surrounding the slit ocellus have a diameter of roughly 5-8 μm. The cells encircling the pit ocelli appear to have an overall smaller size of roughly 3-6 μm although the 10-15 μm long cilia obscure much of the cellular outlines.

Stage 0: the steady-state polyp. The steady-state polyp represents Stage 0 of the transformation from the eyeless polyp form to the eyed and free-swimming medusa form. The main characteristic of the steady-state polyp relative to the transformation process is the radially-distributed and equidistant tentacles surrounding the base of the hypostome (Figure 4A). Under SEM, the surface of the entire polyp is heavily ciliated; each cell has a single cilium which is smooth and thin with a length of approximately 10-15 μm and a diameter of roughly 0.5 μm.

Stage 1. The first evidence of the transformation process can be seen when the tentacles of the steady-state polyp move from being radially distributed to forming four groups of approximately 2-5 tentacles per group (the number of tentacles per group in a single animal is highly variable) (Figure 4B). This rearrangement of the polyp tentacles from a radial distribution to a tetrahedral distribution, a process that takes 1-2 days, defines Stage 1. The bases of the polyp tentacles will then fuse approximately 3 days after transformation began to form the surface on which the eyes will develop. Most of the fused tentacle bases will form the rhopalial body while the proximal part of the fused tentacles will continue to constrict and elongate to become the slender rhopalial stalk. At this point, unfused apical sections of the tentacles continue to resemble those of a steady-state polyp, although some may begin to recede. It is just after tentacle rearrangement (prior to tentacle fusion) that the upper body column, just below the tentacles, forms a cuff which folds up and around the bases of the tentacle groups. It is in the areas between the fused tentacle groups where this cuff of cells either begins to form the primary medusa tentacle buds, which appear by Stage 2 with an approximate length of 100 μm, or folds inward and down (parallel to the body column) underneath

the flattened hypostome. This inward movement of cells marks the beginning of a progressive in-folding which forms the ectodermal-lined cavity destined to become the bell of the medusa (Figure 5). The hypostome will transition to become the manubrium, which is the mouth of the medusa. As the cells fold inward, the junction between the developing bell and polyp can be seen as a dimpled furrow along the outside circumference of the body column; this indentation gradually becomes more defined and constricted as it moves farther down the body column (Figure 5). During this process, the formation of the four septa is also evident as dimpled indentations in the cuff which are parallel with the body column (Figure 5); septa partition the stomach cavities of the medusa and extend down the four corners of the bell to the pedalia. In a Stage 1 animal, the dimpled furrow is located at the base of the cuff of cells roughly 100 μm below the hypostome (Figure 5A). The approximate length of the Stage 1 polyp remains 3 mm.

Stage 2. An initial pigmented eye spot approximately 15 μm in diameter can first be seen around the fourth day and signifies Stage 2 of transformation (Figures 6A, 7A). The encircling bases of the photoreceptors, which are producing this pigment, suggest an overall eye size of approximately 30 μm in diameter (Table 1). This eye spot corresponds to the early pigment formation of the small complex eye based on its location and the simultaneous appearance of the large complex eye, which, under brightfield examination of whole rhopalia of Stage 2 animals, first appears as a non-pigmented cup-shaped primordium of cells in the region of the large complex eye. This cup is roughly 30 μm in diameter (including the cells encircling the cup-shaped concavity) and the center of the cup, which is the future location of the lens of the large complex eye, has the greatest depth of approximately 10 μm below the rhopalial surface (Figure 7B). The primordial eye cup of the small lensed eye can also be seen under brightfield examination of whole rhopalia and is located slightly above the pigment (closest to the point of attachment to the polyp body) in the future location of the small complex eye lens. This cup has roughly the same width of the primordial cup of the large complex eye (roughly 30 μm) and, unlike the cup of the large lensed eye, has a relatively uniform depth of approximately 10 μm across the majority of its diameter (Figure 7B). By the end of Stage 2, faint pigmentation can be

seen around the top half of the cup-shaped primordium of the large complex eye (closest to the small complex eye; Figure 7C). In a Stage 2 animal, the dimpled furrow signifying bell formation is located at the base of the cuff of cells roughly 175 μm below the hypostome (Figure 5B) and the approximate length of the Stage 2 polyp remains 3 mm.

Stage 3. By the fifth day, four clearly defined eye spots can be distinguished and represent the large and small complex eyes and slit ocelli based on corresponding locations in the adult rhopalia (Figures 6B, 7D). The presence of four eyespots defines the beginning of Stage 3. By day 7 (Figure 8A), all six eyespots are visible including the complex eyes, the slit ocelli, and lastly the pit ocelli (Figure 7E). A more faintly-pigmented area in the center of the forming pigment cup of the large lensed eye is where the lens is developing (Figures 7D, E). The Stage 3 polyp remains at a length of approximately 3 mm and bears rhopalia that are approximately 140 μm in length and width. The diameter of the large complex eye is approximately 62 μm, the small complex eye is approximately 63 μm in length and 40 μm in height, the slit ocelli are approximately 44 μm in length and 30 μm in height, and the pit ocelli have an approximate diameter of 32 μm (Table 1). The distance between the pigment boundaries of the large and small complex eye (measured from pigment boundaries at closest distance) is approximately 18 μm along with the distance between the pigment boundaries of the large complex eye and each slit ocellus, the distance between the pigment boundaries of the small complex eye and each slit ocellus, and the distance between the pigment boundaries of the small complex eye and each pit ocellus (Figure 2B). The distance between the pigment boundaries of the large complex eye and each pit ocellus is approximately 45 μm, the distance between the pigment boundaries of a slit ocellus and pit ocellus is approximately 20 μm, the distance between the pigment boundaries of the slit ocelli is approximately 65 μm, and the distance between the pigment boundaries of the pit ocelli is approximately 75 μm (Figure 2B). Tentacle recession, though variable from animal to animal, is obvious during this stage and the buds of the primary set of medusa tentacles can be seen extending upward and resting against the sides of the hypostome, with a length of approximately 250 μm, or, by the end of Stage 3, over the top of the hypostome (Figures 6B, 8A) with a highly variable

length of roughly 500 µm. In a Stage 3 animal, the dimpled furrow which signifies bell formation is located at the base of the cuff of cells roughly 250 µm below the hypostome (Figure 5C). Under scanning electron microscopy, only the large complex eye and occasional slit ocellus are visible due to the position of the fused tentacle bases which rest against the hypostome and therefore obscure the developing eyes from view (Figure 9). The structure of the large lensed eye appears on the surface of the fused tentacles just above the remaining unfused tentacle sections as a rounded sheet of cells which has folded upward (in the direction of the point of attachment/top of the forming rhopalium) and concurrently forms a groove approximately 30 µm in length which faces slightly downward towards the base of the rhopalium (Figure 9). The cells making up the sheet begin to show dramatically shortened cilia the closer they are to the groove. Cells located around the base of the sheet (just above the forming statocyst) have cilia which are the same length (approximately 10-15 µm) of those found in the steady-state polyp and on adult rhopalia. Slightly farther up the sheet are cells with varying cilia lengths of roughly 3-7 µm. The majority of the central region of the up-folding sheet consists of cells with cilia only 1 µm in length or less (Figure 9). By the time the apex of the sheet of cells is reached, almost no cilia can be seen. The diameter of the ciliated cells that make up the surface of the large complex eye is roughly 5-8 µm.

Stage 4. The progression from Stage 3 to Stage 4 (which takes approximately 4-5 days) involves a gradual uprising of the developing rhopalia, which were previously outstretched, up against the hypostome, the base of which is now clearly set inward from the tentacle bases, and the completion of polyp tentacle recession (Figure 8B). By this stage, the eyes/ocelli and rhopalia resemble miniature versions of adult medusa eyes/ocelli and the lenses of the complex eyes can clearly be seen (Figure 7F). By the end of Stage 4, 4-5 days from the start of this stage, the medusa tentacles have receded tip-first into the developing bell adjacent to the point of origin (Figure 8B) and the bell will begin to sporadically pulsate. During Stage 4, the statocyst begins to form at the distal region of the fused polyp tentacles (Figures 8B, 10A). The dimpled furrow which signifies bell formation is now located at the base of the bell roughly 300 µm below the hypostome (Figure 5D).

Under light microscopy, the delineation of the developing bell from the remnant polyp body can now be defined by an increasingly obvious difference in color between the beige-colored polyp (Figure 1A) and the darkening amber-colored bell (Figure 8B). Due to a high variation in stalk length, the length and width of the developing bell (not including the protruding hypostome) will be given from this point forward. The developing bell of a Stage 4 animal is approximately 0.8 mm long and 0.7 mm wide with rhopalia that have an approximate length of 180 μm and width of 165 μm. The diameter of the large complex eye is now approximately 84 μm, the small complex eye is approximately 77 μm in length and 43 μm in height (measured from the top of the lens to the bottom of the retina), the slit ocelli are approximately 56 μm in length and 37 μm in height, and the pit ocelli have an approximate diameter of 38 μm (Table 1). The distance between the pigment boundaries of the large and small complex eyes is approximately 12 μm, the distance between the pigment boundaries of the large complex eye and each slit ocellus remains approximately 18 μm, the distance between the pigment boundaries of the large complex eye and each pit ocellus remains approximately 45 μm, the distance between the pigment boundaries of the small complex eye and each of the four simple ocelli is approximately 20 μm, the distance between the pigment boundaries of a slit ocellus and pit ocellus is approximately 20 μm, the distance between the pigment boundaries of the slit ocelli is approximately 80 μm, and the distance between the pigment boundaries of the pit ocelli is approximately 90 μm (Figure 2C).

Under scanning electron microscopy, a clear difference in ciliation patterns can be seen between the sparsely ciliated front of the rhopalium (where the eyes are developing) and the heavily ciliated backside of the rhopalium (from where the stalk originates; Figure 10A) . The diameter of the cells which cover the surface of the complex eyes and encircle the slit-shaped groove and pit-shaped concavity of the simple ocelli is roughly 5-8 μm and remains this size through the end of transformation. The cells range in shape from cuboidal to more rectangular, especially closer to the grooves of the complex eyes and slit-/pit-shaped indentations of the simple ocelli (Figure 10B). These cells exhibit cilia similar to those seen in the adult eye and steady-state polyp. Each cilium is roughly

10-15 μm in length, 0.5 μm in diameter, and the base of the cilium is surrounded by a ring of slender microvilli that are roughly 0.6 μm long and 0.1 μm wide; these microvilli are also located along the perimeter of most cells (Figures 10C, D, E, F). Some cells have a smooth surface (Figures 10B, E) while others are rougher in appearance as they exhibit microvilli (roughly 0.6 μm long and 0.1-0.4 μm wide) sporadically across the cell surface in varying numbers (Figures 10D, F). The length of the cilium of cells exhibiting microvilli across the surface remains 10-15 μm with the exception of an occasional cell with a shortened cilium: the cilium of these cells, which tend to be more spherical in shape with a diameter of approximately 5-8 μm, is shortened to a length of only roughly 1.5 μm and remains at a thickness of roughly 0.5 μm (Figure 10F). All three different ciliation/microvilli patterns (microvilli absent/long cilium, microvilli present/long cilium, microvilli present/short cilium) are not found in any specific location and appear to be randomly distributed. Many of the smooth-surface cells can be found on the up-folding lip of cells and down-folding lip of cells of the complex eyes, but there appears to be an equal amount of rough-surface cells. The cells which have a shortened cilium and microvilli across the surface are the least common. The two complex eyes and both pairs of simple ocelli are now clearly visible (Figure 10A), as during the previous stages the developing eyes were obscured from view due to the position of the fused tentacle bases which rest against the hypostome. For orientation, the fused tentacles will form the basal statocyst and thus represent the bottom of the rhopalium: the downward-facing groove, which is now approximately 35 μm long and is more curved, of the large complex eye sits centered on a raised circular area (roughly 75 μm in diameter) representing the developing retina of photoreceptors. The circumference of the circular area is more clearly defined along the edge of the lower half (from which the lip originates) and sits higher (relative to the rhopalial surface) than the upper half (Figure 11A). The ciliation pattern of the cells making up the up-folding sheet of cells is similar to that seen during Stage 3, but now a greater portion of the cells exhibit the shortened cilia roughly 1 μm in length (Figures 10B, 11A). The upper half of the developing retina of the large complex eye (located above the downward-facing groove) is made up of cells which exhibit cilia approximately 10-15 μm long. The up-folding sheet of cells seen

on the surface hides the cup-shaped primordium of the large complex eye and, along with the downward-facing groove it forms, can still be distinguished in scanning electron microscopy examination of adult rhopalia. Above the large complex eye, the small complex eye first appears as a groove that faces slightly upward towards the top of the rhopalium and this groove is created by a less obvious down-folding sheet of cells (Figure 10A). The raised retina below the upward-facing groove of the small complex eye is more oval in shape with edges that are less clearly delineated than that of the large lensed eye. Although less defined than the original groove of the large complex eye, the upward-facing groove of the small complex eye can still be distinguished in adult rhopalia. The pit ocelli appear as small concave dimples on either side of the developing small lensed eye and are roughly 10 μm in diameter (Figures 10A, 11B). Lastly, the slit ocelli appear as grooves, roughly 25 μm in length, which slant slightly upward towards the top of the rhopalium/ inward towards the center of the rhopalium and are located slightly above and on either side of the developing large lensed eye (Figures 10A, 11C). This slit-shaped groove differs in width along its length: the region of the groove situated closest to the side of the rhopalium (away from the complex eyes) is wider and more spherically shaped with a width of roughly 10 μm while the inner portion of the groove (closest to the complex ocelli) is tapered and has a width of no more than 3 μm (Figure 11C). By adulthood, the ciliated cavities of the slit ocelli will no longer be able to be seen upon formation of photoreceptor cells, which span the surface of the cavity and are covered with lens-like material. In the small complex eye and simple ocelli, shortening of the cilia is only apparent in cells found within the grooves of the small complex eye, slit ocelli, and the dimple of the pit ocelli, exhibiting cilia with approximate lengths of 1-3 μm (Figures 11B, C).

Stage 5. The progression to Stage 5 involves an in-folding of the eyes, medusa tentacles (which have developed from the medusa tentacle buds), and hypostome into the developing bell where the hypostome will transition to form the medusal manubrium (Figures 12A, B). In a Stage 5 animal, the dimpled furrow, which signifies bell formation, is located at the base of the developing bell (where it is attached to the polyp remnants) roughly 800 μm below the hypostome (Figure 5E).

The developing bell of a Stage 5 animal is approximately 1 mm long and 1.2 mm wide with rhopalia that are approximately 200 μm in length and 170 μm in width. The eyes/ocelli and rhopalia continue to resemble miniature versions of adult eyes/ocelli and rhopalia (Figures 12B, 13A) and have grown in size: the large complex eye has a diameter of approximately 93 μm, the small complex eye is approximately 88 μm in length and 46 μm in height (measured from the top of the lens to the bottom of the retina), the slit ocelli are approximately 65 μm in length and 36 μm in height, and the pit ocelli have an approximate diameter of 41 μm (Table 1). The distance between the pigment boundaries of the large and small complex eyes is approximately 9 μm, the distance between the pigment boundaries of the large complex eye and each slit ocellus is approximately 15 μm, the distance between the pigment boundaries of the large complex eye and each pit ocellus remains approximately 45 μm, the distance between the pigment boundaries of the small complex eye and each of the four simple ocelli remains approximately 20 μm, the distance between the pigment boundaries of a slit ocellus and pit ocellus is approximately 22 μm, the distance between the pigment boundaries of the slit ocelli is approximately 90 μm, and the distance between the pigment boundaries of the pit ocelli is approximately 100 μm (Figure 2D).

Under scanning electron microscopy, the eyes/ocelli of a Stage 5 animal resemble those seen in a Stage 4 animals but have increased in size: the down-facing groove created by the up-folding sheet of cells in the large lensed eye now has a width of approximately 40 μm (Figure 14A) and sits on a raised circular area that is approximately 80 μm in diameter. The up-facing groove created by the down-folding sheet of cells in the small complex eye is now approximately 37 μm wide (Figures 14A, B). The cell sizes, ciliation patterns, and cilia lengths remain the same and the distribution of the ciliation patterns remains relatively random (Figures 14B, C, D). As in Stage 4, more rectangular-shaped cells are found closest to the grooves of the complex eyes and closest to the slit-/pit-shaped indentations of the simple ocelli (Figures 14B, D). The slit-shaped indentations of the slit ocelli are approximately 35 μm in length (Figure 14C) and the concave dimple of the pit ocellus remains roughly 10 μm in diameter (Figure 14D).

Stage 6. After only 1-2 days at Stage 5, the transformation is nearly complete and the animal resembles a young medusa with rhopalia that remain approximately 200 μm long and 180 μm wide. At this stage, the animal may detach from the substrate (leaving its polyp remnants behind) or may remain to mature further (Figure 15A). Further maturation of the medusa is characterized by an uncoiling of the medusa tentacles, an increase in size and cuboidal shaping of the bell, and an increase in bell transparency; the increase in size of the bell (which goes from being approximately 1.2 mm in length and width to approximately 2 mm in length and width) coupled with a perceived decrease and/or reorganization of pigmentation is presumably caused by an out-folding of cells along the four septa. As the time of detachment is highly variable, Stage 6 does not represent a specific stage during rhopalial development but only signifies that the medusa resulting from the transformation process is not yet free-swimming.

Stage 7. After the medusa detaches and is free-swimming, the animal has reached Stage 7 and the transformation is complete (Figure 15B). The bell of a newly metamorphosed animal is approximately 1.2-2 mm long and 1.2-2 mm wide with rhopalia that remain approximately 200 μm in length and 180 μm in width. The eyes/ocelli and rhopalia continue to resemble miniature versions of adult eyes/ocelli and rhopalia but with slight changes in size, as shown in Table 1: the large complex eye has an approximate diameter of 96 μm (Figure 13B), the small complex eye remains at a length of approximately 89 μm and a height of approximately 55 μm (Figure 13C), the slit ocelli have reached an approximate length of 72 μm and a height of 41 μm (Figure 13D), and the pit ocelli have an approximate diameter of 44 μm (Figure 13E). The distance between the pigment boundaries of the large and small complex eyes remains approximately 9 μm, the distance between the pigment boundaries of the large complex eye and each slit ocellus remains approximately 15 μm, the distance between the pigment boundaries of the large complex eye and each pit ocellus is 50 μm, the distance between the pigment boundaries of the small complex eye and each of the four simple ocelli remains approximately 20 μm, the distance between the pigment boundaries of a slit ocellus and pit ocellus is approximately 25 μm, the distance between the pigment boundaries of the slit ocelli remains

approximately 90 µm, and the distance between the pigment boundaries of the pit ocelli remains approximately 100 µm (Figure 2E).

Under scanning electron microscopy, the eyes/ocelli of a Stage 7 animal resemble those seen in a Stage 5 animal and remain relatively the same size: the downward-facing groove created by the up-folding sheet of cells in the large complex eye remains approximately 37 µm in width along with the up-facing groove created by the down-folding sheet of cells in the small complex eye. The raised retina of the large complex eye remains at a diameter of approximately 80 µm. The slit-shaped indentation of the slit ocelli remains at an approximate length of 35 µm and the concave dimple of the pit ocelli remains at an approximate diameter of 10 µm. A polyp may completely transform into a free-swimming medusa in about 14 days. A schematic diagram of eye development is shown in Figure 16.

Regression. The term regression refers to the return of an animal to a former or less developed state. This phenomenon was observed during the metamorphosis of *Carybdea marsupialis* when eye-forming animals revert back to the eyeless polyp state through the reabsorbance of the eyes, rhopalia, and statocyst. The time it takes to return to the polyp form varies from one to two weeks, depending on the stage at which regression begins, which can range from Stage 3 to Stage 6, just prior to medusal detachment (Figure 17). The first evidence indicating regression is seen in the dispersal of the melanin pigment granules which move from being neatly contained within the boundaries of the photoreceptors to being unevenly distributed across the entire front-facing surface of the rhopalium where the eyes were developing. This occurs in just one day. It appears that the melanin granules previously contained within the photoreceptors making up the developing large complex eye are dispersed first, followed by the small complex eye and simple ocelli. The retraction of the individual rhopalia is variable with some disappearing along the same timeline while other regressing animals are left with one or two rhopalia that have yet to be reabsorbed. For most of the animals observed, the medusa tentacles are reabsorbed quickly, often within two days of beginning the regression, although they are not necessarily reabsorbed at the same time. The earlier the animal is

in the transformation process, the shorter amount of time it takes for the medusal structures to be reabsorbed; for example, an animal regressing from Stage 4 takes approximately 2 days to completely reabsorb the medusa tentacles and rhopalia, while an animal regressing from Stage 6 takes approximately a week. For animals regressing later in transformation, the last structure to be reabsorbed is the statocyst, while in earlier stages all structures within the rhopalia appear to be reabsorbed around the same time. Once polyp tentacles have begun to emerge, remnant pigment can often be seen within the polyp body and appears as darkened diffuse patches. All regressing polyps take approximately 5 days after reabsorbing all medusal components to exhibit polyp tentacle buds which then lengthen. All resulting polyps are healthy and normal.

Hematoxylin and Eosin

A hematoxylin and eosin stain was performed on polyp sections and transforming animals to provide structural reference of the developing rhopalium and corresponding ocelli.

Stage 0. In longitudinal sections of the steady-state polyp, the polyp tentacles, hypostome, body column, and gastrovascular cavity are visible (Figure 18A). In addition, the two layers which make up the body are visible, consisting of the outer ectoderm and the inner endoderm, are separated by a gelatinous substance referred to as mesolgea (Figure 18B). The hypostome base is vertically aligned parallel with the body column.

Stage 1. In Stage 1 sections, the fusion of tentacles can be seen (Figures 18C, D) and the early stages of the in-folding cuff (which will result in the development of the medusa bell) is also visible as the base of the hypostome is now set inward approximately 75 μm relative to the body column surface. Concentrations of darkly-stained spherical nuclei approximately 3 μm in diameter can be seen only within the ectoderm of the fused tentacles with the higher and thicker concentrations in the region where the ocelli will develop (Figures 18C, D). The thickness of the region of nuclei below the surface, which corresponds to the thickness of the ectoderm, is roughly 12 μm below the majority of the rhopalial surface. The thickness of the nuclei below the surface on which the eyes/ocelli will develop ranges in thickness from a depth of roughly 18 μm along the surface of the

developing rhopalium to a shallower depth of roughly 12 µm closest to the point of attachment of the polyp body and tentacles. The staining in this region appears darker due to the increased number of nuclei (Figures 18C, D) but no organization of these cells which would indicate eye formation is visible at this stage.

Stage 2. In Stage 2, the base of the hypostome remains inset approximately 75 µm from the body column surface. The eyes/ocelli are developing on the surface of the fused tentacles which face towards the extended hypostome (Figure 19A). The cup-shaped primordium of both complex eyes is visible along with the initial pigmented eyespot of the small complex eye (which defines Stage 2) which is located approximately12 µm below the rhopalial surface (Figure 19B). The location and appearance of this pigment is similar to that seen during brightfield examination of whole rhopalia. The cup-shaped primordium of the large lensed eye and the pigment of the small complex eye are encircled by darkly-stained nuclei that appear slightly longer than the surrounding nuclei which remain roughly 3 µm in diameter (Figure 19B). Based on the close association with the developing eyes and pigment of the small complex eye, these nuclei are presumed to be photoreceptor nuclei and are roughly 4-6 µm in length and 3 µm wide. The region of photoreceptor nuclei surrounding the upper region of the large complex eye (closest to the small complex eye) is separated from the photoreceptor nuclei of the lower region of the small complex eye by a thin and lightly stained region roughly 3 µm wide (Figure 19B) which most likely corresponds to the neural region located below the tapered base of the photoreceptors.

Stage 3. In Stage 3, the in-folding of the cuff has progressed to a depth of approximately 125 µm below the point of attachment of the rhopalia to the body column and the ocelli continue to develop on the surface of the fused tentacles (Figure 19C). The developing velarium, which is a thin circular shelf of muscle that sits along the bottom margin of the bell and aids in directional swimming (Gladfelter, 1973; Satterlie et al., 2005) can now be distinguished. The retinal pigment of the complex eyes and simple ocelli are now clearly visible and is encircled by photoreceptor nuclei that are roughly 6 µm long and approximately 3 µm wide (Figure 19D). The region of nuclear staining

surrounding each of the six ocelli, which spans outward from the outer edge of the pigment, remains at an approximate width of 6-12 µm through the end of transformation. The developing lens of the large complex eye stained lighter than the surrounding cells and no nuclei are visible within the lens, which is located within the opening of the retinal cup (Figure 19D). A sheet of overlying cells (which was seen in the SEM results) is attached to the forming lens of the large complex eye and appears to fold into the opening of the retinal cup; this sheet of cells is roughly 20 µm thick, although at this point (Stage 3) it is difficult to differentiate between the cells at the periphery of the lens and the cells making up the overlying sheet. The topmost region of the developing pigment cup (closest to the point of attachment to the polyp body) reaches close to the surface of the rhopalium while the bottommost portion (closest to the statocyst) ends just underneath the sheet of cells and developing lens, roughly 20 µm below the surface of the sheet of cells (Figure 19D). The pigment has a much more defined boundary along the inner periphery of the cup (which encircles the lens) while the outer circumference has many outward wisps of migrating pigment granules. The upper region of the photoreceptor cells (which spans from the middle pigmented portion to just below the lens) cannot yet be easily discerned in the large complex eye, but the distance from the bottom of the lens (which rests in the opening of the pigment cup) to the pigmented cup is approximately 10 µm. The region of photoreceptor nuclei surrounding each eye/ocellus is separated from the photoreceptor nuclei of the adjacent eyes/ocelli by a thin and lightly stained region roughly 5 µm wide; this width of separation remains through the end of transformation and corresponds to the neural region which can be found just below the tapered photoreceptor bases.

Stage 4. In Stage 4, the in-folding of the cuff is very deep, approximately 275 µm below the point of rhopalial attachment to the body column, and partial sections of withdrawn medusa tentacles can be seen resting inside the forming bell (Figure 20A). The rhopalia now resemble miniature versions of the adult visual structures and the forming lenses of the complex eyes are easily distinguished (Figure 20B). The lens of the large complex eye now sits within the retinal cup just below the cup opening. The overlying sheet of cells, which appears to eventually form the cornea,

attached to the developing lens is now approximately 6 μm thick and easily differentiated from the lens. The length of the upper portions of the photoreceptors (which span from the pigmented cup to just below the lens) making up the large complex eye remains roughly 10 μm. Photoreceptor nuclei, which remain roughly 6 μm in length and 3 μm in width, can be seen around the periphery of each eye/ocellus (Figure 20B). The width of the light-staining region separating the photoreceptor nuclei of each eye/ocellus from the photoreceptor nuclei of the surrounding eye/ocelli remains approximately 5 μm (Figure 20B). The dark-staining nuclei that are not associated with the complex eyes or simple ocelli, remain at a diameter of approximately 3 μm and span a depth of roughly 20 μm from the rhopalial surface inward. These spherical nuclei are not found in most of the interior region surrounding the gastric cavity extension. The photoreceptor nuclei at the back of the large complex eye rest against the edge of the gastric cavity and span a depth of roughly 10 μm from the edge of the retinal pigment to the cavity. Also by Stage 4, the three regions of the photoreceptors can easily be distinguished in rhopalial cross sections: the apical light-receptive portion of the photoreceptors stains very lightly and is located just behind the lens, the pigment granules can be found in the middle region of the photoreceptor cells and make up the pigmented cup, and the basal region of the photoreceptor cells located within the outer perimeter of the eye contain the nucleus of the cell (see Stage 7 below for a figure reference).

Stage 5. In Stage 5, the bell is nearly fully-formed and the invagination of the cuff is complete and nearly reaches the boundary between the developing bell and the remnant polyp body (Figure 20C). The overlying sheet of corneal cells attached to the developing lens of the large complex eye is now approximately 5 μm thick. The length of the apical light-receptive portions of the photoreceptors (which span from the pigmented cup to just below the lens) remains roughly 10 μm. The width of the light-staining region separating the photoreceptors of each eye/ocellus from the photoreceptors of the surrounding eye/ocelli remains approximately 5 μm (Figure 20D). The darkly-stained photoreceptor nuclei remain at a length of roughly 6 μm and width of 3 μm while the nuclei that are not associated with the complex eyes or simple ocelli remain at a diameter of approximately 3

μm and span a depth of roughly 20 μm from the rhopalial surface inward (Figure 20D). The photoreceptor nuclei spanning from the back of the large complex eye rest against the edge of the gastric cavity and still span a depth of roughly 10 μm from the edge of the retinal pigment to the cavity (Figure 20D).

Stage 7. By the end of transformation, most measurements remain the same from Stage 5 including the length of the apical light-receptive portions of the photoreceptors of the large complex eye (10 μm), the width of the light-stained region separating the photoreceptor nuclei of the eyes/ocelli from the photoreceptor nuclei of the adjacent eye/ocelli (5 μm), the size of the photoreceptor nuclei (6 μm long and 3 μm wide) and nuclei not associated with the eyes/ocelli (3 μm in diameter), the span of the nuclei not associated with the eyes/ocelli from the surface of the rhopalium inward (20 μm), and the span of photoreceptor nuclei located between the back of the large complex eye and the edge of the gastric cavity (10 μm; Figure 21A). The thickness of the sheet of cells overlying the lens of the large complex eye has thinned to approximately 3 μm and is forming the cornea (Figure 21B). The non-ocular nuclei are still not found in close association with the gastrovascular cavity and are confined to a 20 μm depth below the rhopalial surface (Figure 21A). As was seen by Stage 4, all three regions of the photoreceptor cells are distinguishable including the apical light-receptive region, the middle pigmented region, and the basal nuclear region (Figure 21B). A group of cells, which can be seen beginning in Stage 4, at the apex of the rhopalium (above the small complex eye), stains much lighter than the surrounding cells, and although the nuclei within this group of cells are the same size (approximately 3 μm in diameter) as surrounding nuclei, they are much more sparsely distributed (Figure 21C).

Pigment Identification and Development

The Fontana-Masson staining and bleaching procedures reveal the pigment in the ocelli of *Carybdea marsupialis* to be melanin. This pigment is made up of melanin-containing granules, which are brown to black in color, that are within the middle regions of the photoreceptor cells making up the retinas of the complex eyes and simple ocelli. These results coupled with brightfield observations

of whole rhopalia during transformation as well as the Hematoxylin and Eosin (H & E) results clarify the process of pigment appearance and progressive expansion.

Adult rhopalia. In adult rhopalia, the pigment granules contained within the photoreceptors, which make up the retina, comprise the pigment cups of each complex eye and ocellus. The diameter of the pigment cup of the large complex eye in an adult rhopalium is roughly 350μm with a thickness of roughly 25μm (Figures 22A, B, C); the length of the pigment cup of the small complex eye is roughly 250μm with a height of approximately 100μm (Figure 22D); the length and height of the pigment of the slit ocelli is roughly 200μm and 40μm, respectively (Figure 23A); and the diameter of the pigment cup of the pit ocellus is roughly 100μm (Figure 23B). The morphology of the pigment cups consists of a relatively smooth interior edge (closest to the lens in the complex eyes and closest to the center of the ocellus in the pit and slit ocelli) compared to a much rougher periphery (Figures 22, 23). This rough edge resembles a sunburst pattern of fainter pigment radiating outward (away from the center of the eye/ocellus) from the main pigment cup. These finger-like extensions of pigment indicate the movement of melanin granules along the length of the photoreceptors, a characteristic which has been documented in adult photoreceptors (Martin, 2002, 2004). These granules are located in the central pigmented region of the photoreceptors which is below the apical light-receptive region and above the basal nuclear region (Figure 22C). Two different types of photoreceptors are distinguishable in the stained cross-sections, those which are stained lightly and those which have stained darkly (Figure 22C). A small vitreous space can also be seen separating the lens and surrounding retina in the large complex eye (Figure 22A). The depth of the pigment cup of the large complex eye (measured from the rhopalial surface inward) is roughly 200 μm in the top half of the cup (closest to the small complex eye) and roughly 100 μm in the bottom half of the cup (closest to the statocyst; Figure 22B). The back of the pigment cup in both complex eyes (located the farthest inward from the rhopalial surface) is slightly flattened (Figures 22 A, B, D) and closer to the surface of the rhopalium, the pigment cup of the large complex eye constricts inward towards the center of the eye and then has a gentle curve outward forming a somewhat tulip-shaped opening

(Figure 22A). The pigment cup of the small complex eye reaches a depth of roughly 175 μm and is more rectangular in shape (Figure 22D).

Stage 0 and Stage 1. No pigment appears until Stage 2 therefore no animals prior to Stage 2 are subjected to the staining procedure.

Stage 2. The first pigment appears during Stage 2 of transformation, following the fusion of the polyp tentacle bases and corresponds with the initial eyespot appearance seen in the staging results. Appearing as a small, concentrated, circular-to-linearly shaped spot approximately 15 μm wide, the initial pigment is located in the central region of the developing rhopalial face, at a depth of approximately 12 μm below the surface (Figures 7A, B, 24A). The location and appearance of the initial pigment in the melanin-stained slides and brightfield images of whole rhopalia corresponds to that which was seen in the H & E sections. The circular-to-linearly shaped pigment then stretches out laterally to form a semicircle roughly 20 μm in length which faces upward towards the fused tentacle bases. This semicircle increases in length to roughly 25 μm and becomes more flattened in shape by the end of Stage 2 (Figure 7A). The pigment making up this changing band appears in a sunburst pattern, radiating outward from the center with the greatest pigment concentrations along the lateral axis and sparser pigment along the top and bottom edges of the pigment band. The top edge of the pigment band is more clearly linear than the bottom as was seen in adult eyes. The initial upward-facing semicircle of pigment represents the early appearance of the small lensed eye. The early appearance of the large complex eye can be seen in conjunction with the emergence of the small complex eye pigment as a concave cup-shaped primordium located just below the small complex eye (Figures 7B, 24A). By the time the pigment of the small complex eye is readily visible, very faint pigment can be visualized along the upper half of the circular cup-shaped primordium of the large complex eye (closest to the small complex eye; Figure 7B); by the end of Stage 2, this pigment has increased but is still localized to the upper half of the cup-shaped primordium of the large complex eye (Figure 7C).

Stage 3. By Stage 3, the faint pigment seen along the upper half of the cup-shaped primordium (closest to the small complex eye) of the large complex eye has progressed to form a spherical pigment cup roughly 40-50 μm in diameter. The upper half of the pigment cup (closest to the small complex eye) is more concentrated than the lower half and both halves have a thick perimeter of fainter pigment radiating outward from the central heavily-pigmented cup (Figures 7D, 24B). By the end of Stage 3, this outer perimeter of fainter pigment does not stray as far from the central cup as was seen in the beginning of Stage 3 (Figure 7E). At this point in development, the perimeter of fainter pigment is most likely due to a combination of gradual photoreceptor maturation and the migration of the pigment granules within the photoreceptors. Within the forming cup, a more faintly pigmented region is visible where the lens has begun to develop (Figures 7D, E, 24B). In addition to the sunburst pattern of pigmentation, other characteristics which were seen in the H & E slides are also visible in the sections stained for melanin such as the up-folding sheet of cells in the large lensed eye which is attached to the developing lens. Due to the up-folding sheet of cells, the bottom portion of the pigment cup (closest to the forming statocyst) does not reach the rhopalial surface (Figure 24B). The depth of the pigment cup of the large complex eye, measured from the rhopalial surface inward, reaches approximately 25 μm and cross-sections of the retinal cup reveal a relative pigment thickness of 6 μm (Figure 24B). The pigment of the small complex eye has made an interesting development by Stage 3: it now appears as two separate upward-facing semicircular bands of pigment. These semicircles are initially very contracted, with an approximate diameter of 15μm each, and are slightly tilted in towards each other (Figure 7D). The bottom periphery of the bands (closest to the large complex eye) has diffuse pigment radiating outward but only a short distance from the band itself. The inner region between the two semicircular bands, which is roughly 15μm in length, has sporadic areas of pigment which stretch upward from within each semicircle (towards the point of connection with the polyp body) and inward towards the region separating the bands, occasionally connecting (Figure 7D). The two semicircles then flatten and lengthen to roughly 20μm each, gradually decreasing the empty area between them, now roughly 5μm, until by the end of Stage

3, they are connected in what once again appears as a single long pigment band approximately 50 µm in length and 20 µm in height (Figure 7E). The developing pigment cup of the small complex eye reaches an approximate depth of 20 µm although, as was seen in the initial appearance of the small complex eye pigment during Stage 2, the majority of the pigment is located approximately 10 µm below the surface of the rhopalium. Like the pigment of the large complex eye, the relative thickness of the developing pigment cup is approximately 6 µm (Figure 24B). Following the appearance of pigment in the small complex eye and large complex eye, the next photoreceptors to begin producing melanin pigment are those of the slit ocelli. This pigment is located within slit-shaped indentations found slightly below and on either side of the small complex eye (Figures 7D, E) and has a length of approximately 25 µm and a height of 13 µm; the greatest concentration of pigment is along the inner edges of the slit ocellus (closest to the large complex eye) and becomes more faint along its length (Figures 7D, E). At the beginning of Stage 3, very faint pigment can be seen along the inner edges of the pit ocellus (closest to the small complex eye; Figure 7D). By the middle of Stage 3, the pit ocelli appear as faint, circular blotches of pigment, approximately 14 µm in diameter, located on either side of the small complex eye (Figure 7E).

Stage 4. During Stage 4, the pigment cup of the large lensed eye has increased to a diameter of approximately 70 µm (Figures 7F, 24C), the pigment of the small lensed eye has increased and is now approximately 60 µm long and 25 µm tall (Figures 7F, 24C), the pigment of the slit ocelli has increased to a size of approximately 35 µm long and 20 µm tall (Figure 7F), and the pigment of the pit ocelli has increased to a diameter of approximately 20 µm (Figure 7F). By this point, very little pigment can be seen radiating outward from the more heavily pigmented central regions forming much smoother pigment boundaries (Figures 7F, 24C). As was seen in the H & E sections, the developing lens attached to the up-folding sheet of cells in the large complex eye is readily visible within the opening of the pigment cup (Figure 24C). Due to the overlying sheet of cells, the basal portion of the pigment cup (closest to the forming statocyst) still does not reach the rhopalial surface (Figure 24C). The depth of the forming pigment cup of the large complex eye, measured from the

rhopalial surface inward, now reaches a depth of approximately 50 µm while the forming pigment cup of the small complex eye now reaches a depth of approximately 45 µm and remains roughly 10 µm below the rhopalial surface. The relative thickness of the pigment cups of the complex eyes remains approximately 6 µm (Figure 24C).

Stage 5. In Stage 5, the pigment cup of the large complex eye has increased to a diameter of approximately 80 µm (Figures 13A, 24D), the pigment of the small complex eye has increased to a size of approximately 70 µm long and 30 µm tall, the pigment of the slit ocelli has increased to a size of approximately 45 µm long and 20 µm tall, and the pigment of the pit ocelli has increased to a diameter of approximately 22 µm. The depth of the forming pigment cup of the large complex eye, measured from the rhopalial surface inward, now reaches a depth of approximately 55 µm while the forming pigment cup of the small complex eye now reaches a depth of approximately 50 µm and remains roughly 10 µm below the rhopalial surface (Figure 13A). The relative thickness of the pigment cups of the complex eye remains approximately 6 µm (Figure 24D). As was seen in the H & E sections, the up-folding sheet of cells overlying the large complex eye and attached to the developing lens has thinned to a thickness of 3 µm (Figure 24D).

Stage 7. By the end of transformation, the pigment cup of the large complex eye has increased to a diameter of approximately 85 µm (Figures 13B, 24A, B), the pigment of the small complex eye remains at a length of approximately 70 µm and a height of 30 µm (Figure 13C), the pigment of the slit ocelli has increased to a size of approximately 55 µm long and 25 µm tall (Figure 13D), and the pigment of the pit ocelli has increased to a diameter of approximately 25 µm (Figure 13E). The depth of the forming pigment cup of the large complex eye, measured from the rhopalial surface inward, now reaches approximately 60 µm (Figures 13B, 25B) while the forming pigment cup of the small complex eye now reaches a depth of approximately 55 µm and is now roughly 6 µm below the rhopalial surface. The forming pigment cup of the large complex eye, when seen from a profile-view in whole rhopalia and in cross-sections, is tulip-shaped as, in coming closer to the front of the eye closest to the rhopalial surface, the cup tightens in and then flares outward slightly (Figure

13B). This is not seen in the forming pigment cup of the small complex eye. The relative thickness of the pigment cups of the complex eyes remains approximately 6 μm (Figure 25B). As could be seen in the H & E slides from Stage 4 onward, the faintly stained area with more sparsely-distributed nuclei at the top of the rhopalium is also visible from Stage 4 onwards in the melanin-stained slides (Figure 25A). Stage 7 controls, which were bleached of melanin prior to the Fontana-Masson staining procedure, show a clear decrease in melanin staining after being bleached for 20 minutes (Figure 25C) and a complete absence of melanin staining after being bleached for 30 minutes (Figure 25D), further confirming the presence of melanin as the retinal pigment.

UV Opsin-Like Staining

Adult rhopalia. In the small complex eye, all photoreceptors which stained positive for the UV (ultraviolet) opsin-like protein are localized to the central bottom portion of the retina (directly behind the small complex eye lens) and are not found along the sides of the eye (Figure 26A). These photoreceptors exhibit staining roughly 30-40 μm from the tapered base of the cell (located around the eye perimeter) to a brightly-stained rounded bulge located farther towards the center of the retina, giving the stained region a "lollypop" shape (Figure 26B). The tapered base of the photoreceptor (located along the perimeter of the small complex eye) has a width of roughly 1 μm but widens to roughly 3 μm just beneath the apical spherical bulge. This rounded tip ranges from spherical to oval in shape with an approximate length (parallel to the photoreceptor axis) of 8 μm and a width of 6 μm. The nuclei of the photoreceptor cells could not be visualized but are likely located within the brightly-stained rounded tip based on the typical photoreceptor cell structure, which places the nucleus just past the tapered region of the cell. The distinct edges of the stained spherical bulges indicate that these brightly-shaped structures represent the apical tip of the photoreceptor. The apical tips of the distal bulges of the photoreceptors have a rather rigid stopping point due to similar positioning within the retina and collectively form a very linear boundary (Figure 26B). The entire length of the photoreceptors appears to rest on top of the dark retinal pigment indicating that these cells represent a subset of photoreceptor cells that do not contain pigment and are located on top of other

photoreceptor cells that do (Figure 26A). Some unstained photoreceptor cells can be seen interspersed with cells which stained positive for the UV opsin-like protein (Figure 26B).

In the large complex eye, at least three types of photoreceptors can be seen which, unlike those which were positively stained in the small complex eye, encircle the entire retina: the first type resembles those found in the small complex eye and these appear isolated to the top-center region of the retina (closest to the small complex eye; Figures 26C, D). These photoreceptors have the same characteristic lollypop shape of the positively-stained photoreceptors found in the small complex eye. In addition to having a similar length of 30-40 µm, the tapered base, which is roughly 1 µm wide, widens to roughly 3 µm just beneath the brightly-stained round to oval-shaped bulge which is approximately 8 µm long and 6 µm wide. Unlike in the small complex eye, the collective tapered regions of the photoreceptors and corresponding tips do not line up with each other but instead form a more jagged boundary (Figures 26C, D). Approximately halfway down the sides of the retina, closest to the sides of the rhopalium, the photoreceptors change in appearance; intermingled with the bulbous and brightly stained photoreceptors are longer photoreceptors of a different shape (Figures 27A, B). These cells are much longer, stretching farther towards the center of the retina with an approximate staining length of 60-70 µm, and have a more slender spindle-like shape. The positively-stained tapered base, roughly 1 µm in width, stretches roughly 40-50 µm before gradually widening to a width of approximately 5 µm just below the location of a dark oval-shaped structure which corresponds in both size (approximately 6 µm long and 3 µm wide) and location to the nucleus of the positively-stained cell (Figure 27B). Shortly past the nucleus, the staining quickly fades having covered roughly two-thirds of the distance to the lens sitting at the center of the retina (Figures 27A, C). The termination of staining is not as abrupt as in the shorter positively-stained photoreceptors, indicating that only a portion of the photoreceptor cell stained and that the apical portion of the cell did not stain positive for the UV opsin-like protein (Figure 27C). The transition from the shorter photoreceptors found in the upper region of the large complex eye (closest to the small complex eye) to the longer photoreceptors found in the lower portion of the large complex eye is shown in Figures

28A and B. The third type of photoreceptor is the unstained photoreceptors seen interspersed with and beneath those staining positively for the UV opsin-like protein (Figure 27B). Controls of adult rhopalia, which were not exposed to the primary antibody targeting the UV opsin-like protein, show no staining (Figure 28C).

Stage 0, Stage 1, and Stage 2. As photoreceptors are not found in the eyeless steady-state polyp (Stage 0), no animals at this stage are subjected to the procedure which tests for the presence of the UV opsin-like protein within photoreceptor cells. No Stage 1 animals are tested due to the difficulty of isolating individual forming rhopalia. The first stage that is tested for the presence of photoreceptors exhibiting opsin-like properties is Stage 2 which stains negative for the presence of UV opsin-like protein (Figure 29A).

Stage 3. UV opsin-like staining is first seen early during Stage 3 in association with only the small complex eye (Figures 29B, C). Brightly-stained photoreceptor cells can be seen directly along the lower perimeter of the central pigmented portion of the forming small complex eye (closest to the large complex eye). The staining within these cells is rectangular in shape with a length of approximately 10 μm (parallel to the long axis of the rhopalium) and a width of 6 μm. Occasional brightly-stained photoreceptor bases are visible. Staining within cells closer to the periphery of the forming retina is more diffuse and not as bright (Figures 29B, C) By the end of Stage 3, sporadic cells in the large complex eye begin to exhibit very faint and diffuse staining resembling wisps radiating outward from the perimeter of the forming pigment cup. The staining within these cells has a length of roughly 15 μm and a width of 3 μm (Figure 29D). No staining is seen in Stage 3 controls that are not subjected to the primary antibody targeting the UV opsin-like protein (Figure 29E).

Stage 4. In the rhopalium of a Stage 4 specimen, the photoreceptors continue to form and staining is brighter and more expansive in the photoreceptors of both complex eyes (Figure 30A, B). The staining of the UV opsin-like protein found in the photoreceptors of the small complex eye remains much brighter than that within the photoreceptors of the large complex eye (Figure 30B). As during initial formation in Stage 3, the cells located along the lower perimeter of the central

pigmented portion of the forming small complex eye are much brighter than those farther to the sides. The cells still have a rectangular shape, remaining at a width of approximately 6 μm, although the base of staining within the cells (closest to the large complex eye) is now tapered to a narrow 1 μm in width which originates in the thin region between the complex eyes (Figure 30B). By this stage, staining is visible interspersed within the band of pigment as well as along the upper perimeter of the pigment cup (closest to the top of the rhopalium just below the small complex eye lens) resulting in a staining length of roughly 30 μm (Figure 30B). This indicates that these photoreceptors, which do not appear to contain any pigment, thread in among the pigmented photoreceptors. In the large complex eye, numerous positively stained photoreceptors are now visible in the forming retina (Figure 30C). These photoreceptors appear much more slender in shape and do not stain as brightly as those seen in the forming small complex eye. The width of staining within positively-stained photoreceptors of the large complex is approximately 4 μm and the length of staining is roughly 20-25 μm which gradually becomes fainter at the distal end (located farthest from the tapered base of the cell). All staining is located closer to the outside of the retina (located farthest from the central developing lens), indicating that only the lower portions of the photoreceptors contain the UV opsin-like protein. Some tapered bases, which are roughly 1 μm wide, are visible but do not stain as brightly as those of the small complex eye photoreceptors. All positively-stained photoreceptors in the large complex eye are morphologically identical and appear to rest on top of the retinal pigment, indicating that no pigment is contained within these cells (Figure 30C). In both complex eyes, other photoreceptors are visible which did not stain positive for the presence of UV opsin-like protein. No staining is seen in Stage 4 controls that are not subjected to the primary antibody targeting the UV opsin-like protein (Figure 30D).

Stage 5. During Stage 5, the number of photoreceptors has increased for both complex ocelli with a corresponding increase in the brightness of staining for the UV opsin-like protein (Figure 31A). As in previous stages, the staining within the photoreceptors of the small complex eye is brighter than that seen in the photoreceptors of the large complex eye. The positively-stained

photoreceptors in the small complex eye, which now span almost the complete length (parallel to the horizontal axis of the rhopalium) of the pigment cup, have begun to take on a more slender shape as they remain at a staining length of approximately 30 μm but with a slightly smaller width of 4-5 μm (Figure 31B). Unlike in Stage 4, the staining does not stretch all the way to just below the lens of the small complex eye, but appears to taper off roughly midway across the retinal pigment; this most likely corresponds to the increase in height of the pigment band (Figure 31B). The staining within photoreceptors of the large complex eye, spanning from the now easily seen tapered bases (which remain at a width of roughly 1 μm) at the periphery of the retina in toward the central forming lens, now has a length of approximately 30-35 μm and a width of approximately 3 μm, which gives the photoreceptor an even more slender shape (Figure 31C). As in Stage 4, these positively-stained photoreceptors still appear to be located on top of the retinal pigment. More positively-stained photoreceptors can be seen in the lower half of the large complex eye (closest to the bottom of the rhopalium) than in the top half and appear brighter. In this lower region, a new pattern has begun to take shape where photoreceptors in the central lower portion, the region of the aforementioned up-folding sheet of cells, appear to be intertwined with one another, both positively stained and unstained, giving the region a "checkered" appearance (Figure 31D). 3D imaging indicates that the photoreceptors for both complex eyes are now arranged in multiple layers, though still located close to the surface. No staining is seen in Stage 5 controls that are not subjected to the primary antibody targeting the UV opsin-like protein (Figure 31E).

Stage 7. By the end of transformation, the number of photoreceptors in both complex eyes have increased, although all positively-stained photoreceptors in the small complex eye are still confined to being found along the length of the pigment cup, directly behind the forming lens, and are not located elsewhere in the eye (Figure 32A). The photoreceptors continue to maintain a relatively rectangular shape with the basal end being tapered with a width of roughly 1 μm and the rest of the staining exhibiting a width of 3-5 μm. The length of staining has increased to approximately 30-40 μm (Figure 32B). The bulk of the staining length of the photoreceptors is located just below the

retinal pigment (closest to the large complex eye) and, although some staining is still visible in the retinal pigment region of the eye, this portion of the photoreceptors now appears to rest on top of the pigment as opposed to threading in among the pigmented photoreceptors as was seen in earlier stages. Some unstained photoreceptors are still visible interspersed with the positively-stained ones (Figure 32B). Staining within the photoreceptors of the large complex eye also exhibits a length of approximately 30-40 μm and remains at a slender width of approximately 3 μm. Controls of Stage 7, which are not subjected to the primary antibody targeting the UV opsin-like protein, show no staining (Figure 32D) and at no point during transformation are any photoreceptors within the simple ocelli positively stained (Figure 32E).

J1-Crystallin Staining

Adult rhopalia. The spherical lens of the large complex eye sits within the concave retina. The spherical lens of the small complex eye also sits in the opening of the retinal cup but protrudes much farther than the lens of the large complex eye. Both lenses have a rough diameter of 150μm. The center of the large complex lens has more globular cells, which range in shape from spherical to cuboidal with a diameter of roughly 15-20μm, while the outer portion is made up of stacks of fibrous cells (Figure 33A). In the small complex eye lens, the globular cells, which also have a rough diameter of 15-20μm but are more spherical in shape than those found in the large complex eye, are found along the outer third of the lens in the region which rests within the pigment cup opening. The fibrous cells taper and angle inward towards the portion of the lens which is farthest from the pigment cup closest to the top of the rhopalium (Figure 33B); this congregation of the fibrous cells indicates a point of origin from which the cells spread outward. Staining for the J1-crystallin protein in adult lenses indicates that staining is restricted to the fibrous cells. Staining seen on the surface of the lenses reflects the fibrous nature of the cells which run along the outer perimeter (Figures 33C, D). No staining was seen in controls of adult complex eye lenses which were not subjected to the primary antibody (Figures 33A, B). Lenses which were cut in half prior to staining clearly show that only the outer-fibrous portions of the lenses are positively stained for J1 crystallin and the globular regions

exhibit little to no staining (Figure 34A). In large lenses which have been cut in half, the underside portion of the lens (which rests within the retinal cup) exhibits brighter staining than in the portion which protrudes out of the cup. Like the lens of the small complex eye, the large lens also has an apparent point of origin from which all cells spread outward; for the large lens, this point appears to be located on the underside of the lens, which faces inward towards the inside of the retinal cup, with both the central globular cells splaying towards the center and the fibrous cells spreading out around the outer perimeter of the lens (Figure 34A). Just above the lens of the small complex eye, a few bright spots of punctate staining are visible within the down-folding sheet of cells along with very faint staining across the entire surface of the sheet of cells (Figure 34B); no other extraocular staining is visible in adult rhopalia (Figure 34C).

In the slit ocelli, the brightest staining can be seen running linearly along the top inner edge of the pigment cup (Figure 35A); the top edges of these cells rest perpendicular to the surface of the upper half of the ocellus (Figure 35B). Faint and diffuse staining can be seen in the lens-like material on the surface of the photoreceptor cells in a pattern which reflects the bumpy surface which is visible under scanning electron microscopy (Figure 35C). Immunopositive staining was also seen in the pit ocelli of adult rhopalia. Appearing within the confines of the dimple-shaped pigment cup, the staining is very punctate and is organized into thin linear strands which clump together (Figures 36A, B). No staining was seen in controls of the simple ocelli which were not subjected to the primary antibody targeting the J1-crystallin protein (Figure 36C). Often, spherical patches of pigment can be found between the pit and slit ocelli and can range in size from a very sparsely pigmented region roughly 25μm in diameter (Figure 37A) to a heavily pigmented cup roughly 50μm in diameter (Figure 37C). These structures are most often unpaired (only one structure is seen per rhopalium) and are located closer to the slit ocellus than to the pit ocellus. Although only in the larger structures is the presence of lens-like material visible under brightfield examination of whole rhopalia (Figure 37C), staining for J1-crystallin is seen in both types of structures and appears as a spherical area of even, diffuse staining located in the center of the pigmented area (Figures 37B, D). No staining is seen in controls

of the structure that are not subjected to the primary antibody targeting the J1-crystallin protein (Figure 36C).

Stage 0, Stage 1, and Stage 2. Individual developing rhopalia were first isolated from Stage 2 animals, as rhopalia from Stage 1 animals are too difficult to separate. During Stage 2, only the pigment of the early-forming small lensed eye is visible with no evidence of lens formation. Evenly distributed punctate staining for J1-crystallin was seen across the entire rhopalial surface (Figure 38A) and, due to its location relative to the ectodermal cells, the staining appears to be confined to the outer cellular membranes (Figure 38B) and does not penetrate very deep below the surface of the rhopalium. No staining is seen in Stage 2 controls that are not subjected to the primary antibody targeting the J1-crystallin protein (Figure 38C).

Stage 3. During Stage 3, the area of the forming lens of the large complex eye begins to exhibit faint diffuse staining both within the up-folding sheet of cells and below, within the developing retinal cup where the lens is beginning to form (Figures 39A, B). At this point, the lens is roughly 15μm in diameter. In addition, an increased amount of the punctate staining across the rhopalial surface can be seen within the up-folding sheet of cells of the forming large complex eye (Figure 39B). A subsurface spherical clump of globular cells can be seen in the location of the future lens of the small complex eye despite the absence of lens-specific staining for the J1-crystallin protein (Figure 39C). Other than the prolific surface staining, no staining is visible in the slit ocelli or the pit ocelli. No staining is seen in Stage 3 controls that are not subjected to the primary antibody targeting the J1-crystallin protein (Figure 39D).

Stage 4. During Stage 4, there is more of the punctate staining on the surface of and within the up-folding sheet of cells in the lower half (closest to the bottom of the rhopalium) of the forming large complex eye than in the top half (closest to the small complex eye; Figures 40A, B). The diffuse staining is visible across the surface of the developing lens but does not appear to penetrate within the forming structure. The lens is roughly 30μm in diameter. The small complex eye now shows similar characteristics to the large complex eye in that there is a greater concentration of the punctate surface

staining within the down-folding sheet of cells and that faint diffuse staining is now seen within the sheet of cells and below it in the area of the developing lens (Figures 40A, C). The staining of the small complex eye appears brighter than in the large complex eye. As in the large complex eye, the diffuse staining of the small complex eye is only seen along the surface of the forming lens and does not appear to penetrate very far within the structure. The lens of the small complex eye is roughly 25μm in diameter. By this stage, it is evident that the majority of staining is becoming restricted to the area of lens formation and the extralenticular staining becomes less pronounced. During Stage 4, staining also begins to be seen in the slit ocelli and appears as a diffuse outline of the photoreceptor cells in the center of the ocellus indicating the early formations of the lens-like material positioned on the cells' surfaces. (Figure 40D). Roughly three to five stained cells are visible. As in earlier stages, the punctate surface staining does not penetrate to the interior regions of the rhopalium except for within a cluster of cells found above the small complex eye at the top of the rhopalium (Figure 40E); here, the staining appears very bright and spans the depth of the rhopalium from front to back across the top-central region of the rhopalium. The base of the sheet of cells covering the developing small complex lens appears to feed into this cluster. No staining is visible within the developing pit ocelli and no staining is seen in Stage 4 controls that are not subjected to the primary antibody targeting the J1-crystallin protein (Figure 40F).

Stage 5. By Stage 5, the diffuse staining on the surface of the large and small complex eye lenses has increased in brightness and appears to penetrate farther within the forming lenses (Figures 41A, B, C). The size of the lenses of the large and small complex eyes is roughly 37μm and 27μm, respectively. More of the punctate surface staining can be seen in the lower portion of the large lensed eye (closest to the bottom of the rhopalium) than in the top half (closest to the small complex eye; Figures 41A, B). The staining in the slit ocelli has made a marked progression: the surfaces of the photoreceptor cells in the center of the ocellus are still only stained along the surface, but the brightness of the staining has increased as well as the number of stained cells, which is now roughly ten (Figure 41D). The brightly stained region spanning the top of the rhopalium, just above the small

complex eye, has not changed in appearance (Figure 41E) and no staining is visible in the developing pit ocelli. No staining is seen in Stage 5 controls that are not subjected to the primary antibody targeting the J1-crystallin protein (Figure 41F).

Stage 7. By the end of transformation, the diffuse staining in both the large and small complex eye lenses and in the lens-like material of the slit ocelli has continued to increase in brightness and, in the case of the complex eye lenses, in depth to slightly beneath the surface of the lens (Figure 42A). The size of the lenses of the large and small complex eyes is now roughly 40μm and 30μm, respectively. As in previous stages, the amount of the punctate surface staining is greater in the bottom half of the large lensed eye (closest to the basal statocyst) than in the top half (closest to the small complex eye; Figures 42A, B). Staining in the small lensed eye still appears brighter than in the large lensed eye (Figures 42A, C). The number of slit ocelli photoreceptor cells staining positive for the presence of J1-crystallin in the lens-like material covering their surface has increased to roughly 12-15 (Figure 42D). The bright patch of cells found just above the lens of the small complex eye at the top of the rhopalium has not changed in appearance (Figure 42E). As in earlier stages, no staining is seen in the forming pit ocelli and no staining is seen in Stage 7 controls that are not subjected to the primary antibody targeting the J1-crystallin protein (Figure 42F).

The comparison of the staining seen in the final stage of transformation (Stage 7) and in adult rhopalia shows a dramatic change between metamorphosis and adulthood in the localization of the crystallin protein, which goes from being found across the entire rhopalial surface (e.g., Figure 38A) to being almost exclusively confined to the lens in adults (Figure 34B).

FMRFamide Staining

Stage 0. FMRFamide-positive nerves are found throughout the body of the steady-state polyp ranging from the hypostome mouth opening to the foot connecting the animal to the substrate (Figure 43A). All positively-stained nerves appear to be restricted to the ectoderm with neuronal processes primarily oriented parallel with the body column with the exception of a circular nerve ring which is roughly 6 μm thick and is found near the tentacular region below the hypostome (Figures 43A, B).

The long neurites found along the body column often stretch the length of the animal and are roughly 1-3 μm in width. The grouping of these neurites often leaves unstained spaces around the circumference of the body column (Figures 43A, B). These neurites differ in complexity and structure in the upper body column versus in the stalk; this difference is more easily defined in polyps that are undergoing asexual reproduction and have a new polyp budding off of the body column or in polyps that have recently lost a bud (Figure 44A). Above the point of bud emergence, in the upper body column, the FMRFamide-positive nerves are more abundant and interconnected with thicker, more punctate neurites (defined by groups of neuropeptide vesicles and perikarya) and numerous laterally branching processes connecting the adjacent neurites (Figure 44B). Below the point of bud emergence, the positively-stained neurites are less abundant and simpler with thinner, smoother (having fewer vesicles and perikarya), and with few branching processes connecting the adjacent neurites (Figure 44C). The spherical neuropeptide vesicles found along the lengths of the neurites have a diameter of 1-2 μm and, in general, the thinner neurites have a greater number of vesicles. No nerve ring is visible at the base of the foot, instead the number of processes tapers down the length of the stalk.

There are three types of neural cells found within the body column. First, two types of ganglion cells make up the long neurites spanning the length of the body column including multipolar (Figure 45A) and bipolar (Figure 45B) nerves. A greater proportion of multipolar cells are found in the upper body column than in the stalk region, which consists primarily of bipolar nerve cells. The perikarya of the ganglion cells, both bipolar and multipolar, range in size from roughly 3-6 μm in diameter and are spherical to oval in shape. Most multipolar nerves that were observed have three processes originating from the cell body (Figure 45A). Second, the surface of the upper body column has numerous sensory neurons that feed down into subsurface processes (Figure 45C). These sensory neurons, which appear to be unipolar and are responsible for relaying external stimuli to the ganglion cells located deeper beneath the ectoderm surface (Hadži, 1909; Schneider, 1890), have a cell body approximately 12 μm in length and 6 μm in width. The single neurite connecting the sensory neuron

body to a ganglion cell, which is located deeper underneath the surface of the ectoderm, is roughly 30 μm in length (Figure 45D). The nerves can become more difficult to visualize in the upper body column primarily due to the increase in concentration of both small nematocytes (stinging cells), found just below the ectoderm surface, and also to the large nematocytes, which are usually slightly deeper. The small nematocytes found throughout the body column are also found in the greatest concentration across the entire hypostome surface, thereby greatly decreasing the ability to discern the numerous linear processes which run from the base of the hypostome up to the oral opening. Many of these hypostome processes are continuous with those running down the body column. An oral nerve ring encircling the mouth opening is not visible, instead a cluster of sensory neurons line the oral opening (Figures 45E, F).

The tentacular nerves consist of a mix of both thick and thin processes running the length of the tentacles (Figures 46A, B), many of which are continuous into the body column. As in the neurites running the length of the body column, these processes range in width from roughly 1-3 μm and the thinner neurites tend to be more heavily vesiculated (Figure 46B). All of the tentacular neurites have bipolar cell bodies and neuropeptide vesicles located along their lengths (Figure 46B) with multipolar neuron bodies located in the apical section of the tentacle (Figure 46A). Usually branching off from these multipolar bodies is a sensory neuron whose cell body has the same dimensions as the sensory neurons seen along the body column (Figure 46C). Some of the multipolar cell bodies are larger, approximately 10 μm in diameter, and could be mistaken for sensory neuron bodies if not for appearing to have more than one neurite extension. Processes originating from the apical multipolar cells bodies connect to other nearby multipolar neurons, which results in a nerve net in the apical half of the tentacle (Figures 46A, E). The processes making up this nerve net are very thin, having a width of roughly 1 μm, are heavily vesiculated, and are primarily oriented perpendicular to the tentacle length. Due to the similar sizing of the neuropeptide vesicles found along the lengths of the neurites, both those along the body column and along the length of the tentacles, and the perikarya, it is often difficult to distinguish potential bipolar neurons from vesicles.

Above the region where the sensory neurons are found, closest to the tip of the tentacles, are structures at the surface of each tentacle that are highly immunoreactive. These spherical structures resemble stemmed cherries and appear to have a cell body that is approximately 3 μm in diameter with a single extension into the external environment that is 1-2 μm wide and roughly 10 μm long (Figure 46D). Despite not resembling the location, size, or shape of other sensory neurons found throughout the body, the absence of a nematocyst capsule indicates that these structures are sensory neurons and not nematocytes.

Stage 1. Once the tentacles have rearranged to form four tentacle groups, signifying Stage 1 of transformation, the individual tentacle nerves still resemble those of steady-state polyps. The grouping of the tentacles does, however, cause an apparent shift in nerves running from the tentacles down into the body column as nerves that were once vertically continuous from the length of the tentacle into the body column take on a more angled shape. As the tentacles group together and begin to fuse at their bases, the tentacles at the edges of the bunch move from being parallel with the body column to bending slightly outward due to the constricting group of bases. As the nerves remain parallel with the tentacles, they too appear more angled in relation to the body column. Upon reaching the fusing bases, the neurites are once again parallel with the body column and then spread out as the constrictions of the columnar base widen when fusing with the body column (Figure 47A). Also during this stage, it begins to become difficult to visualize nerves in the upper body column, in the area where the bell will begin to develop, as they do not appear as bright and take on a more diffuse appearance (Figure 47B).

Stage 2. In Stage 2, the immunoreactive nerves in the apical unfused sections of the polyp tentacles continue to resemble those seen in the steady-state polyp, as the tentacles begin to be reabsorbed and begin to shorten. Within the fused tentacle base, the neurites are grouped even more closely together than in Stage 1. The nerves continue to be difficult to visualize in the upper body column.

Stage 3. From the merging of the tentacles to the end of Stage 3 (when all six eye spots are present and polyp tentacles continue to recede), the apical sections of unfused tentacles continue to resemble those seen in a steady-state polyp. More of the interconnected apical nerve net appears to comprise the length of the tentacles due to their continued reabsorption. The linear neurites flowing from the remaining tentacles, through the fused columnar base and into the body column show no change in appearance from Stage 2, although the progression of the nerves from the fused base into the body column becomes more difficult to visualize as the cuff of cells begins to fold up around the tentacle bases (Figure 48). Also, the sensory neurons which were previously found in the apical region of the tentacles in previous stages are now located closer to the fused tentacle bases and those which are within the tentacles stretching out perpendicular to the body column are also perpendicular to the body column (Figure 48).

Stage 4, Stage 5, and Stage 7. The immunoreactive nerves and their arrangement in the forming rhopalia are very similar from Stage 4 until the end of transformation and will therefore be described collectively. When the bell begins to take obvious shape during Stage 4, fewer neurites can be seen in the upper body column. Often, the difference in the number of neurites seen on either side of the junction of the developing bell and remaining polyp body is substantial, especially by Stage 5 (Figure 49A). At this point, very few neurites can still be seen crossing from the polyp body into the bell as the developing medusa prepares to detach; FMRFamide-immunoreactive neurites observed within the bell are often completely isolated to the areas within and proximal to the emerging nematocyte batteries. By Stage 4 and through the end of transformation, nerves show a more complex arrangement in the developing rhopalia. The brightest-staining nerves can be seen on the back of the rhopalium, where the stalk originates. Beginning along the top edge of the statocyst, which is encircled by bipolar nerve bodies and neurites with the brightest nerves along the backside edge of the structure (Figure 49B), this collection of ganglion nerves spans slightly above the statocyst in the region between the statocyst and stalk origin and consists of numerous intertwined neurites which are primarily oriented perpendicular to the rhopalial length with some fainter central neurites oriented

parallel with the rhopalial length (Figure 49C). Often seen running back and up from the thick and brightly stained region of nerves encircling the base of the statocyst on the backside of the rhopalium are thin neurite extensions (roughly 13 μm in length and 1 μm thick) that each connect to one of several positively-stained oval shaped structures, resembling the sensory neurons seen in the tentacles of steady-state and regressing polyp tentacles; these structures have a length of roughly 10-12 μm and a width of roughly 6 μm (Figure 49B). Brightly-stained spherical structures can also often be seen just below the rhopalial surface at either end of the nerves spanning across the back of the rhopalium (perpendicular to the rhopalial length) in a paired symmetrical fashion (Figure 49C), although these are more brightly-stained and more spherical in shape with a small diameter of roughly 6 μm. Occasionally, some thin neurites can be seen stretching down across the surface of the statocyst.

Due to the sheer number of perikarya and intertwining of the neurites, it is difficult to isolate individual multipolar neurons but bipolar neurons are visible and most identifiable perikarya have a diameter of roughly 3 μm. An exception to this is found in occasional larger multipolar ganglion nerves which are roughly 9 μm in diameter and are found in close proximity to where the stalk enters the rhopalial body; these large cells have approximately five processes which are roughly 1-2 μm wide (Figure 50A). Neurites branching off of the central nerves on the backside of the rhopalium curve outward around the sides of the gastric cavity extension and then curve upward resulting in a group of neurites which are predominantly parallel with the rhopalial length oriented behind and in closer contact with the simple ocelli, particularly the pit ocelli (Figures 50C, 51A). Another group of brightly stained interconnected neurites can be found spanning the top of the rhopalium just beneath and slightly above the small complex eye in between the pit ocelli (Figure 50B). The neurites, which are oriented parallel with the rhopalial length, appear to feed into this apical collection of ganglion nerves primarily oriented perpendicular to the rhopalial length. Although many neurites can be seen along the length of the rhopalial stalk, there are often one or two groups of thicker and more brightly stained neurites that, at the base of the stalk (closest to the body), are more spread out, but converge

together just before entering the back of the rhopalium; the area of convergence is most often on the underside of the stalk closest to the basal statocyst (Figure 51B).

Close to the surface on the front of the rhopalium (where the eyes/ocelli are forming), FMRFamide staining in ganglion nerve cells can be seen running along the photoreceptor cell bases encircling the eyes/ocelli. Most obvious is the staining surrounding the large lensed eye (Figures 52A, B): the circle of nerves around the large lensed eye has a width of roughly 5 μm; these nerves are very diffusely stained and consist of many faintly-stained cell bodies, which are roughly 1 μm in diameter, and neuropeptide vesicles, which range in size from roughly 0.25-0.5 μm. Cell processes extending from the cell bodies are faint and are no more than 1 μm in width. The nerves encircling the large lensed eye merge with the nerves encircling the base of the statocyst in the region between the two structures (Figure 52B). The nerves along the sides of the large complex eye widen into a triangular-shaped region of interconnected nerves upon reaching the junction between the large and small complex eyes (Figures 52A, B); the base of this triangular region, which is parallel with the bottommost portion of the small lensed eye pigment cup, is roughly 20 μm wide. It is in the region between the large and small complex eyes where these nerves are the least visible. One group of nerves coming off of these triangular regions continues around the top of the large lensed eye and the bottom of the small lensed eye to connect in the middle. Another group of nerves branches in the opposite direction out towards the sides of the rhopalium in the region between the lower slit ocelli and upper pit ocelli (Figures 52A, B). The nerves surrounding the majority of the perimeters of the simple ocelli are more punctately-stained and easier to visualize: these neurites are thicker, roughly 1 μm in width, and have numerous bipolar cell bodies and vesicles along their length. The nerves encircling the perimeter of the slit ocelli have a sparse and more faintly stained region connecting to the triangular-shaped nerve regions of the large complex eye and also connect to nerves on the sides of the rhopalium which wrap around the gastric cavity extension and come together on the back of the rhopalium. A nearly complete to complete ring of bipolar ganglion nerve cells encircles each of the pit ocelli and this ring becomes sparser and thin on the far side closest to the side of the rhopalium

(Figures 52C, D). The inner section of the circle is thicker, roughly 3 μm, and feeds into the band of nerves spanning the top of the rhopalium, which connects the two pit ocelli on either side of the small lensed eye (Figure 52C). The outer portion of the circle (closest to the side of the rhopalium) is only roughly 0.5 μm thick. The nerves found closest to the ocelli feed into the nerves spanning the areas on either side of the gastric cavity extension as well as the region above the cavity at the top of the rhopalium.

In juvenile jellyfish, a preliminary nerve ring and nerve net is readily apparent. Upon exiting the rhopalial stalk, the nerves branch in three directions (Figure 53A): two separate neurites angle downward to join with nerves at the base of an adjacent medusa tentacle or secondary tentacle bud. In younger medusa, these nerves are straight and very thin (often only a single thin neurite is seen and is only roughly 1 μm thick) while in older specimens they become more sinuous in shape and consist of a slightly thicker group of neurites that is roughly 12 μm thick (Figures 53B, C). These laterally branching neurites, which connect the alternating rhopalia and medusa tentacles/medusa tentacle buds, form the preliminary nerve ring. A third, thicker group of neurites moves in a straight line up the bell where it ends in a cluster of brightly stained spherical cell bodies (roughly 3 μm in diameter) located at the corner of each of the four gastric pouches, just above the lateral junction of the gastric pouches and manubrium. Smaller neurites branching out from these clusters connect to each other forming a faint rudimentary ring and feed downward into the manubrium. The neural connection running from the rhopalial stalk to the apex of the bell is much thicker (Figure 53D) than the lateral extensions and directly follows an underlying band of muscle (Figure 53E), which corresponds in location to the perradial smooth muscle bands that are located on each side of the bell and run parallel with the bell length in contrast to the circular, striated swim musculature (Satterlie et al., 2005). The group of nerves is thickest, roughly 40 μm wide, closest to the rhopalial stalk and thins to 25 μm as it moves up the bell and by the time it ends, it is only roughly 13 μm wide. Multiple linear neurites make up this band and thinner neurites can be seen branching off of the sides, occasionally feeding into the developing nerve net. The forming nerve net branches off of the nerves found at the bases of

the tentacles and tentacle buds as well as nerve processes branching off of all three rhopalial nerve extensions. These processes often taper and end unless they are able to feed into nearby portions of the FMRFamide-positive nerve net which (excluding the aforementioned areas) are isolated to nerves found within and stretching out from nematocyte batteries on the surface of the bell. Both multipolar and bipolar neurons roughly 3 μm in diameter make up the nerve net with neurites ranging in width from 0.5-1 μm (Figure 54A). The multipolar neurons have approximately three to five branching neurites. Small clusters of neuropeptide vesicles, roughly 1 μm in diameter, are visible along the length of the branching neurites and, as was seen in the nerves of the steady-state polyp, the thinner neurites are more heavily vesiculated. The tentacular nerve net is very brightly stained and consists of vesiculated neurites ranging in width from 1-3 μm, which are interconnected by both bipolar and multipolar nerve bodies which range in size from 3-10 μm in diameter (Figures 54B, C). Large multipolar neurons with a diameter of roughly 10 μm appear similar in morphology to the large multipolar neurons seen in the rhopalia near the stalk and have approximately five processes (Figure 54B). Very brightly stained areas of interconnecting neurites are visible at the bases of the medusa tentacles and secondary medusa buds as well as at the bases of the rhopalial stalks. In addition, staining was also observed in the manubrium and along the edge of the velarium.

No staining is seen in controls that are not exposed to the primary antibody targeting the FMRFamide neuropeptide (Figure 55).

Summary of Results (Table 2)

Of the three analyzed components absent in the steady-state polyp prior to transformation, photoreceptors in the forming small complex eye are the first to begin producing melanin during Stage 2 of transformation. The pigment which stained positive for melanin corresponds to the location and appearance of the pigment seen in the area of the forming small lensed eye under brightfield examination of whole rhopalia as well as in H & E sections. By the end of Stage 2, faint pigment in the developing large complex eye stained positive for melanin and is visible in brightfield examination of whole rhopalia as well as in H & E sections. Photoreceptor nuclei are now visible

encircling the forming complex eyes on the surface of the fused tentacles bases. Despite the presence of photoreceptor nuclei and melanin production, no photoreceptors stain positive for the presence of the UV opsin-like protein. In all three instances (brightfield, Fontana-Masson, and H & E), cup-shaped primordiums of both the large and small complex eyes can be seen in the area where the lenses will begin developing. Although the entire rhopalial surface exhibits crystallin staining, no evidence of lens formation is visible. The FMRFamide-positive nerves within the forming rhopalium resemble those of the tentacles seen in steady-state polyps and primarily consist of multiple neurites, which are oriented parallel with the tentacle length. By the beginning of Stage 3, melanin pigment is well established in the forming pigment cups of both complex eyes, the slit ocelli, and, eventually, the pit ocelli as was detected by the Fontana-Masson stain. This pigment is also visible under brightfield examination of whole rhopalia as well as in H & E sections. The first detection of the UV opsin-like protein appears in photoreceptors of the small complex eye and, by the end of Stage 3, some staining is also visible in photoreceptors of the large complex eye. At no point during transformation was the UV opsin-like protein detected in either type of simple ocelli. J1-crystallin protein is now present in the forming lens of the large complex eye and has brighter extralenticular staining in an up-folding sheet of cells which sits over the eye. This sheet of cells is visible using scanning electron microscopy (SEM) and in sections stained with H & E and for melanin where it is clearly attached to the underlying forming lens. Despite the presence of a clump of cells in the area of the forming lens, no lens-specific staining is visible in the small complex eye. By Stage 4, the amount of melanin in the photoreceptor cells making up the forming retinas of all six eyes/ocelli has increased as detected by the Fontana-Masson stain and is also visible under brightfield and in H & E sections. The staining for the UV opsin-like protein in the photoreceptor cells has also increased in both complex eyes and the positively-stained cells do not appear to contain any pigment. The positively-stained photoreceptors in the large complex eye are all morphologically identical and are more slender than those found in the small complex eye. Lens-specific J1-crystallin is now present in both lenses of the forming complex eyes along with brighter extralenticular staining in the up- and down-folding sheets of cells

which cover the large and small complex eye. These sheets of cells are visible under SEM, where they exhibit different ciliation patterns, as well as in sections stained for both melanin and with H & E. In sections, an increased differentiation between the forming lens of the large complex eye and the overlying sheet of cells, which is thinning, is apparent. J1-crystallin protein is now also evident in the developing slit ocelli on the surface of the photoreceptor cells. This lens-like material is not visible under SEM, as the slit ocellus only appears as a concave groove. No staining is seen in the pit ocelli, which are only positive for melanin and remain as such until the end of transformation. Under SEM, the pit ocelli appear as small concave dimples.

First easily seen during Stage 4, a region of cells spanning much of the top of the rhopalium, just above the small complex eye, is visible in sections stained for melanin and with H & E, where it appears as a more sparsely nucleated region. In samples tested for the presence of J1-crystallin, this region exhibits very bright punctate staining, and, in samples tested for the presence of FMRFamide, it exhibits a collection of brightly-stained and interconnected neurites between the pit ocelli. In addition to this group of nerves, the FMRFamide-positive nerves now consist of a group of interconnected neurites on the back of the rhopalium that are primarily perpendicular to the rhopalial length; these nerves wrap around the sides of the rhopalium and up to form a group of interconnected nerves behind the simple ocelli that are primarily oriented parallel with the rhopalial length. These nerves connect to fainter nerves encircling the large complex eye and to more pronounced nerves encircling the pit ocelli.

By Stage 5, the pigment cups of all six eyes/ocelli continue to stain positive for melanin as well as expand in size. The presence and expansion of the pigment remains detectable in whole rhopalia and in sections stained for melanin and with H & E. The number of photoreceptors producing the UV opsin-like protein and the brightness of staining continues to increase. Lens-specific J1-crystallin staining now appears to penetrate farther into the lenses of the complex eyes but remains the brightest on the surface; the extralenticular staining remains bright in the up- and down-folding sheet of cells covering the complex eyes and an increased number of the photoreceptor cells

in the slit ocellus have bright staining in the lens-like material forming on their surface. By Stage 7 (the end of transformation when the metamorphosed medusa is free-swimming), the amount of melanin has continued to increase as the pigment cups continue to expand as was seen in the sections stained for melanin, under brightfield examination, and in sections stained with H & E. The number of photoreceptors producing the UV opsin-like protein and the brightness of staining continues to increase. Lens-specific J1-crystallin staining now appears to penetrate farther into the lenses of the complex eyes but remains the brightest on the surface; the extralenticular staining remains bright in the up- and down-folding sheet of cells covering the complex eyes and an increased number of the photoreceptor cells in the slit ocellus have bright staining in the lens-like material forming on their surface. Nerves leaving the rhopalial stalk branch laterally to each side forming a rudimentary nerve ring which connects the alternating rhopalia and medusa tentacles/medusa tentacle buds. A third, and thicker, branch of nerves spans upward towards the apex of the bell. Throughout transformation, an overall increase in the size of the eyes/ocelli and their components (primarily including the pigment cups and lenses) was observed, although the distances between the eyes/ocelli remained relatively close together. A summary of results can be seen in Table 2.

In adult rhopalia, the pigment cups of all six eyes/ocelli stain positive for the presence of melanin and, as in the transforming animals, only photoreceptors of the complex eyes exhibit positive staining for the UV opsin-like protein. Like the transforming animals, the positively-stained photoreceptor cells do not appear to contain pigment, but, unlike in transforming animals, at least two types of positively-stained photoreceptors make up the retina of the large complex eye. As is also seen in transforming animals, only the outer portion of the lenses (the fibrous cells) demonstrates the presence of J1-crystallin while the inner globular cells remain unstained. Although staining is evident in the lens-like material on the surface photoreceptors of the slit ocelli, staining is also observed in the pit ocelli unlike in transforming animals. Multiple features seen in developing rhopalia under SEM are still visible in adult rhopalia including the up- and down-folding sheets of cells covering the

lenses of the complex eyes as well as the grooves which are formed due to the in-pocketing of these cells. Unlike in forming slit ocelli, the lens-like material is distinctly visible under SEM in adults.

Discussion

Mechanisms of Development in Vertebrates and Invertebrates

The development of the eyes/ocelli in *Carybdea marsupialis* exhibit both similarities and differences to the modes of development utilized in vertebrates and other invertebrates. While the mode of development in vertebrates is relatively consistent, invertebrates exhibit much more diverse developmental strategies. As was seen in the eyes of the hydromedusan *Cladonema radiatum* (Weber, 1981b), the eyes/ocelli of *C. marsupialis* were each derived completely from primordia of cells located on the surface ectoderm. This first indication of ocular development is comparable to the presence of placodes in the optic neuroepithelium and surface ectoderm during the development of the camera-type eyes of vertebrates (Creuzet, Vincent, & Couly, 2005; Hyer, et al., 2003; Smith, Kao, & John, 2002), to optic placodes observed in invertebrates such as in the formation of the camera-type eyes in cephalopods (Meinertzhagen, 1990), and in the formation of the compound eyes in *Drosophila* (Green, Hartenstein, & Hartenstein, 1993). An optic placode is defined as a thickened region of ectoderm which identifies the area destined to form an eye (Smith et al., 2002), and the thickened layer of nuclei seen on the surface of the rhopalia where the eyes will form could share this terminology. Similar structures in other invertebrates during early eye formation include the optic anlagen seen in the developing pigment-cup eyes of polychaetes (Arendt, Tessmar, de Campos-Baptista, Dorresteijn, & Wittbrodt, 2002; Rhode, 1992; Suschenko & Purschke, 2009) and in the developing eyes of onychophorans (velvet worms; Eakin and Westfall, 1965; Mayer, 2006) as well as the ophthalmic groove in scallops (Butcher, 1930).

The subsequent invagination of the eye primordia on the surface of the developing rhopalia to form the cup-shaped structure of the early retinal cup is comparable in structure to the optic vesicle seen in both vertebrates and invertebrates (Eakin & Brandenburger, 1967; Hyer et al., 2003;

Meinertzhagen, 1990). However, during vertebrate eye development, the optic vesicles are formed from evaginations of the anterior portion of the neural tube (the precursor to the brain and spinal cord; Gehring, 2004; Hyer et al., 2003) as opposed to an invagination of the surface non-neural ectoderm. Despite the initial evagination forming the optic vesicle in vertebrates, the optic cup is ultimately formed by an invagination of the neuroectoderm (Gehring, 2004; Hyer et al., 2003). The first steps of ocular development in invertebrates can vary but there are many examples that are comparable with early eye formation beginning from an invagination of the surface ectoderm, as was seen in *C. marsupialis*, such as the invagination of the surface eye primordium in *Drosophila* to form the eye-antennal imaginal disc (the tissue destined to become the eye and antenna; Gehring, 2004; Ready, Hanson, & Benzer, 1976), the invagination/internalization of the optic placode in onychophorans (Eakin & Westfall, 1965; Eriksson, Tait, & Budd, 2003; Mayer, 2006) and cephalopods to form the optic vesicle (Meinertzhagen, 1990), and in the invagination of the tentacular ectoderm to form the optic vesicle in developing gastropod eyes (Demian & Yousif, 1975; Eakin & Brandenburger, 1967). In the invertebrate polychaete worm *Platynereis dumerilii*, which exhibits pigment-cup eyes, the first evidence of eye formation in both the development of larval and adult eyes is the appearance of pigment spots in the optic anlagen (located on either side of the developing brain) with no mention of surface indentations (Arendt et al., 2002; Rhode, 1992) like those seen in the developing eyes/ocelli of *C. marsupialis*. However, the anlagen is believed to be a part of the epidermis (Rhode, 1992; Suschenko & Purschke, 2009), as it is only later in development that the eyes sink below the epidermis. Unlike most other annelids (Dorsett & Hyde, 1968), some adult polychaete photoreceptors contain a shielding pigment (Arendt et al., 2002; Rhode, 1991; Singla, 1975) and are therefore similar to the pigmented photoreceptors found in *C. marsupialis* eyes (Martin, 2004). Despite this similarity, the second pair of eyes in polychaetes forms from the splitting of the eye anlagen on either side of the head splitting in half (Rhode, 1992), whereas each eye/ocellus in *C. marsupialis* appears to originate from its own primordium. In other invertebrates, eye development is completely subepidermal, forming in close vicinity of or within the brain with no involvement of epidermal cell populations.

For example, the eyes of the nemertean *L. viridis* are believed to be initiated by cerebral nerve cells (which will become the rhabdomeric sensory cells) with surrounding undifferentiated cells becoming both pigment and corneal cells (von Döhren & Bartolomaeus, 2007). A subepidermal origin is also shown for the pigmented eyes in platyhelminthes such as in the flatworms *Mesostoma lingua* (Younossi-Hartenstein, Ehlers, & Hartenstein, 2000), *Macrostomum sp.* (Morris et al., 2004), and *Schmidtea polychroa* (Cardona, Hartenstein, & Romero, 2005), the eyes of which differentiate within either side of the forming brain.

The SEM results, coupled with the sections stained for both the H & E and melanin procedures, indicate that lens formation in the complex lensed eyes of *C. marsupialis* begins with an in-pocketing of ectodermal cells into the forming primoridal cups in the region of subsequent lens formation. In vertebrates, the optic vesicle induces the overlying ectoderm to form the lens placode which will invaginate to form the cellular lens (Grainger, 1992; Jacobson & Sater, 1988; McAvoy, 1980; Saha, Spann, & Grainger, 1989). The lens placode, in turn, induces the optic vesicle to invaginate to form the optic cup (Hyer et al., 2003). The inner region of the optic cup will then give rise to the retina, comprised of photoreceptors, and the outer layer gives rise to the pigmented layer (Cvekl & Piatigorsky, 1996). The method of cellular lens formation utilized by vertebrates is somewhat similar to that seen in lens formation during eye development in the complex eyes of *C. marsupialis*, as the invagination of the lens placode in vertebrates is comparable to the in-pocketing of cells forming the cellular lens in *C. marsupialis*. Most invertebrate lenses are acellular and are formed by the secretion of crystallin proteins and not from crystallin-containing cells (Fernald, 2000). The lenses in onychophorans consist of a dense, spherical, vitreous body which is secreted by an inner layer of the cornea and sits in the optic cavity (Eakin and Westfall, 1965; Mayer, 2006). The lenses of gastropods are believed to be secreted by both corneal and retinal cells; specifically, the corneal cells, retinal pigment cells, and retinal sensory cells are believed to contribute equally during early lens development; whereas, the retinal pigment cells are believed to be the primary contributor late in development and in adulthood (Eakin & Brandenburger, 1967). Lenses and lens-like structures

in polychaete worms have been reported to be formed by (or are part of) pigment cells (Purschke, 2005; Purschke, Arendt, Hausen, & Müller, 2006; Suschenko & Purschke, 2009), specialized un-pigmented supportive cells (Rhode, 1992; Suschenko & Purschke, 2009), or as a result of lens material secretion by corneal cells (Rhode, 1991). In onychophorans, the lens material is also secreted by corneal cells (Eakin & Westfall, 1965). The cephalopod camera-type eye lens is cellular, like those of vertebrates and cubomedusae, but forms very differently: the primary eye fold, consisting of two ectodermal layers separated by a mesodermal layer, grows around the optic vesicle. The inner ectoderm layer gives rise to the inner segment of the cellular lens, while the outer ectodermal layer gives rise to the outer segment of the cellular lens and the iris (Meinertzhagen, 1990). In squid, the site of crystallin production is thought to originate from the overlying ectoderm (Arnold, 1967; West, Sivak, Pasternak, & Piatigorsky, 1994) from which the lens is derived (Arnold, 1967; West, 1993), although a study by West et al. (1994) admitted production of crystallin protein by the lens primordia is also possible despite lacking nuclei (Arnold, 1966a, 1966b; West, 1993), as non-nucleated lens fibers in vertebrates have been demonstrated to synthesize lens crystallins (Lieska, Krotzer, & Yang, 1992; Piatigorsky, 1981; Shinohara & Piatigorsky, 1980; Thomas, Zelenka, Cutherbertson, Norman, & Piatigorsky, 1990; Treton, Shinohara, & Piatigorsky, 1982). In vertebrate eyes, structures large enough to scatter incoming light (such as nuclei and mitochondria) are broken down and removed (Greiling & Clark, 2008; Piatigorsky, 1998). The ectodermal cells overlying the complex ocelli in developing rhopalia appear to be the source of lens formation and, as no apparent nuclei could be distinguished in the developing lenses of the complex ocelli, the overlying cells as well as the lens primorida could both potentially produce the lens crystallins. The lens material of the hydrozoan *Cladonema radiatum* is formed by pigment cell processes where pigment granules in the distal portion of the cell change to crystallin bodies (Weber, 1981a, 1981b). As the eyes of *C. marsupialis* do not possess nonsensory pigment cells in the retina and appear to form from an inpocketing of cells into the retinal cup, this is a distinct difference. During the formation of the retinal cups in *C. marsupialis*, the differentiation of the photoreceptor cells were observed as they gradually lost their

rounded shape and became long and skinny with three clearly defined regions. Cell elongation during photoreceptor differentiation is seen in both vertebrates (Hendrickson et al., 2008; Raymond, 1985) and invertebrates (Mayer, 2006; Rhode, 1992; Richard, Muschalik, Grawe, Özüyaman, & Knust, 2009). In vertebrates, retinal differentiation is a result of the formation of the optic vesicle from the optic cup, a transition which is signaled by the lens placode, although signal interaction with the pre-lens ectoderm has been shown to be sufficient (Hyer et al., 2003). As the retinas of the lensed eyes differentiate (as evidenced by the production of melanin) prior to the detection of J1-crystallin in forming lenses, the study by Hyer et al. (2003) indicates a possible parallel in the retinal differentiation of vertebrates and in cubozoan eyes in addition to the similarities that exist in the method of lens formation. Also, as the inpocketing of cells (which will form the lens) appears to happen concurrently with the invagination of the cup-shaped primorida, this process is similar to the simultaneous invaginations of the optic vesicle and lens placode seen in vertebrates (Hyer et al., 2003).

The forming lens material in the complex eyes of *C. marsupialis* appears histologically different than the attached overlying sheet of cells. It was shown that the lens material gradually becomes more distinct from the overlying sheet of cells and that this sheet gradually thins and appears to form the overlying cornea. The cornea in vertebrates is formed by the signaling of the surface ectoderm by the underlying lens (Meier, 1977; Thut, Rountree, Hwa, & Kingsley, 2001). During cephalopod eye development, the cornea forms last and is from extra-ocular ectodermal tissue from a skin fold of the forward growing arms (Arnold, 1984). It is unclear at what point in development the cornea forms in the lensed eyes of *C. marsupialis*, as it simply results from a gradual thinning of the cells attaching to the underlying developing lens. The developing cornea in vertebrates initially thickens until the fusion of the eyelids, where it subsequently thins and remains at this thickness until birth (Zieske, 2004).

The establishment of a neuronal pathway connecting the retina to the central nervous system of an animal, thereby enabling the transmission and subsequent processing of visual information, is

another important landmark in eye development. In the developing larvae of the polychaete *Platynereis dumerilii*, nerves are visible connecting the forming larval photoreceptor cell axons to the larval central nervous system. Once the adult eyes begin to develop slightly later in development, nerves can also be seen connecting the photoreceptor cells to the optic commissure of the brain (Arendt et al., 2002). In onychophorans, after the formation of the optic vesicle, the optic nerves begin to form and consist of an optic neuropil which feeds into an optic tract that enters the brain (Eriksson et al., 2003; Mayer, 2006). In the squid, after the eyes begin to differentiate, the optic ganglia begin to form; shortly afterwards, optic nerves connect the eye vesicles to the anlagen of the optic lobe (Shigeno, Tsuchiya, & Segawa, 2001). In vertebrates, when the retinal ganglion cells begin to differentiate in the optic vesicle, the axons extend towards the forming optic nerve which feeds into the brain (Brown, Patel, Brzezinski, & Glaser, 2001). It is the retinal ganglion cells which transmit visual information collected by the photoreceptors (Gilbert, 2006). In *Drosophila*, the eye-anntenal imaginal disc exists in the larvae before becoming the adult compound eye during metamorphosis. As a morphogenetic furrow moves across the eye disc, the photoreceptor-containing ommatidia are formed (Ready et al., 1976; Tomlinson & Ready, 1987) and the axons extend through the optic stalk into the forming optic lobes of the brain (Jan, Ghysen, Christoph, Barbel, & Jan, 1985; Steller, Fischbach, & Rubin, 1987).

As seen in all of the aforementioned examples, only after the formation of the eyes begins are neuronal connections established from the developing retina to the central nervous system. FMRFamide-immunoreactive nerves are not seen in close contact with the retina of the large lensed eye until after the formation of the primordial cup and the beginning of retinal cell differentiation. The lack of involvement of a brain in stimulating eye formation, as is seen in *C. marsupialis* and in many other invertebrates, is not surprising as it has been proposed that eyes evolved before the brain (Gehring & Ikeo, 1999) based on the simple explanation that if the brain is meant to process sensory information, then there would be no need for information-processing if a sensory structure was not there to collect it in the first place. This is supported by a study by Nördstrom et al. (2003) which

showed that *Tripedalia* larvae (a cnidarian cubozoan) possess numerous single-celled ocelli but have no nervous system at all.

Despite the variety of developmental strategies used in invertebrate eye formation, it is very common for eye formation to begin with an invagination of the outer ectoderm as opposed to the very different strategy utilized in vertebrate eye formation. This key first step in eye development is shared with that which is seen in the developing eyes/ocelli of *C. marsupialis*. The method of lens formation in *C. marsupialis*, however, can best be compared to the process used by vertebrates. Thus, *C. marsupialis* appears to share similarities with the developmental mechanisms used by both vertebrates and invertebrates. As the aforementioned similarity with vertebrate eye development is not as easily defined as the obvious agreement in the early strategies of eye development used by *C. marsupialis* and many other invertebrates, this could suggest a closer relationship between the ocular development in *C. marsupialis* and other invertebrates as opposed to vertebrates. It is important to remember, however, that the retinas of the invertebrates compared exhibit many morphological differences with those of *C. marsupialis* , including the usage of rhabdomeric photoreceptors as opposed to ciliary photoreceptors. The differences in mode of development between vertebrates and invertebrates as well as amongst invertebrates was one characteristic which led to the proposal of the polyphyletic theory of eye evolution (Gehring, 2005; Salvini-Plawen & Mayr, 1977). As recent genetic work involving the eye regulatory gene networks has provided evidence of a monophyletic theory of eye evolution despite the many morphological and developmental differences, a genetic study following eye development in *C. marsupialis* might help reveal similarities and differences not detected at the morphological level.

Regression of Forming Eyes During Transformation

The regression observed during the transformation process is exciting, especially considering how late in the metamorphosis it was able to occur. This could potentially indicate the ability of free-swimming juveniles, or even adult jellyfish, to revert back to the polyp life-form, a phenomenon which has been observed in hydrozoans. In the life cycle of *Hydractinia carnea*, it was found that

medusa buds artificially detached early during formation were able to transform back into polyps while those detached late formed complete medusae that were reduced in size (Frey, 1968; Müller, 1913; Schmid, 1972). The potential for reverse development has also been proposed in the hydromedusans *Laodicea undulata* (De Vito, Piraino, Schmich, Bouillon, & Boero, 2006), *Turritopsis dohrnii* and *Hydractinia carnea* (Schmich et al., 2007). In most cases of hydrozoan reverse development, sexual maturation appears to be the point of no return (Piraino, De Vito, Schmich, Bouillon, & Boero, 2004; Stearns, 1992); however, a study by Piraino, Boero, Aeschbach, and Schmid (1996) showed that reverse development can occur in newly-liberated medusae of *Turritopsis nutricula* as well as in adults with mature gonads. This same study also demonstrated that reverse development is a consequence of unfavorable environmental conditions (Piraino et al., 1996). Unfortunately, this study did not specifically address the regression of the ocelli, which are located on the tentacle bulbs and are of a simpler type to the camera-type eyes found in cubomedusae (Martin, 2002). The first indication of regression in transforming *C. marsupialis* polyps was the dispersal of pigment from the photoreceptors resulting in a uniformly speckled area. A similar occurrence was seen in degenerating *Coryne eximia* medusae where "clusters of colored particles" were described as resulting from the breakdown of the ocelli (Puce, Bavestrello, Azzini, & Cerrano, 2003, p. 250). As the regression from a free-swimming medusa to the polyp stage can occur in approximately three days for the hydromedusans examined (De Vito et al., 2006; Piraino et al., 1996), it is likely that the complex rhopalium and corresponding ocelli contribute to the lengthier regression time observed in *C. marsupialis*.

Other animals are known to exhibit ocular degeneration which can range from an incomplete formation of the eye to a regression from a fully formed eye to an essentially eyeless state. The cavefish *Astayanx mexicanus* has both eyed and eyeless populations, depending on whether or not they are surface-dwelling (eyed) or cave-dwelling (eyeless). Interestingly, the eyeless cavefish exhibit early eye formation (including formation of the lens placode, optic cup formation, retinal cell differentiation, and opsin gene transcription). Subsequently, the lens placode fails to differentiate into

the cellular lens, the cornea does not form, opsin gene transcription ceases, the eye degenerates and is overgrown by a flap of skin (Cahn, 1958; Langecker, Schmale, & Wilkens, 1993; Langecker, Wilkens, & Schmale, 1995). Widespread apoptosis and downregulation of *Pax6* was observed in these degenerating eyes (Jeffery, 2005; Jeffery & Martasian, 1998). The Ozark cave salamander, another cave-dwelling animal, exhibits an aquatic larva with a fully-functional retina which is degenerated during the transition to the terrestrial-dwelling adult (Besharse & Hollyfield, 1977). The armored cave-dwelling catfish *Ancistrus cryptophthalmus*, which do not have visible eyes, are born with structurally intact eyes which are used by offspring during the first 270 days of life. At this point, a reduction of the dark pigment in the eyes can be seen followed by a disorganization of the eye structure which changes from a spherical to horseshoe shape. The eye then sinks in to the optical orbit, changes in shape again to a small elliptical shape, and is covered by skin folds. Also, the degeneration of the two eyes in each animal was never simultaneous (Secutti & Trajano, 2009) as was seen in the asymmetric recession of individual eye-bearing rhopalia during regression in *C. marsupialis*. Successive environmental changes during the lifecycle of an animal can also be accompanied by degeneration of the existing visual system as is seen in the deep-sea hydrothermal vent crab *Bythograea thermydron*: the planktonic larvae of the crab, which can be found in the water column far above the depths of the vents, have image-forming compound eyes which are degenerated during the metamorphosis to the adult crab for a visual system better suited for the dimmer environment where image-forming eyes are largely unnecessary (Jinks et al., 2002). Another example can be seen in the degradation of the larval eyes in polychaetes (Rhode, 1992), beginning with a reduction of the sensory cell and microvilli, as the adult eyes begin to form.

Degeneration has been reported to begin first with apoptosis in the lens followed by the retina (Jeffery, 2005; Peters & Peters, 1973; Wilkens, 1988, 2001). Although forming lenses are clearly present by Stage 6 of transformation in *C. marsupialis*, which is the latest stage where regression was observed, it is difficult to ascertain whether or not degeneration of the lensed eyes begins here or in the retina. The first indication of regression was in the degeneration of the retina as evidenced by the

dispersal of pigment granules from the retinal photoreceptors. To further clarify the regression process, a study following the location of apoptotic cells could be beneficial if this process utilizes apoptosis as is seen in other ocular degenerations (Jeffery, 2005; Jeffery & Martasian 1998).

Common Components of Vision in Developing and Adult Cubozoan Eyes

The results of this study clearly indicate the usage of several ocular components utilized by higher organisms including melanin, opsins, crystalline, and similar neuropeptides.

Melanin and UV opsin-like protein in developing and adult photoreceptors. Photoreceptor maturation begins with the positive detection of melanin by the Fontana-Masson stain in photoreceptors of the small complex eye during Stage 2 (followed closely by the large complex eye) and the subsequent production of the UV opsin-like protein in the small complex eye during Stage 3 and later in the large complex eye during Stage 4. Although previous studies have shown immunoreactivity for a UV opsin-like protein in the complex eyes of *C. marsupialis* (Ekström et al., 2008; Martin, 2004), neither study commented on the apparent lack of pigment in the positive-staining photoreceptor cells as was seen in the present study using DIC imaging. One type of photoreceptor cell in the slit ocelli of *T. cystophora* is also known to be unpigmented (Garm, Andersson, & Nilsson, 2008). The initial production of pigment in the small complex eye indicates that the pigmented photoreceptor cells of the small complex eye begin maturing before the pigmented photoreceptor cells of the large complex eye. A second difference in photoreceptor appearance/maturation seen in both lensed eyes was indicated by the expression of melanin in both eyes prior to the appearance of the UV opsin-like protein, which indicates that the pigmented photoreceptors expressing the shielding pigment either mature or are established before the non-pigmented photoreceptors expressing the UV opsin-like protein.

The detection of the UV opsin-like protein further supports the plethora of evidence suggesting that photosensitivity in cnidarians is opsin-based (Coates et al., 2006; Ekström et al., 2008; Garm, Coates, et al., 2007; Martin, 2002; Musio et al., 2001; O'Connor, Garm, et al., 2010; Suga et al., 2008; Weber, 1982a, 1982b). Of course, just because the antibody targeting the zebrafish UV

opsin labeled photoreceptors in the developing and adult rhopalia, this does not necessarily mean that the opsins in these photoreceptors utilize UV light; it may simply mean that the structure of the UV opsin-like protein is similar enough to the zebrafish UV opsin to be labeled by the antibody and would thereby make hypotheses concerning UV light tentative but plausible. The unpigmented photoreceptors which were positively-stained for the presence of the UV opsin-like protein are primarily located at the surface of the retina above the unstained pigmented photoreceptors; the position and unpigmented nature of these photoreceptors can possibly be explained by the wavelengths of light potentially utilized by the photopigments. The surface layer of photoreceptor cells utilizing the UV light, coupled with the absorption of UV light by the bell (Coates et al., 2006; which the light must first pass through prior to reaching the internally-oriented eyes), might provide a sufficient shield preventing the UV radiation from reaching the photoreceptors beneath. This would also explain why the photoreceptors expressing the UV opsin-like protein did not appear to contain any shielding pigment, as the primary purpose of melanin is to absorb harmful UV light (Cockell & Knowland, 1999) and this would not be necessary in photoreceptors utilizing this light. Although UV light is known to cause DNA damage (Cockell & Knowland, 1999), the surrounding photopigments of the photoreceptor cells could act as a screening pigment themselves in the utilization of the UV light thereby preventing it from reaching the delicate nuclear DNA. If harmful UV light was required to pass through layers of photoreceptors before reaching the UV-specific photoreceptors, substantial damage could be done and explains the surface positioning of the positively-stained photoreceptors. Also, the expression of UV opsin-like protein in the small complex eye before the large complex eye during transformation is intriguing and two possibilities come to mind. First, as the large complex eye appears earliest in development as a primordial cup, it is possible that the increased complexity and size of this lower eye merely takes more time to form its foundation before the cells begin to mature and are able to begin expressing the melanin and UV opsin-like proteins, which first appear in the smaller and simpler complex eye. Second, due to the upward orientation of the small complex eye, it is possible that early expression of the UV opsin-like protein is necessary because of the increased

exposure of this eye to the downwelling UV light; the increased concentration of the UV opsin-like protein in the photoreceptors of the small complex eye and in the upper photoreceptors of the large complex eye in adult rhopalia support this theory.

J1-crystallin protein in developing and adult lenses. Despite that pigmentation and therefore photoreceptor maturation was first evident in the small complex eye, the large complex eye is the first eye to show immunopositive staining for J1-crystallin. It is possible then that lens formation begins first in the large complex eye. However, due to the spherical clump of globular cells seen in the location of the future lens of the small complex eye, it is also possible that lens formation begins simultaneously but that the lens cells of the small complex eye are expressing different crystallin proteins that were not detected by the anti-J1-crystallin antibody. As the ocelli develop, the increase in staining for J1-crystallin demonstrates not only the appearance and growth of lenses, but the increase in concentration of the crystallin proteins. The surface of adult lenses exhibit brightness of staining comparable to that seen in the developing lenses, signifying a continued production of crystallin proteins as the lens increases in size through adolescence and possibly during adulthood, as lens crystallin production in adults has been indicated in other invertebrates such as squid (West et al., 1994). In the adult slit ocelli, however, the staining is markedly less pronounced than in developing slit ocelli, indicating that at some point between metamorphosis and adulthood, J1-crystallin produced within the slit ocelli stops or slows down dramatically, resulting in a lower concentration of crystallin proteins within the slit ocelli as they expand in size. The lack of staining in the central cells of the complex eye lenses in developing and adult complex eyes indicates the isolation of J1-crystallin to the outer layers of cells. Expression patterns of the genes encoding J1-crystallins show a similar pattern in the cubozoan *Tripedalia cystophora*, which exhibited intense staining on the surface of the lens of the large complex eye; this same study also demonstrated the isolation of J1-crystallin mRNA expression to the outer layers of the lenses of both complex ocelli (Piatigorsky et al., 2001). This pattern of staining is also seen in developing squid lenses, with a lack of S-crystallins in the central core of the lens primordium (West et al., 1994). It is possible that the central region of the developing

and adult lenses is made up of a different type of crystalline, such as J2-crystallin or J3-crystallin, which are found in the lenses of the cubomedusan *Tripedalia cystophora* (Piatigorsky et al., 1989). As the characteristic distribution of proteins within the lens appears to differ in concentration from the heavily concentrated inner region to the less concentrated outer region (Martin, 2004), this could also speak to a potential difference in the structural crystallin used. Differential crystallin patterns and proteins can also be seen in developing and adult vertebrate lenses (for a review see Rabaey, 1965) such as in developing eyes of rats (McAvoy, 1978a, 1978b; van Leen, van Roozendaal, Lubsen, & Schoenmakers, 1987), mice (Robinson & Overbeek, 1996), chickens (Hejtmancik, Beebe, Ostrer, & Piatigorsky, 1985; Li, Zelenka, & Piatigorsky, 1993; Thomas et al., 1990), frogs (Brunekreef, van Gensen, Destrée, & Lubsen, 1997; Mikhailov, Simirskii, Aleinikova, & Gorgolyuk, 1997; Smolich, Tarkington, Saha, & Grainger, 1994; Zhao et al., 2011), and in toad lenses, where α- and β-crystallin are found in the outer lens layers and not in the central lens where a different protein, γ-crystallin, exists by itself in its highest concentrations (Keenan, Elia, Dunn, Orr, & Pierscionek, 2009). As there is no lens-like material visible in the pit ocellus in histological sections, SEM, or under brightfield examination of whole rhopalia, the positive staining for the presence of J1-crystallin was surprising. Previous detection of J1-crystallin in the simple ocelli of the cubomedusan *Tripedalia cystophora* has been described (Kozmik, Ruzickova, et al., 2008), although the staining pattern is very different from that seen in *C. marsupialis*. The immunoreactivity of the 7th ocular structure, often located in between one set of the simple ocelli, indicated the presence of J1-crystallin in the center of the spherical area of pigment. Under brightfield imaging of whole rhopalia, the appearance of the larger version of the structure also indicated the presence of lens-like material in the same location. Despite the variation in the structural complexity and unpaired nature, the consistent location and frequent appearance of these extra structures indicates the presence of a newly-described ocellus.

The extralenticular staining is not surprising, as lens crystallins are multifunctional proteins which are often expressed and have non-optical roles in tissue outside of the lens (Kozmik, Swamynathan, et al., 2008; Piatigorsky et al., 2001; Wistow & Piatigorsky, 1987, 1988); the use of a

single protein encoded by one gene for dual functions has been referred to as "gene sharing" (Piatigorsky, 1998, 2007; Piatigorsky & Wistow, 1989). Extralenticular expression of crystallin proteins has been well-documented in vertebrates (for αB-crystallin see Bhat & Nagineni, 1989; Iwaki, Kume-Iwaki, & Goldman, 1990; Robinson & Overbeek, 1996; for αA-crystallin see Srinivasan, Nagineni, & Bhat, 1992; for ρ-crystallin see Mikhailov et al., 1997; for β-crystallins see Head, Peter, & Clayton, 1991; Magabo, Horwitz, Piatigorsky, & Kantorow, 2000; for γ-crystallin see Smolich et al., 1994; for δ-crystallin see Agata, Yasuda, & Okada, 1983; Li et al., 1993) and in invertebrates such as the scallop (Ω-crystallin: Piatigorsky et al., 2000) and fly (drosocrystallin: Janssens & Gehring, 1999). The vertebrate lens crystallin αB-crystallin functions not only as a lens crystallin but also as a widely-expressed heat shock protein (Klemenz, Fröhli, Steiger, Schäfer, & Aoyama, 1991). In jellyfish, J1-crystallins have been shown to be similar in sequence to the ADP-ribosylglycohydrolases (Castellano et al., 2005; Piatigorsky & Kozmik, 2004) and J3-crystallin is similar in sequence to saposins (multifunctional enzymes which function in membrane turnover; Piatigorsky et al., 2001). Due to these similarities as well as expression in regions outside of the lens (Kozmik et al., 2003; Kozmik, Swamynathan, et al., 2008; Piatigorsky et al., 2001), it has been suggested that cubomedusan crystallins have non-optical functions. The pattern of crystallin staining seen over the course of development indicates that the J1-crystallin is initially widely expressed at the beginning of ocular development and gradually becomes more pronounced in the lenses before being almost exclusively isolated to the lenses by the time the animal has reached adulthood. Similar results were shown in a study following δ-crystallin in developing chicken embryos; extralenticular crystallin was found in several areas of the embryo during early development but was completely isolated to the lenses by the time the chickens were 1-day-old (Agata et al., 1983). In the future, it would be interesting to determine the extent of the extralenticular staining outside of the developing rhopalium; is it found across the surface of the entire steady-state polyp and, if so, how does this change over the course of transformation? Like in adult rhopalia, is there a complete lack of the extralenticular staining in the entire medusal body?

FMRFamide immunoreactivity in developing and adult animals. The FMRFamide immunoreactivity seen in the steady-state polyp and in the body of early transforming polyps has both similarities and differences to the RFamide/FMRFamide immunoreactivity seen in many polyps of other cnidarian species such as the presence of sensory neurons along the body column in addition to a high concentration of sensory neurons in the hypostome, the presence of a tentacular nerve net, nerve rings, and staining primarily restricted to the ectoderm (Golz, 1994; Grimmelikhuijzen, 1983; Grimmelikhuijzen et al., 1996; Gröger & Schmid, 2000). The presence of a dual ectodermal/endodermal nerve ring could not be discerned, as only an ectodermal nerve ring could be visualized at the junction of the hypostome and tentacular origin, although the presence of a dual ectodermal/endodermal nerve ring pair has been indicated in the polyp of an unknown *Carybdea* species (Werner et al., 1976). A similar situation has been reported in a study by Grimmelikhuijzen (1983) who demonstrated staining only in the outer nerve ring of the hydropolyp *Leucarthiara nobilis*. The increased difficulty in seeing the nerves in the upper body column and in the area of the forming bell during the early stages of transformation is most likely an indication of the degeneration of the majority of the polyp nerves followed by the differentiation of the medusal nervous system. Nerve degeneration, reorganization of nerves, and differentiation of new nerves have been documented during many metamorphic processes, such as in insects (Levine, 1986), hydrozoan planulae (Martin, 2000), and scyphozoan planulae (Nakanishi, Yuan, Jacobs, & Hartenstein, 2008; Yuan, Nakanishi, Jacobs, & Hartenstein, 2008).

The FMRFamide-immunoreactive nerves seen during transformation and within the rhopalia are found in similar locations in adults, including within the rhopalia, nerve ring, subumbrella, tentacles, and velarium (Satterlie, 2002, 2011). As early as Stage 4, the bilaterally symmetric neuronal organization seen within adult rhopalia (Parkefelt et al., 2005; Plickert & Schneider, 2004, Satterlie, 2002; Skogh et al., 2006) is apparent in the rhopalia of transforming animals. The bulk of the immunoreactivity seen in developing rhopalia is not directly associated with the eyes/ocelli but is located along the back (from where the stalk originates) and sides of the rhopalium as is seen in adults

(Parkefelt & Ekström, 2009). Two nerve groups which were seen in the rhopalia during development appear to correspond to the neural commissures in adults which interconnect the two sides of the FMRFamide immunoreactive system (Parkefelt & Ekström, 2009; Parkefelt et al., 2005; Satterlie, 2002; Skogh et al., 2006). The difference in neurite density seen in developing rhopalium consisted of the densest areas being more concentrated in the lower half of the rhopalium in close association with the basal statocyst; whereas, in adult rhopalia, this density is shifted upward with relatively low densities occurring in the lower half of the structure (Parkefelt & Ekström, 2009). On either side of the stalk in adult animals are large FMRFamide-immunoreactive cells of undiscerned polarity (Parkefelt & Ekström, 2009; Skogh et al., 2006) which correspond in size and location to the large multipolar cells seen in developing rhopalia in close association with the rhopalial stalk; in adults, these cells have been proposed to be a part of the pacemaker system due to their close association with the rhopalial stalk (Parkefelt & Ekström, 2009). As the pacemaker system is clearly in place by the end of transformation, as is evidenced by the swimming ability of the juvenile medusa, the span of nerves corresponding to the posterior commissure along with the large multipolar cells seen in close association with the rhopalial stalk likely together represent the early formation of the pacemaker region and, potentially, a portion of the adjacent rhopalial neuropil (Gray et al., 2009). Close to the surface on the front-facing side of the developing rhopalium, diffuse nerves were seen encircling the large complex eye; in adult eyes, all nerves are localized behind the ocelli (Parkefelt & Ekström, 2009). The diffuse staining seen along the periphery of the large complex eye could correspond to the immunolabeling seen just below the retina of this eye in adult rhopalia (Martin, 2002, 2004; Parkefelt & Ekström, 2009); it is possible that as the rhopalia and corresponding ocelli expanded during growth to adulthood these nerves matured and became located deeper within the rhopalium. As a faint connection was seen from the triangular nerve group of the large complex eye to the region between the simple ocelli, it is possible that this represents an early formation of a subset of neural connectivity between these eye types. In support of this, Electroretinography (ERG) recordings in the similar species *T. cystopho*ra revealed that responses to stimulation of the lower lensed eye could be

detected in the slit ocelli (Garm & Ekström, 2010). In addition, it has been speculated that since the slit eyes have the same visual field as the large lensed eye (Coates, 2005), the visual signals from these two eye types are integrated while the visual signals from the pit ocelli and small lensed eye, which also share the same visual field (Coates, 2005), are integrated; the information from both sets of visual fields are then integrated probably in an area close to the rhopalial stalk (Parkefelt et al., 2005). Previous studies have found RFamide (Martin, 2002, 2004) and non-specific FMRFamide immunoreactivity (Satterlie, 2002) in the slit ocelli of adult rhopalium; this was not seen in any of the transformative stages in the current study.

As the multicellular ocelli are advanced in structure compared to the single-celled ocelli found in planulae of the cubozoan *Tripedalia cystophora*, which lack neurons (Nordström et al., 2003), it makes sense to have a way in which to convey and process the increased amount and complexity of sensory information collected by the visual structures. As the FMRFamide immunoreactivity seen in the developing rhopalia clearly expands in size and complexity from the simple linear neurites seen at the fusion of the polyp tentacles by Stage 2, which corresponds to the simultaneous development of the eyes/ocelli, this adds to the increasing amount of evidence implicating the involvement of the rhopalial nervous system in conveying, if not also interpreting, visual information collected by the eyes/ocelli (Garm et al., 2006; Parkefelt & Ekström, 2009; Parkefelt et al., 2005). Since the purpose of the rhopalium is to hold the visual structures, any associated neural system is surely in existence to enable the animal to convey and interpret valuable sensory information. Despite the extensive staining seen in the nerves detected by the antibody directed against FMRFamide, the complexity of the polyp nervous system, transforming nervous system, and resulting nervous system in juvenile medusae is surely an underestimate when acknowledging that the FMRFamide-immoreactive nerves represent only a subpopulation of the overall nervous system.

Ocular Growth and Spacing

Although growth of the eyes/ocelli occurs from the start of ocular development until adulthood, the percentage of growth from the start of development to the end of metamorphosis and from the end of metamorphosis until adulthood differs. For all six eyes/ocelli, a higher percentage of growth (large lensed eye: 300%, small lensed eye: 200%, slit ocelli: 250%, pit ocelli: 240%) was observed for the size of the eyes/ocelli from the end of metamorphosis to adulthood than for the percentage increase of the eyes/ocelli from the start of transformation to the end of transformation (large and small lensed eyes: 200%, slit ocelli: 60%, pit ocelli: 40%). For the simple ocelli, a much higher percentage of growth was observed from metamorphosis to adulthood with relatively little growth occurring during metamorphosis. Overall, from the start of metamorphosis until adulthood, the large lensed eye increased in size approximately 1200%, the small lensed eye increased in size approximately 900%, the slit ocelli increased in size approximately 450%, and the pit ocelli increased in size approximately 350%. The vast increase in size of the eyes and ocelli corresponds to the relative lack of significant lengthening of the photoreceptor staining length observed during transformation to those in adults, which are roughly only 1-1.5- times bigger. The eyes/ocelli remained in close association with each other throughout the course of transformation; the distance between the complex eyes and the simple ocelli remained relatively constant while the distance between the large and small complex eye actually shrunk during transformation. This indicates that the eyes/ocelli maintain a close association with one another from early during transformation until adulthood.

Photoreceptor Populations

Although morphological differences in photoreceptor populations between the two complex eyes have been acknowledged (Martin, 2004), there was no mention of differing morphologies in the large lensed eye in either of the studies which looked at photoreceptors indicating the presence of the UV opsin-like protein (Ekström et al., 2008; Martin, 2004). However, the study by Ekström et al. (2008) was conducted on large lensed eyes of newly metamorphosed medusa and, as was seen in the

present study, the photoreceptors in the large lensed eye of newly metamorphosed medusa appear to be morphologically identical. A conclusion based only on the staining seen in the developing eyes would be that the large complex eye had at least two types of photoreceptors including the morphologically identical immunopositive cells expressing the UV opsin-like protein and the interspersed unstained photoreceptors. Results from adult rhopalia indicate that the large complex eye has at least three different photoreceptors including the short stained photoreceptors in the apical region of the eye, the long stained photoreceptors, and the unstained photoreceptors. The differences in photoreceptor populations of the large complex eye between a newly metamorphosed animal and an adult indicate that a vast majority of the morphological differentiation of the photoreceptors occurs after transformation, between juvenility and adulthood.

Staining for the UV opsin-like protein within the short photoreceptors of the small lensed eye and upper region of the large lensed eye indicate that the entire length of the photoreceptor stained positive for the presence of the UV opsin-like protein based on the brightly-stained apical bulge which appears to be the distal boundary of the photoreceptor cell. Although it is possible that this does not represent the apical edge of the photoreceptor, the distinct boundary of stain indicates otherwise, especially in adult photoreceptors. Staining within the long photoreceptors of the large lensed eye in both developing and adult animals appears to be isolated to the lower portions of the cells as has been previously described in adults and juveniles (Ekström et al., 2008; Martin, 2004). Despite both types of photoreceptors present in the complex eyes (short and long) staining positive for the presence of the UV opsin-like protein, the marked morphological differences between these photoreceptor populations suggests alternative functions. Specifically, the morphological similarities and close proximity of the short photoreceptors in the upper portion of the large lensed eye and the photoreceptors of the small complex eye suggest a common function of these short photoreceptors and a different function of the long photoreceptors in the large complex eye. This morphological difference in photoreceptor populations and the relative locations of the two photoreceptor types is comparable to the organization of the vertebrate retina, which consists of both rod and cone

photoreceptors. The cones are shorter than the rods and have a short conically-shaped outer light-sensing segment; whereas, the outer segment of the rods are slender and cylindrical in shape (Szymonowicz & MacCallum, 2010). Although located at the back of the eye due to the inverted design of the retina (Svet & Khazen, 2009), the cone cells are predominant in the area directly behind the lens whereas the rods are predominant along the periphery of the retina (Masson, 2011). This is similar to the organization of the photoreceptor populations in the retinas of the lensed eyes of *C. marsupialis* where the short photoreceptors were more closely associated with the lens and, in the small complex eye, were located directly behind the lens with dwindling numbers to the periphery of the retina. Overall, there are at least three different types of photoreceptors making up the complex eyes including the long photoreceptors of the large complex eye, which stained positive for the UV opsin-like protein; the short photoreceptors of the large and small complex eye, which stained positive for the UV opsin-like protein; and the unstained photoreceptors in the complex eyes and simple ocelli. As the unstained photoreceptors obviously utilize a different opsin than the ones that positively stained for the presence of the UV opsin-like protein, this indicates the usage of at least two different opsins (the UV opsin-like protein and the opsin found in the unstained photoreceptors of the complex eyes and simple ocelli) in the eyes/ocelli of *C. marsupialis*. The use of a different photopigment in the simple ocelli than in the lensed eyes has been suggested by several authors (Ekström et al., 2008; Koyanagi et al., 2008; O'Connor, Garm, et al., 2010), as no indication has been found of what photopigment are used in the simple ocelli (Garm & Ekström, 2010).

Functionality During Development

Early functioning of the eyes during the course of transformation has not been established, although results of this study indicate possible functionality of the eyes/ocelli and integration of visual stimuli as early as Stage 4. Recently, Garm & Bielecki (2008) demonstrated that pacemaker neurons, which control contractions of the swim musculature (Satterlie, 1979, 2002; Satterlie & Nolen, 2001; Satterlie & Spencer, 1979), are modulated by visual input; as the bell begins pulsating as early as Stage 4, it is possible that visual input begins to play a role in the sporadic contractions

indicating functionality of the ocelli by this point along with the ability to integrate and convey visual stimuli from the rhopalium to the main nerve ring which then innervates the swim musculature. If the pacemaker region directly controls contractions of the swim musculature (Satterlie, 1979, 2002; Satterlie & Nolen, 2001; Satterlie, & Spencer, 1979), and visual input modulates the pacemaker region, then it only makes sense that for there to be contractions at this stage, there must be visual stimuli collected by the ocelli. Although peptides in the RFamide family have been implicated in the transmission of photic stimuli to the epitheliomuscular system (Plickert & Schneider, 2004), evidence of a forming medusal nerve ring in the FMRFamide-immunoreactive system and connection of said ring to the rhopalia is not visible until the end of transformation, Stage 7. Despite this, visual information collected by functioning eyes or ocelli appears to be reaching the swim musculature by this point in transformation as evidenced by the increasing frequency of bell pulsation, and this indicates that although it is possible for the FMRFamide-immunoreactive nerves to play a part in the collection and integration of visual stimuli, a different subset of the nervous system is at least partially responsible for conveying the information leaving the rhopalial stalk and going to the swim musculature.

Alternative Functions of the Lensed Eyes

Several results of this study indicate a different function of the two lensed eyes including differences in lens development and morphology, differences in photoreceptor population, and differences in FMRFamide immunoreactivity. Differences in lens formation are visible early in transformation due to the variation of ciliation patterns on the surface of the up-folding and down-folding sheets of cells of the large and small lensed eyes, respectively. Where the reduction of cilia was seen in cells overlying the forming large complex eye lens, no change in ciliation pattern was seen in cells overlying the forming small complex eye lens; this characteristic was also seen in adult rhopalia along with the morphological differences in the lens structure. An additional morphological difference is in the arrangement of the lens in reference to the retinal cups of the large and small complex eyes. The lack of staining for the UV opsin-like protein in the slit and pit ocelli also suggests

that the simple ocelli serve a different visual task as has been suggested in a similar study by Ekström et al. (2008) and in a study investigating the morphological properties of the simple ocelli (Garm et al., 2008). The photoreceptor populations of the large complex eye, consisting of both long and short photoreceptors which stained positive for the presence of the UV opsin-like protein in addition to the unstained photoreceptors, are very different from the photoreceptor populations of the small complex eye, which consist only of short positively-stained photoreceptors in addition to unstained photoreceptors. The organization of these photoreceptors is also different between the two lensed eyes, as the photoreceptors of the large complex eye encircle the entire perimeter of the central lens; whereas, the photoreceptors of the small complex eye are centralized behind the lens (closest to the large complex eye). There was a lack of FMRFamide immunoreactive nerves in close proximity to the neural layer of the retina in the small complex eye system in developing rhopalia, a pattern also seen in adult rhopalia (Parkefelt & Ekström, 2009). This indicates the probable involvement of a different neuronal subset other than FMRFamide in the transmission of sensory information collected here. Based on the aforementioned differences, it is possible that the small complex eye may have a different visual function than that of the large complex eye, a hypothesis suggested by previous studies based on varying synapse morphologies (Gray et al., 2009), photoreceptor populations (Laska & Hündgen, 1982; Martin, 2004), temporal properties (Coates, 2005; Garm et al., 2008; Nilsson et al., 2005; O'Connor, Nilsson, & Garm, 2010), monitored visual fields (Coates, 2005; Garm & Ekström, 2010; Garm et al., 2011), and differing effects on pacemaker frequency (Garm & Mori, 2009).

Conclusions

From the results obtained during this study, it is apparent that the morphological components traditionally required for vision, including the opsin, melanin, and crystallin proteins utilized in higher animals, are present in the first multicellular organisms to possess complex camera-type eyes. The process by which the eyes/ocelli develop shows similarities to the developmental mechanisms utilized by both vertebrates and other invertebrates and results in eyes/ocelli which utilize

morphological components traditionally required for vision in higher animals, including opsin, melanin, and crystallin proteins. A newly-described 7th eye was discovered and the presence of a retina and crystallin material was indicated. During ocular development, the process was able to be halted and reversed resulting in a regression of the eye-forming animal back to the eyeless polyp state, a phenomenon which is also seen in vertebrates and other invertebrates.

References

Agata, K., Yasuda, K., & Okada, T. S. (1983). Gene coding for a lens-specific protein, δ-crystallin, is transcribed in nonlens tissues of chicken embryos. *Developmental Biology, 100*(1), 222-226. doi:10.1016/0012-1606(83)90214-2.

Anderson, P. A. V. (2004). Cnidarian neurobiology: what does the future hold? *Hydrobiologia, 530/531*(1-3), 107-116. doi:10.1007/978-1-4020-2762-8_13.

Arendt, D. (2003). Evolution of eyes and photoreceptor cell types. *International Journal of Developmental Biology, 47*(7-8), 563-571.

Arendt, D., Tessmar, K., de Campos-Baptista, M.-I., Dorresteijn, A., & Wittbrodt, J. (2002). Development of pigment-cup eyes in the polychaete *Platynereis dumerilii* and evolutionary conservation of larval eyes in Bilateria. *Development, 129*, 1143-1154.

Arendt, D. K., Tessmar-Rabile, K., Snyman, H., Dorresteijn, A. W., & Wittbrodt, J. (2004). Ciliary photoreceptors with a vertebrate-type opsin in an invertebrate brain. *Science, 306*(5697), 869-871. doi:10.1126/science.1099955.

Arendt, D., & Wittbrodt, J. (2001). Reconstructing the eyes of Urbilateria. *Philosophical Transactions of the Royal Society of London B, 356*(1414), 1545-1563. doi:10.1098/rstb.2001.0971.

Arkett, S.A., & Spencer, A. N. (1986). Neuronal mechanisms of a hydromedusan and shadow reflex. II. Graded response of reflex components, possible mechanisms of photic integration and functional significance. *Journal of Comparative Physiology A, 159*(2), 201-213. doi:10.1007/BF00612303.

Arnold, J. M. (1966a). On the occurrence of microtubules in the developing lens of the squid *Loligo pealei*. *Journal of Ultrastructure Research, 14*, 534-539.

Arnold, J. M. (1966b). Squid lens development compounds that affect microtubules. *Biological Bulletin, 131*, 383.

Arnold, J. M. (1967). Fine structure of the development of the cephalopod lens. *Journal of Ultrastructure Research, 17*(5-6), 527-543. doi:10.1016/S0022-5320(67)80139-4.

Arnold, J. M. (1984). Closure of the squid cornea: a muscular basis for embryonic tissue movement. *Journal of Experimental Zoology, 232*(2), 187-195. doi:10.1002/jez.1402320206.

Bahar, S. (2002). Evolution of the eye: lessons from freshman physics and Richard Dawkins. *Biological Physicist, 2*(2), 2-5.

Bebenek, I. G., Gates, R. D., Morris, J., Hartenstein, V., & Jacobs, D. K. (2004). *sine oculis* in basal Metazoa. *Development Genes and Evolution, 214*(7), 342-351. doi:10.1007/s00427-004-0407-3.

Berger, E. W. (1898). The histological structure of the eyes of cubomedusae. *Journal of Comparative Neurology, 8*(3), 223-230. doi:10.1002/cne.910080317.

Berger, E. W. (1900). Physiology and histology of the Cubomedusae, including Dr. F. S. Conant's notes on the physiology. *Memoirs of the Biological Laboratory. Johns Hopkins University, IV*, 1-84.

Berrill, N. J. (1949). Developmental analysis of scyphomedusae. *Biological reviews, 24*(4), 393-409. doi:10.1111/j.1469-185X.1949.tb00581.x.

Besharse, J. C., & Hollyfield, J. G. (1977). Ultrastructural changes during degeneration of photoreceptors and pigment epithelium in the Ozark cave salamander. *Journal of Ultrastructure Research, 59*(1), 31-43. doi:10.1016/S0022-5320(77)80026-9.

Bhat, S. P., & Nagineni, C. N. (1989). αB subunit of lens-specific protein α-crystallin is present in other ocular and non-ocular tissues. *Biochemical and Biophysical Research Communications, 158*(1), 319-325. doi:10.1016/S0006-291X(89)80215-3.

Bloemendal, H. (1982). Lens proteins. *Critical Reviews in Biochemistry, 12*(1), 1-38. doi:10.3109/10409238209105849.

Bliss, A. F. (1943). Derived photosensitive pigments from invertebrate eyes. *Journal of General Physiology, 26*(4), 361-367. doi:10.1085/jgp.26.4.361.

Bliss, A. F. (1948). The absorption spectra of visual purple of the squid and its bleaching products. *Journal of Biological Chemistry, 176*, 563-569.

Blumer, M. J. F., Salvini-Plawen, L. V., Kikinger, R., & Büchinger, (1995). Ocelli in a Cnidaria polyp: the ultrastructure of the pigment spots in *Stylocoronella riedli* (Scyphozoa, Stauromedusae). *Zoomorphology, 115*(4), 21-227. doi:10.1007/BF00393802.

Brown, N. L., Patel, S., Brzezinski, J., & Glaser, T. (2001). *Math5* is required for retinal ganglion cell and optic nerve formation. *Development, 128*, 2497-2508.

Brumwell, G. B., & Martin, V. J. (2002). Immunocytochemically defined populations of neurons progressively increase in size through embryogenesis of *Hydra vulgaris*. *Biological Bulletin, 203*(1), 70-79.

Brunekreef, G. A., van Gensen, S. T., Destrée, O. H. J., & Lubsen, N. H. (1997). Extralenticular expression of *Xenopus laevis* α-, β-, and γ-crystallin genes. *Investigative Ophthalmology and Visual Science, 38*(13), 2764-2771.

Buskey, E. J. (2003). Behavioral adaptations of the cubozoan medusa *Tripedalia cystophora* for feeding on copepod (*Dioithona oculata*) swarms. *Marine Biology, 142*(2), 225-232. doi:10.1007/s00227-002-0938-y.

Butcher, E. O. (1930). The formation, regeneration and transplantation of eyes in Pecten *(Gibbus borealis*). *Biological Bulliten, 59*, 154.

Cahn, P. H., (1958). Comparative optic development in Astyanax mexicanus and two of its blind cave derivatives. *Bulletin of the American Museum of Natural History, 115*, 75–112.

Calder, D. R. (1972). Development of the sea nettle *Chrysaora quinquecirrha* (scyphozoa, semaeostomeae). *Chesapeake Science, 13*(1), 40-44. doi:10.2307/1350549.

Callaerts, P., Munoz-Marmol, A. M., Glardon, S., Castillo, E., Sun, H., Li, W.-H.,…Salo, E. (1999). Isolation and expression of a *Pax-6* gene in the regenerating and intact planarian *Dugesia(G)tigrina*. *Proceedings of the National Academy of Sciences U.S.A., 96(*2), 558-563. doi:10.1073/pnas.96.2.558.

Cardona, A., Hartenstein, V., & Romero, R. (2005). The embryonic development of the triclad Schmidtea polychroa. *Development Genes and Evolution, 215*, 109-131. doi:10.1007/s00427-004-0455-8.

Carroll, J. (2008). Focus on molecules: the cone opsins. *Experimental Eye Research, 86*, 865-866. doi:10.1016/j.exer.2007.09.004.

Cashmore, A. R., Jarillo, J. A., Wu, Y.-J., & Liu, D. (1999). Cryptochromes: blue light receptors for plants and animals. *Science, 284*(5415), 760-765. doi:10.1126/science.284.5415.760.

Castellano, S., Lobanov, A. V., Chapple, C., Novoselov, S. V., Albrecht, M., Hua, D.,…Guigó, R. (2005). Diversity and functional plasticity of eukaryotic selenoproteins: identification and characterization of the SelJ family. *Proceedings of the National Academy of Sciences U.S.A., 102*(45), 16188-16193. doi:10.1073_pnas.0505146102.

Catmull, J., Hayward, D. C., Macintyre, N. E., Reece-Hoyes, J. S., Mastro, R., Callaerts, P.,… Miller, D. J. (1998). Pax-6 origins-implications from the structure of two coral Pax genes. *Development Genes and Evolution, 208*(6), 352-356. doi:10.1007/s004270050191.

Coates, M. M. (2003). Visual ecology and functional morphology of Cubozoa (Cnidaria). *Integrative and Comparative Biology, 43*(4), 542-548. doi:10.1093/icb/43.4.542.

Coates, M. M. (2005). *Vision in a cubozoan jellyfish,* Tripedalia cystophora. (Unpublished doctoral dissertation). Stanford University, Stanford, USA.

Coates, M. M., Garm, A., Theobald, J. C., Thompson, S. H., & Nilsson, D.-E. (2006). The spectral sensitivity of the lens eyes of a box jellyfish, *Tripedalia cystophora* (Conant). *Journal of Experimental Biology, 209*, 3758-3765. doi:10.1242/jeb.02431.

Cockell, C. S., & Knowland, J. (1999). Ultraviolet radiation screening compounds. *Biological Reviews, 74*(3), 311-345. doi:10.1111/j.1469-185X.1999.tb00189.x.

Conant, F. S. (1898). The cubomedusae. *Memoirs of the Biological Laboratory. Johns Hopkins University, 4*, 1-61.

Conn, H. W. (1900). *The method of evolution*. New York: G.P. Putnam's Sons.

Creuzet, S., Vincent, C., & Couly, G. (2005). Neural crest derivatives in ocular and periocular structures. *International Journal of Developmental Biology, 49*, 161-171. doi:10.1387/ijdb.041937sc.

Cvekl, A., & Piatigorsky, J. (1996). Lens development and crystallin gene expression: many roles for Pax-6. *BioEssays, 18*, 621-630.

Darwin, C. (1859). *On the origin of species by means of natural selection, or the preservation of favoured races in the struggle for life* (1st ed). London: John Murray.

Darwin, C. (1882). *The origin of species by means of natural selection* (6th ed). London: John Murray.

de Queiroz, A. (1999). Do image-forming eyes promote evolutionary diversification? *Evolution: International Journal of Organic Evolution, 53*(6), 1654-1664.

De Vito, D., Piraino, S., Schmich, J., Bouillon, J., & Boero, F. (2006). Evidence of reverse development in Leptomedusae (Cnidaria, Hydrozoa): the case of *Laodicea undulata* (Forbes and Goodsir 1851). *Marine Biology, 149*(2), 339-346. doi:10.1007/s00227-005-0182-3.

Demian, E. S., & Yousif, F. (1975). Embryonic development and organogenesis in the snail *Marisa cornuarietis* (Mesogastropoda: Ampullariidae). V. Development of the nervous system. *Malacologica, 15*(1), 29-42.

Dorsett, D. A., & Hyde, R. (1968). The fine structure of the lens and photoreceptors of Nereis virens. *Zeitschrift für Zellforschung, 85*(2), 243-255. doi:10.1007/BF00325039.

Dulai, K. S., von Dornum, M., Mollon, J. D., & Hunt, D. M. (1999). The evolution of trichromatic color vision by opsin gene duplication in New World and Old World primates. *Genome Research, 9*, 629-638. doi:10.1101/gr.9.7.629.

Duncan, M. K., Cvekl, A., Kantorow, M., & Piatigorsky, J. (2004). Lens crystallins. In F. J. Lovicu & M. L. Robinson (Eds.), *Development of the ocular lens.* Cambridge: Cambridge University Press.

Eakin, R. M. (1979). Evolutionary significance of photoreceptors: in retrospect. *American Zoologist, 19*(2), 647-653. doi:10.1093/icb/19.2.647.

Eakin, R. M., & Brandenburger, J. L. (1967). Differentiation in the eye of a pulmonate snail *Helix aspersa*. *Journal of Ultrastructure Research, 18*(3-4), 391-421. doi:10.1016/S0022-5320(67)80126-6.

Eakin, R. M., & Westfall, J. A. (1962). Fine structure of photoreceptors in the hydromedusan, *Polyorchis penicillatus. Proceedings of the National Academy of Sciences U.S.A., 48*(5), 826-833.

Eakin, R. M., & Westfall, J. A. (1965). Fine structure of the eye of peripatus (Onychophora). *Zeitschrift für Zellforshung, 68*, 278-300. doi:10.1007/BF00342434.

Ekström, P., Garm, A., Pålsson, J., Vihtelic, T. S., & Nilsson, D.-E. (2008). Immunohistochemical evidence for multiple photosystems in box jellyfish. *Cell and Tissue Research, 333*(1), 115-124. doi:10.1007/s00441-008-0614-8.

Eriksson, B. J., Tait, N. N., & Budd, G. E. (2003). Head development in the onychophoran *Euperipatoides kanangrensis* with particular reference to the central nervous system. *Journal of Morphology, 225*, 1-23. doi:10.1002/jmor.10034.

Fernald, R. D. (1997). The evolution of eyes. *Brain, Behavior and Evolution, 50*, 253-259. doi:10.1159/000113339.

Fernald, R. D. (2000). Evolution of eyes. *Current Opinion in Neurobiology, 10*(4), 444-450. doi:10.1016/S0959-4388(00)00114-8.

Fernald, R. D. (2004a). Evolving eyes. *International Journal of Developmental Biology, 4*, 701-705. doi:10.1387/ijdb.041888rf.

Fernald, R. D. (2004b). Eyes: variety, development and evolution. *Brain, Behavior and Evolution, 64*(3), 141-147. doi:10.1159/000079743.

Fischer, A. B., & Hofmann, D. K. (2004). Budding, bud morphogenesis, and regeneration in *Carybdea marsupialis* Linnaeus, 1758 (Cnidaria: Cubozoa). *Hydrobiologia, 530/531*(1-3), 331-337. doi:10.1007/s10750-004-2658-4.

Fox, D. L., & Crane, S. (1942). Concerning the pigments of the two-spotted octopus and the opalescent squid. *Biological Bulletin, 82*(2), 284-291.

Frey, J. (1968). Die Entwicklungsleistungen der Medusenknospen und Medusen von *Podocoryne carne*a M. Sars nach Isolation und Dissoziation. *Wilhelm Roux' Archiv für Entwicklungsmechanik der Organismen, 160*, 428-464.

Garm, A., Andersson, F., & Nilsson, D.-E. (2008). Unique structure and optics of the lesser eyes of the box jellyfish Tripedalia cystophora. *Vision Research, 48*, 1061-1073. doi:10.1016/j.visres.2008.01.019.

Garm, A., & Bielecki, J. (2008). Swim pacemakers in box jellyfish are modulated by the visual input. *Journal of Comparative Physiology A, 194*(7), 641-651. doi:10.1007/s00359-008-0336-0.

Garm, A., Coates, M. M., Gad, R., Seymour, J., & Nilsson, D.-E. (2007). The lens eyes of the box jellyfish *Tripedalia cystophora* and *Chiropsalamus* sp. are slow and color-blind. *Journal of Comparative Physiology, 193*, 547-557. doi:10.1007/s00359-007-0211-4.

Garm, A., & Ekström, P. (2010). Evidence for multiple photosystems in jellyfish. *International Review of Cell and Molecular Biology, 280*, 41-78. doi:10.1016/S1937-6448(10)80002-4.

Garm, A., Ekström, P., Boudes, M., & Nilsson, D.-E. (2006). Rhopalia are integrated parts of the central nervous system in box jellyfish. *Cell and Tissue Research, 325*(2), 333-343. doi:10.1007/s00441-005-0134-8.

Garm, A., & Mori, S. (2009). Multiple photoreceptor systems control the swim pacemaker activity in box jellyfish. *Journal of Experimental Biology, 212*, 3951-3960. doi:10.1242/jeb.031559.

Garm, A., O'Connor, M., Parkefelt, L., & Nilsson, D.-E. (2007). Visually guided obstacle avoidance in the box jellyfish *Tripedalia cystophora* and *Chiropsella bronzie*. *Journal of Experimental Biology, 210*, 3616-3623. doi:10.1242/jeb.004044.

Garm, A., Oskarsson, M., & Nilsson, D.-E. (2011). Box jellyfish use terrestrial visual cues for navigation. *Current Biology, 21*, 798-803. doi:10.1016/j.cub.2011.03.054.

Garm, A., Poussart, Y., Parkefelt, L., Ekström, P., & Nilsson, D.-E. (2007). The ring nerve of the box jellyfish *Tripedalia cystophora*. *Cell and Tissue Research, 329*, 147-157. doi:10.1007/s00441-007-0393-7.

Gehring, W. J. (2004). Historical perspective on the development and evolution of eyes and photoreceptors. *International Journal of Developmental Biology, 48*, 707-717. doi:10.1387/ijdb.041900wg.

Gehring, W. J. (2005). New perspectives on eye development and the evolution of eyes and photoreceptors. *Journal of Heredity, 96*(3), 171-184. doi:10.1093/jhered/esi027.

Gehring, W. J., & Ikeo, K. (1999). Pax 6: mastering eye morphogenesis and eye evolution. *Trends in Genetics, 15*(9), 371-377. doi:10.1016/S0168-9525(99)01776-X.

Gehring, W. J. & Seimiya, M. (2010). Eye evolution and the origin of Darwin's eye prototype. *Italian Journal of Zoology, 77*(2), 124-136. doi:10.1080/11250001003795350.

Gerl, E. J., & Morris, M. R. (2008). The causes and consequences of color vision. *Evolution: Education and Outreach, 1*(4), 476-486. doi:10.1007/s12052-008-0088-x.

Gershwin, L.-A., & Dawes, P. (2008). Preliminary observations on the response of *Chironex fleckeri* (Cnidaria: Cubozoa: Chirodropida) to different colors of light. *Biological Bulletin, 215*, 57-62.

Gilbert, S. F. (Ed.). (2006). *Developmental biology*. Sunderland, MA: Sinauer Associates.

Gladfelter, W. G. (1973). A comparative analysis of the locomotory systems of medusoid Cnidaria. *Helgolander Wissenschaftliche Meeresuntersuchungen, 25*, 228-272. doi:10.1007/BF01611199.

Gohar, H. A. F., & Eisawy, A. M. (1960). The development of *Cassiopea andromeda* (Scyphomedusae). *Publications of the Marine Biological Station, Ghardaqa, 11*, 148-190.

Goldsmith, T. H. (1990). Optimization, constraint, and history in the evolution of eyes. *Quarterly Review of Biology, 65*(3), 281-322.

Golz, R. (1994). Occurrence and distribution of RFamide-positive neurons within the polyps of *Coryne sp.* (Hydrozoa, Corynidae). *Biological Bulletin, 186*, 115-123. doi:10.2307/1542041.

Gould, S. J. (1994). Common pathways of illumination. *Natural History, 103*(12), 10-20.

Grainger, R. M. (1992). Embryonic lens induction: shedding light on vertebrate tissue determination. *Trends in Genetics, 8*(10), 349-355. doi:10.1016/0168-9525(92)90280-H.

Gray, G. C., Martin, V. J., & Satterlie, R. A. (2009). Ultrastructure of the retinal synapses in cubozoans. *Biological Bulletin, 217*, 35-49.

Gregory, T. R. (2008). The evolution of complex organs. *Evolution: Education and Outreach, 1*(4), 358-389. doi:10.1007/s12052-008-0076-1.

Green P., Hartenstein, A. Y., & Hartenstein, V. (1993). The embryonic developmentof the *Drosophila* visual system. *Cell and Tissue Research,* 273(3), 583-598.

Greiling, T. M. S., & Clark, J. I. (2008). The transparent lens and cornea in the mouse and zebra fish eye. *Seminars in Cell and Developmental Biology, 19*(2), 94-99. doi:10.1016/j.semcdb.2007.10.011.

Grimmelikhuijzen, C. J. P. (1983). FMRFamide immunoreactivity is generally occurring in the nervous system of coelenterates. *Histochemistry, 78*(3), 361-381. doi:10.1007/BF00496623.

Grimmelikhuijzen, C. J. P., Graff, D., & Spencer, A. N. (1988). Structure, location and possible actions of Arg-Phe-amide peptides in coelenterates. In M. C. Thorndyke & G. J. Goldsworthy (Eds.), *Neurohormones in invertebrates* (pp. 199-217). Cambridge: Cambridge University Press.

Grimmelikhuijzen, C. J. P., Leviev, I., & Carstensen, K. (1996). Peptides in the nervous system of cnidarians: structure, function, and biosynthesis. *International Review of Cytology, 167*, 37-89. doi:10.1016/S0074-7696(08)61345-5.

Grindley, J. C., Davidson, D. R., & Hill, R. E. (1995). The role of *Pax-6* in eye and nasal development. *Development, 121*, 1433-1442.

Gröger, H., Callaerts, P., Gehring, W. J., & Schmid, V. (2000). Characterization and expression analysis of an ancestor-type *Pax* gene in the hydrozoan jellyfish *Podocoryne carnea*. *Mechanisms of Development, 94*(1-2), 157-169. doi:10.1016/S0925-4773(00)00286-0.

Gröger, H., & Schmid, V. (2000). Nerve net differentiation in medusa development of *Podocoryne carnea*. *Scientia Marina, 64*(S1), 107-116. doi:10.3989/scimar.2000.64s1107.

Hadži, J. (1909). Über das Nervensystem von *Hydra*. *Arbeiten Zoologischen Institut der Universität Wien und der Zoologischen Station in Triest. Wien., 17*, 225-268.

Halder, G., Callaerts, P., & Gehring, W. J. (1995a). Induction of ectopic eyes by targeted expression of the eyeless gene in *Drosophila. Science, 267*(5205), 1788-1792. doi:10.1126/science.7892602.

Halder, G., Callaerts, P., & Gehring, W. J. (1995b). New perspectives on eye evolution. *Current Opinions in Genetics and Development, 5*(5), 602-609. doi:10.1016/0959-437X(95)80029-8.

Hamner, W. M. (1994). Australia's box jellyfish: a killer down under. *National Geographic Magazine, 186*(2), 116-130.

Hartwick, R. F. (1991). Observations on the anatomy, behavior, reproduction and life cycle of the cubozoan *Carybdea sivickisi*. *Hydrobiologia, 216/217*(1), 171-179. doi:10.1007/BF00026459.

Head, M. W., Peter, A., & Clayton, R. M. (1991). Evidence for the extralenticular expression of members of the β-crystallin gene family in the chick and a comparison with δ-crystallin during differentiation and transdifferentiation. *Differentiation, 48*(3), 147-156. doi:10.1111/j.1432-0436.1991.tb00253.x.

Hejtmancik, J. F., Beebe, D. C., Ostrer, H., & Piatigorsky, J. (1985). δ- and β-crystallin mRNA levels in the embryonic and posthatched chicken lens: temporal and spatial changes during development. *Developmental Biology, 109*(1), 72-81. doi:10.1016/0012-1606(85)90347-1.

Hendrickson, A., Bumsted-O'Brien, K., Natoli, R., Ramamurthy, V., Possin, D., & Provis, J. (2008). Rod photoreceptor differentiation in fetal and infant human retina. *Experimental Eye Research, 87*, 415-426. doi:10.1016/j.exer.2008.07.016.

Hermans, C. O., & Eakin, R. M. (1974). Fine structure of the eyes of an Alciopid Polychaete, *Vanadis tagensis* (Annelida). *Zoomorphology, 79*(4), 245-267. doi:10.1007/BF00277508.

Hill, A., Boll, W., Ries, C., Warner, L., Osswalt, M., Hill, M., & Noll, M. (2010). Origin of Pax and Six gene families in sponges: Single *PaxB* and *Six1/2* orthologs in *Chalinula loosanoffi*. *Developmental Biology, 343*(1-2), 106-123. doi:10.1016/j.ydbio.2010.03.010.

Hoshiyama, D., Suga, H., Iwabe, N., Koyanagi, M., Nikoh, N., Kuma, K.,…Miyata, T. (1998). Sponge *Pax* cDNA related to *Pax-2/5/8* and ancient gene duplications in the *Pax* family. *Journal of Molecular Evolution, 47*(6), 640-648. doi:10.1007/PL00006421.

Hyer, J., Kuhlman, J., Afif, E., & Mikawa, T. (2003). Optic cup morphogenesis requires pre-lens ectoderm but not lens differentiation. *Developmental Biology, 259*(2), 351-363. doi:10.1016/S0012-1606(03)00205-7.

Hyman, L. H. (1940). Phylum Cnidaria. In *The invertebrates: Protozoa through Ctenophora.* (Vol. 1., pp. 365-661). New York: McGraw-Hill.

Ingolia, T. D., & Craig, E. A. (1982). Four small *Drosophila* heat shock proteins are related to each other and to mammalian α-crystallin. *Proceedings of the National Academy of Sciences U.S.A., 79*(7), 2360-2364. doi:10.1073/pnas.79.7.2360.

Iwaki, T., Kume-Iwaki, A., & Goldman, J. E. (1990). Cellular distribution of alpha B-crystallin in non-lenticular tissues. *Journal of Histochemistry and Cytochemistry, 38*(1), 31-39. doi:10.1177/38.1.2294148.

Jacobs, D. K., Nakanishi, N., Yuan, D., Camara, A., Nichols, S. A., & Hartenstein, V. (2007). Evolution of sensory structures in basal metazoa. *Integrative and Comparative Biology, 47*(5), 712-723. doi:10.1093/icb/icm094.

Jacobson, A. G., & Sater, A. K. (1988). Features of embryonic induction. *Development, 104*, 341-359.

Jager, M., Quéinnec, E., Houliston, E., & Manuel, M. (2006). Expansion of the SOX gene family predated the emergence of the Bilateria. *Molecular Phylogenetics and Evolution, 39*(2), 468-477. doi:10.1016/j.ympev.2005.12.005.

Jan, Y. N., Ghysen, A., Christoph, I., Barbel, S., & Jan, L. Y. (1985). Formation of neuronal pathways in the imaginal discs of *Drosophila melanogaster*. Journal of Neuroscience, 5(9), 2453-2464.

Janssens, H., & Gehring, W. J. (1999). Isolation and characterization of drosocrystallin, a lens crystallin gene of *Drosophila melanogaster*. *Developmental Biology, 207*(1), 204-214. doi:10.1006/dbio.1998.9170.

Jeffery, W. R. (2005). Adaptive evolution of eye degeneration in the Mexican blind cavefish. *Journal of Heredity, 96*(3), 185-196. doi:10.1093/jhered/esi028.

Jeffery, W. R., & Martasian, D. P. (1998). Evolution of eye regression in the cavefish *Astyanax*: apoptosis and the *Pax-6* gene. *American Zoologist, 38*, 685-696. doi:10.1093/icb/38.4.685.

Jinks, R. N., Markley, T. L., Taylor, E. E., Perovich, G., Dittel, A. I., Epifanio, C. E., & Cronin, T. W. (2002). Adaptive visual metamorphosis in a deep-sea hydrothermal vent crab. *Nature, 420*, 68-70. doi:10.1038/nature01144.

Kamachi, Y., Uchikawa, M., Tanouchi, A., Sekido, R., & Kondoh, H. (2001). Pax6 and Sox2 form a co-DNA-binding partner complex that regulates initiation of lens development. *Genes and Development, 15*, 1272-1286. doi:10.1101/gad.887101.

Kaufman, H. E., Barron, B. A., & McDonald, M. B. (1998). *The Cornea* (2nd ed.). Boston: Butterworth-Heinemann.

Keenan, J., Elia, G., Dunn, M. J., Orr, D. F., & Pierscionek, B. K. (2009). Crystallin distribution patterns in concentric layers from toad eye lenses. *Proteomics, 9*, 5340-5349. doi:10.1002/pmic.200800986.

Klemenz, R., Fröhli, R., Steiger, R. H., Schäfer, R., & Aoyama, A. (1991). Alpha B-crystallin is a small heat shock protein. *Proceedings of the National Academy of Sciences U.S.A., 88(*9), 3652-3656.

Koyanagi, M., Takano, K., Tsukamoto, H., Ohtsu, K., Tokunaga, F., & Terakita, A. (2008). Jellyfish vision starts with cAMP signaling mediated by opsin-G_s cascade. *Proceedings of the National Academy of Sciences U.S.A., 105*(40), 15576-15580. doi:10.1073/pnas.0806215105.

Kortschak, R. D., Samuel, G., Saint, R., & Miller, D. J. (2003). EST analysis of the cnidarian *Acropora millepora* reveals extensive gene loss and rapid sequence divergence in the model invertebrates. *Current Biology, 13*(24), 2190-2195. doi:10.1016/j.cub.2003.11.030.

Kozmik, Z. (2005). Pax genes in eye development and evolution. *Current Opinion in Genetics and Development, 15*(4), 430-438. doi:10.1016/j.gde.2005.05.001.

Kozmik, Z., Daube, M., Frei, E., Norman, B., Kos, L., Dishaw, L. J.,…Piatigorsky, J. (2003). Role of Pax genes in eye evolution: A cnidarian *PaxB* gene uniting Pax2 and Pax6 functions. *Developmental Cell, 5*(5), 773-785. doi:10.1016/S1534-5807(03)00325-3.

Kozmik, Z., Ruzickova, J., Jonasova, K., Matsumoto, Y., Vopalensky, P., Kozmikova, I.,… Vlcek, C. (2008). Assembly of the cnidarian camera-type eye from vertebrate-like components. *Proceedings of the National Academy of Sciences U.S.A., 105*(26), 8989-8993. doi:10.1073/pnas.0800388105.

Kozmik, Z., Swamynathan, S. K., Ruzickova, J., Jonasova, K., Paces, V., Vlcek, C., & Piatigorsky, J. (2008). Cubozoan crystallins: evidence for convergent evolution of pax regulatory sequences. *Evolution and Development, 10*(1), 52-61. doi:10.1111/j.1525-142X.2007.00213.x.

Kumar, J. P. (2001). Signaling pathways in *Drosophila* and vertebrate retinal development. *Nature Reviews Genetics, 2*, 846-857. doi:10.1038/35098564.

Kumar, J. P., & Moses, K. (2001). Expression of evolutionarily conserved eye specification genes during Drosophila embryogenesis. *Development Genes and Evolution, 211*(8-9), 406-414. doi:10.1007/s004270100177.

Lam, D. M.-K., Frederick, J. M., Hollyfield, J. G., Sarthy, P., & Marc, R. E. (1982). Identification of neurotransmitter candidates in invertebrate and vertebrate photoreceptors. In J. A. Westfall (Ed.), *Visual cells in evolution* (pp. 65-80). New York: Raven Press.

Lamb, T. D. (2009). Evolution of vertebrate retinal photoreception. *Philosophical Transactions of the Royal Society B, 364*(1531), 2911-2924. doi:10.1098/rstb.2009.0102.

Land, M. F., & Fernald, R. D. (1992). The evolution of eyes. *Annual Review of Neuroscience, 15*, 1-29. doi:10.1146/annurev.ne.15.030192.000245.

Land, M. F., & Nilsson, D.-E. (2002). *Animal eyes*. Oxford: Oxford University Press.

Lane, F. (1960). *Kingdom of octopus*. New York: Sheridan House.

Langecker, T., Schmale, H., & Wilkens, H. (1993). Transcription of the opsin gene in degenerate eyes of cave dwelling *Astyanax fasciatus* (Teleostei,Characidae) and its conspecific ancestor during early ontogeny. *Cell and Tissue Research, 273*(1), 183-192. doi:1007/BF00304625.

Langecker, T. G., Wilkens, H., & Schmale, H. (1995). Developmental constraints in regressive evolution: studies of the expression of the γ_s-crystallin gene in the developing lens of cave-dwelling *Astyanax fasciatus* (Cuvier, 1819) (Teleostei, Characidae) by *in situ* hybridization. *Journal of Zoological Systematics and Evolutionary Research, 33*(3-4), 123-128. doi:10.1111/j.1439-0469.1995.tb00966.x.

Laska, V.G. & Hündgen, M. (1982). Morphologie und Ultrastruktur der Lichtsinnesorgane von *Tripedalia cystophora* Conant (Cnidaria, Cubozoa). *Zoologische Jahrbuecher Abteilung fuer Anatomie und Ontogenie der Tiere 108*, 107-123.

Levine, R. B. (1986). Reorganization of the insect nervous system during metamorphosis. *Trends in Neuroscience, 9*, 315-319. doi:10.1016/0166-2236(86)90096-2.

Li, X., Zelenka, P. S., & Piatigorsky, J. (1993). Differential expression of the two δ-crystallin genes in lens and non-lens tissues: shift favoring δ2 expression from embryonic to adult chickens. *Developmental dynamics, 196*(2), 114-123. doi:10.1002/aja.1001960205.

Lieska, N., Krotzer, K., & Yang, H. (1992). A reassessment of protein synthesis by lens nuclear fiber cells. *Experimental Eye Research, 54*, 807-811.

Luna, L. G. (Ed.). (1968). *AFIP manual of histologic staining methods* (3rd ed., pp. 104). New York: McGraw-Hill.

Lythgoe, J. N., & Partridge, J. C. (1989). Visual pigments and the acquisition of visual information. *Journal of Experimental Biology, 146*, 1-20.

Mackie, G. O. (1990). The elementary nervous system revisited. *American Zoologist, 30*(4), 907-920. doi:10.1093/icb/30.4.907.

Mackie, G. O. (1999). Coelentrate organs. *Marine and Freshwater Behaviour and Physiology, 32*(2-3), 113-127. doi:10.1080/10236249909379043.

Magabo, K. S., Horwitz, J., Piatigorsky, J., & Kantorow, M. (2000). Expression of βB_2-crystallin mRNA and protein in retina, brain, and testis. *Investigative Ophthalmology and Visual Science, 41*(10), 3056-3060.

Martin, V. J. (2000). Reorganization of the nervous system during metamorphosis of a hydrozoan planula. *Invertebrate Biology, 119*(3), 243-253. doi:10.1111/j.1744-7410.2000.tb00011.x.

Martin, V. J. (2002). Photoreceptors of cnidarians. *Canadian Journal of Zoology, 80*(10), 1703-1722. doi:10.1139/z02-136.

Martin, V. J. (2004). Photoreceptors of cubozoan jellyfish. *Hydrobiologia, 530/531*(1-3), 135-144. doi:10.1007/s10750-004-2674-4.

Martin, V., & Givens. J. (1999). Structure of cubozoan jellyfish eyes. *American Zoologist, 39*, 115A.

Masson, P. (1928). Carcinoids (argentaffin-cell tumors) and nerve hyperplasia of the appendicular mucosa. *American Journal of Pathology, 4*(3), 181-212.19.

Masson, P. (2011). Perception. In *Medical neurobiology* (pp. 383). New York: Oxford University Press.

Matus, D. Q., Pang, K., Daly, M., & Martindale, M. Q. (2007). Expression of *Pax* gene family members in the anthozoan cnidarian, *Nematostella vectensis*. *Evolution and Development, 9*(1), 25-38. doi:10.1111/j.1525-142X.2006.00135.x.

Mayer, G. (2006). Structure and development of onychophoran eyes: what is the ancestral visual organ in arthropods? *Arthropod Structure and Development, 35*, 231-245. doi:10.1016/j.asd.2006.06.003.

Mayr, E. (2001). *What evolution is*. New York: Basic Books.

McAvoy, J. W. (1978a). Cell division, cell elongation and distribution of α-, β-, and γ-crystallins in the rat lens. *Journal of Embryology and Experimental Morphology, 44*, 149-165.

McAvoy, J. W. (1978b). Cell division, cell elongation and the co-ordination of crystallin gene expression during lens morphogenesis in the rat. *Journal of Embryology and Experimental Morphology, 45*, 271-281.

McAvoy, J. W. (1980). Induction of the eye lens. *Differentiation, 17*(1-3), 137-149. doi:10.1111/j.1432-0436.1980.tb01091.x.

Meier, S. (1977). Initiation of corneal differentiation prior to cornea-lens association. *Cell and Tissue Research, 184*(2), 255-267. doi:10.1007/BF00223073.

Meinertzhagen, A. (1990). Development of the squid's visual system. In D. L. Gilbert, W. J. Adelman & J. M. Arnold (Eds.), *Squid as experimental animals*. New York: Plenum.

Mikhailov, A. T., Simirskii, V. N., Aleinikova, K. S., & Gorgolyuk, N. A. (1997). Developmental patterns of crystallin expression during lens fiber differentiation in amphibians. *International Journal of Developmental Biology, 41*, 883-891.

Miller, D. J., Hayward, D. C., Reece-Hoyes, J. S., Scholten, I., Catmull, J., Gehring, W. J.,…Ball, E. E. (2000). *Pax* gene diversity in the basal cnidarian *Acropora millepora* (Cnidaria, Anthozoa): Implications for the evolution of the *Pax* gene family. *Proceedings of the National Academy of Sciences U.S.A., 97*(9), 4475-4480. doi:10.1073/pnas.97.9.4475.

Miller, K. R. (1994). Life's grand design. *Technology Review, 97*(2), 24-32.

Morris, J., Nallur, R., Ladurner, P., Egger, B., Rieger, R., & Hartenstein, V. (2004). The embryonic development of the flatworm *Macrostomum sp*. *Development Genes and Evolution, 214*(5), 220-239. doi:1007/s00427-004-0406-4.

Müller, H. C. (1913). Die Regeneration der Gonophore bei den Hydroiden und anschliessende biologische Beobachtungen I. *Athecata. Wilhelm Roux' Archiv fur Entwicklungsmechanik der Organismen, 37*, 319-419.

Müller, P., Yanze, N., Schmid, V., & Spring, J. (1999). The homeobox gene *Otx* of the jellyfish *Podocoryne carnea*: role of a head gene in striated muscle and evolution. *Developmental Biology, 216*(2), 582-594. doi:10.1006/dbio.1999.9522.

Musio, C., Santillo, S., Taddei-Ferretti, C., Robles, L. J., Vismara, R., Barsanti, L., & Gualtieri, P. (2001). First identification and localization of a visual pigment in Hydra (Cnidaria, Hydrozoa). *Journal of Comparative Physiology A, 187*(1), 79-81. doi:10.1007/s003590100180.

Nadakal, A. M. (1960). Chemical nature of cercarial eye-spot and other tissue pigments. *Journal of Parasitology, 46*(4), 475-483.

Nakanishi, N., Hartenstein, V., & Jacobs, D. K. (2009). Development of the rhopalial nervous system in *Aurelia* sp. 1 (Cnidaria, Scyphozoa). *Development Genes and Evolution, 219*, 301-317. doi:10.1007/s00427-009-0291-y.

Nakanishi, N., Yuan, D., Hartenstain, V., & Jacobs, D. K. (2010). Evolutionary origin of rhopalia: insights from cellular-level analysis of Otx and POU expression patterns in the developing rhopalial nervous system. *Evolution and Development, 12*(4), 404-415. doi:10.1111/j.1525-142X.2010.00427.x.

Nakanishi, N., Yuan, D., Jacobs, D. K., & Hartenstein, V. (2008). Early development, pattern, and reorganization of the planula nervous system in *Aurelia* (Cnidaria, Scyphozoa). *Development Genes and Evolution, 218*, 511-524. doi:10.1007/s00427-008-0239-7.

Nilsson, D.-E. (1989). Vision optics and evolution: Nature's engineering has produced astonishing diversity in eye design. *Bioscience, 39*(5), 298-307.

Nilsson, D.-E. (1990). From cornea to retinal image in invertebrate eyes. *Trends in Neurosciences, 13*(2), 55-64. doi:10.1016/0166-2236(90)90069-M.

Nilsson, D.-E. (1996). Eye ancestry: old genes for new eyes. *Current Biology, 6*(1), 39-42. doi:10.1016/S0960-9822(02)00417-7.

Nilsson, D.-E. (2009). The evolution of eyes and visually guided behaviour. *Philosophical Transactions of the Royal Society B, 364*(1531), 2833-2847. doi:10.1098/rstb.2009.0083.

Nilsson, D.-E., Coates, M. M., Gislén, I., Skogh, C., & Garm, A. (2005). Advanced optics in a jellyfish eye. *Nature, 435*, 201-205. doi:10.1038/nature03484.

Nilsson, D.-E., & Pelger, S. (1994). A pessimistic estimate of the time required for an eye to evolve. *Proceedings of the Royal Society of London B, 256*(1345), 53-58. doi:10.1098/rspb.1994.0048.

Nordström, K., Wallen, R., Seymour, J., & Nilsson, D. (2003). A simple visual system without neurons in jellyfish larvae. *Proceedings of the Royal Society B, 270*(1531), 2349-2354. doi:10.1098/rspb.2003.2504.

Oakley, T. H. (2003). The eye as a replicating and diverging, modular developmental unit. *Trends in Ecology and Evolution, 18*(12), 623-627. doi:10.1016/j.tree.2003.09.005.

O'Connor, M., Garm, A., Marshall, J. N., Hart, N. S., Ekström, P., Skogh, C., & Nilsson, D.-E. (2010). Visual Pigment in the lens eyes of the box jellyfish *Chiropsella bronzie*. *Proceedings of the Royal Society B, 277*, 1843-1848. doi:10.1098/rspb.2009.2248.

O'Connor, M., Garm, A., & Nilsson, D.-E. (2009). Structure and optics of the eyes of the box jellyfish *Chiropsella bronzie*. *Journal of Comparative Physiology A, 195*, 557-569. doi:10.1007/s00359-009-0431-x.

O'Connor, M., Nilsson, D.-E., & Garm, A. (2010). Temporal properties of the lens eyes of the box jellyfish *Tripedalia cystophora*. *Journal of Comparative Physiology, 196*, 213-220. doi:10.1098/rspb.2009.2248.

Osorio, D. (1994). Eye evolution: Darwin's shudder stilled. *Trends in Ecology and Evolution, 9*(7), 241-242.

Parkefelt, L., & Ekström, P. (2009). Prominent system of RFamide immunoreactive neurons in the rhopalia of box jellyfish (Cnidaria: Cubozoa). *Journal of Comparative Neurology, 516*(3), 157-165. doi:10.1002/cne.22072.

Parkefelt, L., Skogh, C., Nilsson, D.-E., & Ekström, P. (2005). Bilateral symmetric organization of neural elements in the visual system of a coelenterate, *Tripedalia cystophora* (Cubozoa). *Journal of Comparative Neurology, 492*(3), 251-262. doi:10.1002/cne.20658.

Pearse, J. S. & Pearse, V. B. (1978). Vision in cubomedusan jellyfishes. *Science, 199*(4327), 458. doi:10.1126/science.22934.

Peters, N. & Peters G. (1973). Problemes genetiques de l' evolution regressive des cavernicoles. In L. H. Schroeder (Ed), *Genetics and Mutagenesis is Fish* (pp. 187-201). New York, Springer-Verlag.

Piatigorksy, J. (1981). Lens differentiation in vertebrates: a review of cellular and molecular features. *Differentiation, 19*(1-3), 134-153. doi:10.1111/j.1432-0436.1981.tb01141.x.

Piatigorsky, J. (1998). Multifunctional lens crystallins and corneal enzymes: more than meets the eye. *Annals of the New York Academy of Sciences, 842*, 7-15. doi:10.1111/j.1749-6632.1998.tb09626.x.

Piatigorsky, J. (2007). *Gene sharing and evolution: the diversity of protein functions*. Cambridge: Harvard University Press.

Piatigorsky, J. (2008a). Evolution of mollusc lens crystallins: glutathione S-transferase/S-crystallins and aldehyde dehydrogenase/ Ω-crystallins. *American Malacological Bulletin, 26*(1-2), 73-81. doi:10.4003/006.026.0208.

Piatigorsky, J. (2008b). A genetic perspective on eye evolution: gene sharing, convergence and parallelism. *Evolution: Education and Outreach, 1*, 403-414. doi:1007/s12052-008-0077-0.

Piatigorsky, J., Horwitz, J., Kuwabara, T., & Cutress, C. E. (1989). The cellular eye lens and crystallins of cubomedusan jellyfish. *Journal of Comparative Physiology, 164*(5), 577-587. doi:10.1007/BF00614500.

Piatigorksy, J., Horwitz, J., & Norman, B. L. (1993). J1-crystallins of the cubomedusan jellyfish lens constitute a novel family encoded in at least three intronless genes. *Journal of Biological Chemistry, 268*, 11894-11901.

Piatigorsky, J., & Kozmik, Z. (2004). Cubozoan jellyfish: an Evo/Devo model for eyes and other sensory systems. *International Journal of Developmental Biology, 48*(8-9), 719-729. doi:10.1387/ijdb.041851jp.

Piatigorsky, J., Kozmik, Z., Horwitz, J., Ding, L., Carosa, E., Robison, W. G.,…Tamm, E. R. (2000). Omega-crystallin of the scallop lens. A dimeric aldehyde dehydrogenase class 1/2 enzyme-crystallin. *Journal of Biological Chemistry, 275*(52), 41064-41073.

Piatigorsky, J., Norman, B., Shaw, L. J., Kos, L., Horwitz, J., Steinbach, P. J., & Kozmik, Z. (2001). J3-crystallins of the jellyfish lens: Similarity to saposins. *Proceedings of the National Academy of Sciences U.S.A., 98*(22), 12362-12367. doi:10.1073/pnas.231310698.

Piatigorsky, J., & Wistow, G. J. (1989). Enzyme/crystallins: gene sharing as an evolutionary strategy. *Cell, 57*, 197–199. doi:10.1016/0092-8674(89)90956-2.

Pierce, K. L., Premont, R. T., & Lefkowitz, R. J. (2002). Seven-transmembrane receptors. *Nature Reviews Molecular Cell Biology, 3*, 639-650. doi:10.1038/nrm908.

Piraino, S., Boero, F., Aeschbach, B., & Schmid, V. (1996). Reversing the life cycle: medusae transforming into polyps and cell transdifferentiation in *Turritopsis nutricula* (Cnidaria, Hydrozoa). *Biological Bulletin, 190*, 302-312.

Piraino, S., De Vito, D., Schmich, J., Bouillon, J., & Boero, F. (2004). Reverse development in Cnidaria. *Canadian Journal of Zoology, 82*, 1748-1754. doi:10.1139/Z04-174.

Plachetzki, D. C., Degnan, B. M., & Oakley, T. H. (2007). The origins of novel protein interactions during animal opsin evolution. *PLoS One, 10*, e1054.

Plaza, S., de Jong, D. M., Gehring, W. J., & Miller, D. J. (2003). DNA-binding characteristics of cnidarian Pax-C and Pax-B proteins *in vivo* and *in vitro*: no simple relationship with the Pax-6 and Pax-2/5/8 classes. *Journal of Experimental Zoology Part B: Molecular and Developmental Evolution, 299B*(1), 26-35. doi:10.1002/jez.b.38.

Plickert, G., & Schneider, B. (2004). Neuropeptides and photic behavior in Cnidaria. *Hydrobiologia, 530/531*(1-3), 49-57. doi:10.1007/s10750-004-2689-x.

Prophet, E. B., Mills, B., Arrington, J. B., & Sobin, L. H. (Eds.). (1992). *Armed Forces Institute of Pathology Laboratory Methods in Histotechnology* (pp. 186). Washington, D. C.: American Registry of Pathology.

Puce, S., Bavestrello, G., Azzini, F., & Cerrano, C. (2003). On the occurrence of *Coryne eximia* Allman (Cnidaria, Corynidae) in the Mediterranean sea. *Italian Journal of Zoology, 70*(3), 249-252. doi:10.1080/11250000309356525.

Purschke, G. (2005). Sense organs in polychaetes (Anneldia). *Hydrobiologia 535/536*, 53–78. doi:10.1007/s10750-004-4358-5.

Purschke, G., Arendt, D., Hausen, H., & Müller, M.C.M. (2006). Photoreceptor cells and eyes in Annelida. *Arthropod Structure and Development, 35*, 211–230. doi:10.1016/j.asd.2006.07.005.

Rabaey, M. (1965). Lens proteins during embryonic development of different vertebrates. *Investigative Ophthalmology & Visual Science, 4*(4), 560-578.

Raymond, P. A. (1985). Cytodifferentiation of photoreceptors in larval goldfish: delayed maturation of rods. *Journal of Comparative Neurology, 236*, 90-105. doi:10.1002/cne.902360108.

Ready, D. F., Hanson, T. E., & Benzer, S. (1976). Development of the *Drosophila* retina, a neurocrystalline lattice. *Developmental Biology, 53*(2), 217-240.

Reber-Müller, S., Streitwolf-Engel, R., Yanze, N., Schmid, V., Stierwald, M., Erb, M., & Seipel, K. (2006). BMP2/4 and BMP5-8 in jellyfish development and transdifferentiation. *International Journal of Developmental Biology, 50*(4), 377-384. doi:10.1387/ijdb.052085sr.

Rhode, B. (1991). Ultrastructure of prostomial photoreceptors in four marine polychaete species (annelida). *Journal of Morphology, 209*(2), 177-188. doi:10.1002/jmor.1052090205.

Rhode, B. (1992). Development and differentiation of the eye in *Platynereis dumerilii*. *Journal of Morphology, 212* (1), 71-85. doi:10.1002/jmor.1052120108.

Richard, M., Muschalik, N., Grawe, F, Özüyaman, S., & Knust, E. (2009). A role for the extracellular domain of Crumbs in morphogenesis of Drosophila photoreceptor cells. *European Journal of Cell Biology,88*(12), 765-777. doi:10.1016/j.ejcb.2009.07.006.

Riley, P. A. (1997). Molecules in focus: melanin. *International Journal of Biochemistry and Cell Biology, 29*(11), 1235-1239. doi:10.1016/S1357-2725(97)00013-7.

Robinson, M. L., & Overbeek, P. A. (1996). Differential expression of alpha A- and alpha B-crystallin during murine ocular development. *Investigative Ophthalmology and Visual Science, 37*(11), 2276-2284.

Saha, M. S., Spann, C. L., & Grainger, R. M. (1989). Embryonic lens induction: more than meets the optic vesicle. *Cell differentiation and development, 28*(3), 153-171. doi:10.1016/0922-3371(89)90001-4.

Salvini-Plawen, L., & Mayr, E. (1977). On the evolution of photoreceptors and eyes. *Evolutionary Biology, 10*, 207-263.

Satterlie, R. A. (1979). Central control of swimming in the cubomedusan jellyfish *Carybdea rastonii.* *Journal of Comparative Physiology, 133*(4), 357-367. doi:10.1007/BF00661138.

Satterlie, R. A. (2002). Neuronal control of swimming in a jellyfish: a comparative story. *Canadian Journal of Zoology, 80*, 1654-1669. doi:10.1139/Z02-132.

Satterlie, R. A. (2011). Do jellyfish have central nervous systems? *Journal of Experimental Biology, 214*, 1215-1223. doi:10.1242/jeb.043687.

Satterlie, R. A., & Nolen, T. G. (2001). Why do cubomedusae have only four swim pacemakers? *Journal of Experimental Biology, 204*, 1413-1419.

Satterlie, R. A., & Spencer, A. N. (1979). Swimming control in a cubomedusan jellyfish. *Nature, 281*, 141-142. doi:10.1038/281141a0.

Satterlie, R. A., Thomas, K. S., & Gray, C. (2005). Muscle organization of the cubozoan jellyfish *Tripedalia cystophora* Conant 1897. *Biological Bulletin, 209*, 154-163.

Schmich, J., Kraus, Y., De Vito, D., Graziussi, D., Boero, F., & Piraino, S. (2007). Induction of reverse development in two marine hydrozoans. *International Journal of Developmental Biology, 51*, 45-56. doi:10.1387/ijdb.062152js.

Schmid, V. (1972). Untersuchungen über Dedifferenzierungsvorgänge bei Medusenknospen und Medusen von *Podocoryne carnea* M. *Sars. Wilhelm Roux' Archiv fur Entwicklungsmechanik der Organismen, 169*, 281-307.

Schneider, K. C. (1890). Histologie von *Hydra fusca* mit besonderer Berücksichtigung des Nervensystems der Hydropopypen. *Archiv für Mikroskopische Anatomie, 35*, 321-379.

Secutti, S., & Trajano, E. (2009). Reproductive behavior, development and eye regression in the cave armored catfish, *Ancistrus cryptophthalmus* Reis, 1987 (Siluriformes: Loricariidae), breed in laboratory. *Neotropical Ichthyology, 7*(3), 479-490. doi:10.1590/S1679-62252009000300016.

Seidou, M., Sugahara, M., Uchiyama, H., Hiraki, K., Hamanaka, T., Michinomae, M.,…Kito, Y. (1990). On the three visual pigments in the retina of the firefly squid, *Watasenia scintillans*. *Journal of Comparative Physiology A, 166*(6), 769-773. doi:10.1007/BF00187321.

Sheehan, D. C., & Hrapchak, B. R. (1980). *Theory and practice of histotechnology* (2nd ed., pp. 220-221). St. Louis: C. V. Mosby Co.

Shigeno, S., Tsuchiya, K., & Segawa, S. (2001). Embryonic and paralarval development of the central nervous system of the loliginid squid Sepioteuthis lessoniana. *Journal of Comparative Neurology, 437*(4), 449-475. doi:10.1002/cne.1295.

Shinohara, T., & Piatigorsky, J. (1980). Persistence of crystallin messenger RNA's with reduced translation in hereditary cataracts in mice. *Science, 210*, 914-916. doi:10.1126/science.7434006.

Simpson, T. I., & Price, D. J. (2002). Pax6; a pleiotropic player in development. *BioEssays, 24*(11), 1041-1051. doi:10.1002/bies.10174.

Singla, C. L. (1974). Ocelli of hydromedusae. *Cell and Tissue Research, 149*(3), 413-429. doi:10.1007/BF00226774.

Singla, C. L. (1975). Ultrastructure of the eyes of Arctonoë vittata grube (polychaeta, polynoidae). *Journal of Ultrastructure Research, 52*(3), 333-339. doi:10.1016/S0022-5320(75)80073-6.

Singla, C. L., & Weber, C. (1982). Fine structure studies of the ocelli of *Polyorchis pencillatus* (Hydrozoa, Anthomedusae) and their connection with the nerve ring. *Zoomorphology, 99*(2), 117-129. doi:10.1007/BF00310304.

Skogh, C., Garm, A., Nilsson, D.-E., & Ekström, P. (2006). Bilaterally symmetrical rhopalial nervous system of the box jellyfish *Tripedalia cystophora*. *Journal of Morphology, 267*, 1391-1405. doi:10.1002/jmor.10472.

Smith, K. M., Gee, L., Blitz, I. L., & Bode, H. R. (1999). *CnOtx*, a member of the Otx gene family, has a role in cell movement in hydra. *Developmental Biology, 212*(2), 392-404. doi:10.1006/dbio.1999.9337.

Smith, R. S., Kao, W. W.-Y., & John, S. W. M. (2002). Ocular development. In R. S. Smith, S. W. M. John, P. M. Nishina, & J. P. Sundberg (Eds.), *Systematic Evaluation of the Mouse Eye* (pp. 45-63). New York: CRC Press.

Smolich, B. D., Tarkington, S. K., Saha, M. S., & Grainger, R. M. (1994). Xenopus γ-crystallin gene expression: evidence that the γ-crystallin gene family is transcribed in lens and nonlens tissues. *Molecular and Cellular Biology, 14*(2), 1355-1353.

Sötje, F., Neues, F., Epple, M., Ludwig, W., Rack, A., Gordon, M.,…Tiemann, H. (2011). Comparison of the statolith structures of *Chironex fleckeri* (Cnidaria, Cubozoa) and *Periphylla periphylla* (Cnidaria, Scyphozoa): a phylogenetic approach. *Marine Biology, 158*(5), 1149-1161. doi:10.1007/s00227-011-1637-3.

Spangenberg, D. B. (1991). Rhopalium development in *Aurelia aurita* ephyrae. *Hydrobiologia, 216/217*(1), 45-49.

Srinivasan, A. N., Nagineni, C. N., & Bhat, S. P. (1992). αA-crystallin is expressed in non-ocular tissues. *Journal of Biological Chemistry, 267*(32), 23337-23341.

Stangl, K., Salvini-Plawen, L. V., & Holstein, T. W. (2002). Staging and Induction of medusa metamorphosis in *Carybdea marsupialis* (cnidaria, cubozoa). *Vie Milieu, 52*(4), 131-140.

Stearns, S. C. (1992). *The evolution of life histories*. New York: Oxford University Press.

Steller, H., Fischbach, K.-F., & Rubin, G. M. (1987). *disconnected*: a locus required for neuronal pathway formation in the visual system of drosophila. *Cell, 50*(7), 1139-1153. doi:10.1016/0092-8674(87)90180-2.

Stewart, S. E. (1996). Field behavior of *Tripedalia cystephora* (class Cubozoa). *Marine and Freshwater Behavioral Physiology, 27*(2-3), 175-188. doi:10.1080/10236249609378963.

Stierwald, M. (2004). *On the evolution of cnidarian eyes*. (Doctoral dissertation, University of Basel, Basel, Switzerland). Retrieved from http://edoc.unibas.ch/100/

Stierwald, M., Yanze, N., Bamert, R. P., Kammermeier, L., & Schmid, V. (2004). The *Sine oculis/Six* class family of homeobox genes in jellyfish with and without eyes: development and eye regeneration. *Developmental Biology, 274*(1), 70-81. doi:10.1016/j.ydbio.2004.06.018.

Straehler-Pohl, I., & Jarms, G. (2005). Life cycle of *Carybdea marsupialis* Linnaeus, 1758 (Cubozoa, Carybdeidae) reveals metamorphosis to be a modified strobilation. *Marine Biology, 147*, 1271-1277. doi:10.1007/s00227-005-0031-4.

Suga, H., Schmid, V., & Gehring, W. J. (2008). Evolution and functional diversity of jellyfish opsins. *Current Biology, 18*(1), 51-55. doi:10.1016/j.cub.2007.11.059.

Suga, H., Tschopp, P., Graziussi, D. F., Stierwald, M., Schmid, V., & Gehring, W. J. (2010). Flexibly deployed *Pax* genes in eye development at the early evolution of animals demonstrated by studies on a hydrozoan jellyfish. *Proceedings of the National Academy of Sciences U.S.A., 107*(32), 14263-14268. doi:10.1073/pnas.1008389107.

Sun, H., Rodin, A., Zhou, Y., Dickinson, D. P., Harper, D. E., Hewett-Emmett, D., & Li, W.-H. (1997). Evolution of paired domains: Isolation and sequencing of jellyfish and hydra *Pax* genes related to *Pax-5* and *Pax-6*. *Proceedings of the National Academy of Sciences U.S.A., 94*(10), 5156-5161.

Suschenko, D., & Purschke, G. (2009). Ultrastructure of pigmented adult eyes in errant polychaetes (Annelida): implications for annelid evolution. *Zoomorphology, 128*, 75-96. doi:10.1007/s00435-008-0075-3.

Svet, V. D., & Khazen, A. M. (2009). About the formation of an image in the inverted retina of the eye. *Biophysics, 54*(2), 193-203. doi:10.1134/S0006350909020146.

Szymonowicz, L., & MacCallum, J. B. (2010). Microscopic anatomy of the organs. In *A textbook of histology and microscopic anatomy of the human body: including microscopic technique* (reprint). Whitefish, Montana: Kessinger Publishing LLC.

Taddei-Ferretti, C., Musio, C., Sentillo, S., & Cotugno, A. (2004). The photobiology of *Hydra's* periodic activity. *Hydrobiologia, 530/531*, 129-134. doi:10.1007/978-1-4020-2762-8_16.

Terakita, A. (2005). The opsins. *Genome Biology 6*, 213-213.9. doi:10.1186/gb-2005-6-3-213.

Thomas, G., Zelenka, P. S., Cutherbertson, R. A., Norman, B. L., & Piatigorsky, J. (1990). Differential expression of the two δ-crystallin/argininosuccinate lysase genes in lens heart and brain of chicken embryos. *New Biology, 2*(10), 903-914.

Thut, C. J., Rountree, R. B., Hwa, M., & Kingsley, D. M. (2001). A large-scale *in situ* screen provides molecular evidence for the induction of eye anterior segment structures by the developing lens. *Developmental Biology, 231*, 63-76. doi:10.1006/dbio.2000.0140.

Toh, Y., Yoshida, M., & Tateda, H. (1979). Fine structure of the ocellus of the hydromedusan, *Spirocodon salatrix*. I. Receptor cells. *Journal of Ultrastructure Research, 68*(3), 341-352. doi:10.1016/S0022-5320(79)90166-7.

Tomarev, S. I., & Piatigorksy, J. (1996). Lens crystallins of invertebrates: diversity and recruitment from detoxification enzymes and novel proteins. *European Journal of Biochemistry, 235*(3), 449-465. doi:10.1111/j.1432-1033.1996.00449.x.

Tomlinson, A., & Ready, D. F. (1987). Neuronal differentiation in the *Drosophila* ommatidium. *Developmental Biology, 120*(2), 366-376. doi: 10.1016/0012-1606(87)90239-9.

Treton, J. A., Shinohara, T., & Piatigorsky, J. (1982). Degradation of δ-crystallin mRNA in the lens fiber cells of the chicken. *Developmental Biology, 92*(1), 60-65. doi:10.1016/0012-1606(82)90150-6.

Tsuda, M. (1987). Photoreception and phototransduction in invertebrate photoreceptors. *Photochemistry and Photobiology, 45*(S1), 915-931. doi:10.1111/j.1751-1097.1987.tb07903.x.

van Leen, R. W., van Roozendaal, K. E. P., Lubsen, N. H., & Schoenmakers, J. G. G. (1987). Differential expression of crystallin genes during development of the rat eye lens. *Developmental Biology, 120*(2), 457-464. doi:10.1016/0012-1606(87)90249-1.

von Döhren, J., & Bartolomaeus, T. (2007). Ultrastructure and development of the rhabdomeric eyes in *Lineus viridis* (Heteronemertea, Nemertea). *Zoology, 110*(5), 430-438. doi:10.1016/j.zool.2007.07.006.

Watanabe, H., Fujisawa, T., & Holstein, T. W. (2009). Cnidarians and the evolutionary origin of the nervous system. *Development, Growth and Differentiation, 51*, 167-183. doi:10.1111/j.1440-169X.2009.01103.x.

Weber, C. (1981a). Lens of the hydromedusan, *Cladonema* studied by SDS gel electrophoresis and immunofluorescent technique. *Journal of Experimental Zoology, 217*(1), 15-21. doi:10.1002/jez.1402170103.

Weber, C. (1981b). Structure, histochemistry, ontogenetic development and regeneration of the ocellus of *Cladonema radiatum* Dujardin (Cnidaria, Hydrozoa, Anthomedusae). *Journal of Morphology, 167*(3), 313-331. doi:10.1002/jmor.1051670306.

Weber, C. (1982a). Electrical activities of a type of electroretinogram recorded from the ocellus of a jellyfish, *Polyorchis pencillatus* (Hydromedusae). *Journal of Experimental Zoology, 223*(3), 231-243. doi:10.1002/jez.1402230305.

Weber, C. (1982b). Electrical activity in response to light of the ocellus of the hydromedusan, *Sarsia tubulosa*. *Biological Bulletin, 162*, 413-422. doi:10.2307/1540993.

Wehner, R. (1987). Matched filters neural models of the external world. *Journal of Comparative Physiology A, 161*(4), 511-532. doi:10.1007/BF00603659.

Werner, B., Chapman, D. M., & Cutress, Ch. E. (1976). Muscular and nervous systems of the cubopolyp (Cnidaria). *Cellular and Molecular Life Sciences, 32*(8), 1047-1049. doi:10.1007/BF01933964.

West, J. A. (1993). *Comparative development of the cephalopod and teleost ocular lens*. (Unpublished doctoral dissertation). University of Waterloo, Waterloo, Ontario, Canada.

West, J. A., Sivak, J. G., Pasternak, J., & Piatigorsky, J. (1994). Immunolocalization of S-crystallins in the developing squid (*Loligo opalescens*) lens. Developmental *Dynamics, 199*(2), 85-92. doi:10.1002/aja.1001990202.

Wilkens, H. (1988). Evolution and genetics of epigean and cave *Astyanax fasciatus* (Characidae: Pisces). *Evolutionary Biology, 23*, 271-367.

Wilkens, H. (2001). Convergent adaptations to cave life in the *Rhamdia latucauda* catfish group (Pimelodidae: Teleostei). *Environmental Biology of Fishes, 62*, 251-261. doi:10.1023/A:1011897805681.

Wistow, G. J., Mulders, J. W. M., & de Jong, W. W. (1987). The enzyme lactate dehydrogensase as a structural protein in avian and crocodilian lenses. *Nature, 326*, 622-624. doi:10.1038/326622a0.

Wistow, G., & Piatigorsky, J. (1987). Recruitment of enzymes as lens structural proteins. *Science, 236*(4808), 1554-1556. doi:10.1126/science.3589669.

Wistow, G., & Piatigorsky, J. (1988). Lens crystallins: The evolution and expression of proteins for a highly specialized tissue. *Annual Review of Biochemistry, 57*, 479-504. doi:10.1146/annurev.bi.57.070188.002403.

Yamamoto, M., & Yoshida, M. (1980). Fine structure of ocelli of an anthomedusan, *Nemopsis dofleini*, with special reference to synaptic organization. *Zoomorphology, 96*(3), 169-181. doi:10.1007/BF00310283.

Yamasu, T., & Yoshida, M. (1976). Fine structure of complex ocelli of a cubomedusan, *Tamoya bursaria* Haeckel. *Cell and Tissue Research, 170*(3), 325-339. doi:10.1007/BF00219415.

Yatsu, N. (1917). Notes on the physiology of *Charybdea rastonii*. *The Journal of the College of Science, Imperial University of Tokyo, 40*, 1-12.

Yoshida, M., & Yoshino, Y. (1980). Differentiation of ocelli in ephyrae of *Aurelia aurita*. In P. Tardent & R. Tardent (Eds.), *Developmental and Cellular Biology of Coelenterates* (pp. 343-346). New York: Elsevier/North-Holland Biomedical Press.

Younossi-Hartenstein, A., Ehlers, U., & Hartenstein, V. (2000). Embryonic development of the nervous system of the rhabdocoel flatworm *Mesostoma lingua* (Abildgaard, 1789). *Journal of Comparative Neurology, 434*, 56-58. doi:10.1002/(SICI)1096-9861(20000124)416.

Yuan, D., Nakanishi, N., Jacobs, D. K., & Hartenstein, V. (2008). Embryonic development and metamorphosis of the scyphozoan *Aurelia*. *Development Genes and Evolution, 218*, 525-539. doi:10.1007/s00427-008-0254-8.

Zhao, Y, Ju, F., Zhao, Y., Wang, L., Sun, Z., Liu, M., & Gao, L. (2011). The expression of αA- and βB1-crystallin during normal development and regeneration, and proteomic analysis for the regenerating lens in *Xenopus laevis*. *Molecular Vision, 17*, 768-778.

Zieske, J. D. (2004). Corneal development associated with eyelid opening. *International Journal of Developmental Biology, 48*, 903-911.

Table 1. Changes in Size (μm) of Eyes and Ocelli Over the Course of Transformation

Eye Type	Adult	Stage 1	Stage2	Stage3	Stage4	Stage5	Stage 7
Large lensed eye	D: 400	N/A	D: 30	D: 62	D: 84	D: 93	D: 96
Small lensed eye	L: 300 H: 250	N/A	D: 30	L: 63 H: 40	L: 77 H: 43	L: 88 H: 46	L: 89 H: 55
Slit ocelli	L: 250 H: 100	N/A	N/A*	L: 44 H: 30	L: 56 H: 37	L: 65 H: 36	L: 72 H: 41
Pit ocelli	D: 150	N/A	N/A*	D: 32	D: 38	D: 41	D: 44

Note. D=diameter; L=length; H=height

*Slit-shaped indentations and pit-shaped indentations representing the early simple ocelli were not able to be accurately measured but are present during this stage.

Table 2. Time-Table of the Appearance of UV Opsin-Like Protein, Melanin, and J1-Crystallin

~Day ⟶	Stage 0 0	Stage 1 1-3	Stage 2 4	Stage 3 5-7	Stage 4 8-11	Stage 5 12	Stage 7 14	Adult	
Large complex eye	-	-	-	-	+	+	+	+	OPSIN
	-	-	-	+	+	+	+	+	
	-	-	-	+	+	+	+	+	
Small complex eye	-	-	-	+	+	+	+	+	MELANIN
	-	-	+	+	+	+	+	+	
	-	-	-	-	+	+	+	+	
Slit ocelli	-	-	-	-	-	-	-	-	CRYSTALLIN*
	-	-	-	+	+	+	+	+	
	-	-	-	-	+	+	+	+	
Pit ocelli	-	-	-	-	-	-	-	-	
	-	-	-	+	+	+	+	+	
	-	-	-	-	-	-	-	+	

Note. (+) = presence of protein; (-) = absence of protein
*Lens-specific crystallin

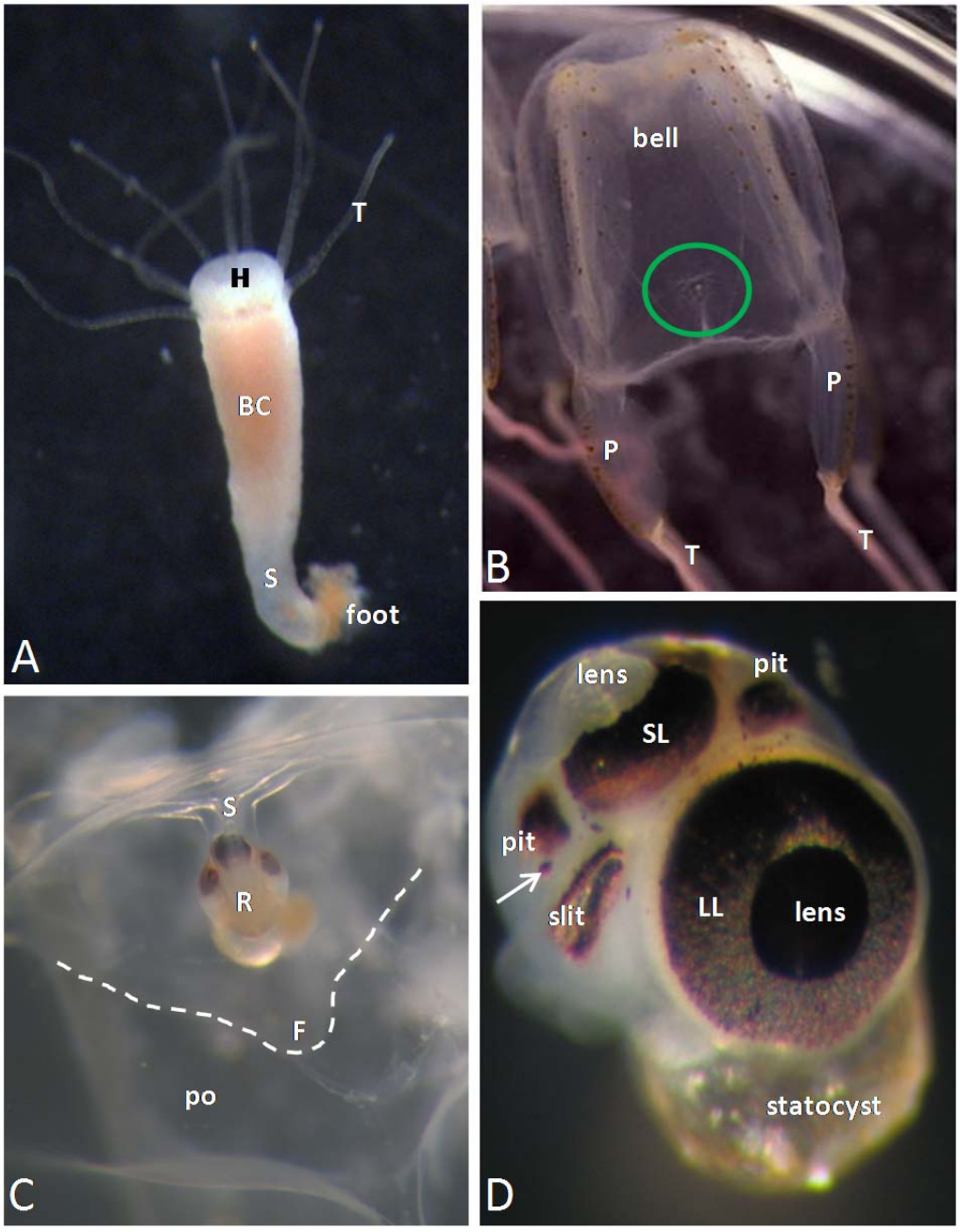

Figure 1. Brightfield images of a steady-state polyp, adult medusa, and adult rhopalium. A. Steady-state polyp. The body column (BC) is attached to the hypostome (H), the base of which is surrounded by a ring of tentacles (T), and to the stalk (S) and foot which attaches the animal to the substrate. B. Adult medusa. Rhopalia (green circle) are located on each quadrant of the bell. A single tentacle (T) hangs from a pedalium (P) located at each of the four bottom corners of the bell. Photo courtesy of Dr. Vicki Martin. C. Each rhopalium (R) in adult medusae is located in an indented pocket of the bell (po) and hangs by a stalk (S). A flap of cells (F/hashed line) covers the rhopalium, acting as a rudimentary eyelid. D. Adult rhopalium. Two complex eyes and two pairs of simple ocelli are located on the rhopalium which has a basal statocyst. The large lensed eye (LL) is oriented inward towards the center of the bell, the small lensed eye (SL) is oriented upward towards the apex of the bell, and the pair of slit ocelli (slit) and the pair of pit ocelli (pit) are oriented inward. The lenses of the complex eyes are oriented within the pigment cup openings. The small structure that is often located between the slit and pit ocellus is also visible (white arrow).

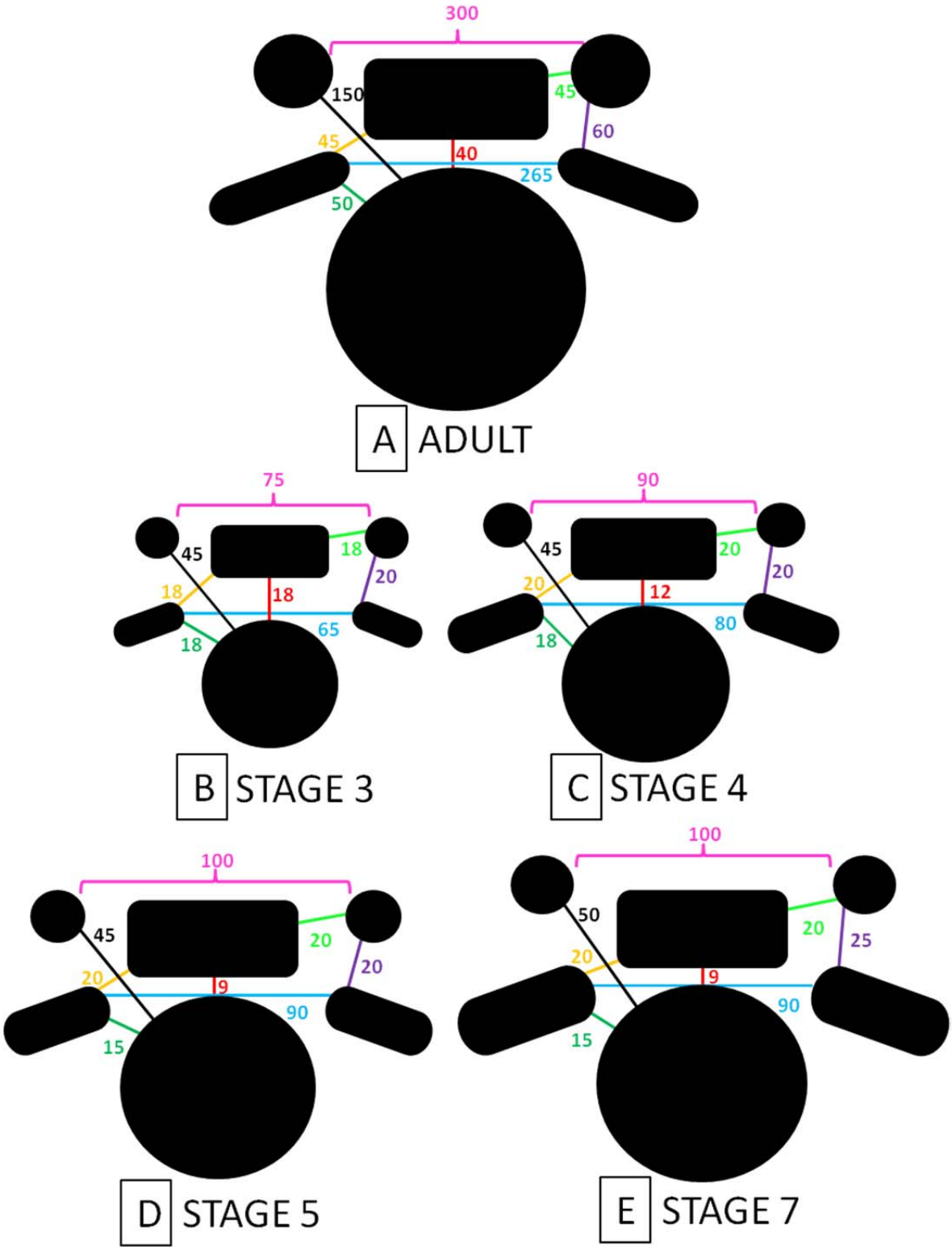

Figure 2. The change in distance (μm) between the developing eyes/ocelli during transformation. The distances were measured between the pigment cups of adjacent eyes/ocelli in adult rhopalia (A), during Stage 3 (B), Stage 4 (C), Stage 5 (D), and Stage 7 (E). The distances given are proportional to the sizes of the pigment cups of the eyes and ocelli at each stage.

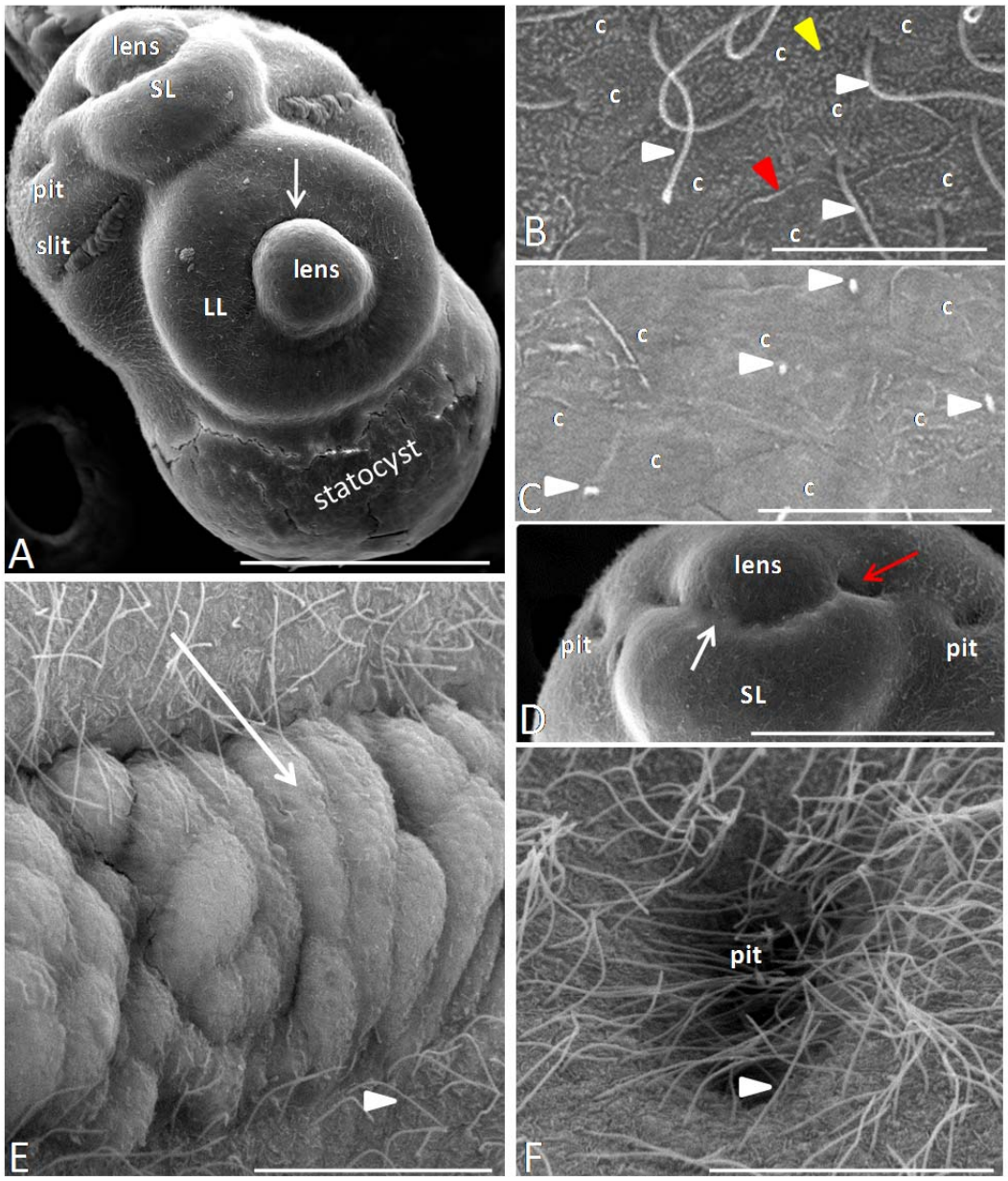

Figure 3. Scanning electron microscope (SEM) images of adult rhopalia. A. Adult rhopalium. The raised doughnut-shaped retina and down-facing deep groove (arrow) of the large complex eye (LL) can be seen. The small complex eye (SL), slit ocelli (slit), and pit ocelli (pit) can also be seen along with the basal statocyst. Scale bar=300 µm. B. Small complex eye surface. The surface cells (c) covering the lens are 5-8 µm in diameter and have a rough surface due to the presence of numerous microvilli along the cell perimeter (red arrowhead) and across the cell surface (yellow arrowhead). The cilia of these cells (white arrowheads) are 10-15 µm in length. Scale bar=10 µm. C. Large complex eye surface. The surface cells (c) of the large complex eye are 5-8 µm in diameter and have a smooth surface. The cilia (arrowheads) of these cells are reduced in length to less than 3 µm. Scale bar=10 µm. D. Small complex eye. The tapering and abrupt ending of the retinal tissue up around the lens of the small complex eye is shown (red arrow) along with the up-facing groove (white arrow). The pit ocelli (pit) are also visible. Scale bar=200 µm. E. Slit ocellus. The bumpy lens-like material can be seen positioned on the surface of the underlying photoreceptor cells (arrow). The slit ocellus is surrounded by cells 5-8 µm in diameter which bear cilia 10-15 µm long (arrowhead). Scale bar=20 µm. F. Pit ocellus. The pit-shaped indentation (pit) is surrounded by cells 3-6 µm in diameter bearing cilia 10-15 µm long (arrowhead). Scale bar=20 µm.

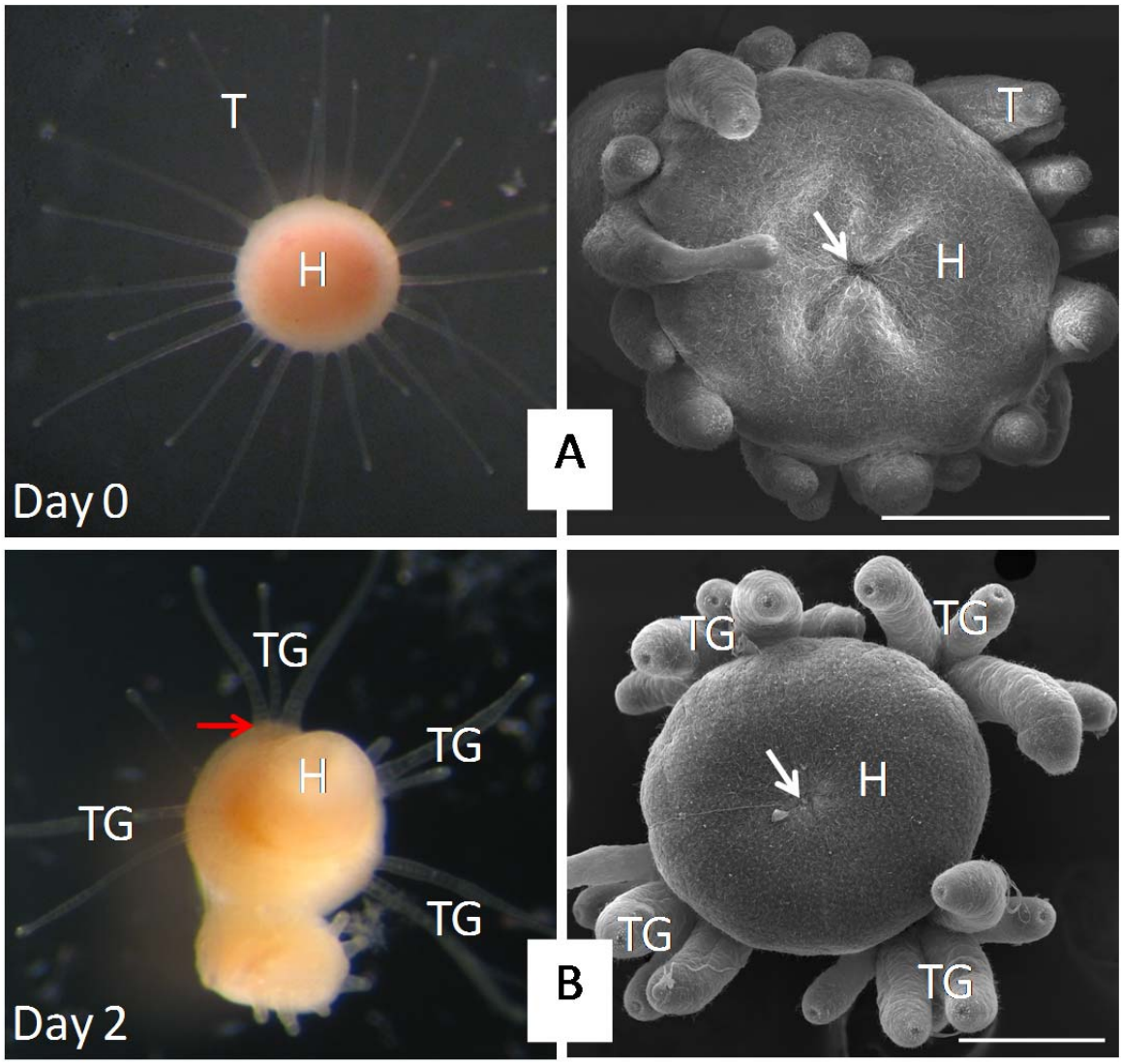

Figure 4. Staging using brightfield (left) and scanning electron microscope images (SEM) images (right) – Steady-state polyp and Stage 1. A. Steady-state polyp. The Stage 0 animal has radially-distributed tentacles (T) surrounding the hypostome (H). The mouth opening can be seen in the center of the hypostome (arrow). B. Stage 1. The tentacles rearrange to form four equidistant groups (TG) of approximately 2-5 tentacles each. The bases of these tentacles will fuse by the end of Stage 1 to form the surface on which the eyes/ocelli will develop (red arrow). The mouth opening (arrow) is visible at the center of the hypostome (H). Scale bars=200μm.

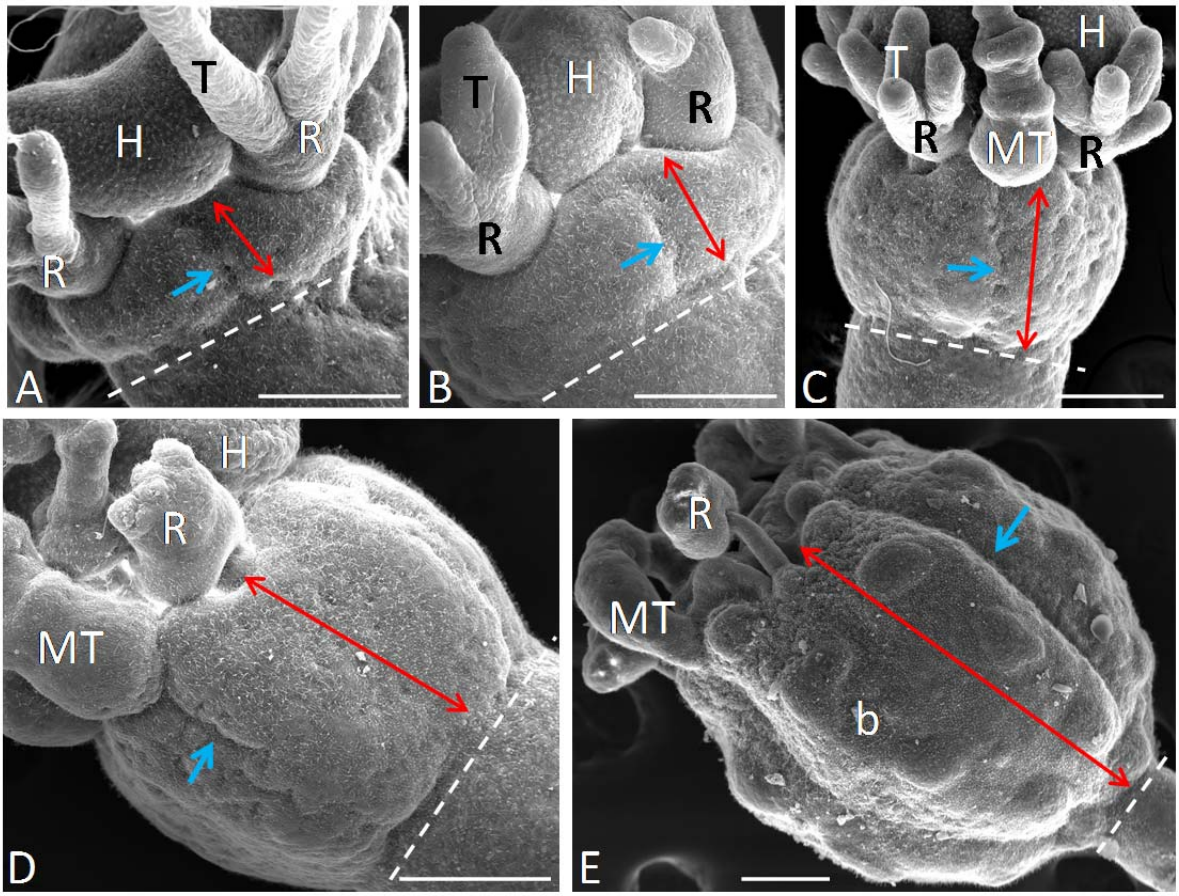

Figure 5. SEM images of bell formation. A. Stage 1. A dimpled furrow (hashed line) can be seen at the base of the cuff of cells (red arrow) roughly 100 µm below the hypostome (H) and represents the beginnings of bell formation as cells fold inward and down underneath the hypostome; septa formation is also visible (blue arrow). B. Stage 2. The length of the cuff (red arrow) has increased as the dimpled furrow (hashed line) is located farther down the body column roughly 175 µm below the hypostome (H); septa formation continues (blue arrow). C. Stage 3. The length of the cuff (red arrow) has increased as the dimpled furrow (hashed line) is now located roughly 250 µm below the hypostome (H); septa formation continues (blue arrow). D. Stage 4. The length of the cuff (red arrow) has increased as the dimpled furrow (hashed line) is now located roughly 300 µm below the hypostome (H); septa formation continues (blue arrow). E. Stage 5. The length of the cuff (red arrow) has increased as the dimpled furrow (hashed line) is now located roughly 800 µm below the rim of the developing bell (b); septa formation continues (blue arrow). T = polyp tentacle, R = rhopalia, MT = medusa tentacles. Scale bars=150µm.

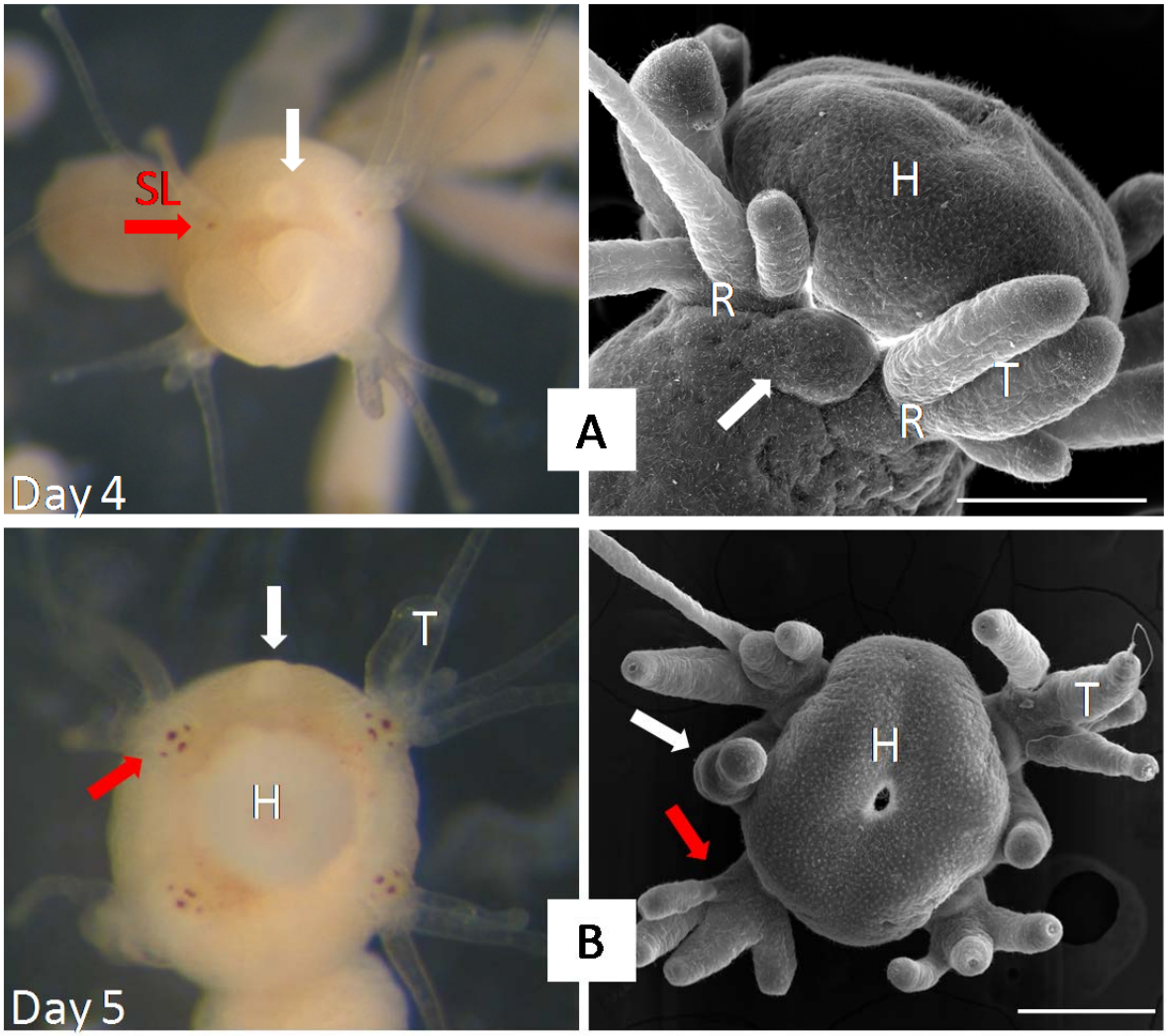

Figure 6. Staging using brightfield (left) and scanning electron microscope (SEM) images (right) – Stage 2 and early Stage 3. A. Stage 2. The appearance of medusa tentacle buds, (white arrow) and initial eyespot of the small lensed eye (SL/red arrow) on the surface of the fused tentacle bases which represent the developing rhopalium (R), are characteristics of this stage. The surface on which the eyes are developing is often obscured from view by the hypostome (H). B. Early Stage 3. In the beginning of Stage 3, four eye spots are visible on the surface of the developing rhopalium (red arrow), which face towards the extended hypostome (H), and represent the large complex eye, small complex eye, and slit ocelli. Medusa tentacles are extending (white arrow). Scale bars=200µm.

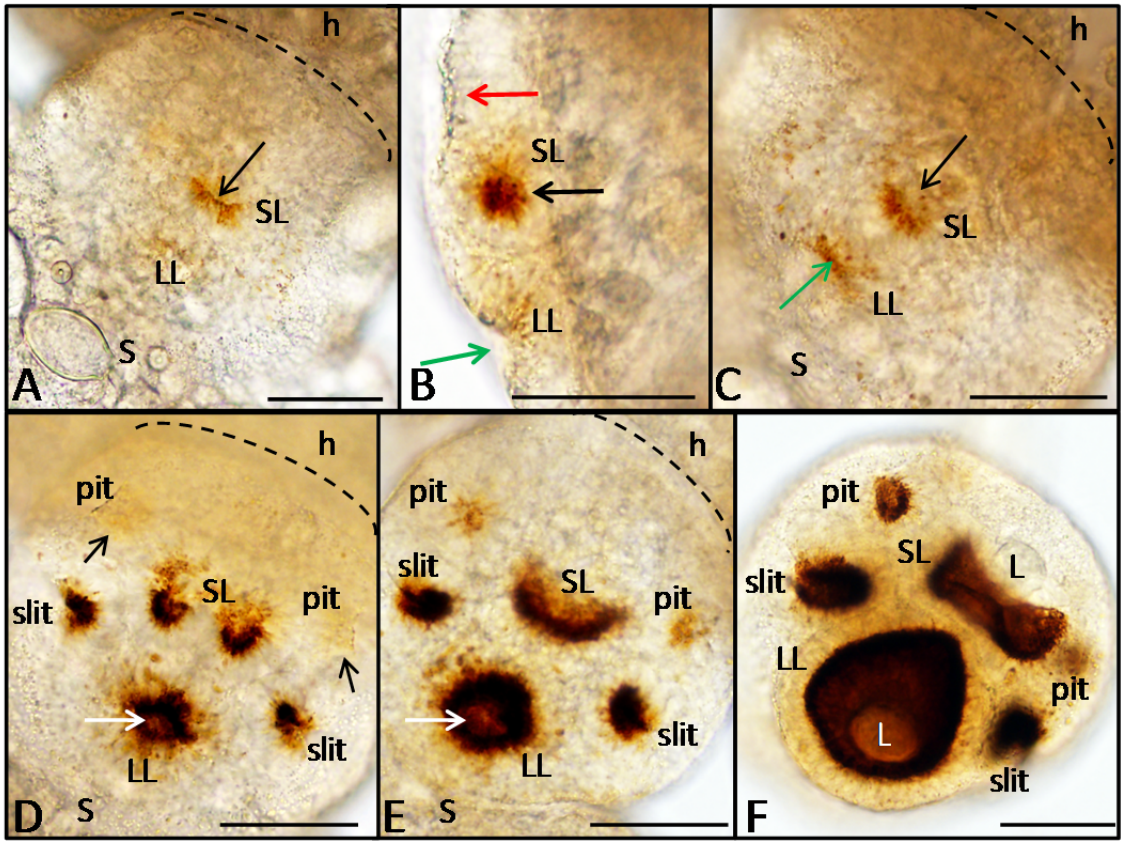

Figure 7. Brightfield images of individual rhopalia – Stage 2 through stage 4. A. Stage 2. The first pigment to appear (arrow) belongs to the small lensed eye (SL). The rhopalial margin is shown (hashed line) in reference to the hypostome (h) and the bottom of the rhopalium is where the statocyst (S) will form. The cup-shaped primordium of the large lensed eye (LL) cannot be seen from this angle and is shown in B. Scale bar=50 µm. B. Stage 2-profile. A profile view of a Stage 2 rhopalium shows the cup-shaped primordium (green arrow) of the large lensed eye (LL) showing faint pigmentation, the pigment (black arrow) of the small lensed eye (SL) and the shallower cup-shaped primordium (red arrow) of the small lensed eye. Scale bar=50 µm. C. Late Stage 2. By the end of Stage 2, the pigment (green arrow) of the large lensed eye (LL) can be seen along the top edge of the cup-shaped primordium along with the pigment (black arrow) of the small lensed eye (SL). The rhopalial margin (hashed line) is shown in reference to the hypostome (h). The bottom of the rhopalium is where the statocyst (S) will form. Scale bar=50 µm. D. Early Stage 3. The pigment of the small lensed eye (SL) is now split into two separate dark pigment bands with sparse pigmentation in between them. The forming pigment cup of the large lensed eye (LL) is clearly visible along with the pigment of the slit ocelli (slit). The faint region in the center of the large lensed eye pigment cup is where the lens is forming (white arrow). Fainter pigment can be seen radiating outward in a sunburst pattern around the more heavily pigmented central region. Very faint pigment can be seen along the inner edges of the pit-shaped indentations on the rhopalial surface (pit/black arrow). The rhopalial margin (hashed line) is shown in reference to the hypostome (h). The bottom of the rhopalium is where the statocyst (S) is forming. Scale bar=50 µm. E. Late Stage 3. The pigment of the small lensed eye (SL) has reconnected in the middle to form a slightly curved pigment band. The pigment of the large lensed eye (LL) has increased in size and concentration along with the pigment of the slit ocelli (slit) and pit ocelli (pit) which are now clearly visible. The faint region in the center of the large lensed eye pigment cup is where the lens is forming (arrow). The perimeter of fainter pigment radiating outward is much smaller around the more heavily pigmented central region. The rhopalial margin (hashed line) is shown in reference to the hypostome (h). The bottom of the rhopalium is where the statocyst (S) is forming. Scale bar=50 µm. F. Stage 4. All six eyes are clearly visible including the large lensed eye (LL), the small lensed eye (SL), the slit ocelli (slit), and pit ocelli (pit). The lenses of the small lensed eye and large lensed eye are also visible (L). Almost no faint pigment radiating outward from the more heavily pigmented central regions can be seen in any of the eyes/ocelli which forms a much smoother pigment boundary. Scale bar=50 µm.

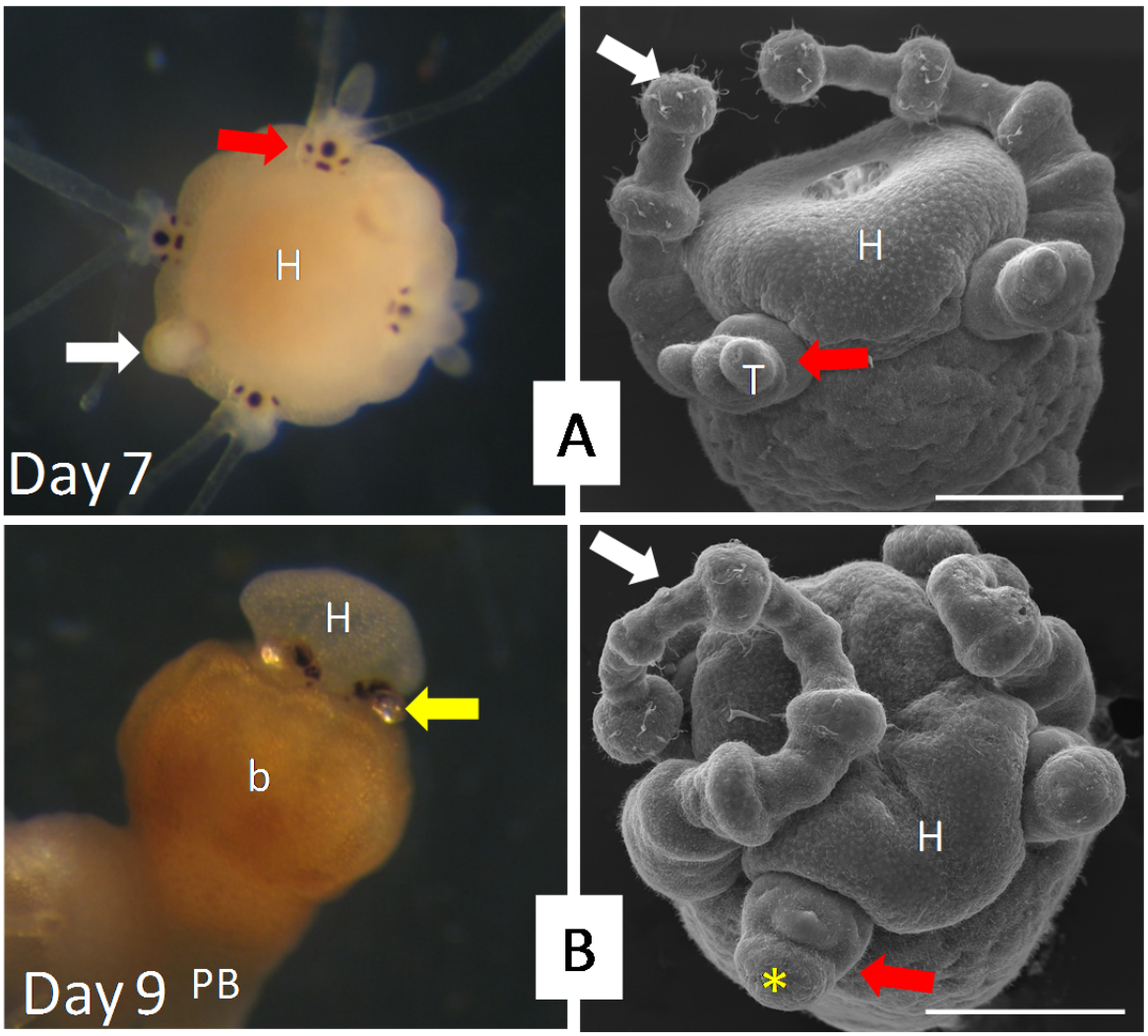

Figure 8. Staging using brightfield (left) and scanning electron microscope (SEM) images (right) – Late Stage 3 and stage 4. A. Late Stage 3. Polyp tentacle recession is nearly complete (T). All six eye spots are visible now, representing the large complex eye, small complex eye, slit ocelli, and pit ocelli, which sit on the surface of the developing rhopalium (red arrow). Medusa tentacles continue to extend (white arrow) and can be seen resting against the sides of the hypostome (H). B. Stage 4. Polyp tentacle recession is complete and the developing statocyst can now be seen (yellow arrow/asterisk). Rhopalia are now distinctive (red arrow) and eyes resemble miniature versions of adult medusa ocelli. The hypostome (H) is still extended. Medusa tentacles (white arrow) begin to fold inside the developing bell (b), which is now much darker in color compared to the remnant polyp body (PB). Scale bars=200µm.

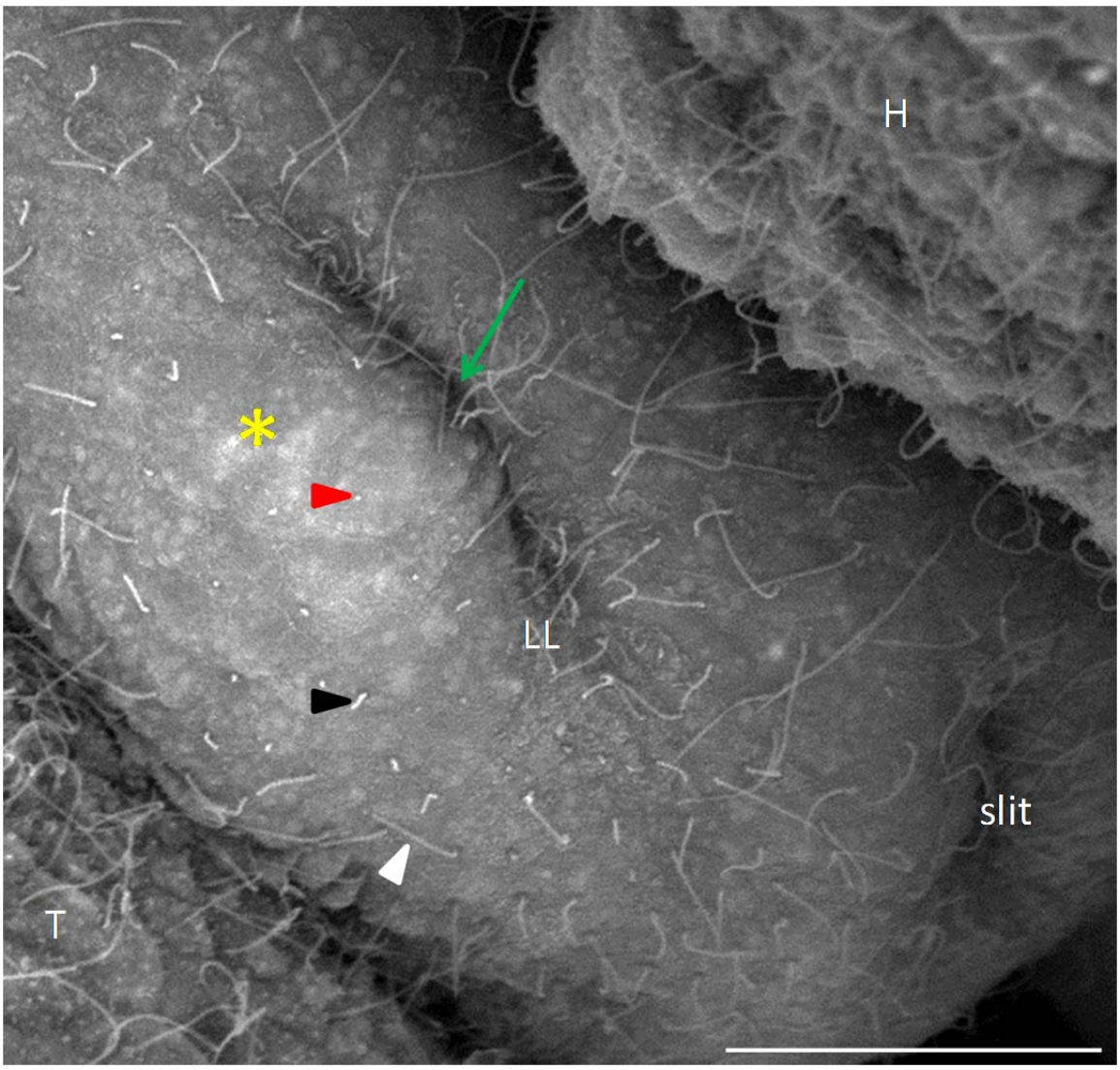

Figure 9. SEM images of developing ocelli. Stage 3. The up-folding sheet of cells (asterisk) of the large lensed eye (LL) is visible on the surface of the fused tentacles along with one of the slit ocelli (slit). The up-folding sheet of cells forms a groove (green arrow) which faces slightly downward towards the remaining polyp tentacles (T). The hypostome (H) obscures the other ocelli from view. Longer cilia (white arrowhead) are found along the bottom portion and sides of the up-folding sheet of cells, while shorter cilia are found in the middle region of the sheet of cells (black arrowhead), and very short cilia are found closest to the lip of the sheet of cells (red arrowhead). Scale bar=25µm.

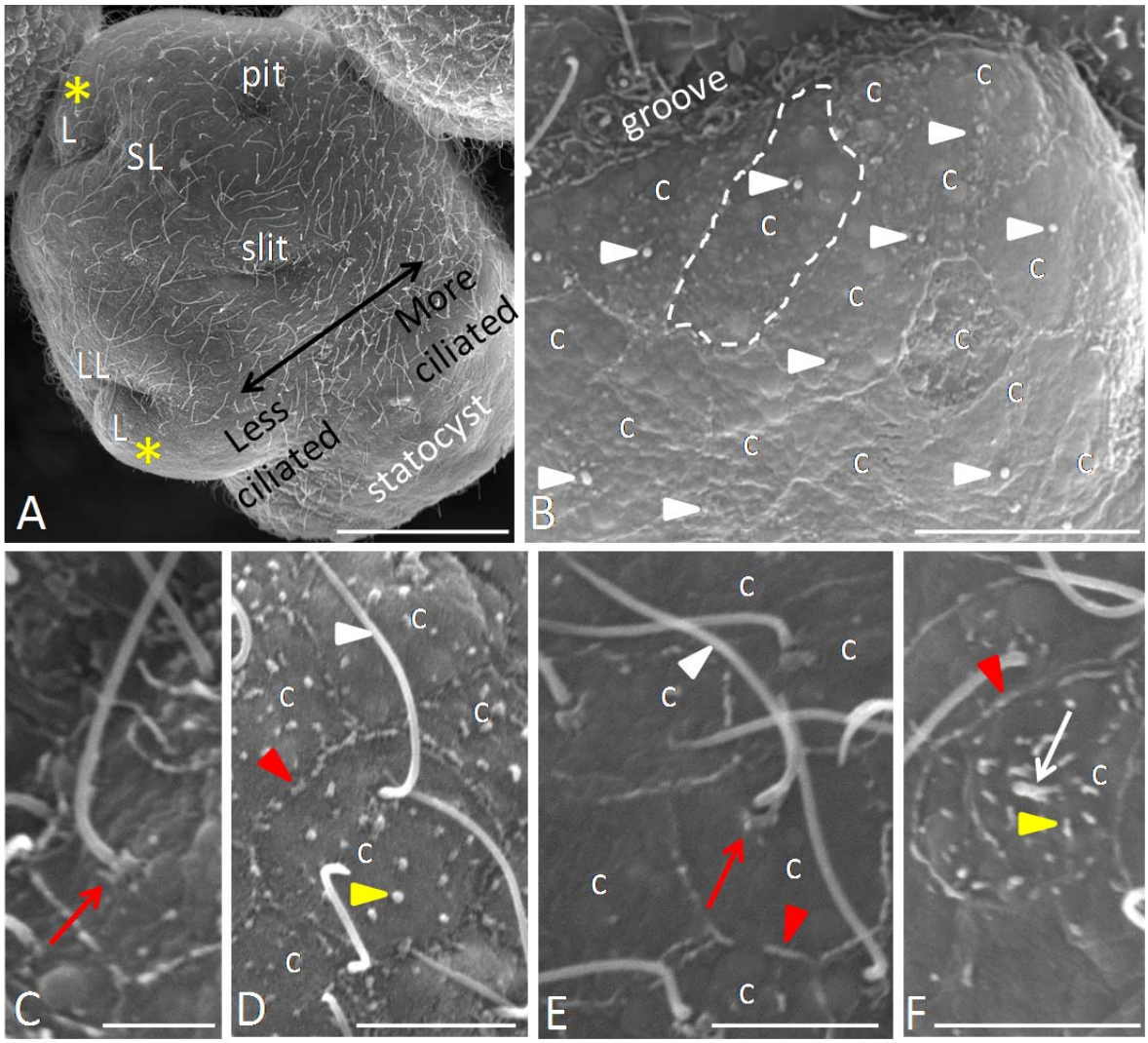

Figure 10. Scanning electron microscope (SEM) images of Stage 4 rhopalia and cells surface patterns. A. A profile of a Stage 4 rhopalium shows the general location of the different eyes/ocelli including the large (LL) and small (SL) lensed eyes, the pit (pit) and slit (slit) ocelli. The up-folding sheet of cells of the large complex eye and down-folding sheet of cells of the small complex eye (asterisks) are visible as well as the difference in ciliation between the more heavily ciliated back of the rhopalium and the less ciliated front (where the eyes are located). The forming lenses (L) of the complex eyes can also be seen. Scale bar=50 µm. B. Large complex eye. A close-up of the apical region of the up-folding sheet of cells (c) shows the shortened cilia (arrowheads) as well as an example of a more rectangular-shaped cell (hashed line) found close to the down-facing groove. Scale bar=10 µm. C. Microvilli. Each cilium is encircled by a ring of microvilli (red arrow) roughly 0.6 µm long. Scale bar=2.5 µm. D. Rough-surface cell with long cilium. These cells (c) have microvilli distributed across the surface (yellow arrowhead) and along the perimeter (red arrowhead) that are roughly 0.6 µm long. The cilium (white arrowhead) is approximately 10-15 µm long. Scale bar=5 µm. E. Smooth-surface cell. These cells (c) have microvilli lining the perimeter (red arrowhead) roughly 0.6 µm long, but none are found across the cell surface. The cilium is 10-15 µm in length (white arrowhead). The microvilli encircling the base of the cilium can also be seen (red arrow). Scale bar=5 µm. F. Rough-surface cell with short cilium. These cells (c), which are more spherical in shape, have microvilli distributed across the surface (yellow arrowhead) and along the perimeter (red arrowhead) that are roughly 0.6 µm long. The cilium (white arrow) is only approximately 1.5 µm in length. Scale bar=5 µm.

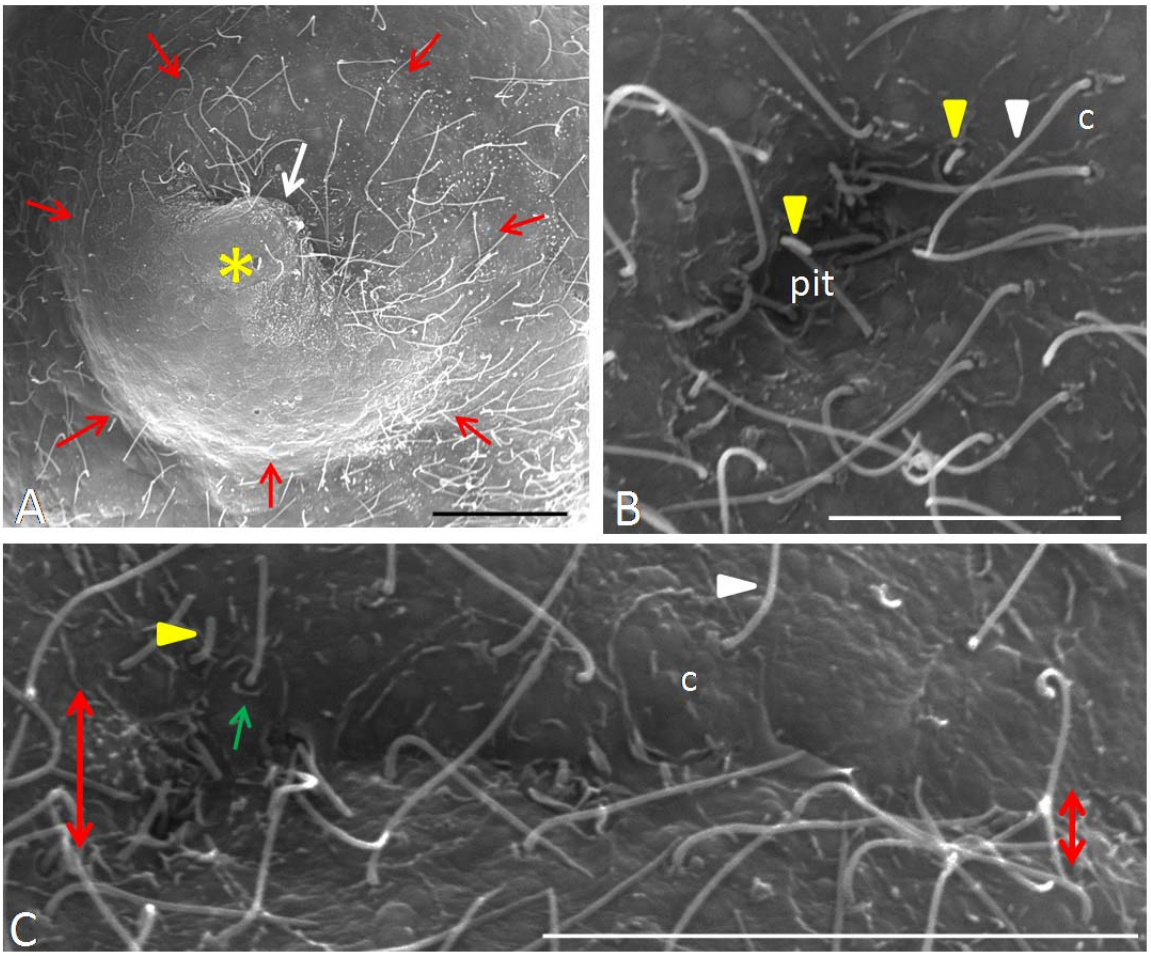

Figure 11. Scanning electron microscope (SEM) images of Stage 4 rhopalia. A. Large lensed eye. The large lensed eye appears as a downward-facing groove (white arrow), formed by the up-folding sheet of cells (asterisk), and is located on the spherical raised retina (red arrows) of the forming large lensed eye retina. The difference in ciliation between the up-folding sheet of cells, which exhibit shortened cilia, and surrounding cells, which exhibit long cilia, is clear. Scale bar=25µm. B. Pit ocellus. Most of the cells (c) surrounding the pit-shaped cavity exhibit long cilia (white arrowhead) while others that are closer or within the pit often exhibit shortened cilia (yellow arrowheads). Scale bar=10µm. C. Slit ocellus. The slit-shaped groove is wider at the end which is located farthest away from the complex eyes and is tapered at the opposite end (red arrows). Most of the cells (c) surrounding the groove exhibit long cilia (white arrowhead) while others that are closer to or within the groove often exhibit shortened cilia (yellow arrowhead). The microvilli surrounding the base of the cilia are also visible (green arrow). Scale bar=20µm.

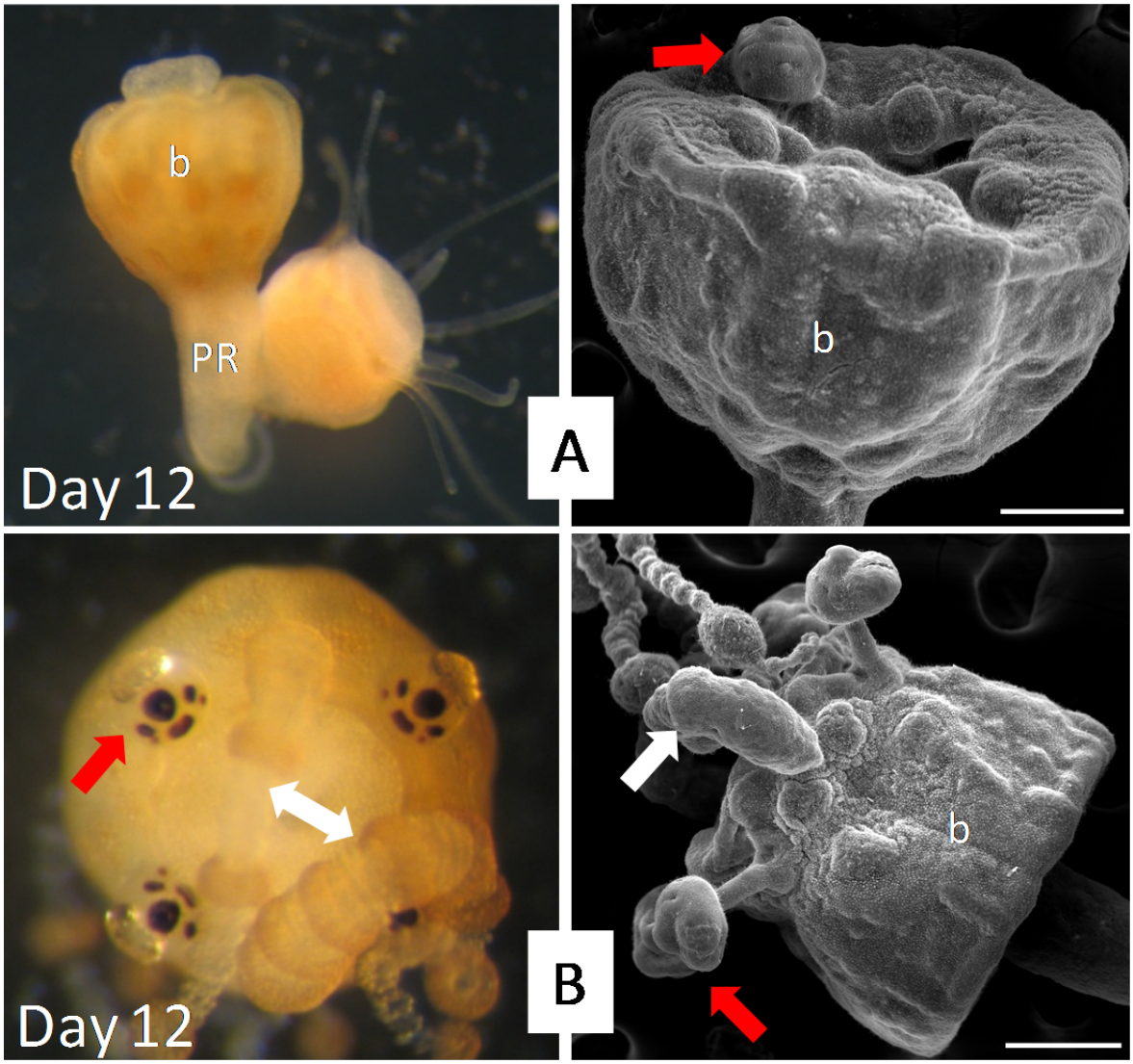

Figure 12. Staging using brightfield (left) and scanning electron microscope (SEM) images (right) – Stage 5. A. Stage 5. The eyes, medusa tentacles, and hypostome have moved inside the developing bell (b) which is attached to the polyp remnants (PR). Rhopalia continue to develop (red arrow). B. Stage 5 everted. The internalized structures within the developing bell (b) have been forced to evert, so the developing rhopalia and eyes/ocelli can now be seen (red arrow). Medusa tentacles have continued to lengthen (white arrow). Scale bars=200 µm.

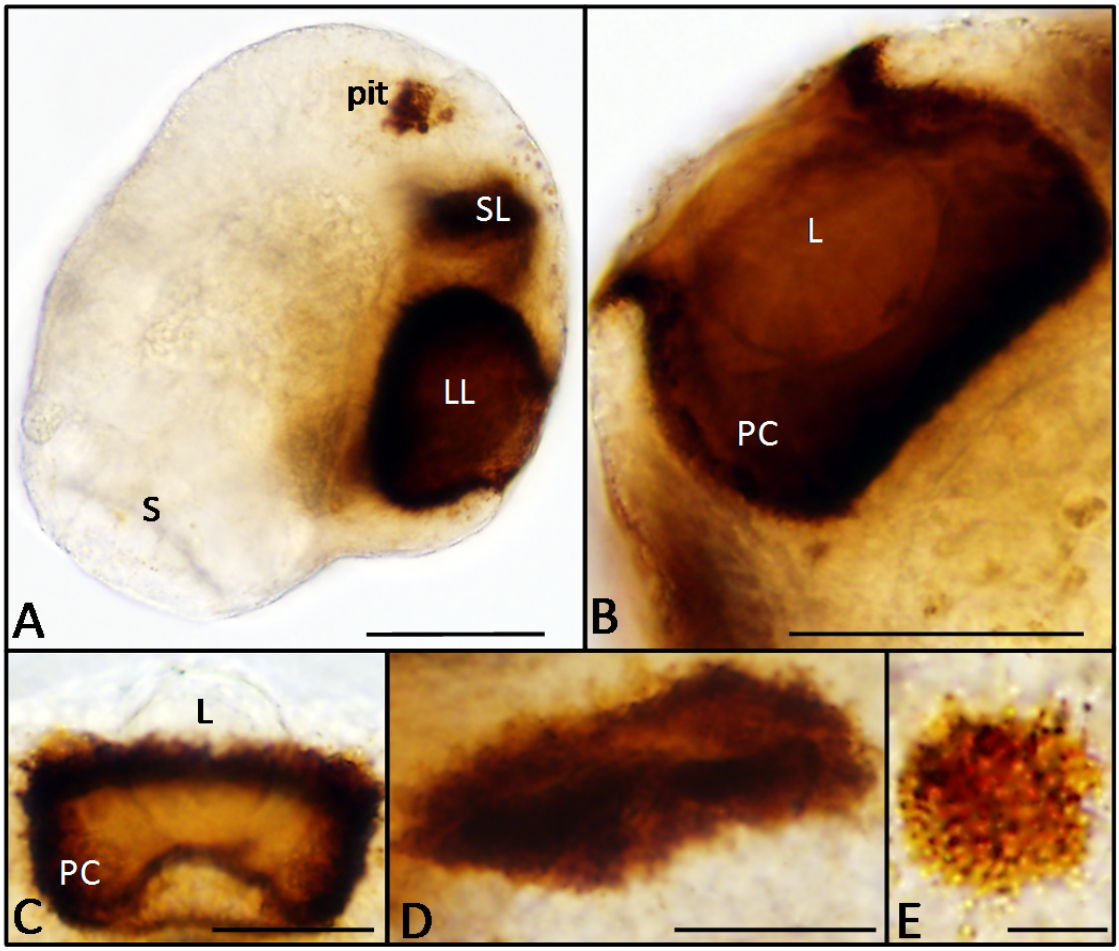

Figure 13. Brightfield images of individual rhopalia – Stage 5 and Stage 7. A. Stage 5. A profile of a Stage 5 rhopalium shows the depth of the pigment cup (roughly 50 µm) of the large lensed (LL) and small lensed (SL) eyes. A pit ocellus is also visible (pit) along with the basal statocyst (S). Scale bar=50 µm. B. Stage 7 large lensed eye. The lens (L) can be seen within the pigment cup (now spanning a depth of roughly 60 µm; PC) of the large complex eye which has a tulip-shaped opening. Scale bar=50 µm. C. Stage 7 small lensed eye. The lens (L) can be seen in the opening of the pigment cup (now spanning a depth of roughly 60 µm; PC) of the small complex eye. Scale bar=25 µm. D. Stage 7 slit ocellus. A slit ocellus in a newly metamorphosed animal. Scale bar=25 µm. E. Stage 7 pit ocellus. A pit ocellus of a newly metamorphosed animal. Scale bar=12.5 µm.

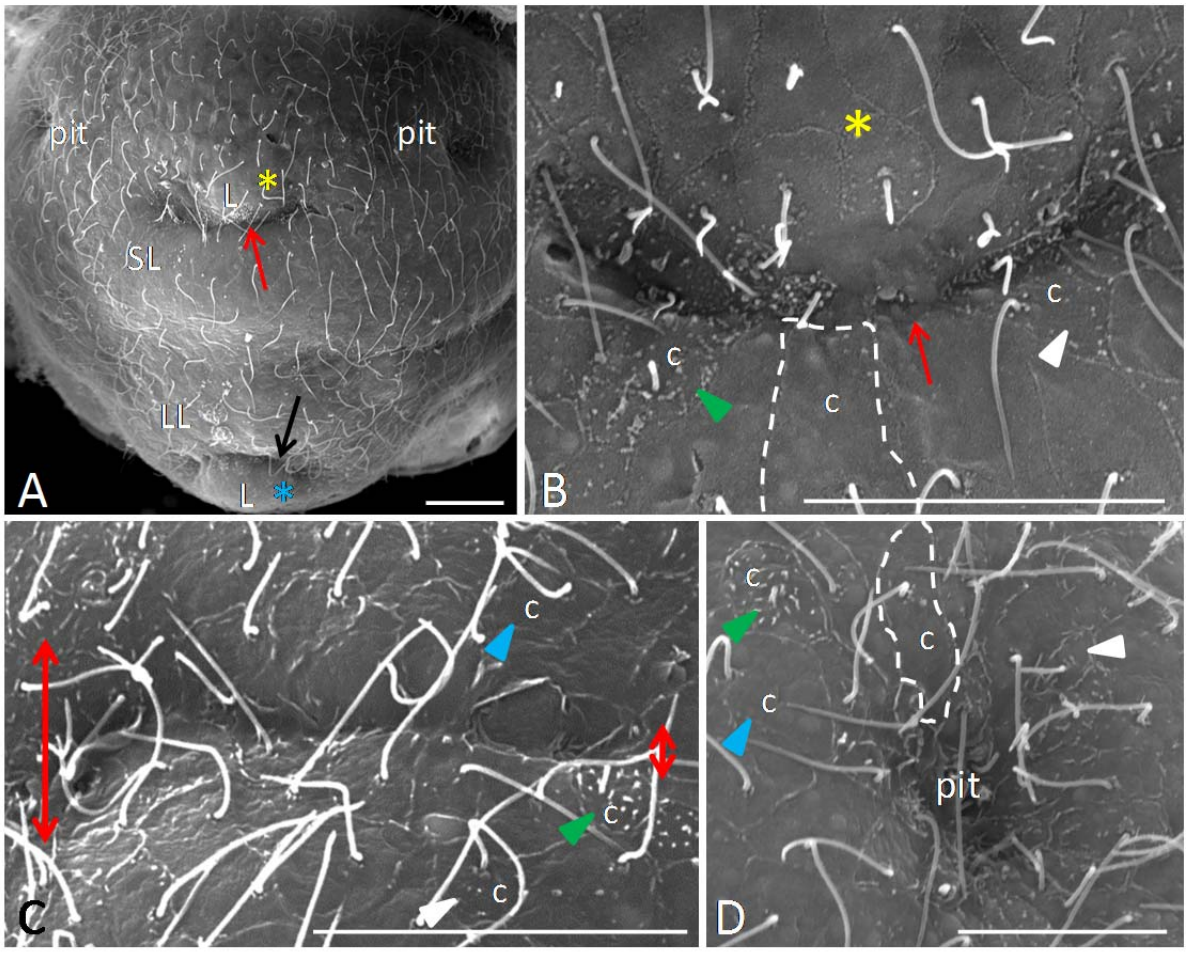

Figure 14. Scanning electron microscope (SEM) images of Stage 5 rhopalia. A. Stage 5 rhopalium. This view from the top of the rhopalium shows the small lensed eye (SL), the two pit ocelli (pit) and the large lensed eye (LL).The developing lenses (L) sit underneath the down-folding sheet of cells (yellow asterisk) in the small lensed eye and underneath the up-folding sheet of cells (blue asterisk) of the large lensed eye. The down-facing groove of the large lensed eye (black arrow) is visible along with the up-facing groove (red arrow) of the small lensed eye. Scale bar=20 µm. B. Small complex eye. The up-facing groove (red arrow) can be seen and is created by the down-folding sheet of cells (asterisk). A rectangular-shaped smooth surface cell (c)/(hashed line) is visible along with rough-surface cells (c) with long cilia (white arrowhead) and rough-surface cells (c) with shortened cilia (green arrowhead). Scale bar=20 µm. C. Slit ocellus. The slit ocellus is wider on the end located farthest away from the complex ocelli and tapers down to a much smaller width at the opposite end (red arrows). Smooth-surface cells (c) are visible (blue arrowhead) along with rough-surface cells (c) with long cilia (white arrowhead), and rough-surface cells (c) with short cilia (green arrowhead). Scale bar=20 µm. D. Pit ocellus. A rectangular-shaped cell (c)/(hashed line) can be seen along the perimeter of the pit-shaped indentation (pit) of the pit ocellus. Smooth-surface cells (c) are visible (blue arrowhead) along with rough-surface cells (c) with long cilia (white arrowhead) and rough-surface cells (c) with short cilia (green arrowhead). Scale bar=10 µm.

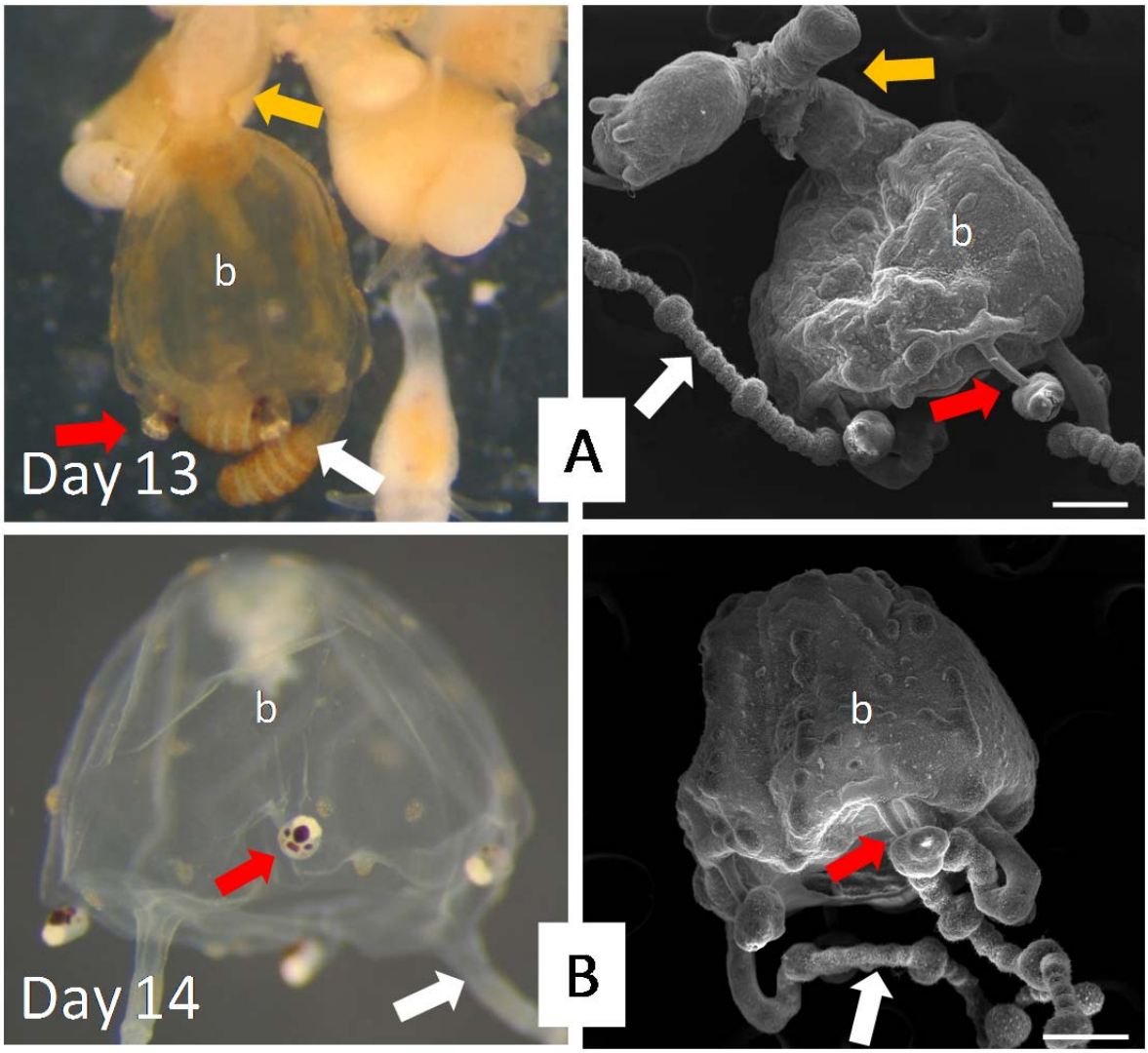

Figure 15. Staging using brightfield (left) and scanning electron microscope (SEM) images (right) – Stage 6 and Stage 7. A. Stage 6. The animal is now a medusa but has not yet detached from the polyp remnants (orange arrow) which remain attached to the substrate. The bell (b), medusa tentacles (white arrow) and rhopalia (red arrow), which hang down near the base of the bell, are visible. The time of detachment is highly variable. B. Stage 7. The free-swimming medusa signifies the end of transformation. The bell (b), medusa tentacles (white arrow), and rhopalia (red arrow), which hang down near the base of the bell, are visible. The rhopalia will eventually be enclosed mid-bell behind an eyelid. Scale bars=200µm.

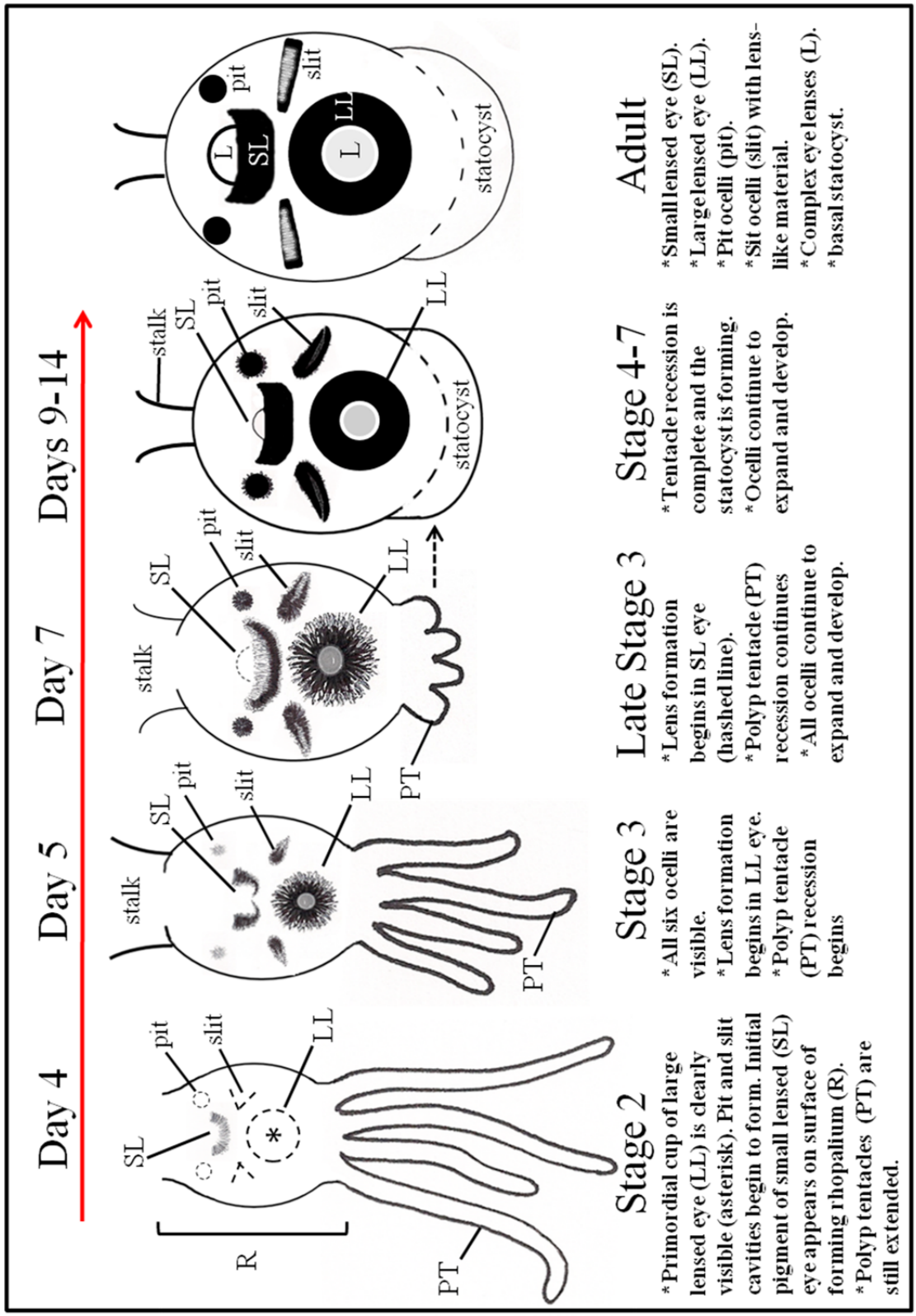

Figure 16. Diagram of eye development. Stage 2 through the end of transformation is shown with the later stages (4-7) combined due to a similar resemblance, although further expansion of the rhopalia and corresponding eyes/ocelli continue through to the end of transformation. Rhopalia are not drawn to scale.

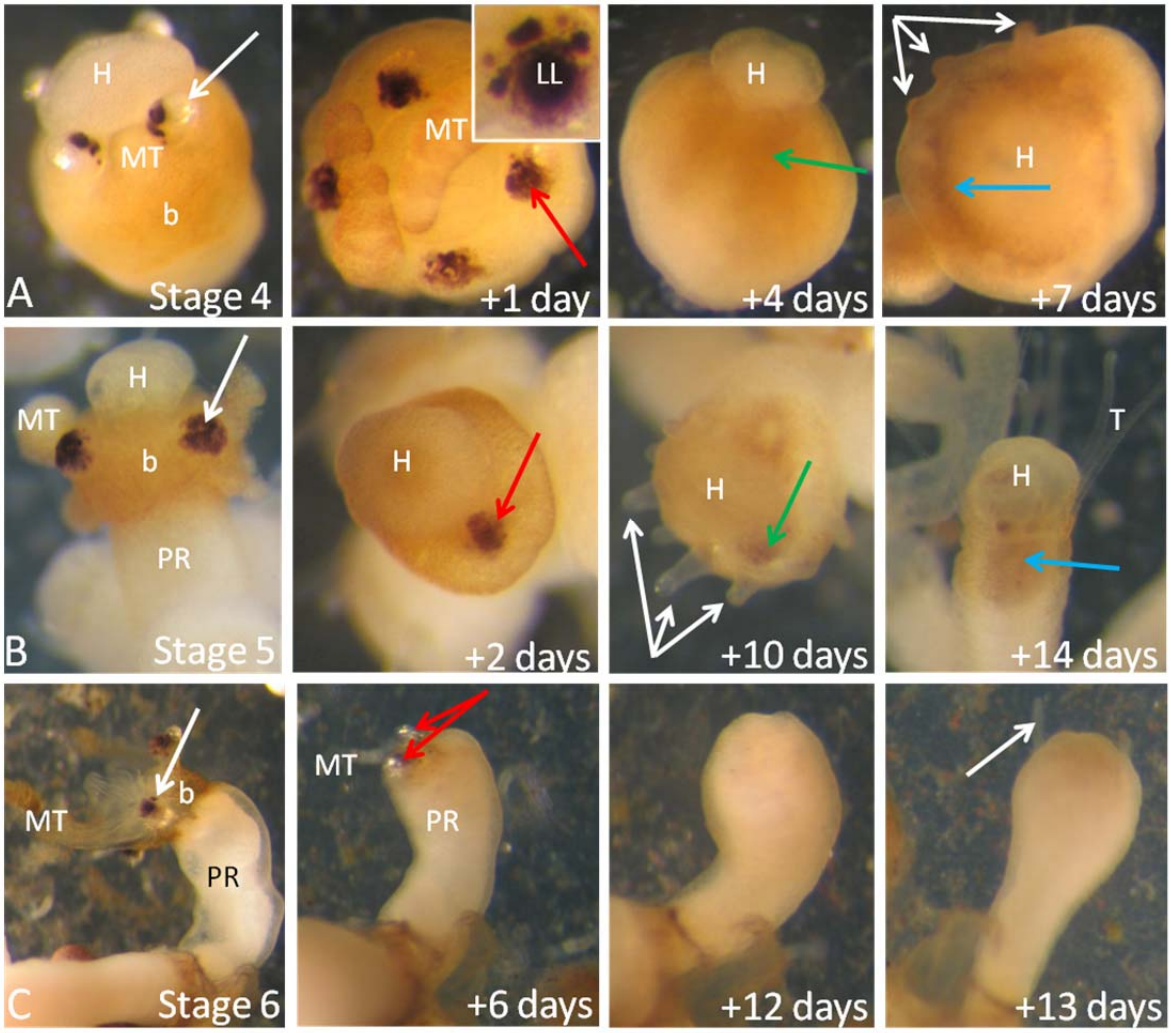

Figure 17. Regression of transformation. A. Regression from stage 4. Before regression begins, four developing rhopalia (white arrow) can be seen encircling the hypostome (H) and medusa tentacles (MT) have inverted into the forming bell (b). The first sign of regression is the dispersal of the photoreceptor pigment in each eye/ocellus (red arrow) which begins in the large lensed eye (inset: LL). The medusa tentacles are now everted. Within four days, all four rhopalia and the medusa tentacles are reabsorbed. Reabsorbed pigment can be seen below the surface of the animal (green arrow). In about a week, polyp tentacles have begun to reappear (white arrows) and reabsorbed pigment is still visible along the base of the hypostome (blue arrow). B. Regression from Stage 5. This animal has already begun to regress. The dispersal of pigment across the rhopalial surface is clear (white arrow) and the medusa tentacles (MT) are still visible. The regressing bell (b) is easily differentiated from the polyp remnants (PR). The re-absorption of the rhopalia does not happen all at once as evidenced by one regressing rhopalium remaining 2 days after regression began to be monitored (red arrow). By this point, the medusa tentacles have been reabsorbed. Within 10 days, polyp tentacles have reappeared (white arrows) and the reabsorbed pigment is apparent beneath the hypostome (H) surface (green arrow). After two weeks, the polyp tentacles (T) have lengthened and some reabsorbed pigment is still visible beneath the surface (blue arrow). C. Regression from Stage 6. This animal has already begun to regress. The pigment is just beginning to be dispersed (white arrow) and the medusa tentacles are still extended (MT). The bell (b) of the newly metamorphosed animal has already been reduced and is easily differentiated from the polyp remnants (PR). Six days after regression began to be monitored, the medusa tentacles (MT) have been almost completely reabsorbed and all that remains of the rhopalia is sparse pigment and the statocysts (red arrows). Twelve days after regression began to be monitored, all medusal structures have been reabsorbed and one day later, polyp tentacles begin to reappear (white arrow).

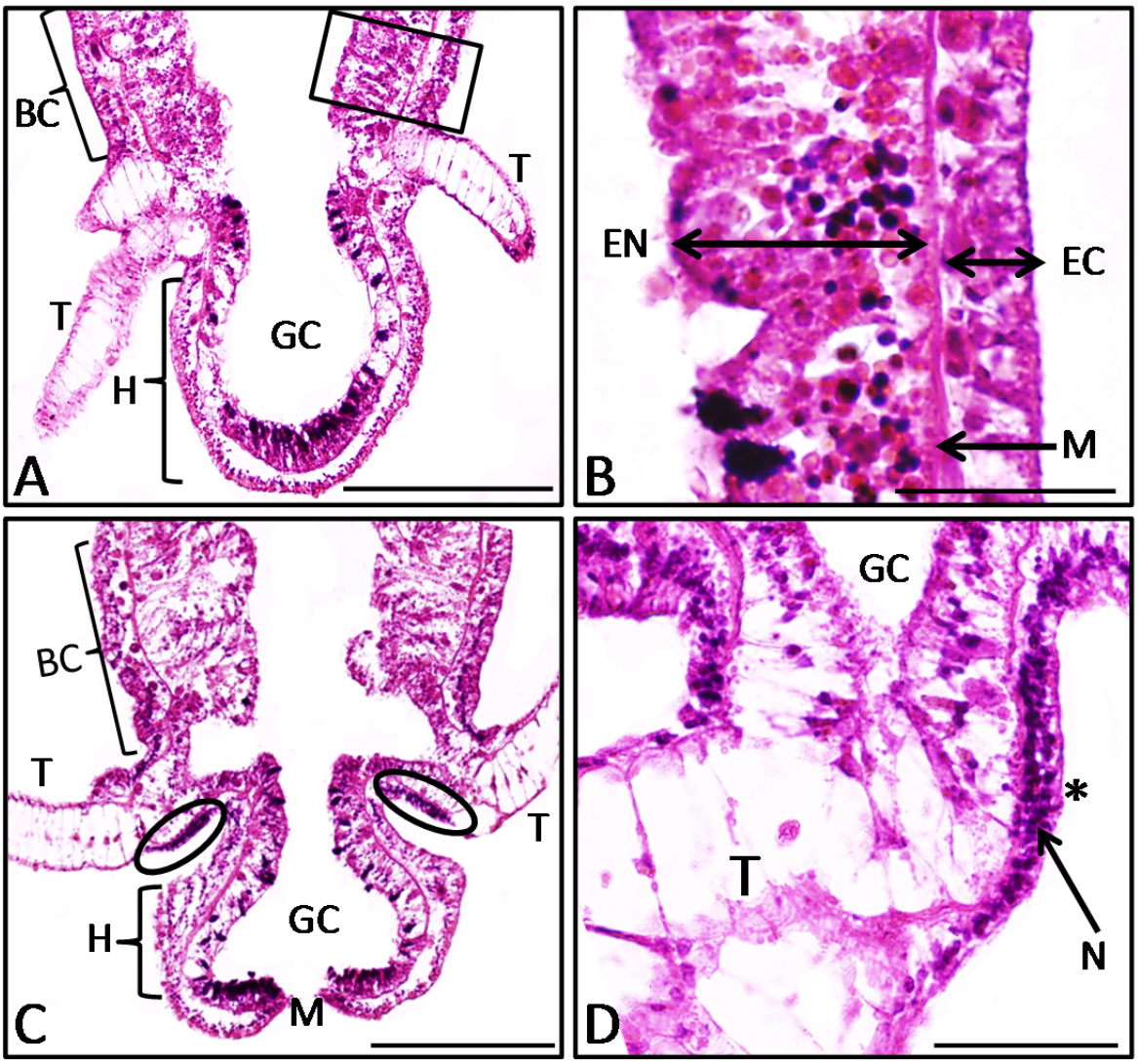

Figure 18. Hematoxylin and eosin stained tissue sections of transforming animals – Stage 0 and Stage 1. A. Stage 0. A longitudinal section of a steady-state polyp (Stage 0) shows the hypostome (H); the tentacles (T), which originate around the base of the hypostome; the body column (BC), which begins below the tentacles; and the gastrovascular cavity (GC), which runs from the hypostome down to the foot of the animal. The different body layers are also visible (rectangle) and are enlarged in B. Scale bar=200 µm. B. Stage 0 body layers. The two body layers are visible and consist of the outer ectoderm (EC) and inner endoderm (EN), which are separated by the gelatinous mesolgea (M). Scale bar=50 µm. C. Stage 1. The bases of the polyp tentacles (T) have now fused to form the surface on which the ocelli will develop (ovals). On this surface, many dark-staining nuclei are visible. In this section, the mouth opening (M) is visible at the distal end of the hypostome (H) whose base is now set inward from the surface of the body column (BC). The gastrovascular cavity (GC) can also be seen. Scale bar=200 µm. D. Stage 1 rhopalium. The ectoderm of the fused tentacles, where the ocelli will develop, (asterisk) has numerous darkly-stained nuclei (N) roughly 3 µm in diameter. The depth span of these nuclei (roughly 18 µm), along with the number of nuclei, is greater on this surface than other regions of the rhopalia. Scale bar=50 µm.

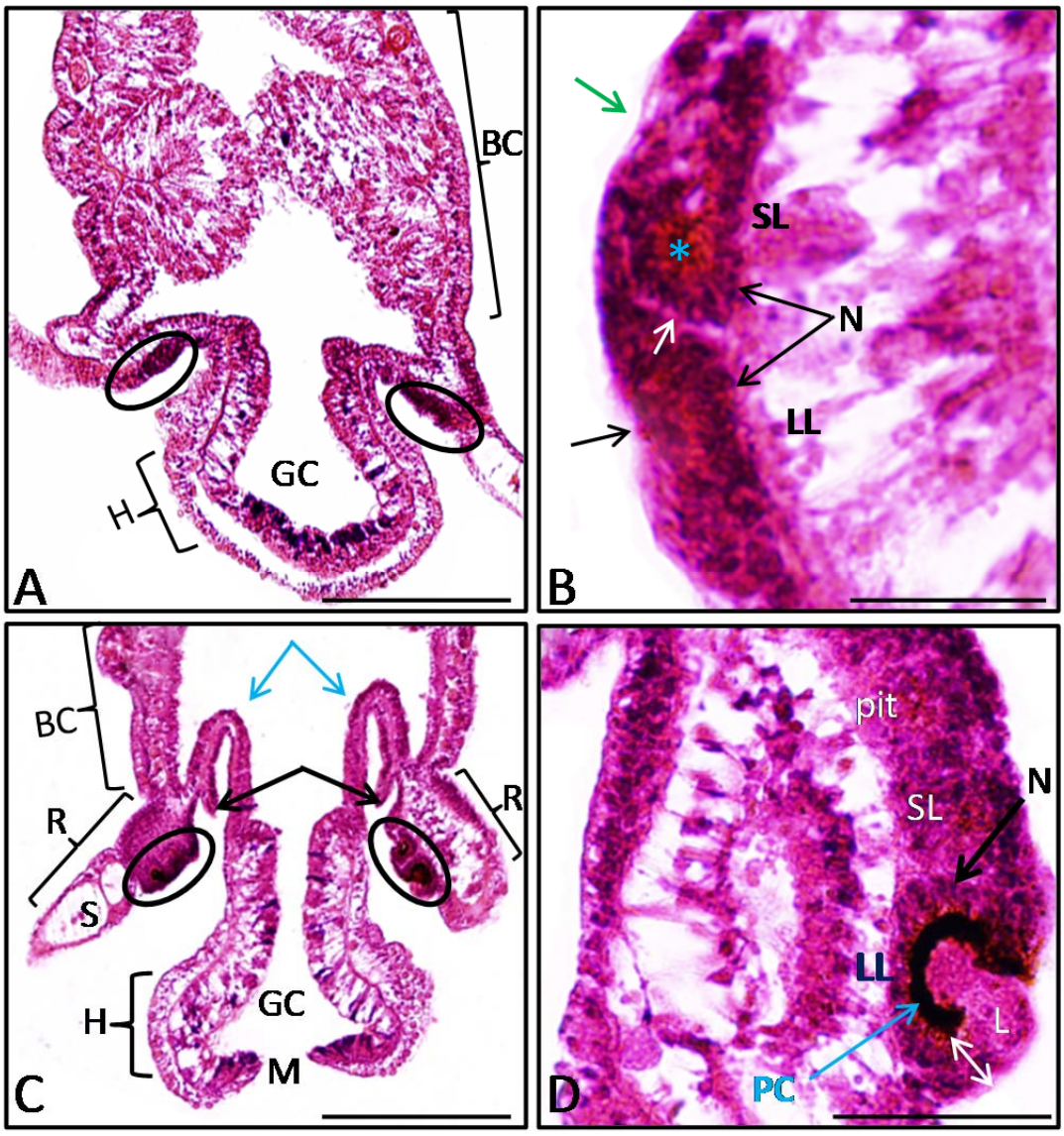

Figure 19. Hematoxylin and eosin stained tissue sections of transforming animals – Stage 2 and Stage 3. A. Stage 2. The eyes/ocelli are now developing on the surface of the fused tentacles (ovals). The gastrovascular cavity (GC) and hypostome (H), whose base is still set inward from the surface of the body column (BC), are visible. Scale bar=200 µm. B. Stage 2 rhopalium. The cup-shaped primordium (black arrow) of the large lensed eye (LL) and the cup-shaped primordium (green arrow) of the small lensed eye (SL) are visible along with the pigmented eyespot (asterisk) of the small lensed eye. The complex eyes are encircled by darkly-stained photoreceptor nuclei (N) and the nuclei of the large complex eye are separated from the nuclei of the small complex eye by a thin, lightly-stained region which corresponds to the forming neural region (white arrow). Scale bar=25 µm. C. Stage 3. The eyes/ocelli (ovals) can be seen developing on the surface of the rhopalia (R) which face towards the central hypostome (H). The mouth opening (M) is visible at the distal end of the hypostome. The remaining tentacles will eventually give rise to the statocyst (S) at the base of the rhopalium. The invagination of cells, which will ultimately form the bell of the medusa (blue arrows). is clearly visible in the gastric cavity (GC) at this point in transformation along with the early formation of the developing medusa velarium (black arrows). Scale bar=200 µm. D. Stage 3 rhopalium. The developing large lensed eye (LL) is visible including the pigment cup (PC/blue arrow), the encircling photoreceptor nuclei (N/black arrow), and the developing lens (L) which sits at the opening of the pigment cup. Due to the overlying sheet of cells, which is attached to the lens, the basal portion of the pigment cup does not reach the surface of the rhopalium (white arrows). A portion of the small lensed eye (SL) and a pit ocellus (pit) is also visible. Scale bar=50 µm.

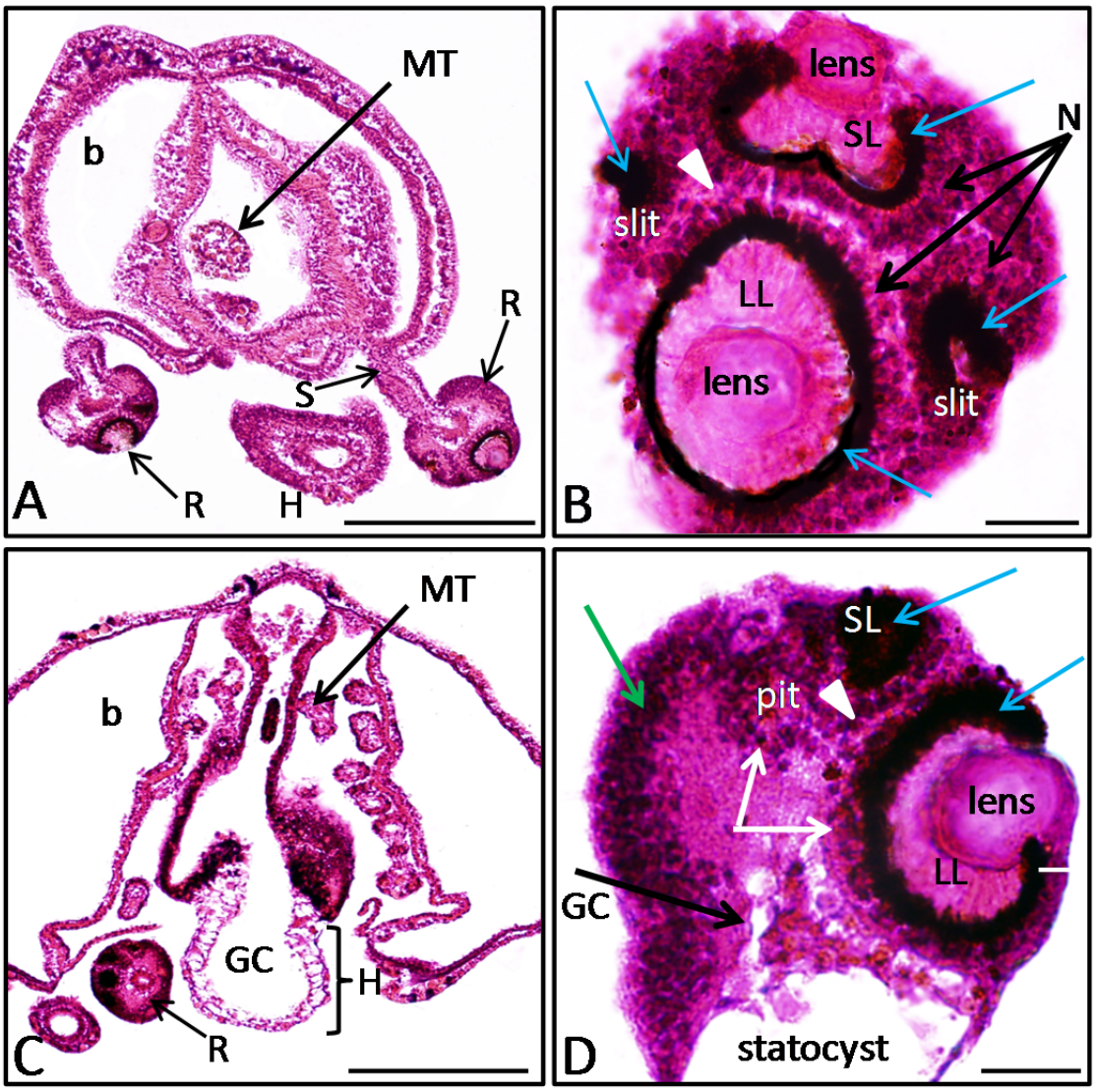

Figure 20. Hematoxylin and eosin stained tissue sections of transforming animals – Stage 4 and Stage 5. A. Stage 4. Two rhopalia (R) are visible along with one rhopalial stalk (S) attaching the rhopalium to the developing bell (b). A section of a medusa tentacle (MT) is visible within the bell along with a portion of the hypostome (H) which has not yet moved inside the bell. Scale bar=200 µm. B. Stage 4 rhopalium. The large lensed eye (LL), small lensed eye (SL), and slit ocelli (slit) are visible in this section along with the forming lenses of the complex eyes, retinal pigment (blue arrows), and the photoreceptor nuclei (N) encircling each of the eyes/ocelli. The thin light-stained region separating the photoreceptor nuclei of the large complex eye from the photoreceptor nuclei of the surrounding eye/ocelli is also visible (white arrowhead). Scale bar=20 µm. C. Stage 5. The developing bell (b) is nearly complete and the hypostome (H) is transitioning to become the manubrium of the medusa. The gastrovascular cavity (GC) is still visible and will become the gastric pouches of the medusa. A single rhopalium (R), which is now within the developing bell, is visible along with portions of medusa tentacles (MT). Scale bar=200 µm. D. Stage 5 rhopalium. The large lensed eye (LL), a portion of the small lensed eye (SL), and a portion of a pit ocellus are visible along with the basal statocyst. The pigment of the complex eyes (blue arrows) and forming lens of the large complex eye are easily distinguished. The sheet of cells overlying the lens of the large complex eye is thinner, although the portion of the pigment cup underneath the sheet of cells still does not reach the surface of the rhopalia (white bar). The photoreceptor nuclei can be seen surrounding the eyes/ocelli (white arrows) and the non-ocular nuclei span the back of the rhopalium (green arrow). A portion of the gastrovascular cavity is also visible (black arrow) along with the thin, lightly-stained region separating the photoreceptor nuclei of the two complex eyes (white arrowhead). Scale bar=20 µm.

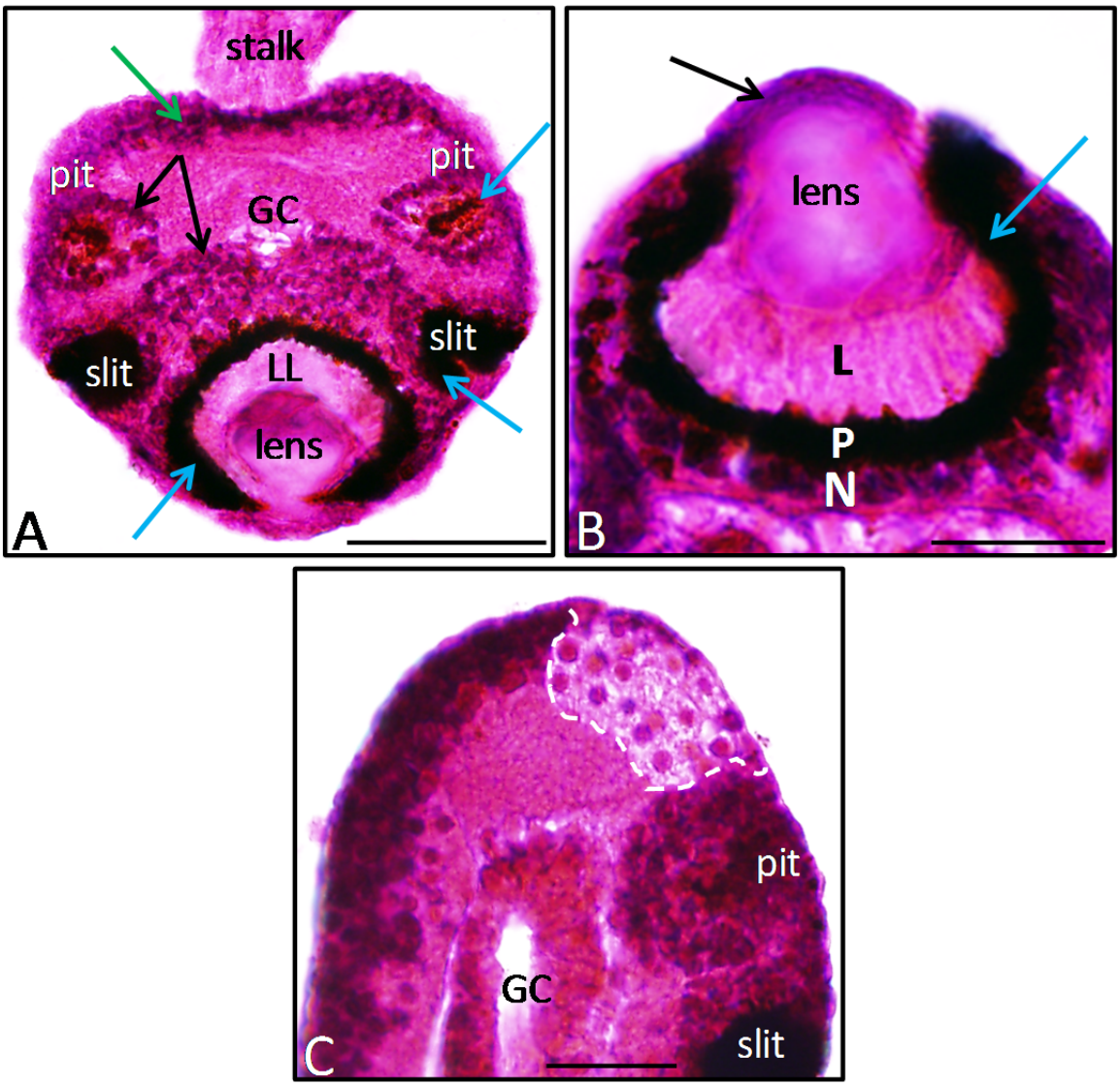

Figure 21. Hematoxylin and eosin stained tissue sections of transforming animals – Stage 7. A. Stage 7 rhopalium. The large lensed eye (LL), slit ocelli (slit), and pit ocelli (pit) are visible. The pigment of the complex eye and ocelli (blue arrows) can be seen as well as the lens of the large complex eye. The nuclei of the photoreceptor cells making up the eye/ocelli can clearly be seen (black arrows) with the non-ocular nuclei along the back of the rhopalium near the stalk (green arrow). A small portion of the gastrovascular cavity (GC) is visible with the lack of non-photoreceptor nuclei surrounding it. Scale bar=50 µm. B. Stage 7 large complex eye. The retinal pigment cup (blue arrow) and lens of the large complex eye can be seen along with the three regions of the photoreceptor cells making up the retina including the apical light-receptive region (L), the middle pigmented region (P), and the basal nuclear region (N). The forming cornea sitting on top of the lens is also visible (black arrow). Scale bar=20 µm. C. Stage 7. The lightly-stained region with sparse nuclei at the top of the rhopalium is visible (hashed line) along with a pit ocellus (pit), slit ocellus (slit), and a portion of the gastrovascular cavity (GC). Scale bar=20 µm.

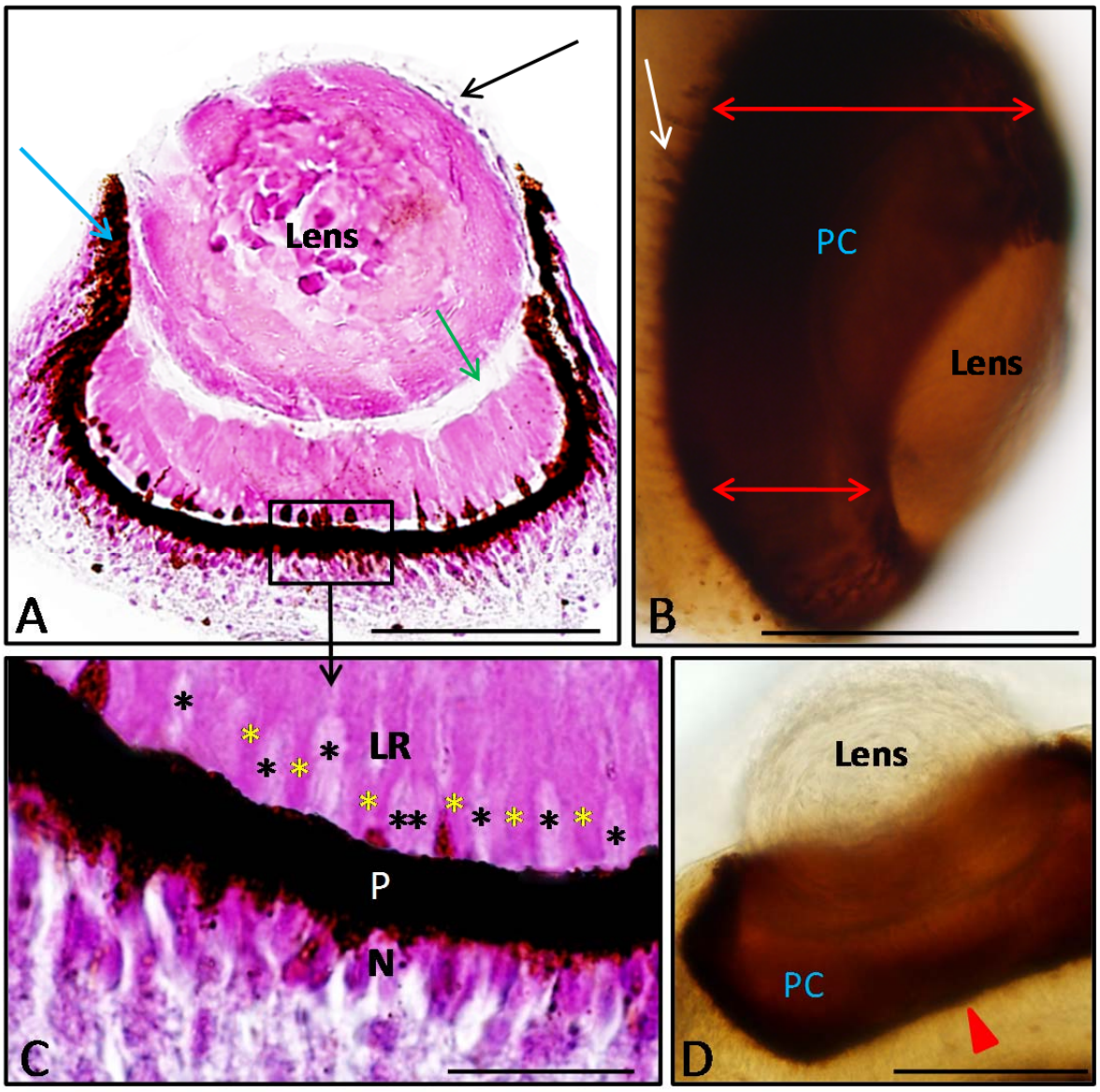

Figure 22. Fontana-Masson staining for melanin (left) and whole-mount brightfield images (right) of adult complex eyes. A. Large complex eye. The pigment cup (blue arrow), having a slightly flattened bottom and tulip-shaped opening, is visible along with the lens and the faintly stained corneal covering (black arrow). The vitreous space separating the lens and retina is also visible (green arrow). An enlargement of the boxed area showing the different photoreceptor regions is shown in C. Scale bar=100µm. B. Whole large complex eye. A portion of the lens can be seen resting in the opening of the pigment cup (PC) which has a greater depth closer to the top of the rhopalium and a thinner depth closer to the bottom of the rhopalium (red arrows). Migrating pigment granules are visible along the outer perimeter of the cup (white arrow). Scale bar=200µm. C. Cross-section of the large complex eye retina. The three regions of the photoreceptors can be seen: the apical light-receptive region (LR), the middle pigmented region (P), and the basal nuclear region (N). The relatively smooth inner edge of the pigment can be seen compared to the migrating pigment granules located along the outer edge within the photoreceptors. Light-staining photoreceptors (black asterisks) and dark-staining photoreceptors (yellow asterisks) are also visible. Scale bar=20µm. D. Whole small complex eye. The lens can be seen within the opening of the pigment cup (PC) and sits higher than the lens of the large complex eye. The bottom of the pigment cup is flattened (red arrowhead). Scale bar=100µm.

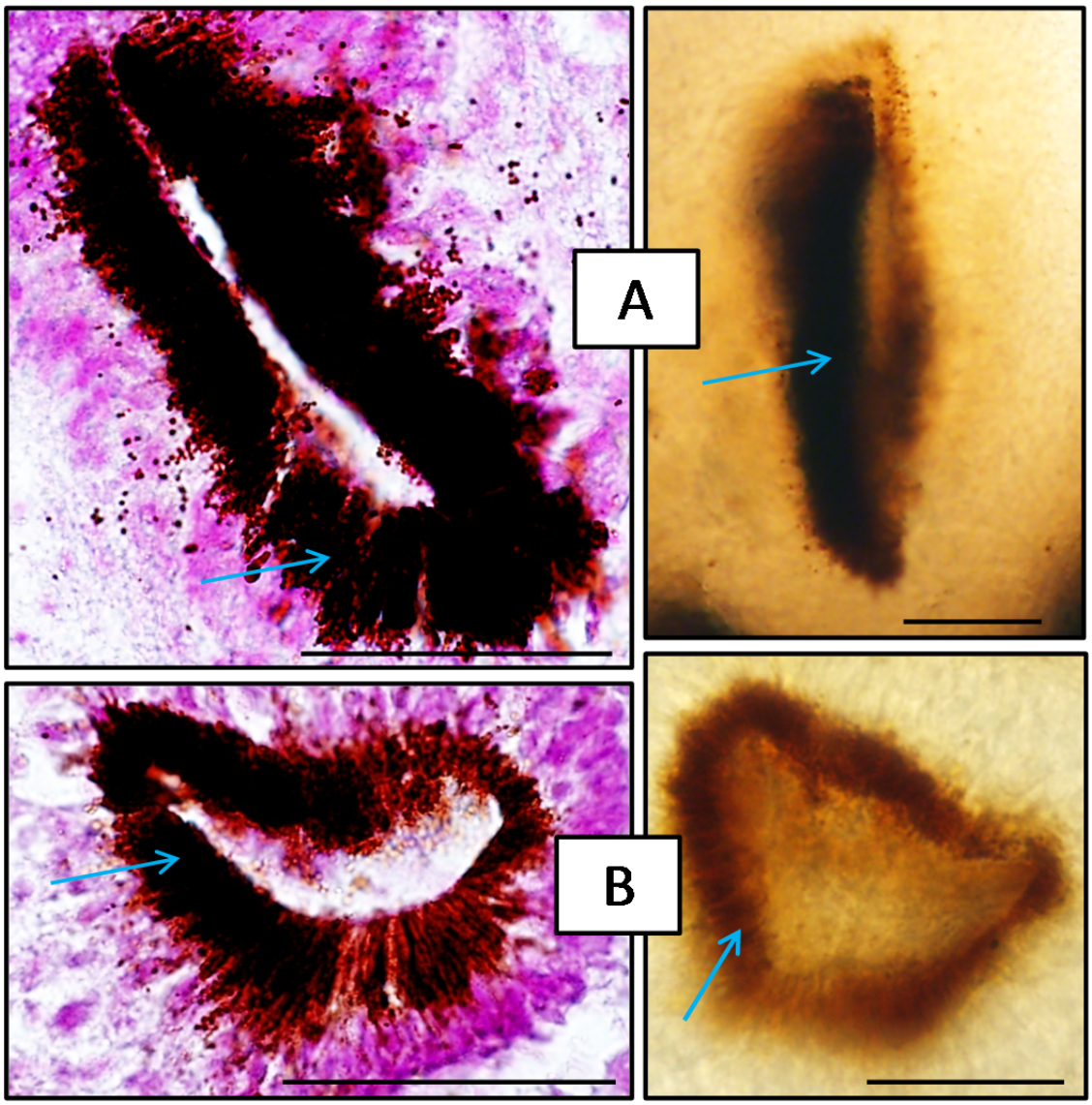

Figure 23. Fontana-Masson staining for melanin on (left) and whole-mount brightfield images (right) of adult simple ocelli. A. Slit ocellus. The inner perimeter of the pigment (blue arrow) is relatively smooth compared to the migrating pigment granules located along the outer perimeter. B. Pit ocellus. The inner perimeter of the pigment (blue arrow) is relatively smooth compared to the migrating pigment granules located along the outer perimeter. Scale bars=50μm.

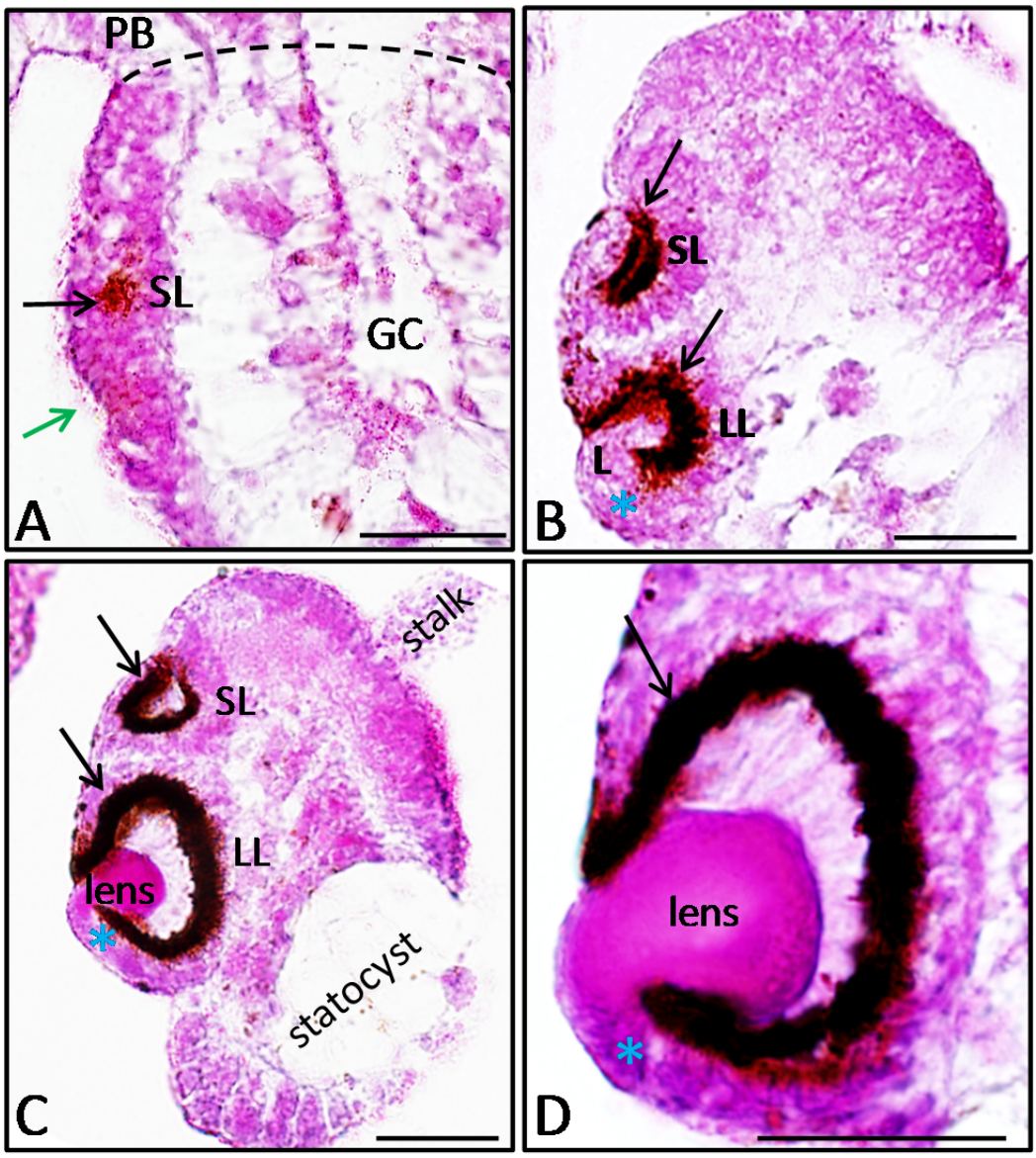

Figure 24. Fontana-Masson staining for melanin in rhopalia during Stage 2 – Stage 5. A. Stage 2. A section of the rhopalial profile shows the initial pigment of the small lensed eye (black arrow), which is located beneath the rhopalial surface, along with the cup-shaped primordium of the large lensed eye (green arrow). The top of the rhopalium (hashed line) is shown relative to the connection to the polyp body (PB). A portion of the gastrovascular cavity (GC) is also visible. Scale bar=25 µm. B. Stage 3. Pigment of the large (LL) and small (SL) lensed eyes is now visible (black arrows). Fainter pigment can be seen radiating from the outer edge of the more heavily pigmented central region. The up-folding sheet of cells (blue asterisk) is visible and is attached to the forming lens (L) which is folding into the forming pigment cup. Due to the thick overlying sheet of cells, the bottom portion of the pigment cup (located farthest from the small complex eye) does not reach the rhopalial surface. Scale bar=25 µm. C. The pigment cups (black arrows) of the large (LL) and small (SL) lensed eyes continue to develop during Stage 4. Much less fainter pigment can be seen radiating out from the main pigment cups of the large and small lensed eyes forming a smoother pigment boundary. The forming lens can be seen within the pigment cup of the large lensed eye along with the up-folding sheet of cells (blue asterisk, which is attached to the lens), the basal statocyst, and a portion of the stalk. Scale bar=25 µm. D. Stage 5. A close-up of a section of the large lensed eye shows the developing pigment cup (black arrow) along with the thinning up-folding sheet of cells (blue asterisk) which is attached to the developing lens. Scale bar=20 µm.

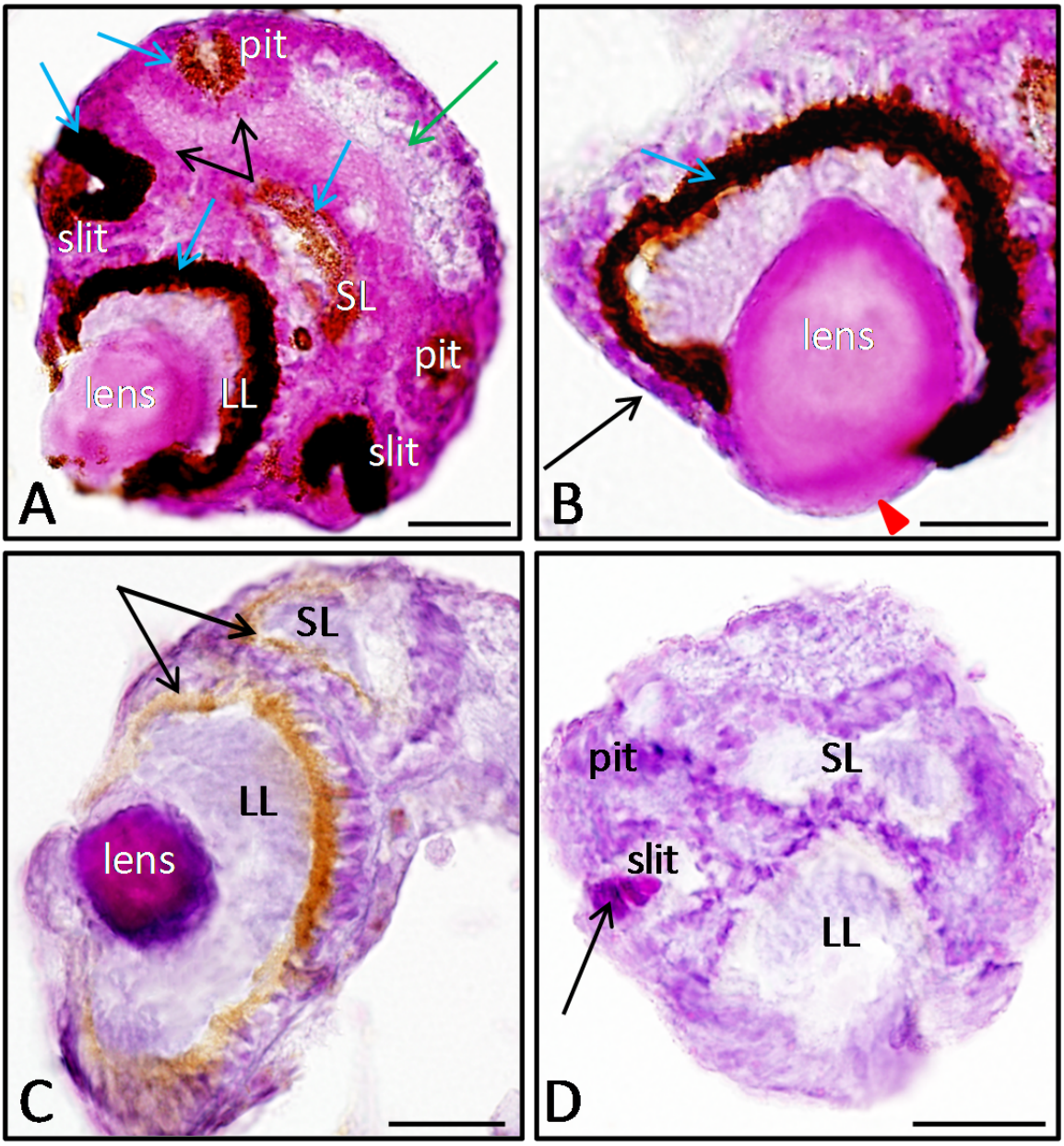

Figure 25. Fontana-Masson staining for melanin in Stage 7 rhopalia and melanin-bleached controls. A. Stage 7. The pigment (blue arrows) of the large lensed eye (LL) and slit ocelli (slit) are visible along with partial portions of the small lensed eye (SL) and pit ocelli (pit). The photoreceptor nuclei encircling the ocelli can also be seen (black arrows) along with the faintly-stained area with sparse nuclei at the top of the rhopalium (green arrow). Scale bar=20 µm. B. Stage 7 large lensed eye. The pigment cup (blue arrow) is visible along with the lens and up-folding sheet of cells (black arrow) which is now very thin and is forming the cornea which sits on top of the lens (red arrowhead). Scale bar=25 µm. C. A Stage 7 rhopalium was bleached for 20 minutes prior to the staining procedure and showed a clear decrease in melanin staining (black arrows) in the large lensed eye (LL) and small lensed eye (SL). Scale bar=20 µm. D. A Stage 7 rhopalium was bleached for 30 minutes prior to the staining procedure and showed a complete lack of melanin staining in the large lensed eye (LL), small lensed eye (SL), slit ocelli (slit), and pit ocelli (pit). The developing lens-like material of a slit ocellus is visible (black arrow). Scale bar=20 µm.

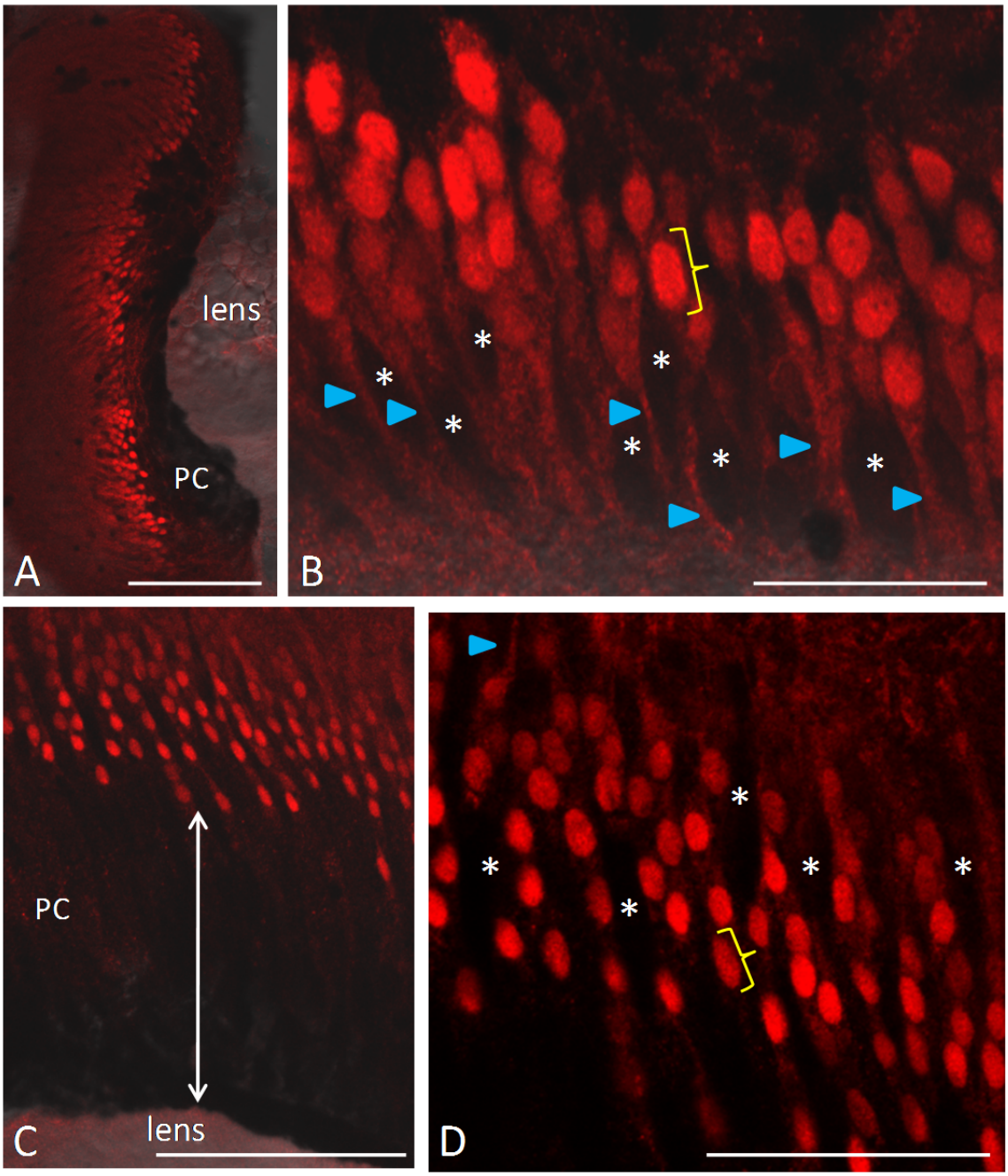

Figure 26. Immunofluorescent staining for UV (ultraviolet) opsin-like protein in adult rhopalia. A. Small lensed eye overview. The positively-stained photoreceptors are localized behind the lens and rest on top of the lower portion of the pigment cup (PC). Scale bar=100 µm. B. Small lensed eye. These photoreceptors have a staining length of 30-40 µm with a tapered base (blue arrowheads) and a brightly-stained bulbous tip (yellow bracket).Unstained photoreceptors (white asterisks) are interspersed with the stained ones which form a rather linear boundary. Scale bar=25 µm. C. Large lensed eye short photoreceptors. These photoreceptors, which are located within the top half of the retina (closest to the small complex eye), rest on top of the pigment cup (PC) and are distanced from the lens (white arrow) Scale bar=100 µm. D. Large lensed eye short photoreceptors close-up. These photoreceptors, like those in the small lensed eye, are 30-40 µm in length with a tapered base (blue arrowhead) and brightly-stained bulbous tip (yellow bracket). Unlike in the small lensed eye, these photoreceptors form a more jagged boundary. Multiple unstained photoreceptors (white asterisks) can be seen interspersed with the stained ones. Scale bar=50 µm. Differential interference contrast (DIC) imaging was used in A-C to provide structural context.

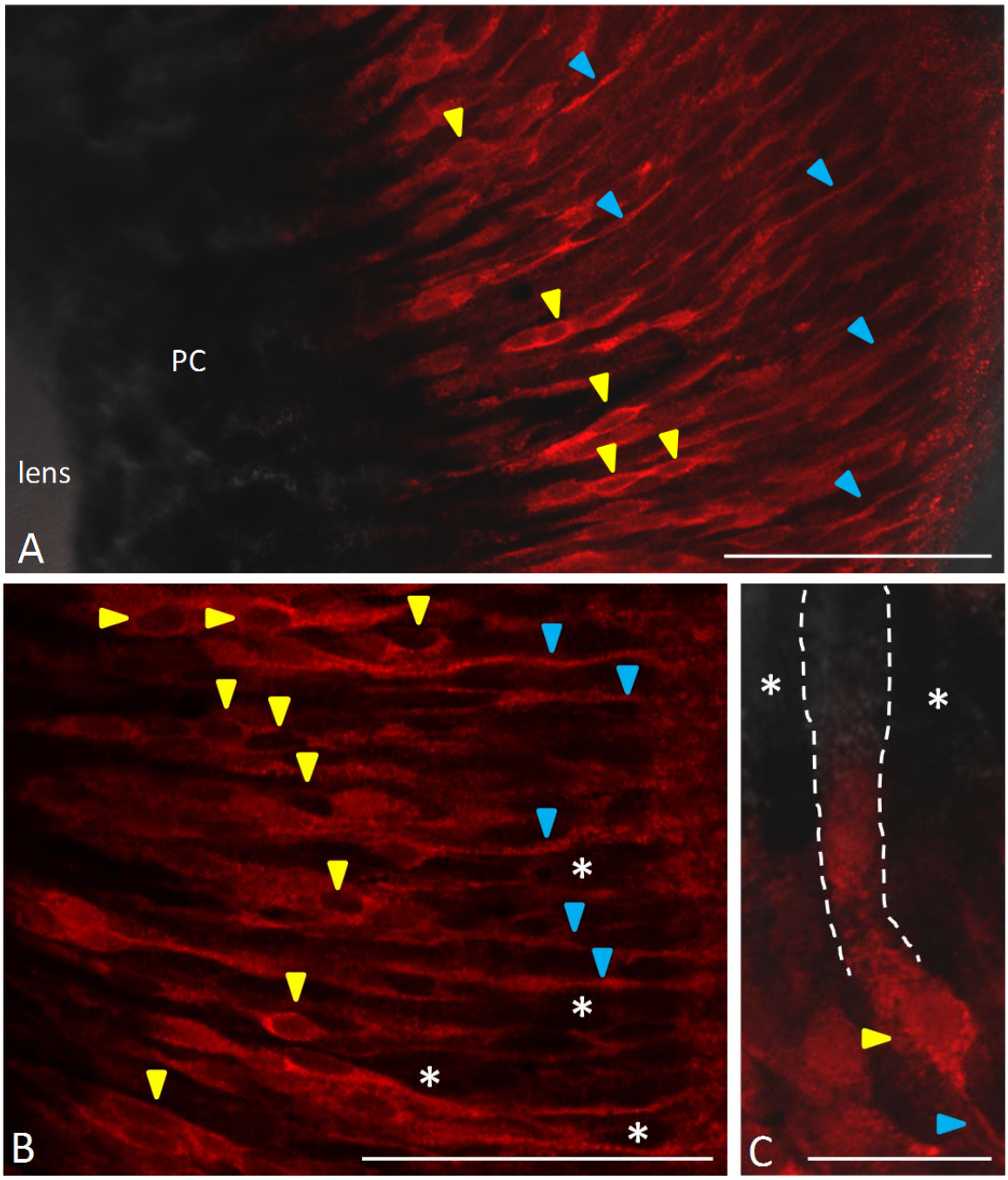

Figure 27. Immunofluorescent staining for UV (ultraviolet) opsin-like protein in adult rhopalia – large complex eye. A. Long photoreceptors overview. These photoreceptors are found in the bottom half of the retina (closest to the basal statocyst) and reach farther inward towards the lens than the short photoreceptors. Resting on top of the pigment cup (PC), these photoreceptors have a staining length of approximately 60-70 µm and exhibit a long tapered base (blue arrowheads) which attaches to the nucleus (yellow arrowheads); staining is restricted to the bottom portions of the photoreceptors. Scale bar=50 µm. B. Long photoreceptors close-up. The thin tapered bases of the photoreceptors (blue arrowheads) are visible along with the nuclei (yellow arrowheads) within the cells. Unstained photoreceptors (examples indicated with asterisks) can be seen interspersed with the stained photoreceptors. Scale bar=50 µm. C. Apical staining in a long photoreceptor. Above the tapered base (blue arrowhead) and nucleus (yellow arrowhead) of a cell, the staining fades and shows the lack of pigmentation within the cell. Two pigmented photoreceptors can be seen on either side (white asterisks). Scale bar=15 µm. Differential interference contrast (DIC) imaging was used in A and C to provide structural context.

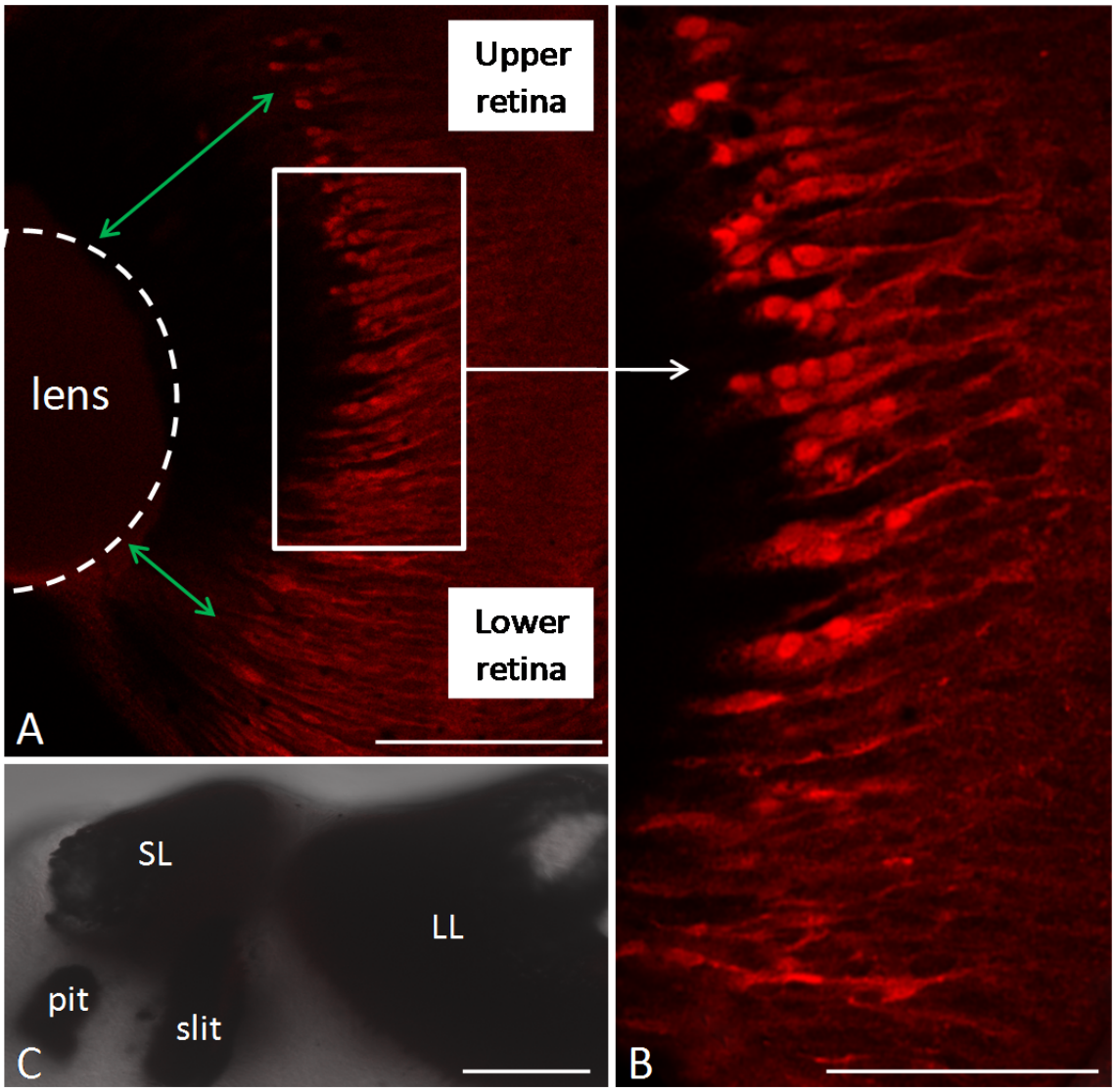

Figure 28. Immunofluorescent staining for UV (ultraviolet) opsin-like protein showing the transition of photoreceptor morphology in the large lensed eye. The upper half of the retina (closest to the small complex eye) exhibits the short stained photoreceptors which transition to the long photoreceptors found in the bottom half (closest to the statocyst). The difference in distance from the lens (hashed line) is visible (green arrows). An enlargement of the boxed area is shown in B. Scale bar=100 µm. B. Transition in photoreceptor morphology close-up. The transition from the short photoreceptors to the long photoreceptors is visible. Scale bar=50 µm. C. Adult rhopalium control. No staining was seen in samples not subjected to the primary antibody; the large (LL) and small (SL) lensed eyes are visible along with a slit and pit ocellus. Scale bar=100 µm. Differential interference contrast (DIC) imaging was used in C to provide structural context.

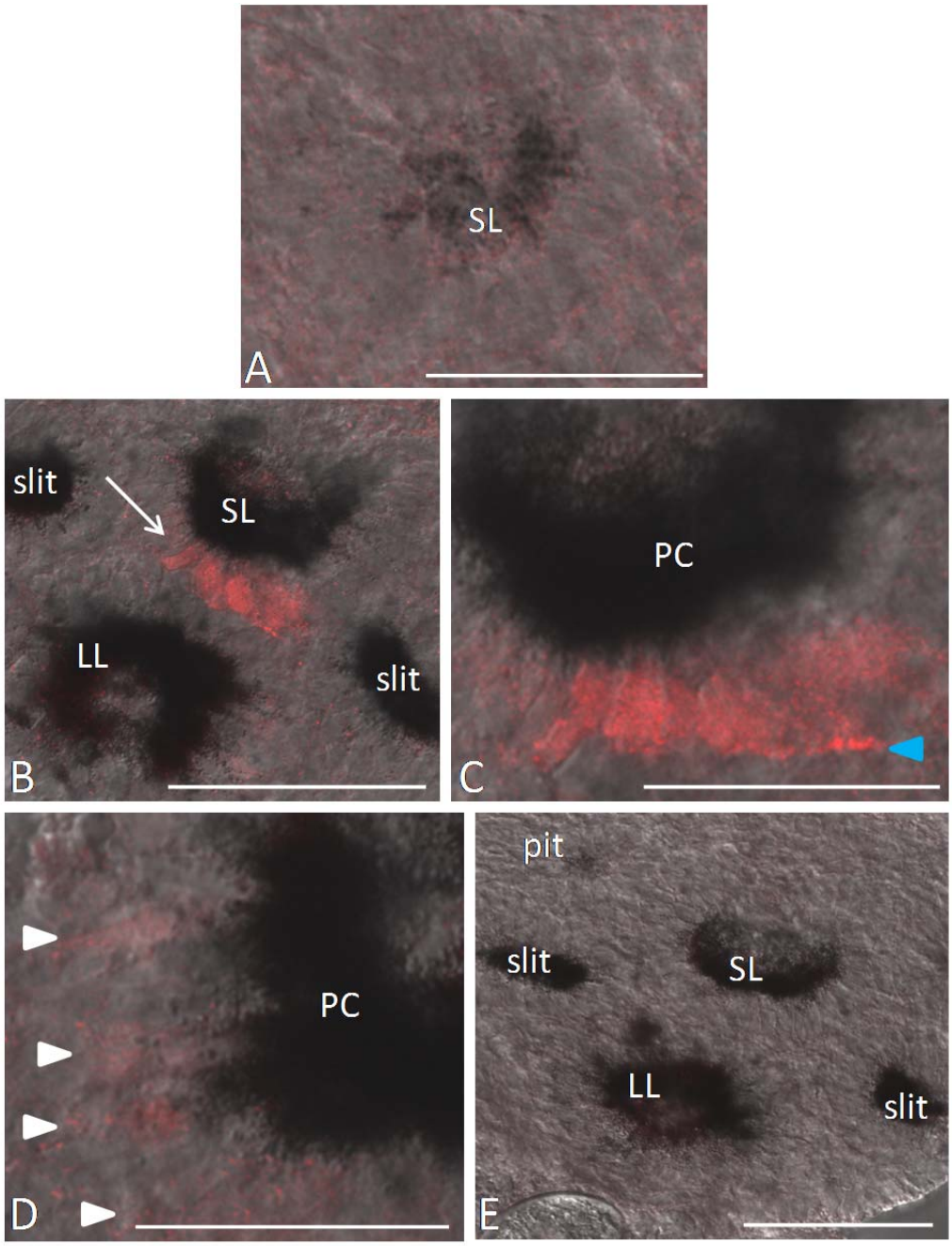

Figure 29. Immunofluorescent staining for UV (ultraviolet) opsin-like protein in Stages 2 and 3. A. Stage 2. No staining is visible in the photoreceptors making up the forming small complex eye (SL). Scale bar=25 µm. B. Stage 3 overview. UV opsin-like positive staining first appears within the photoreceptors of the small lensed eye (SL) which are located in the central portion of the eye (arrow). The large lensed eye (LL) and slit ocelli (slit) are also visible. Scale bar=50 µm. C. Stage 3 small complex eye. The staining within the photoreceptors is located below the forming pigment cup (PC) and has a length of approximately 10 µm. The photoreceptors in the center are brighter than those towards the sides of the forming eye. One brightly-stained photoreceptor base is also visible (blue arrowhead) Scale bar=25 µm. D. Stage 3 large complex eye. The faint staining within the photoreceptors (white arrowheads) of the large complex eye, which also appears outside of the forming pigment cup (PC), has an approximate length of 10-15 µm. Scale bar=25 µm. E. Stage 3 control. No staining was seen in samples not subjected to the primary antibody targeting the UV opsin-like protein. Scale bar=50 µm. Differential interference contrast (DIC) imaging was used in all images to provide structural context.

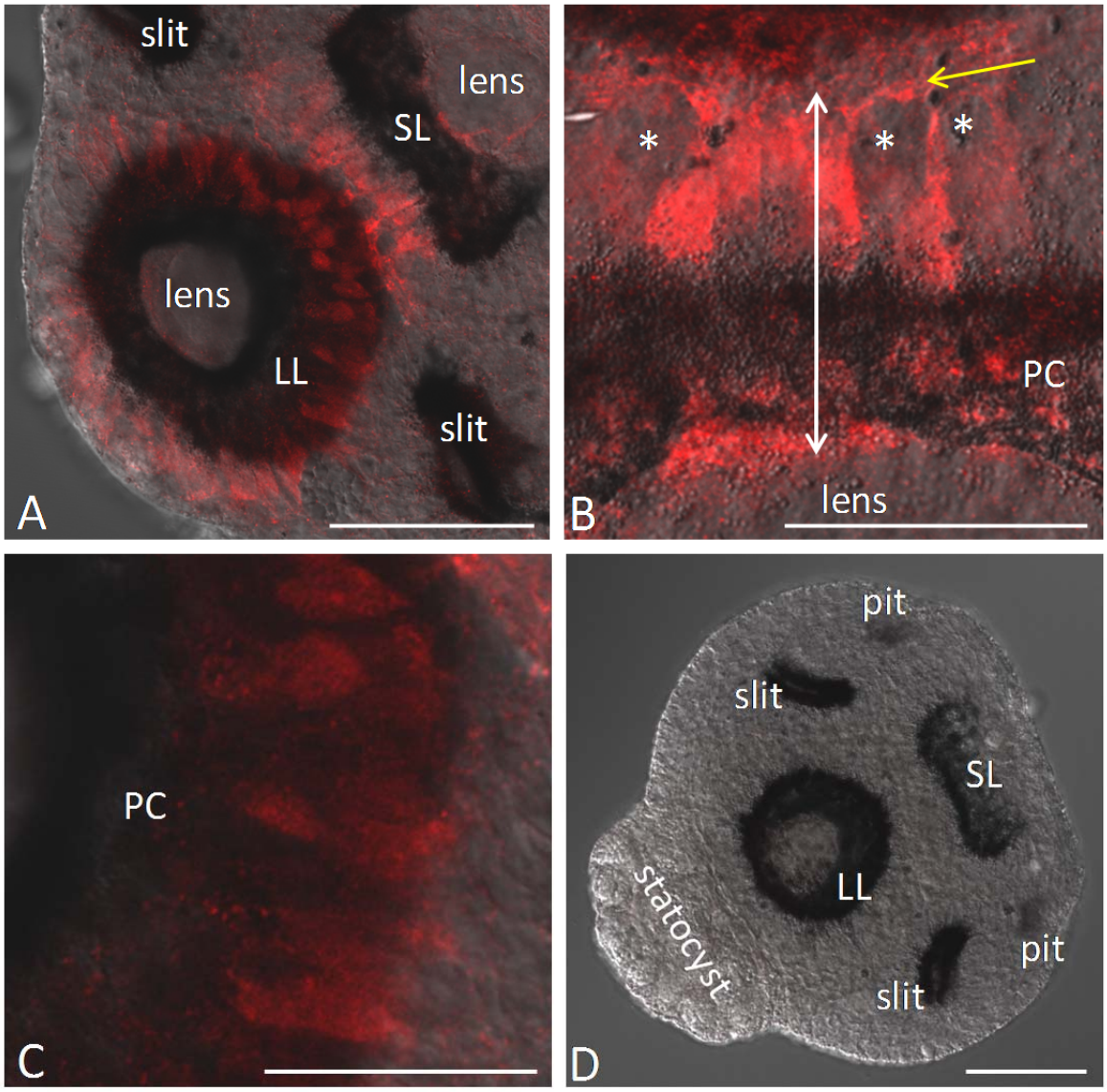

Figure 30. Immunofluorescent staining for UV (ultraviolet) opsin-like protein in Stage 4. A. Stage 4 overview. Staining can be seen within the photoreceptors of both the small (SL) and large (LL) complex eyes. The positively-stained photoreceptors in the small complex eye are still confined to the central region of the forming retina (behind the developing lens) while the photoreceptors of the large complex eye encircle the entire retina. The slit ocelli (slit) are also visible. Scale bar=50 µm. B. Small complex eye. The staining length (white arrow) of the photoreceptors now thread through the pigmented photoreceptors making up the forming pigment cup (PC) to the edge of the forming lens. The staining length has increased to approximately 30 µm and the photoreceptor bases are clearly visible (yellow arrow) along with unstained photoreceptor cells (asterisks). Scale bar=30 C. Large complex eye. Remaining localized in the outer regions of the forming retina, the staining lengths of the photoreceptors are now approximately 20-25 µm and appear to rest on top of the forming pigment cup (PC) which indicates a lack of pigment within the positively-stained cells. Scale bar=20 µm. D. Stage 4 control. No staining was seen in samples not subjected to the primary antibody targeting the UV opsin-like protein. Scale bar=50 µm. Differential interference contrast (DIC) imaging was used in all images to provide structural context.

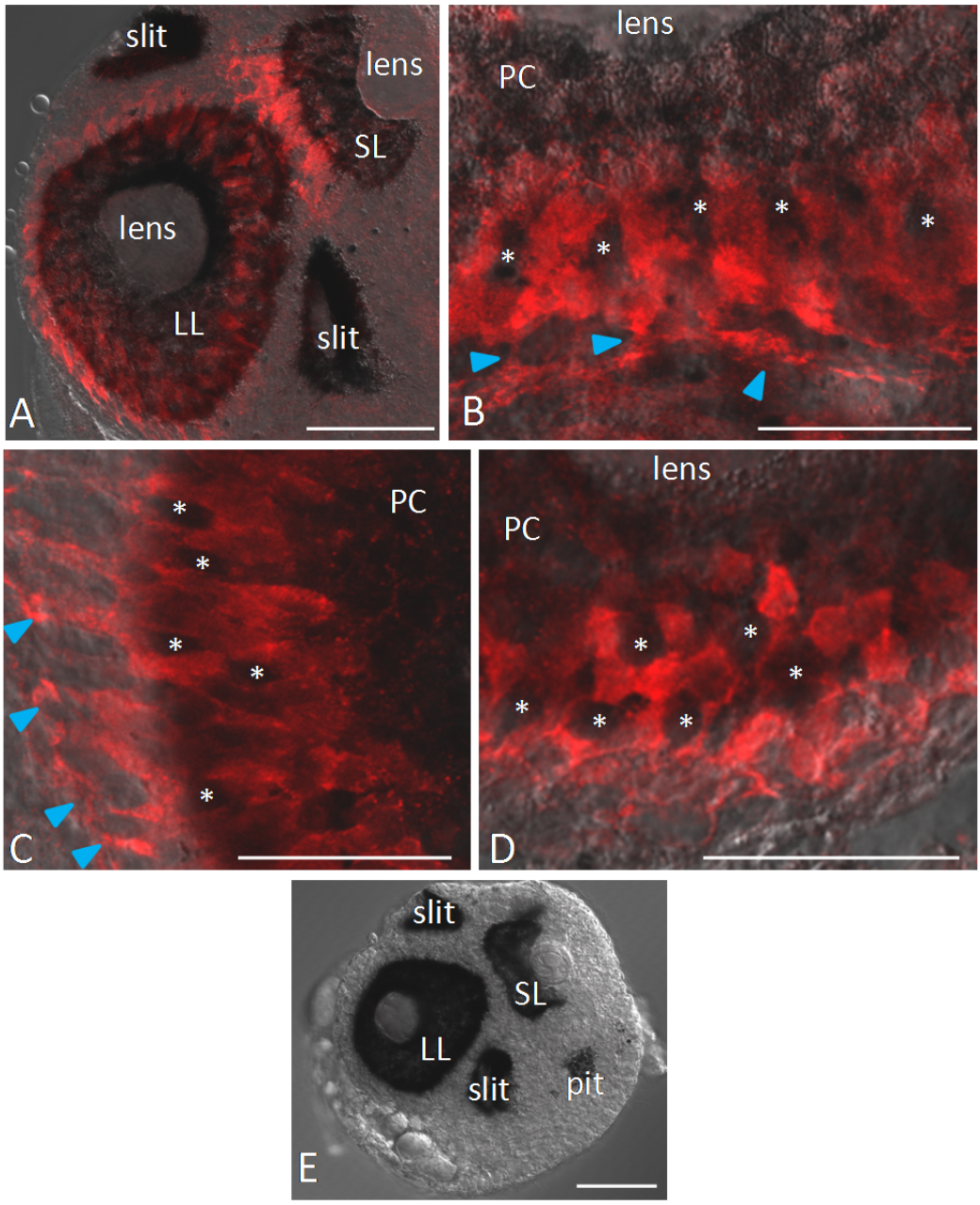

Figure 31. Immunofluorescent staining for UV (ultraviolet) opsin-like protein in Stage 5. A. Stage 5 overview. Staining can be seen within multiple photoreceptors making up the retinas of both the large (LL) and small (SL) lensed eyes although the staining remains brighter in photoreceptors of the small lensed eye which remain localized behind the lens. The unstained slit ocelli (slit) are also visible. Scale bar=50 µm. B. Small lensed eye. The staining lengths of the photoreceptors remain at approximately 30 µm and are now found farther back from the lens and above the pigment cup (PC). Brightly-stained photoreceptor bases are visible (arrowheads). These photoreceptors remain rectangular in shape and are interspersed with unstained photoreceptors (asterisks). Scale bar=25 µm. C. Large complex eye. Now having a staining length of 30-35 µm, the positively-stained photoreceptors remain above the forming pigment cup (PC). Brightly-stained photoreceptor bases are visible (arrowheads) along with unstained photoreceptors (asterisks). Scale bar=25 µm. D. Large lensed eye (bottommost region). Positively-stained photoreceptors can be seen intertwined with unstained photoreceptors giving this region of the eye a checkered appearance. Scale bar=25 µm. E. Stage 5 control. No staining was seen in samples not subjected to the primary antibody targeting the UV opsin-like protein. Scale bar=50 µm. Differential interference contrast (DIC) imaging was used in all images for structural context.

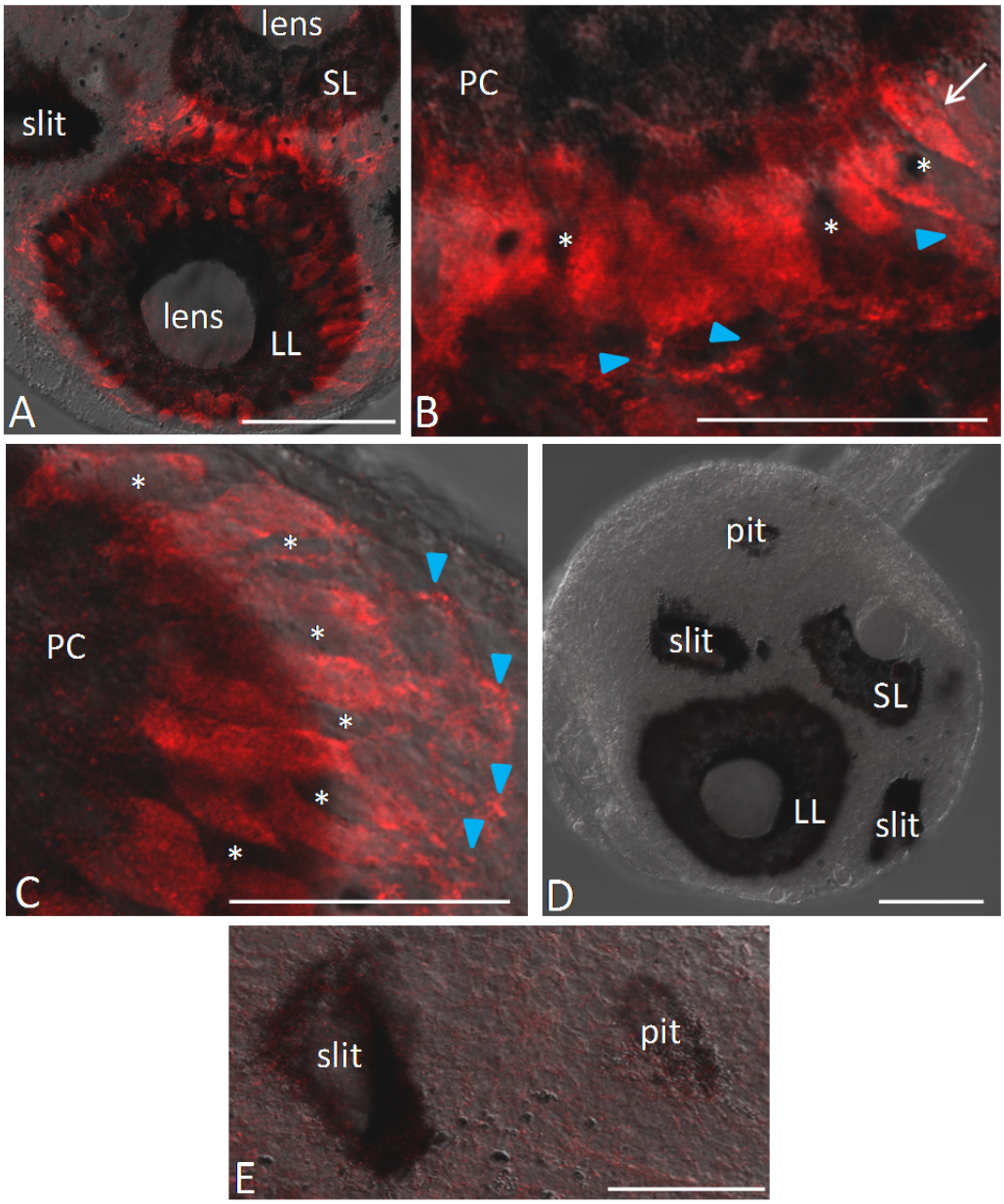

Figure 32. Immunofluorescent staining for UV (ultraviolet) opsin-like protein in Stage 7. A. Stage 7 overview. Staining can be seen within multiple photoreceptors making up the retinas of both the large (LL) and small (SL) lensed eyes, although the staining remains brighter in photoreceptors of the small lensed eye which remain localized behind the lens. A slit ocellus (slit) is also visible. Scale bar=50 µm. B. Small lensed eye. The positively-stained photoreceptors now have a staining length of approximately 30-40 µm and are located farther away from the lens along the outer edge of the pigment cup (PC). Although still somewhat boxy in shape, these photoreceptors are now more slender (arrow). Multiple brightly-stained photoreceptor bases are visible (arrowheads) along with interspersed unstained photoreceptors (asterisks). Scale bar=25 µm. C. Large lensed eye. The photoreceptors now have a staining length of 30-40 µm and remain on top of the pigment cup (PC). Multiple photoreceptor bases are visible (arrowheads) along with unstained photoreceptors (asterisks). Scale bar=25 µm. D. Stage 7 control. No staining was seen in samples not subjected to the primary antibody targeting the UV opsin-like protein. The large (LL) and small (SL) lensed eyes are visible along with the slit (slit) and pit (pit) ocelli. Scale bar=50 µm. E. Slit and pit ocelli. At no point during transformation did any of the photoreceptors of the simple ocelli stain positive for the UV opsin-like protein. Scale bar=25 µm. Differential interference contrast (DIC) imaging was used in all images to provide structural context.

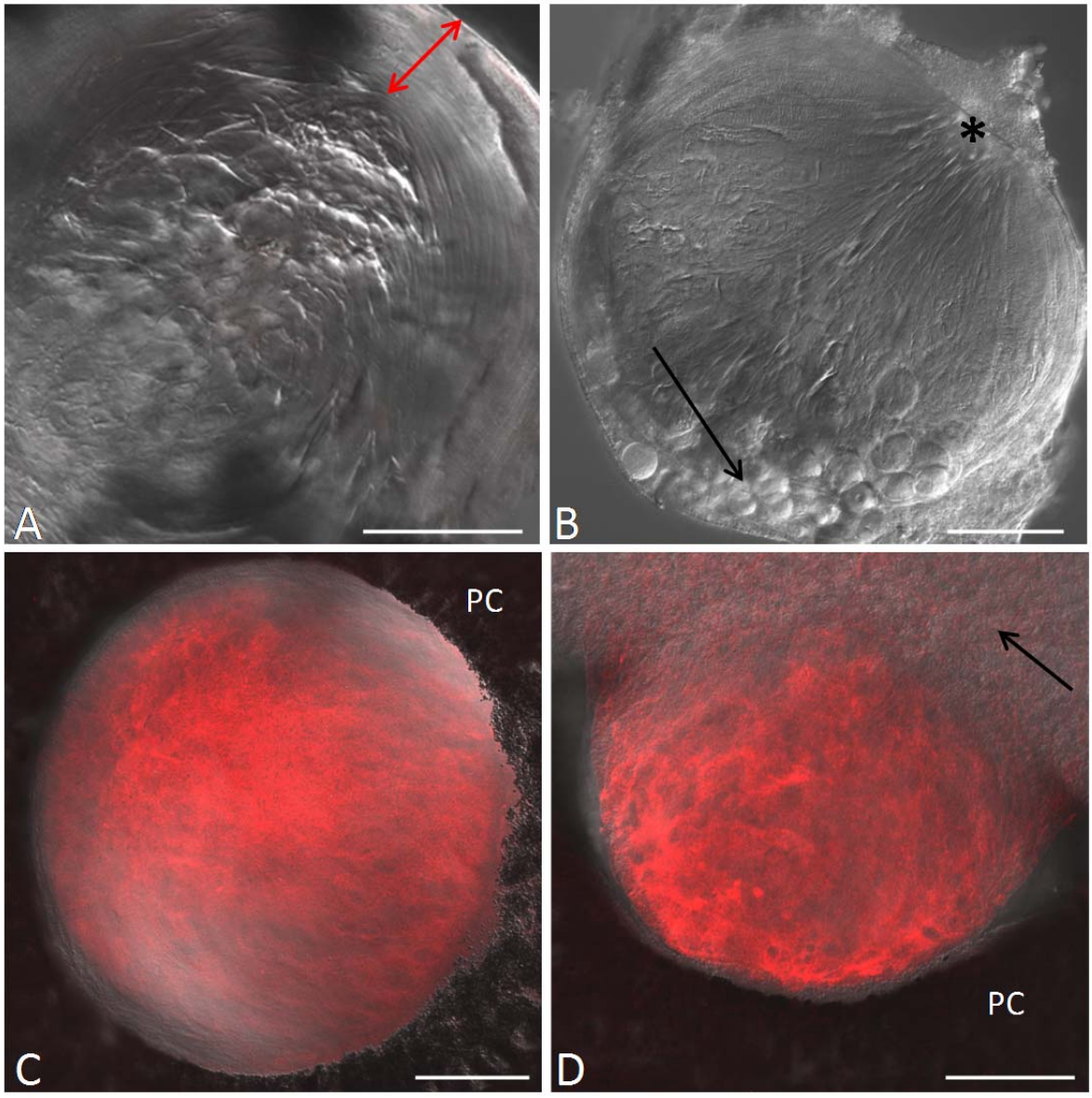

Figure 33. J1-crystallin controls and staining in adult complex eyes. A. Isolated lens of large lensed eye control. No staining was seen in lenses which were not subjected to the primary antibody targeting the J1-crystallin protein. Characteristics of the lens are visible such as the stacked layer of outer fibrous cells (red arrow) surrounding the inner globular cells. B. Isolated lens of small lensed eye control. No staining was seen in lenses which were not subjected to the primary antibody. Characteristics of the lens are visible such as the globular cells (black arrow) in the portion of the lens which rests within the pigment cup opening as well as the tapering of the fibrous cells on the opposite side of the lens to an apparent point of origin (asterisk). C. Large lensed eye. Staining on the surface of the lens, which rests within the encircling pigment cup (PC), reflects the fibrous nature of the cells stained. D. Small lensed eye. Staining on the surface of the lens, which sits within the opening of the pigment cup (PC), reflects the fibrous nature of the cells stained. Very faint staining can be seen in the sheet of cells just above the lens (arrow). Differential interference contrast (DIC) imaging was used in all images to provide structural context. Scale bars=50μm.

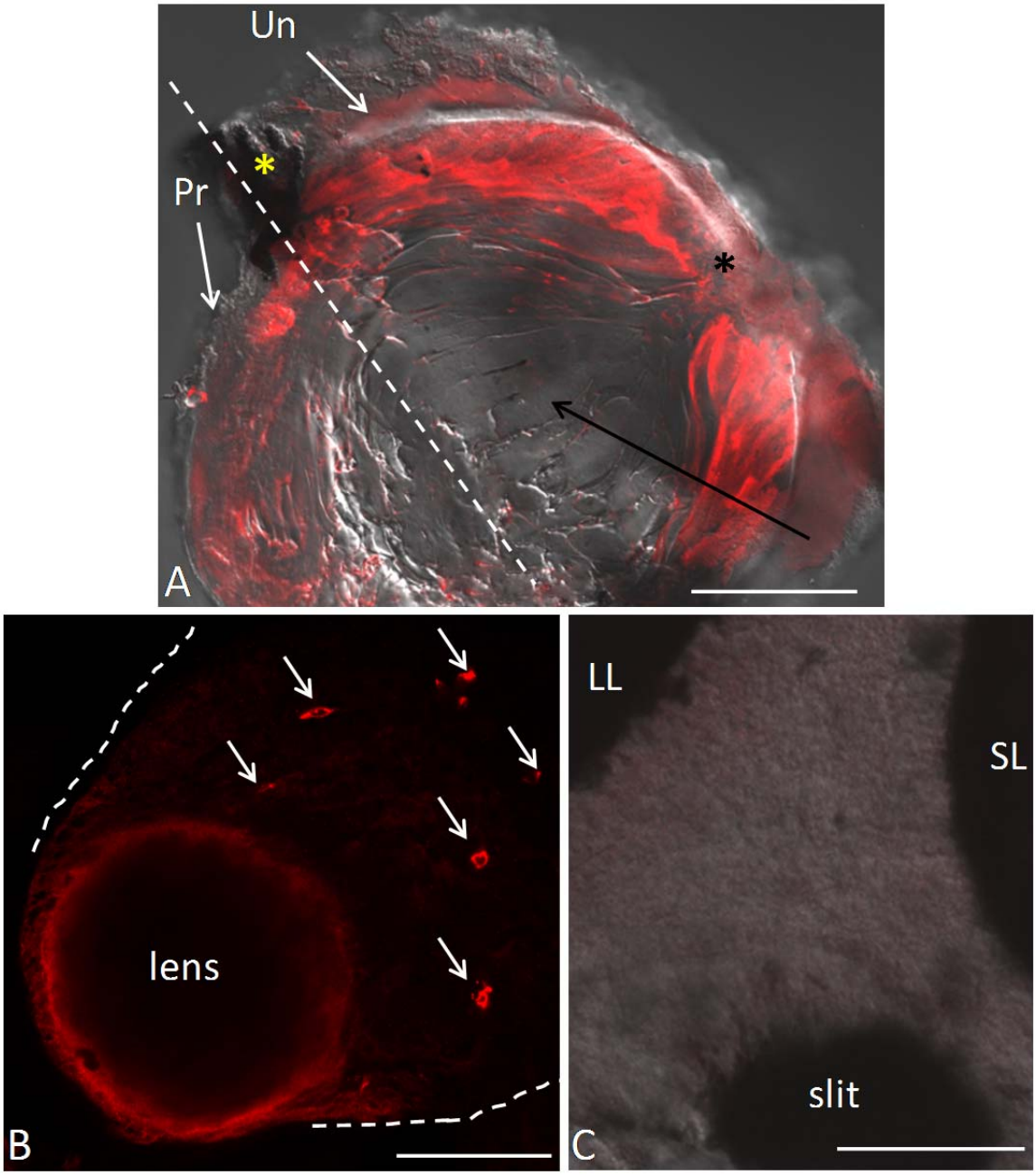

Figure 34. J1-crystallin staining in adult complex eyes and extraocular staining. A. Halved large complex eye lens. For orientation, the portion of the lens to the left of the hashed line protrudes (Pr) from the pigment cup (a portion of which is visible and is labeled with a yellow asterisk) and the region to the right of the hashed line represents the underside of the lens (Un) which sits within the retinal cup. The outer fibrous cells are positively stained and the central globular cells (black arrow) are not stained. The staining of the fibrous cells is brighter in the underside region of the lens than in the protruding region. A point of origin from which all cells spread outward is visible (black asterisk) on the underside of the lens. B. Extraocular staining of the small complex eye. Very faint staining is visible across the surface of the down-folding sheet of cells (within hashed lines) which sits above and connects to the lens of the small complex eye along with several punctate regions of bright staining (white arrows). C. Lack of other extraocular staining. A region of the surface of the rhopalium is shown located near the large lensed eye (LL), small lensed eye (SL), and a slit ocellus (slit) and shows no staining. Scale bars=50μm.

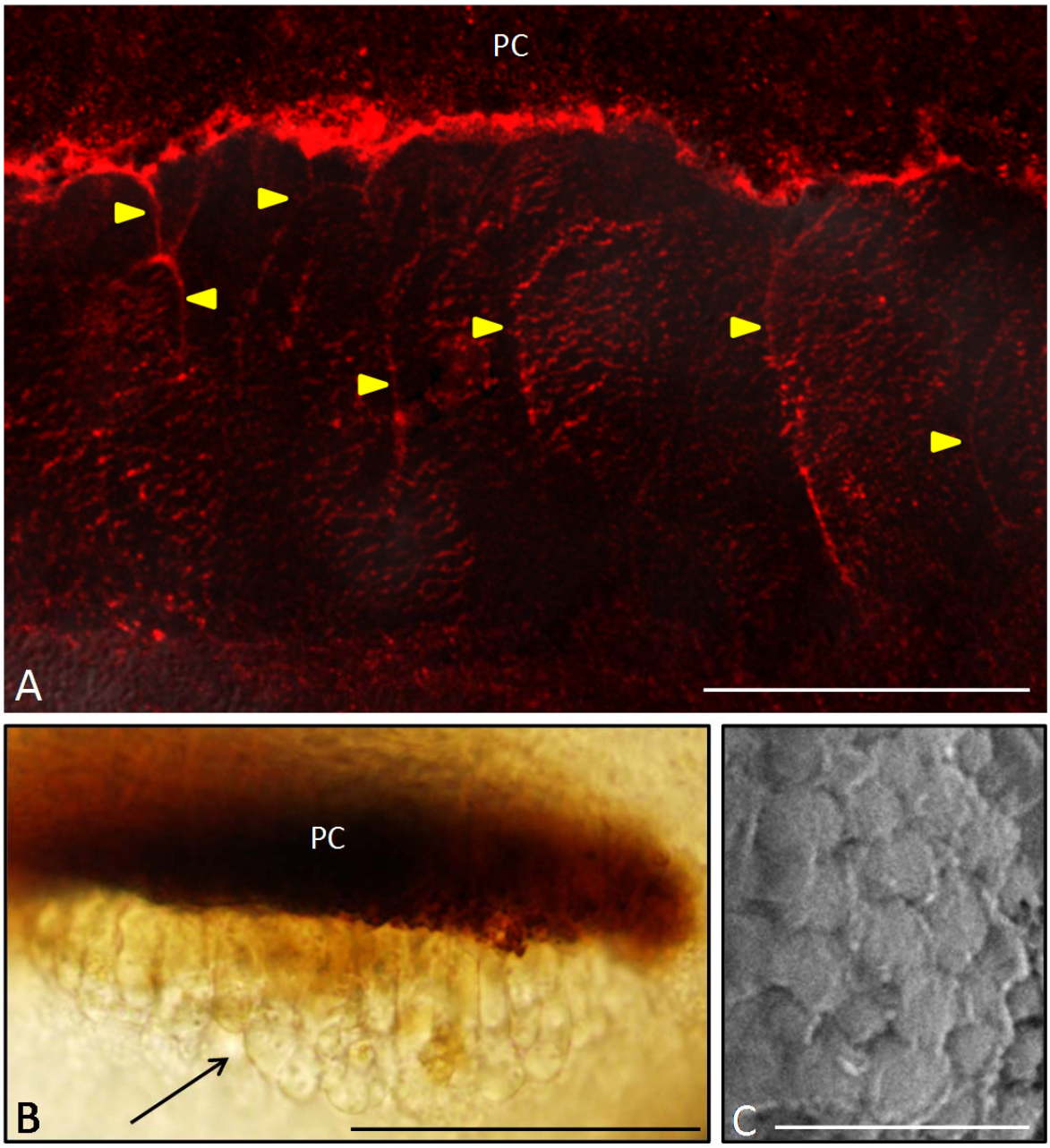

Figure 35. J1-crystallin staining in the slit ocellus. A. Slit ocellus staining. The brightest staining can be seen along the inner edge of the top of the pigment cup (PC). The stained edges of some photoreceptors cells are visible (yellow arrowheads) along with the surface staining which reflects the bumpy surface of the cells shown in C. Scale bar=25µm. B. Brightfield image of whole slit ocellus. The upper edge of the pigment cup is visible (PC) as well as the lens-like material which sits on the surface of the laterally-flatted photoreceptor cells (arrow) that span the opening of the pigment cup. Scale bar=75µm. C. Lens-like material cell surface. The lens-like material gives the surface of the photoreceptor cells a bumpy appearance which causes the pattern of staining seen in A. Scale bar=5µm. Differential interference contrast (DIC) imaging was used in A to provide structural context.

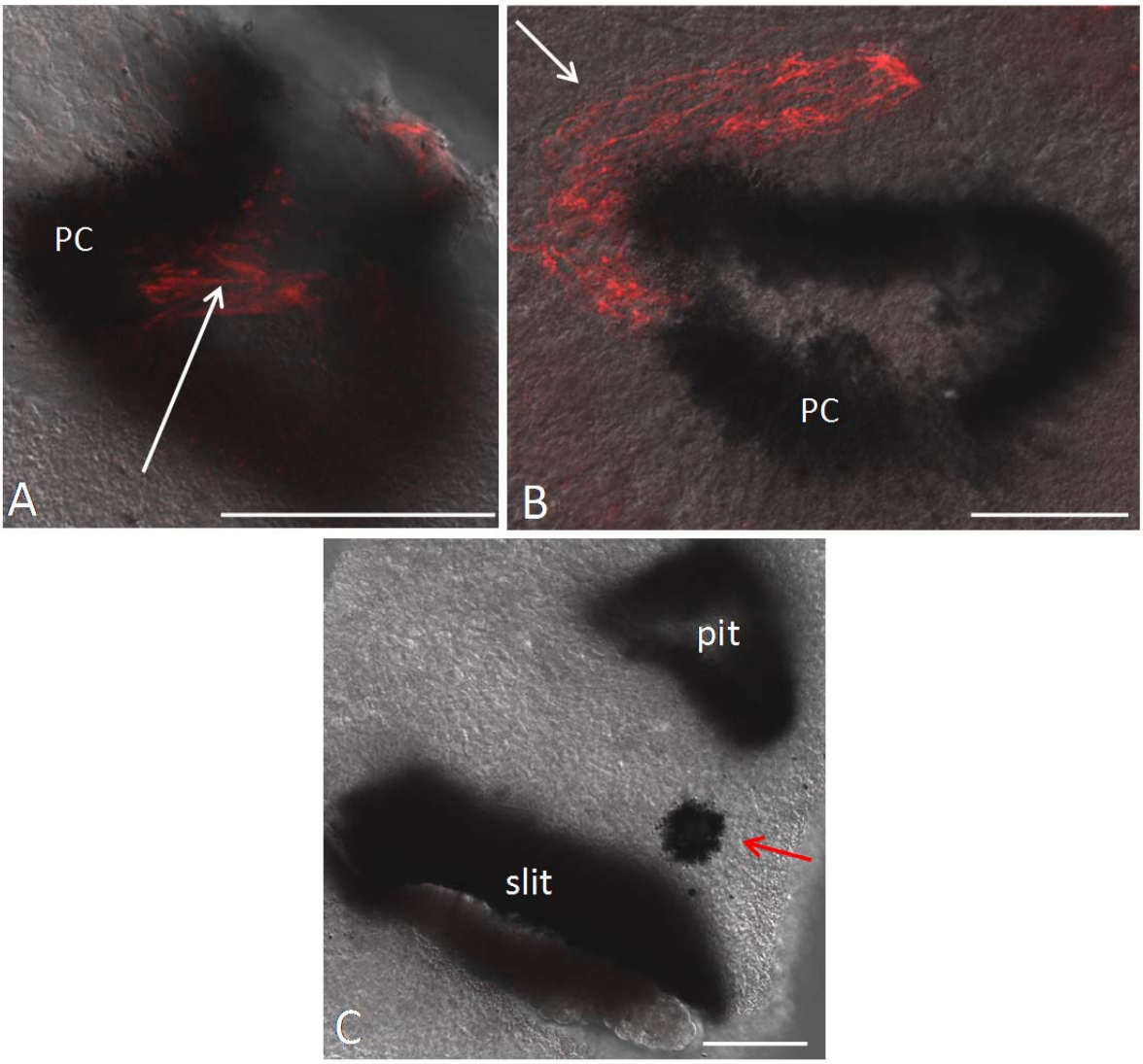

Figure 36. J1-crystallin staining in the pit ocellus. A. Staining of pit ocellus in whole rhopalium. Positive staining (arrow) is seen within the confines of the pigment cup (PC) and is stringy in appearance. B. Staining of pit ocellus - everted. The stained material (white arrow) is artificially everted from the pigment cup (PC). The stained material is stringy, punctuate, and clumps together. C. Simple ocelli control. Simple ocelli not subjected to the primary antibody targeting the J1-crystallin did not exhibit staining. No staining was seen in the circular structure often found in between the slit and pit ocellus (red arrow). Scale bars=50µm. Differential interference contrast (DIC) imaging was used in all images to provide structural context.

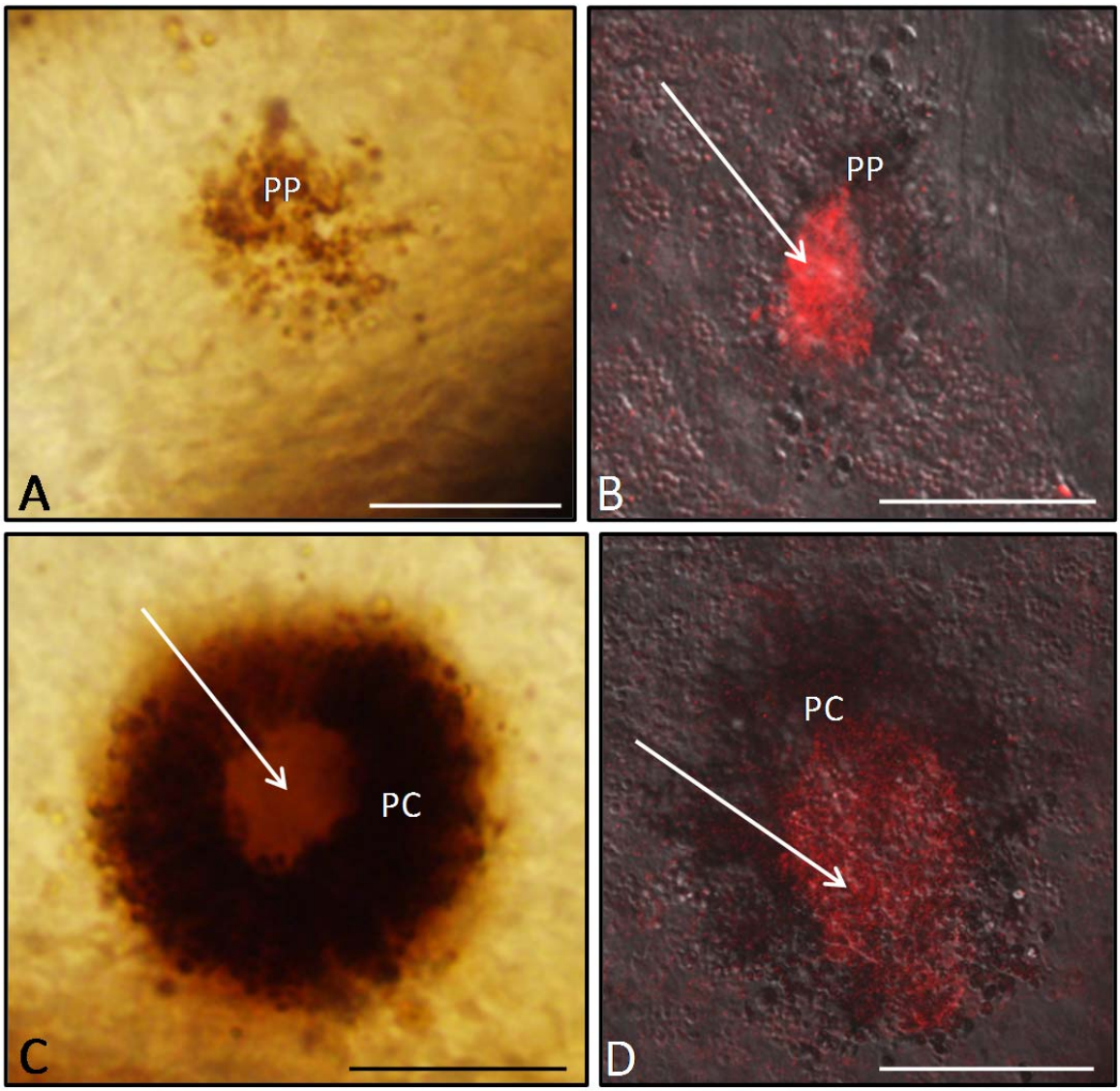

Figure 37. Brightfield images and J1-crystallin staining of structure found between simple ocelli. A. Simple form of structure. The structure can be as simple as a small circular patch of pigment (PP) found in between the slit and pit ocellus. B. J1-crystallin staining of simple form. Bright staining (arrow) is visible in the center of the small patch of pigment (PP). C. Complex form of structure. This form of the structure is heavily pigmented and appears to have some form of lens-like material (arrow) within the pigment cup (PC). D. J1-crystallin staining of complex form. A circular area of staining (arrow) is visible in the center of the encircling pigment cup (PC). Scale bars=25μm. Differential interference contrast (DIC) imaging was used in B and D to provide structural context.

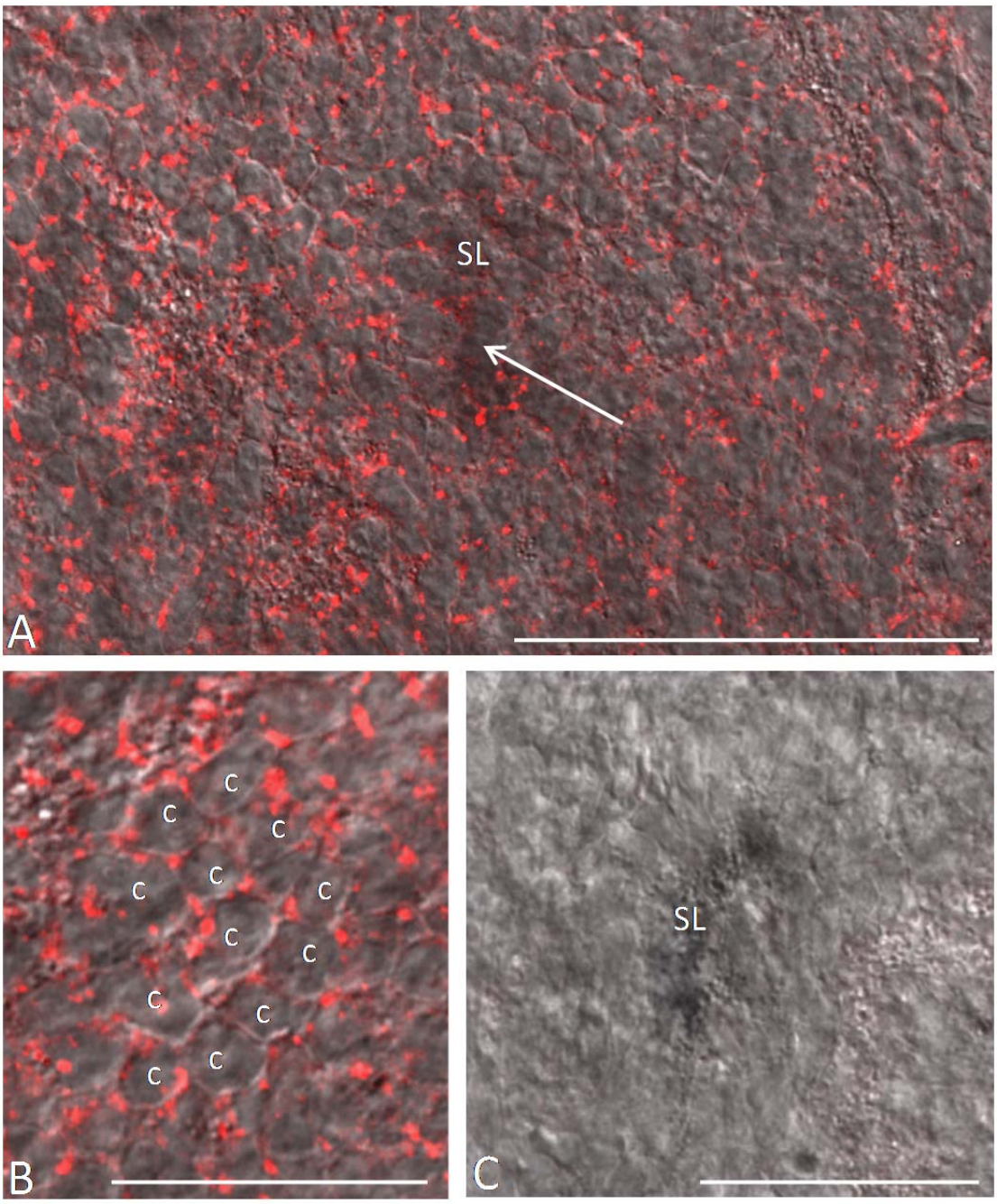

Figure 38. J1-crystallin staining during Stage 2. A. Stage 2. No lens-specific staining is visible yet, as no lenses are forming at this stage. Bright and punctate staining is visible across the surface of the entire rhopalium along with the initial eyespot (white arrow) representing the early formation of the small lensed eye. Scale bar=50µm. B. Surface staining. A close-up of the staining reveals that it is most likely located up against the membrane of the cells (c). Scale bar=20µm. C. Stage 2 control. Samples not subjected to the primary antibody targeting the J1-crystallin protein showed no staining. The pigment of the small lensed eye (SL) is visible. Scale bar=25µm. Differential interference contrast (DIC) imaging was used for all images to provide structural context.

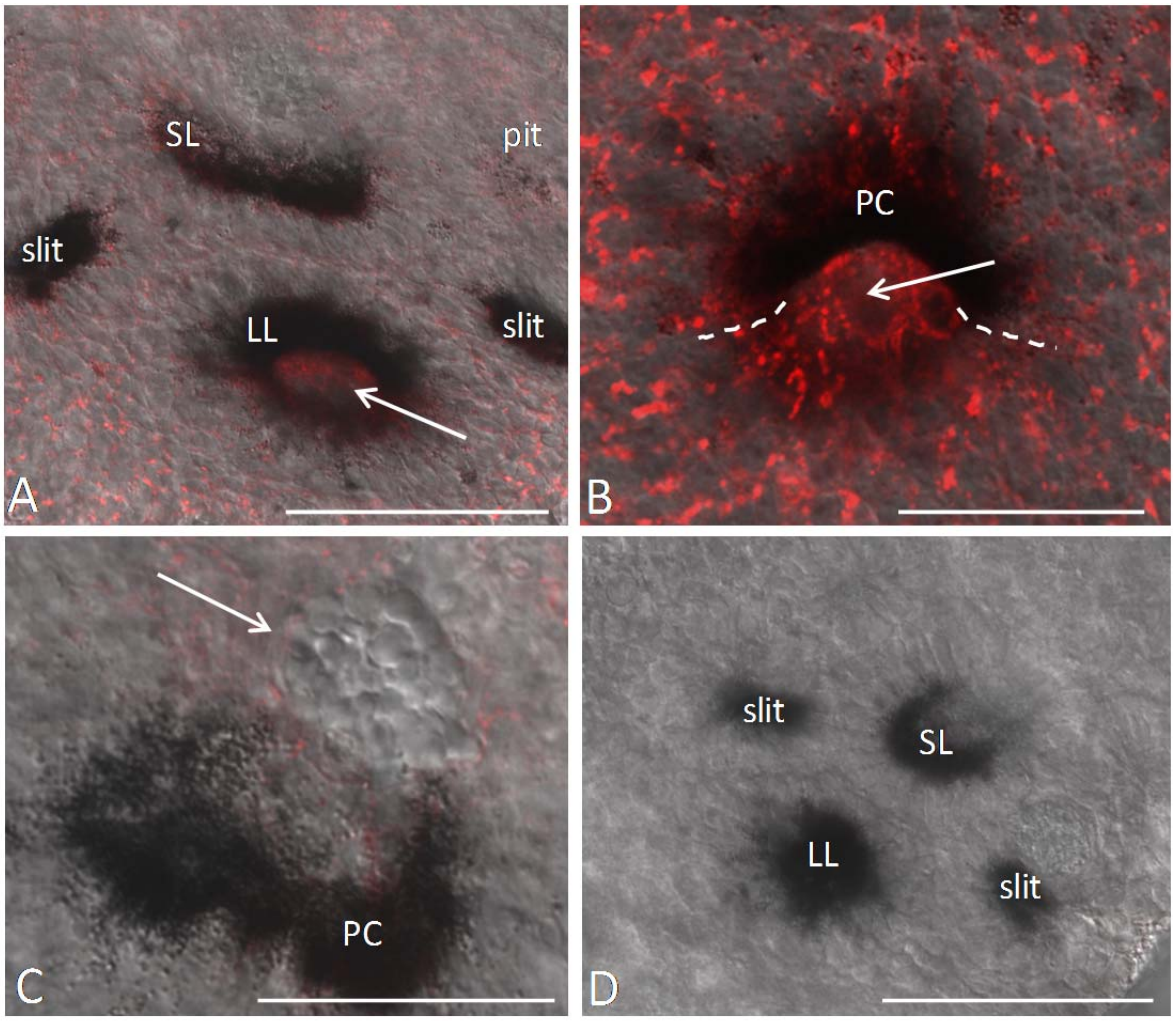

Figure 39. J1-crystallin staining during Stage 3. A. Stage 3 overview. In addition to the extralenticular staining seen across the surface of the entire rhopalium, staining can begin to be seen within the early-forming lens (arrow) of the large lensed eye (LL). The small lensed eye (SL), slit ocelli (slit), and a faint pit ocellus (pit) are also visible. Scale bar=50µm. B. Large lensed eye. Diffuse staining can be seen within the up-folding sheet of cells (hashed lines) which are pocketing into the forming pigment cup (PC). This diffuse staining is most concentrated in the location of the forming lens (arrow). The prolific extralenticular staining is also visible. Scale bar=25µm. C. Small lensed eye. Although a spherical clump of globular cells can be seen in the future location of the lens in the opening of the pigment cup (PC), no lens-specific staining is visible. Scale bar=25µm. D. Stage 3 control. Samples not subjected to the primary antibody targeting the J1-crystallin showed no staining. The large (LL) and small (SL) lensed eyes are visible along with the pair of slit ocelli (slit). Scale bar=50µm. Differential interference contrast (DIC) imaging was used in all images to provide structural context.

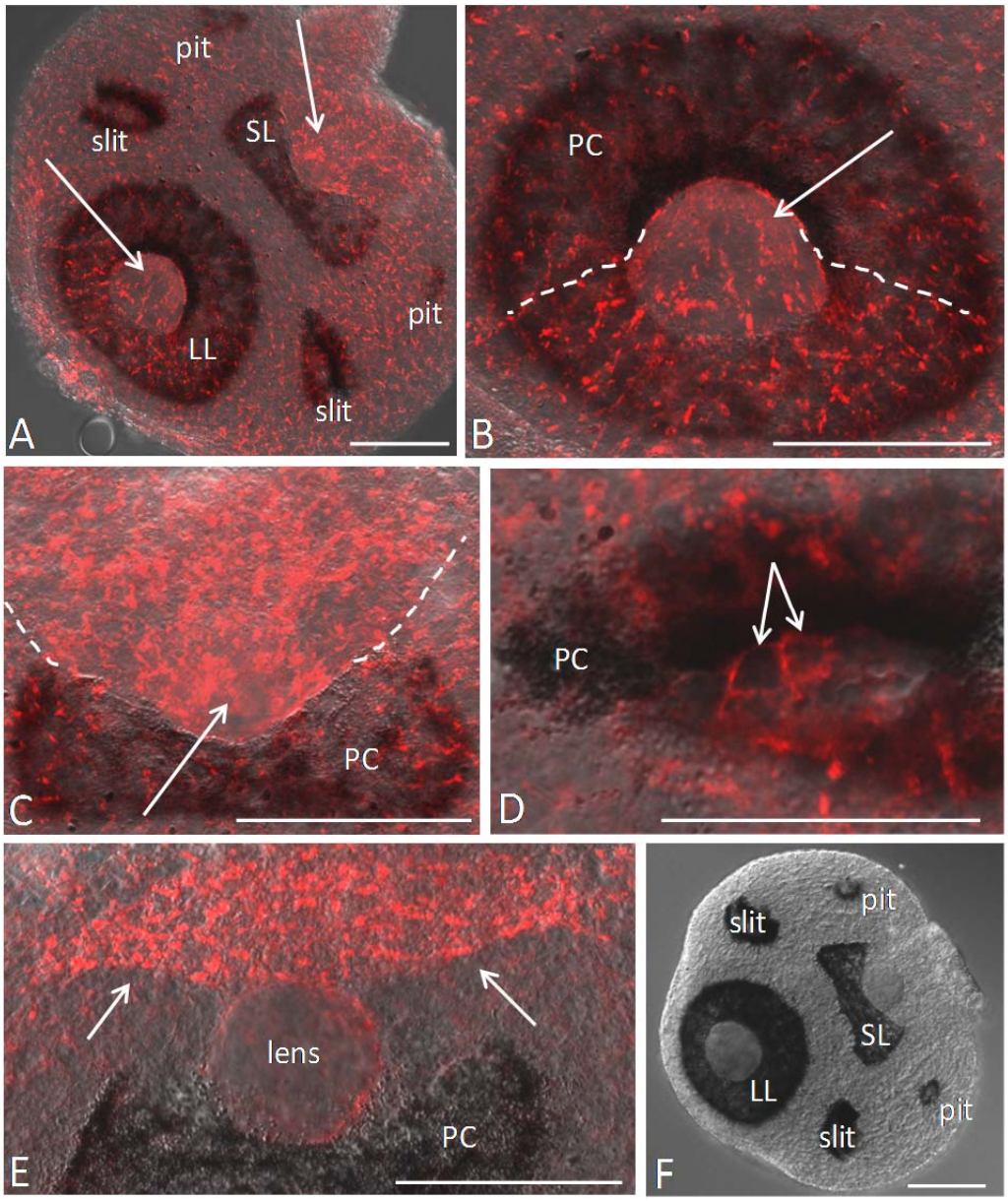

Figure 40. J1-crystallin staining during Stage 4. A. Stage 4 overview. Both the punctate surface staining and diffuse staining are visible in the areas of the forming lenses (arrows) of the large (LL) and small (SL) lensed eyes. Staining of the small lensed eye appears brighter than in the large lensed eye. Staining within the slit ocelli (slit) is also visible by this stage. Scale bar=50µm. B. Large lensed eye. An increased amount of punctate staining is visible within the up-folding sheet of cells (hashed lines) than in the upper portion of the forming large lensed eye. Diffuse staining can now be seen within the sheet of cells and on the surface of the forming lens (arrow) which sits within the opening of the forming pigment cup (PC). Scale bar=50µm. C. Small lensed eye. The bright punctate surface staining is visible within the up-folding sheet of cells (hashed lines) along with the diffuse staining in the area of the forming lens (arrow) which is found at the opening of the pigment cup (PC). Scale bar=50µm. D. Slit ocellus. Diffuse staining can be seen along the surface of the globular cells (arrows) beginning to form the lens-like material at the surface of the pigment cup (PC). Scale bar=25µm. E. Top of rhopalium. A bright patch of staining (arrows) can be seen just above the lens of the small complex eye, which rests in the opening of the pigment cup (PC) and stretches across much of the top of the rhopalium. Scale bar=50µm. F. Stage 4 control. Samples not subjected to the primary antibody targeting the J1-crystallin antibody showed no staining in the large (LL) and small (SL) lensed eyes, the slit ocelli (slit), or the pit ocelli (pit). Scale bar=50µm. Differential interference contrast (DIC) imaging was used in all images to provide structural context.

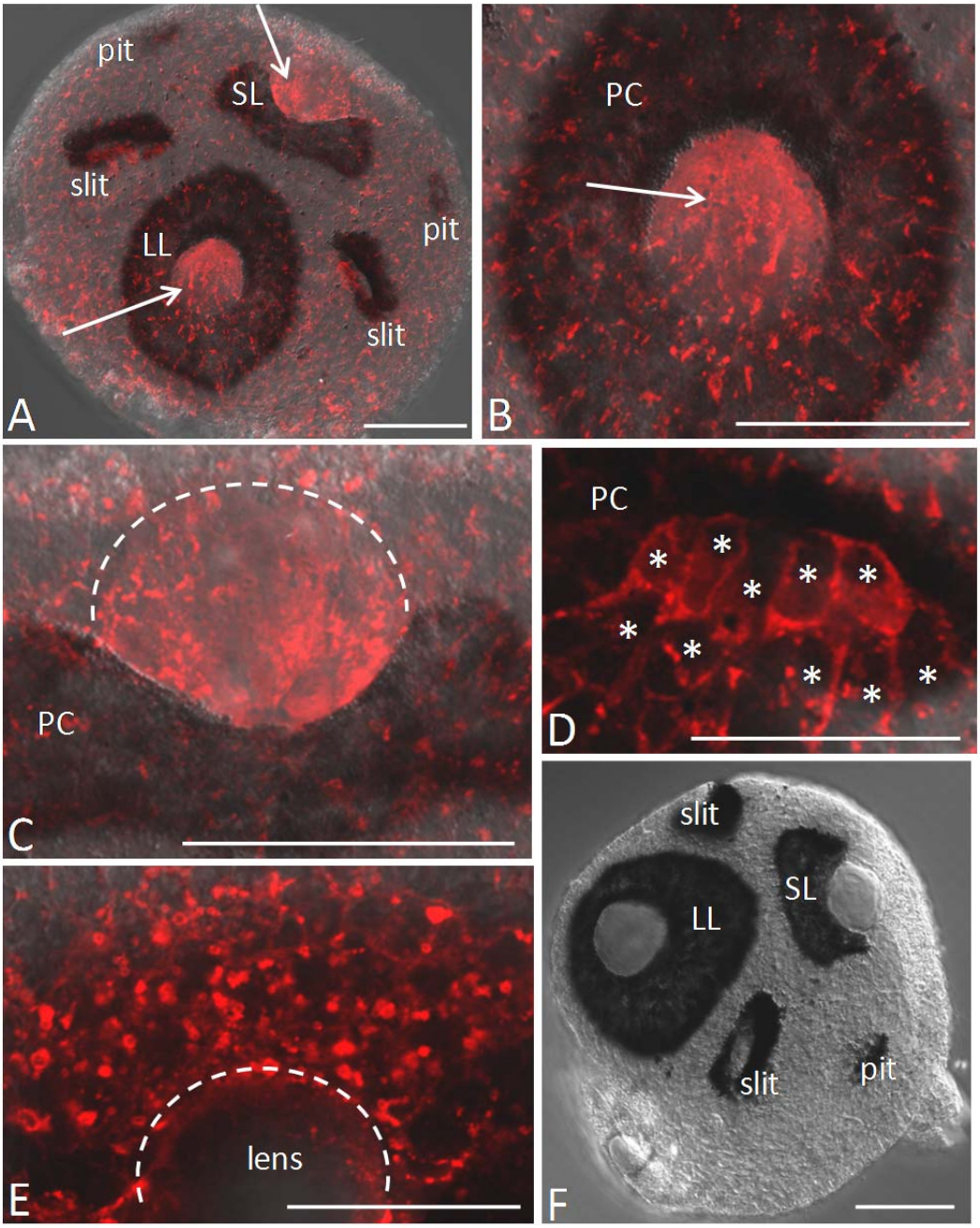

Figure 41. J1-crystallin staining during Stage 5. A. Stage 5 overview. Increased diffuse staining can be seen in the area of both the large (LL) and small (SL) complex eye lenses (arrows). Increased staining is also seen in the slit ocelli. Scale bar=50µm. B. Large lensed eye. Increased diffuse staining is visible along the surface and within the forming lens (arrow) which sits in the center of the forming pigment cup (PC). Scale bar=50µm. C. Small lensed eye. Increased diffuse staining can be seen along the surface and within the forming lens (hashed line) which sits in the opening of the forming pigment cup (PC). Scale bar=50µm. D. Slit ocellus. An increased number of the globular cells (asterisks), exhibiting the lens-like material, sit in the pigment cup (PC) opening and show bright staining along the surface. Scale bar=25µm. E. Top of rhopalium. The bright patch of staining just above the lens (hashed line) of the small complex eye shows no change in appearance. Only the outer portion of the lens is positively stained. Scale bar=25µm. F. Stage 5 control. Samples not subjected to the primary antibody targeting the J1-crystlalin protein showed no staining in the large (LL) and small (SL) lensed eyes, the slit ocelli (slit), or the pit (pit) ocelli. Scale bar=50µm. Differential interference contrast (DIC) imaging was used in all images to provide structural context.

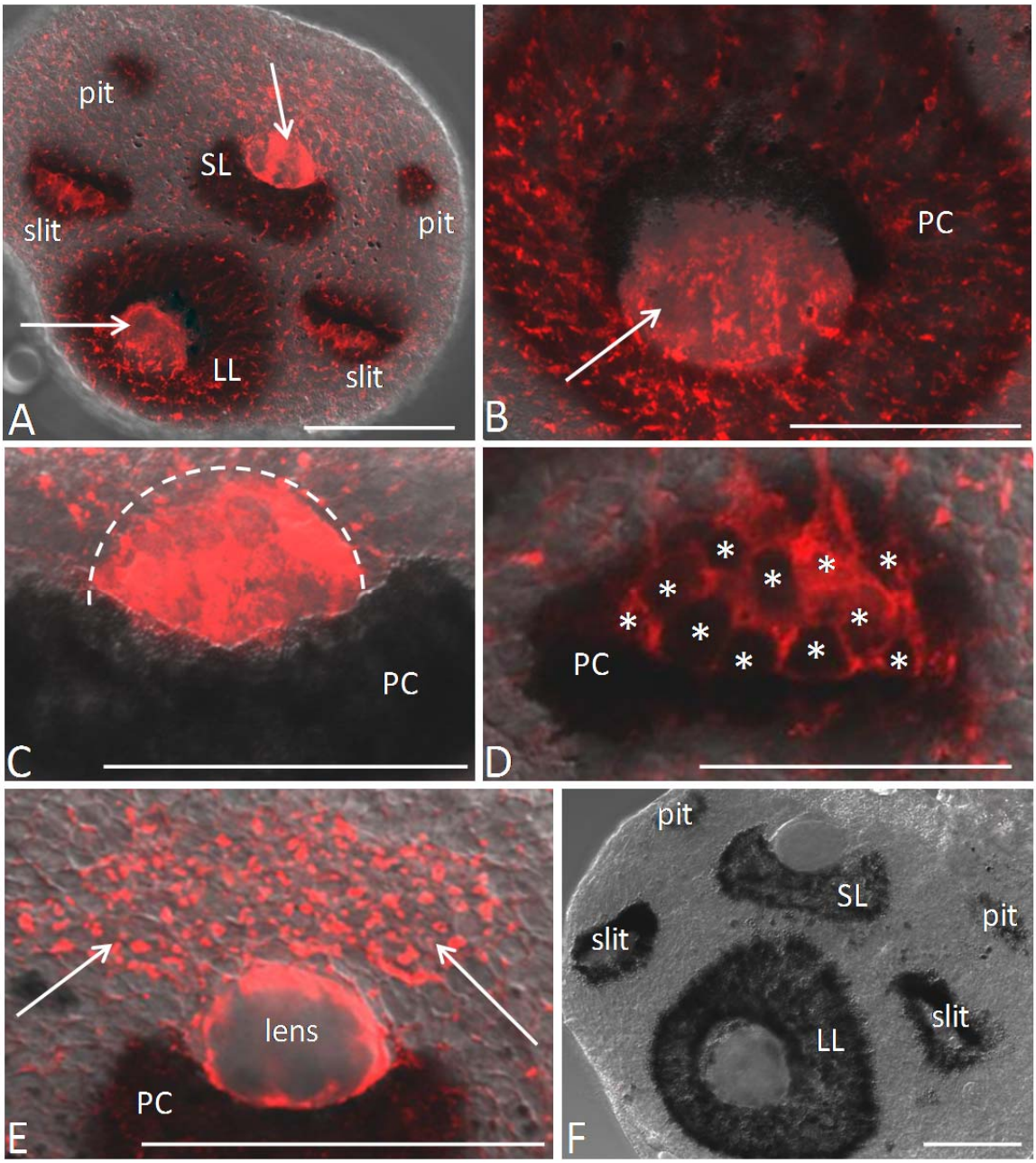

Figure 42. J1-crystallin staining during Stage 7. A. Stage 7 overview. Increased diffuse staining can be seen in the area of both the large (LL) and small (SL) complex eye lenses (arrows). The lens of the small lensed eye stains brighter than the lens of the large lensed eye. Increased staining is also seen in the slit ocelli (slit). Scale bar=50µm. B. Large lensed eye. Increased diffuse staining is visible along the surface and within the forming lens (arrow) which sits in the center of the forming pigment cup (PC). Scale bar=50µm. C. Small lensed eye. Increased diffuse staining can be seen along the surface and within the forming lens (hashed line) which sits in the opening of the forming pigment cup (PC). Scale bar=50µm. D. Slit ocellus. An increased number of the globular cells (asterisks) making up the developing lens-like material which sits in the pigment cup (PC) opening show bright staining along the surface. Scale bar=25µm. E. Top of rhopalium. The bright patch of staining (arrows) just above the lens of the small complex eye shows no change in appearance. Only the outer portion of the lens, which sits at the pigment cup (PC) opening, is positively stained. Scale bar=50µm. F. Stage 7 control. Samples not subjected to the primary antibody targeting the J1-crystallin protein showed no staining in the large (LL) and small (SL) lensed eyes, the slit ocelli (slit) or the pit (pit) ocelli. Scale bar=50µm. Differential interference contrast (DIC) imaging was used in all images to provide structural context.

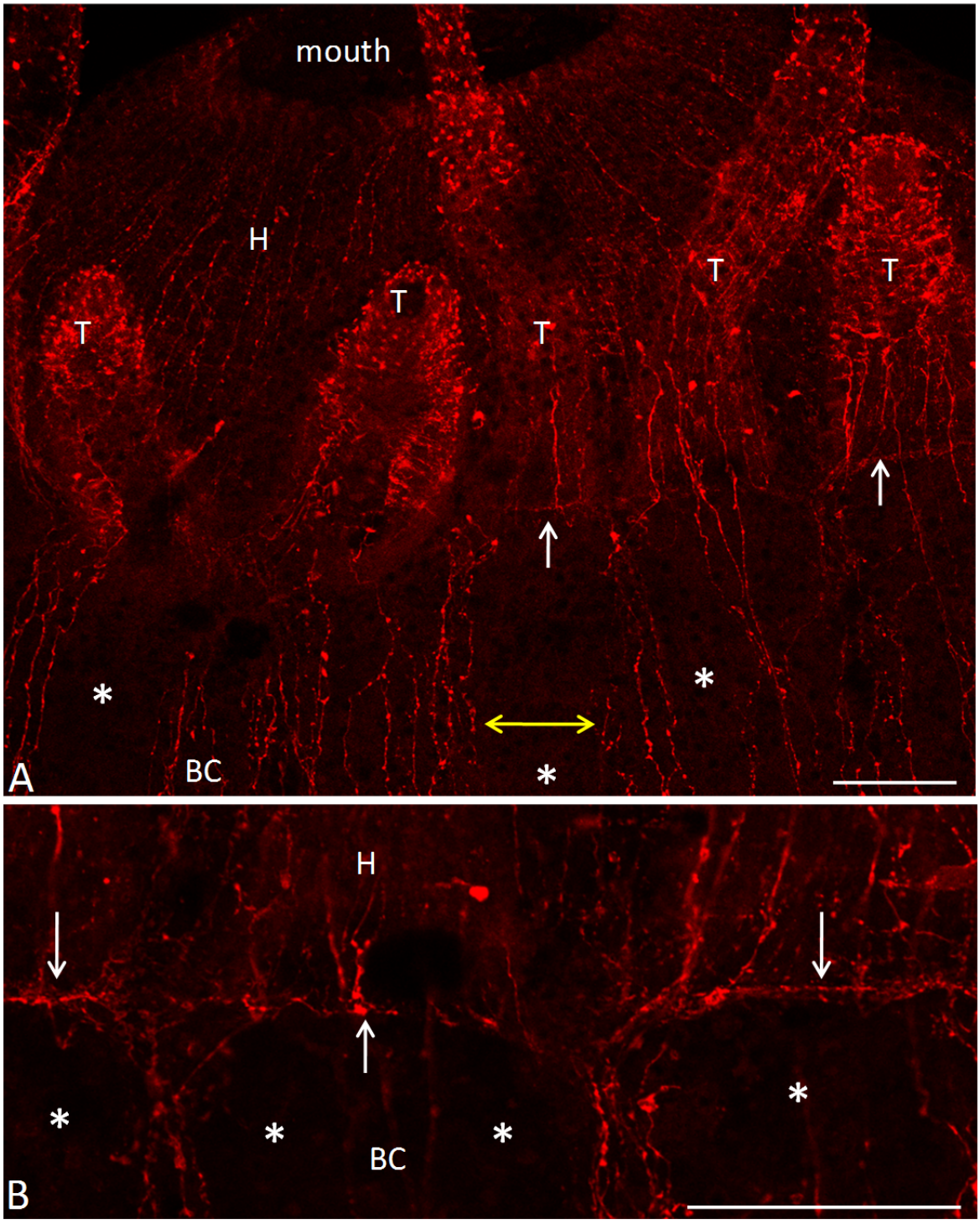

Figure 43. FMRFamide immunoreactivity in steady-state polyps. A. Steady-state polyp overview. Long neurites (yellow arrow) can be seen spanning from the mouth opening (mouth), down the sides of the hypostome (H), down the body column (BC), as well as along the length of each tentacle (T). The grouping of the neurites in the body column often leaves unstained spaces (asterisks). Portions of the circular nerve ring are visible (white arrows). B. Nerve ring. The thin, circular nerve ring (white arrows) runs along the bases of the tentacles in between the hypostome (H) and body column (BC). The grouping of the neurites in the body column often leaves unstained spaces (asterisks). Scale bars=100µm.

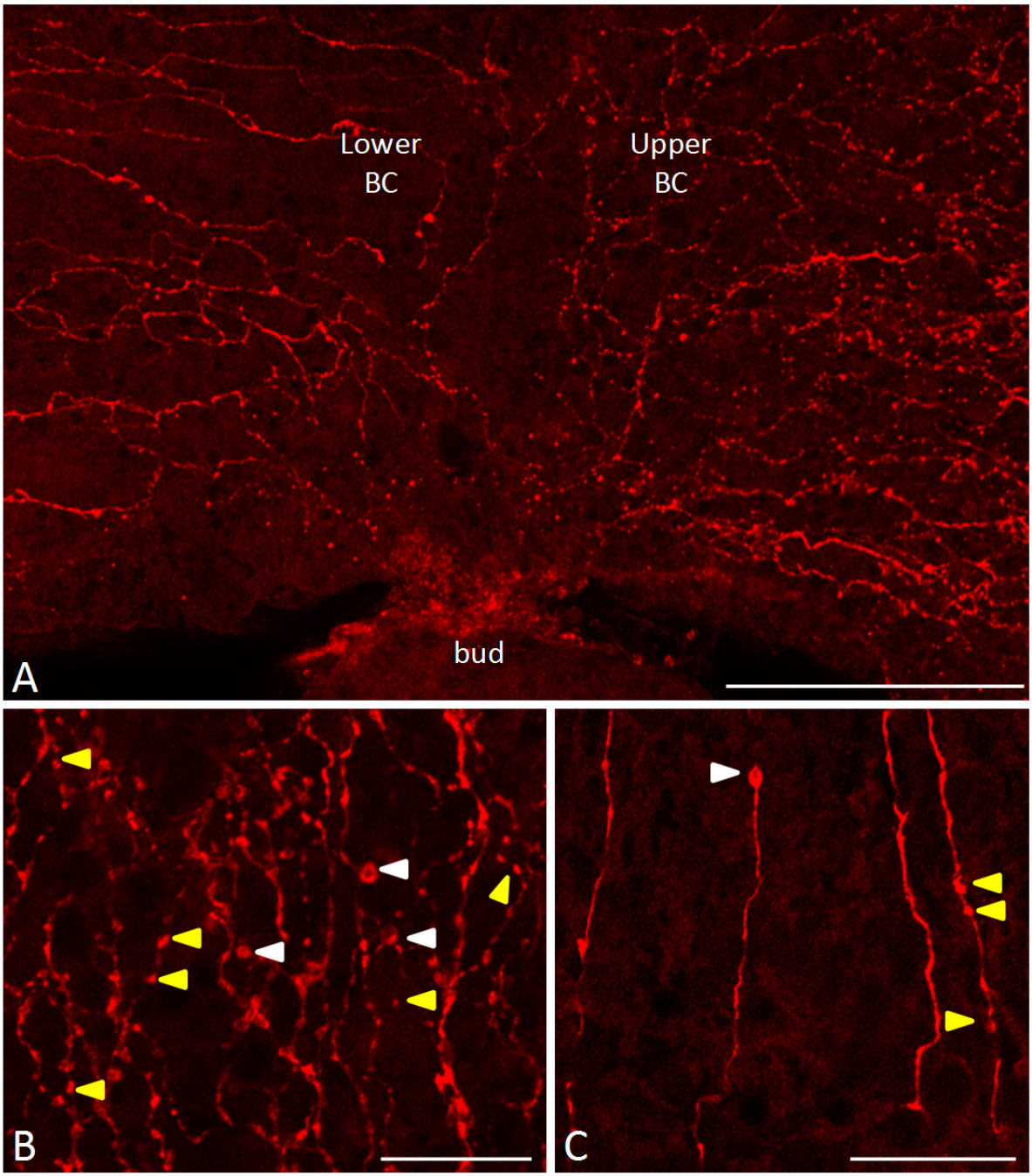

Figure 44. FMRFamide immunoreactivity showing nerve differences along the body column in a steady-state polyp. A. Nerve differences along body column at bud location. The differences in nerve morphology between the upper (Upper BC) and lower (Lower BC) body column can easily be seen at the location of a lateral bud (bud). Scale bar=200µm. B. Upper body column. Here, the nerves are more abundant, thicker, interconnected, and have a higher occurrence of perikarya (white arrowheads) and neuropeptide vesicles (yellow arrowheads). Scale bar=50µm. C. Lower body column. Here the nerves are less abundant, less interconnected, and thinner with fewer perikarya (white arrowhead) and neuropeptide vesicles (yellow arrowheads). Scale bar=50µm.

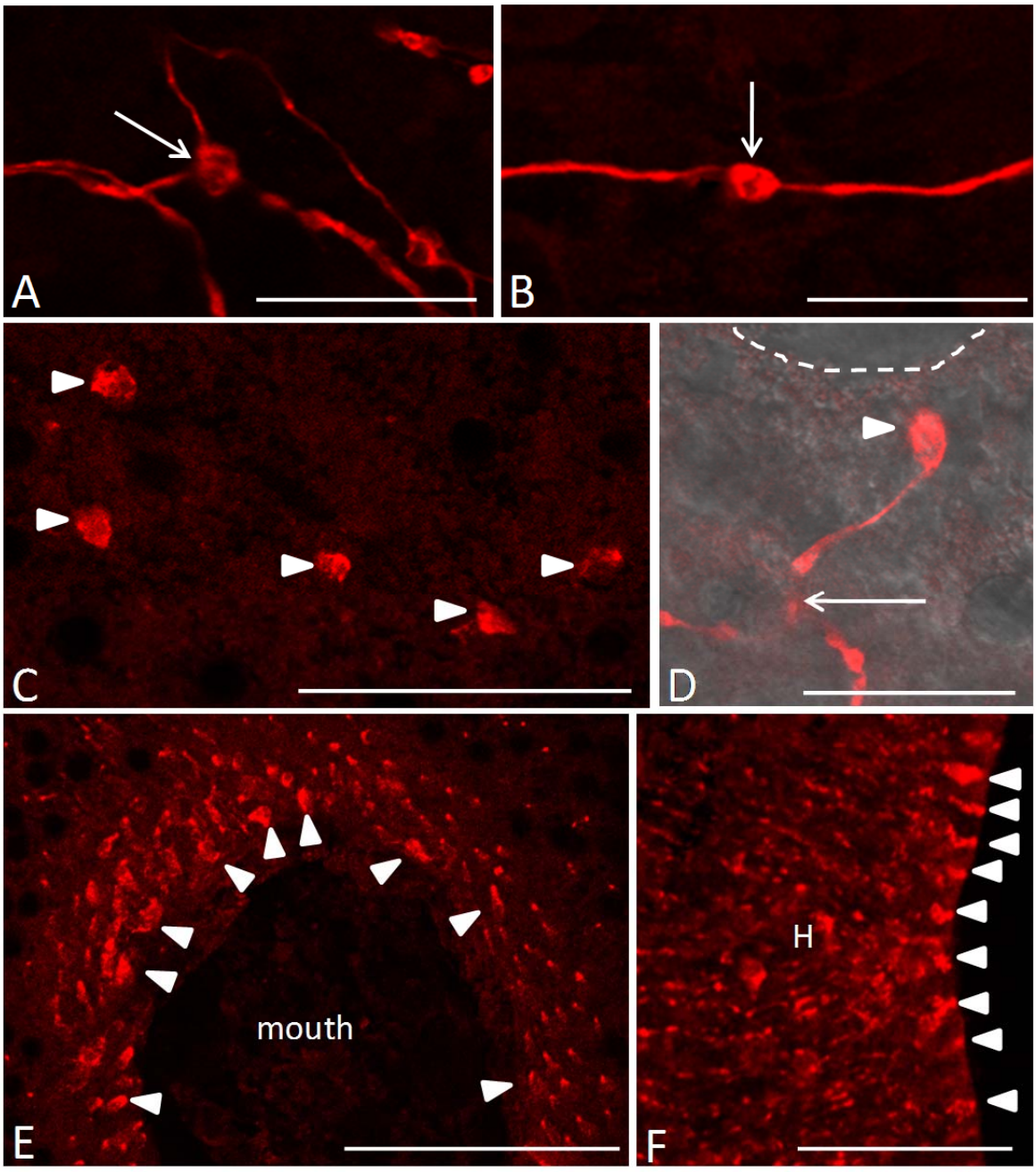

Figure 45. FMRFamide immunoreactivity in nerve types of a steady-state polyp. A. Multipolar ganglion cell. A multipolar nerve cell body (white arrow) is visible with three processes. Scale bar=20µm. B. Bipolar ganglion cell. A bipolar nerve cell body (white arrow) is visible with one process extending from each end. Scale bar=20µm. C. Sensory neurons at body column surface. Several sensory neuron tips (white arrowheads) are visible just below the surface of the ectoderm. Scale bar=50µm. D. Sensory neuron whole. The cell body (white arrowhead) of a sensory neuron is visible just below the ectoderm surface (hashed line) and connects via a single neurite to a basal ganglion cell (white arrow). Scale bar=25µm. E. Hypostome mouth opening. Many sensory neurons (examples shown with white arrowheads) can be seen encircling the mouth opening. Scale bar=100µm. F. Sensory neurons along mouth opening edge. Many sensory neurons (white arrowheads) are visible lining the mouth opening and connect to neurites spanning the hypostome (H). Scale bar=50µm. Differential interference contrast (DIC) imaging was used in D to provide structural context.

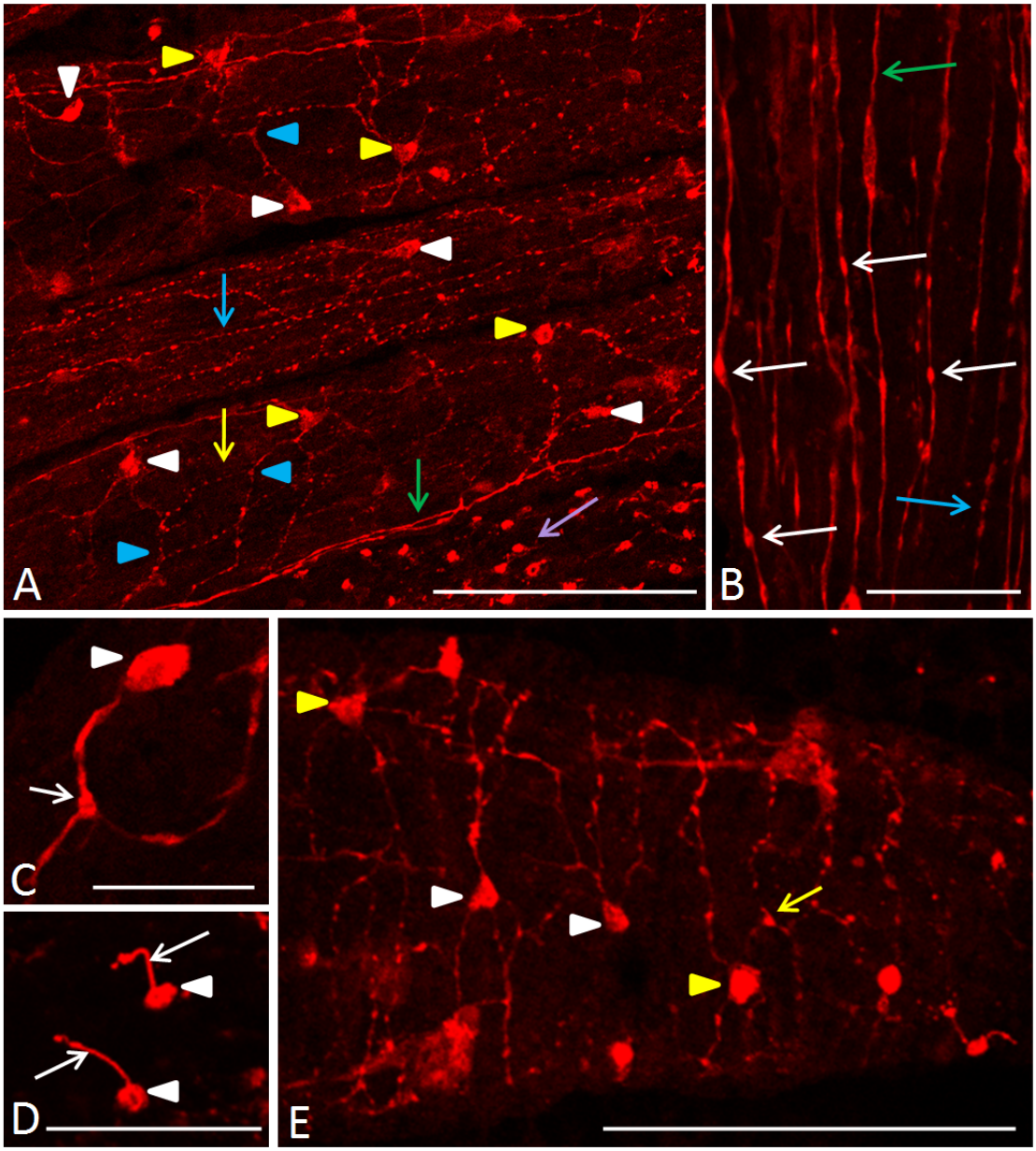

Figure 46. FMRFamide immunoreactivity in the tentacle nerves of a steady-state polyp. A. Tentacle nerve overview. Both thick (green arrow) and thin (blue arrow) processes can be seen along the length of the tentacles. Large multipolar ganglion neurons (yellow arrowheads) and small multipolar ganglion neurons (blue arrowheads) are visible and have thin vesiculated processes (yellow arrow) which form a tentacular nerve net in the upper portion of the tentacles. Sensory neurons (white arrowheads) extending from the multipolar neurons are also visible along with the brightly-stained structures found near the tentacle tip (purple arrow). Scale bar=100µm. B. Tentacular neurites. Both thick (green arrow) and thin (blue arrow) neurites can be seen along the tentacle length. The thin neurites are more vesiculated and both types have bipolar ganglion neurons (white arrows) located along their length. Scale bar=25µm. C. Multipolar neuron. A small multipolar ganglion cell body (white arrow) has three processes extending from it including a sensory neuron (white arrowhead) which stretches toward the ectoderm surface. Scale bar=20µm. D. Cherry structures. Found at the surface in the apical portion of the tentacle, these structures have a cell body with an extension into the external environment. Scale bar=25µm. E. Tentacle nerve net. In the upper portion of each tentacle is a nerve net enabled by interconnecting large (yellow arrowheads) and small (yellow arrow) multipolar ganglion neurons which often have a sensory neuron (white arrowheads) branching off of them. Scale bar=100µm.

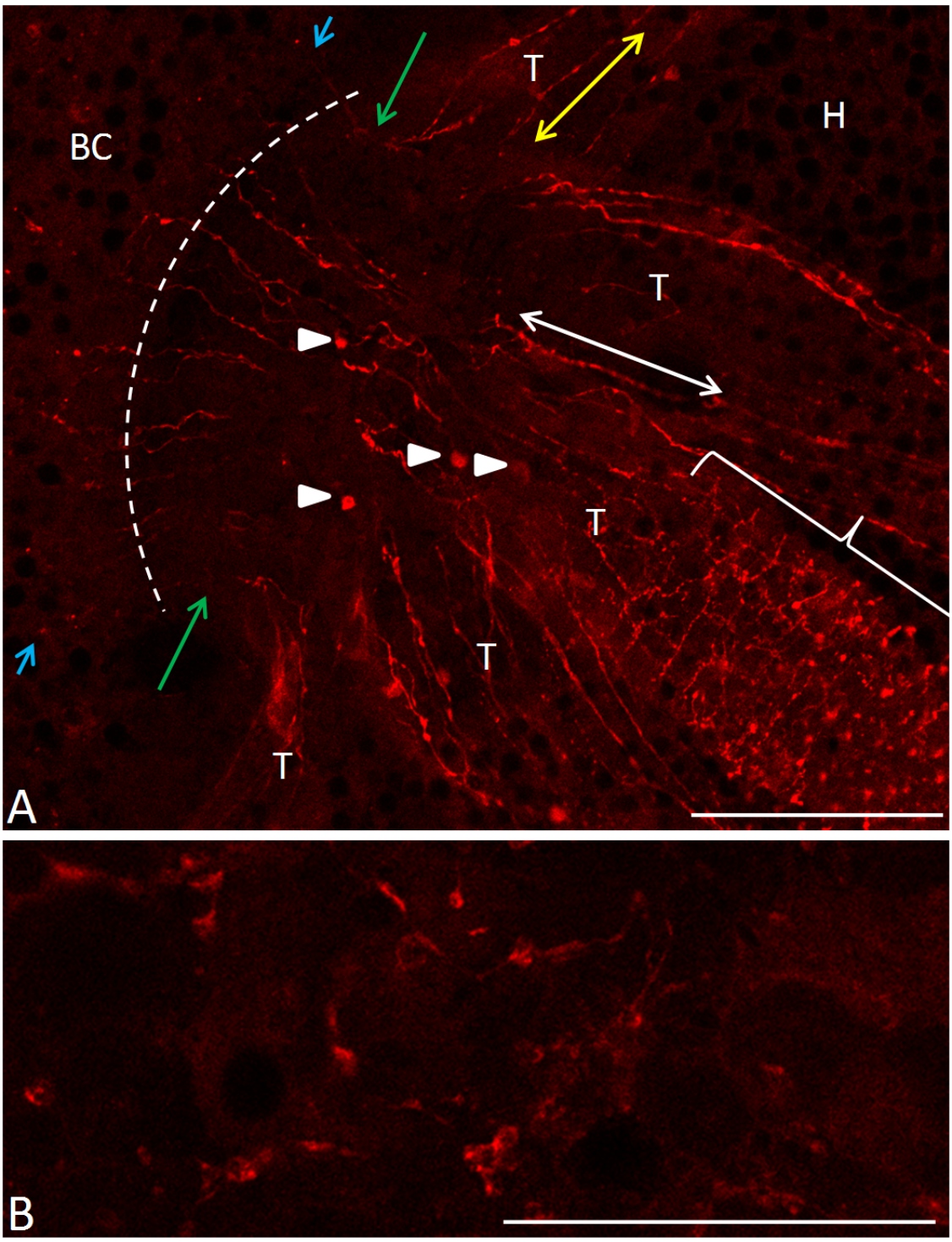

Figure 47. FMRFamide immunoreactivity during Stage 1. A. Grouping and fusing of polyp tentacles. Bending of tentacles (T) due to the constricting tentacle group causes some neurites (yellow arrow) to be oriented perpendicular to the body column (BC/hashed line) while others remain parallel (white arrow). In the area of tentacle fusion, the neurites constrict together in the narrow area (green arrows) and spread out again once entering the body column (blue arrows). The apical nerve net of a receding tentacle is visible (white bracket) along with multiple sensory neurons (white arrowheads). The tentacles rest up against the hypostome (H). Scale bar=100µm. B. Nerves in the upper body column. During Stage 1, it becomes more difficult to visualize nerves in this area as they appear fainter and more diffusely stained. Scale bar=50µm.

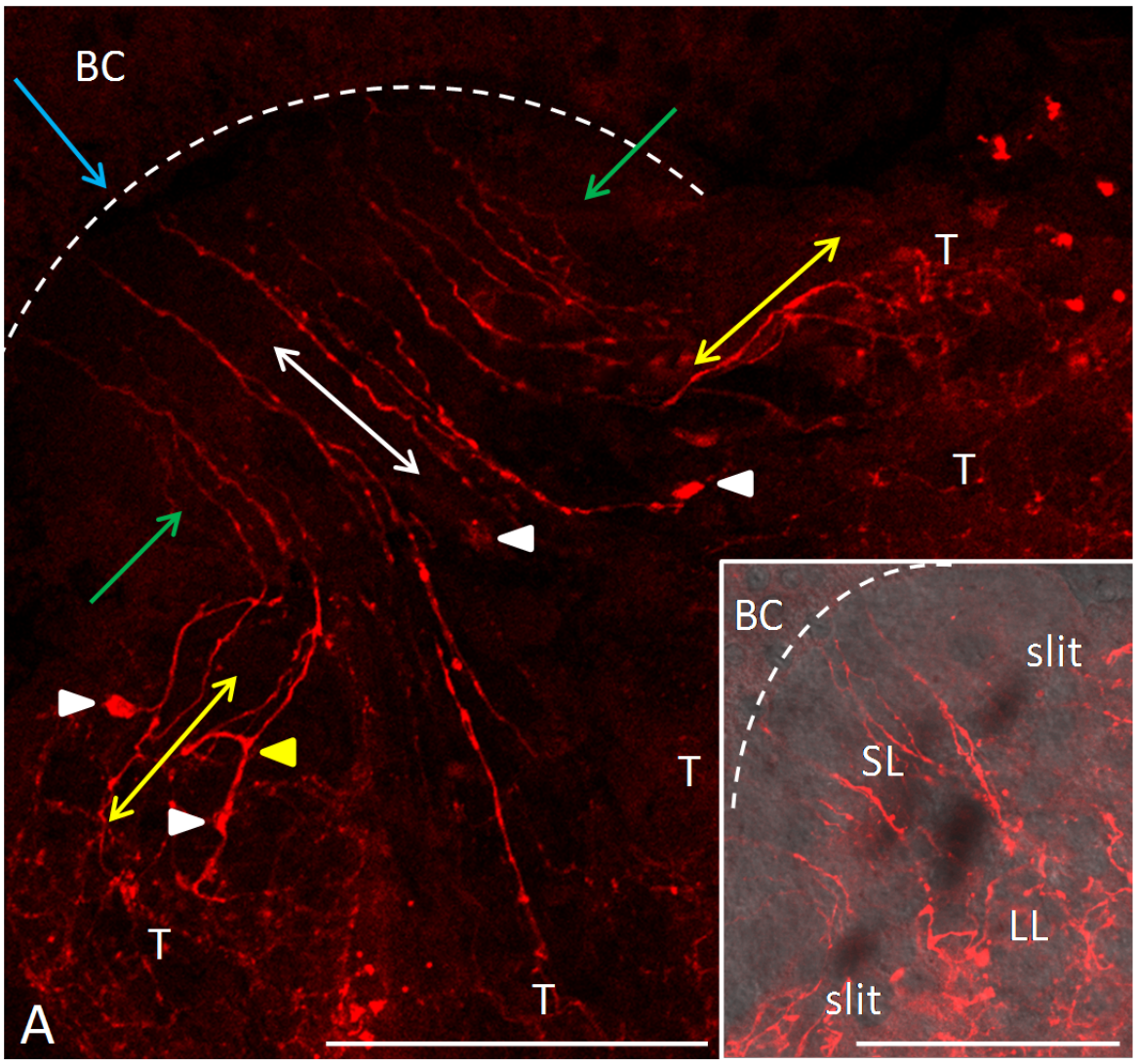

Figure 48. FMRFamide immunoreactivity during Stage 3. A. Neurites within fused tentacle bases. Bending of tentacles (T) due to the continued constriction of the tentacle group (green arrows) bases causes some neurites (yellow arrows) to be oriented perpendicular to the body column (BC/hashed line) while others remain parallel, especially within the fused bases (white arrow). The up-folding cuff of cells (blue arrow) in the body column makes it more difficult to see the progression of the tentacular neurites down into the body column. Multiple sensory neurons (white arrowheads) are visible along with a multipolar ganglion neuron (yellow arrowhead). Inset is a differential interference contrast (DIC) comparison of Stage 3. The location of the developing ocelli on the opposite side of the fused tentacle bases is visible using DIC imaging including the large (LL) and small (SL) lensed eyes and the slit ocelli (slit). The boundary of the body column (BC) is indicated by the hashed line. Scale bars=100µm.

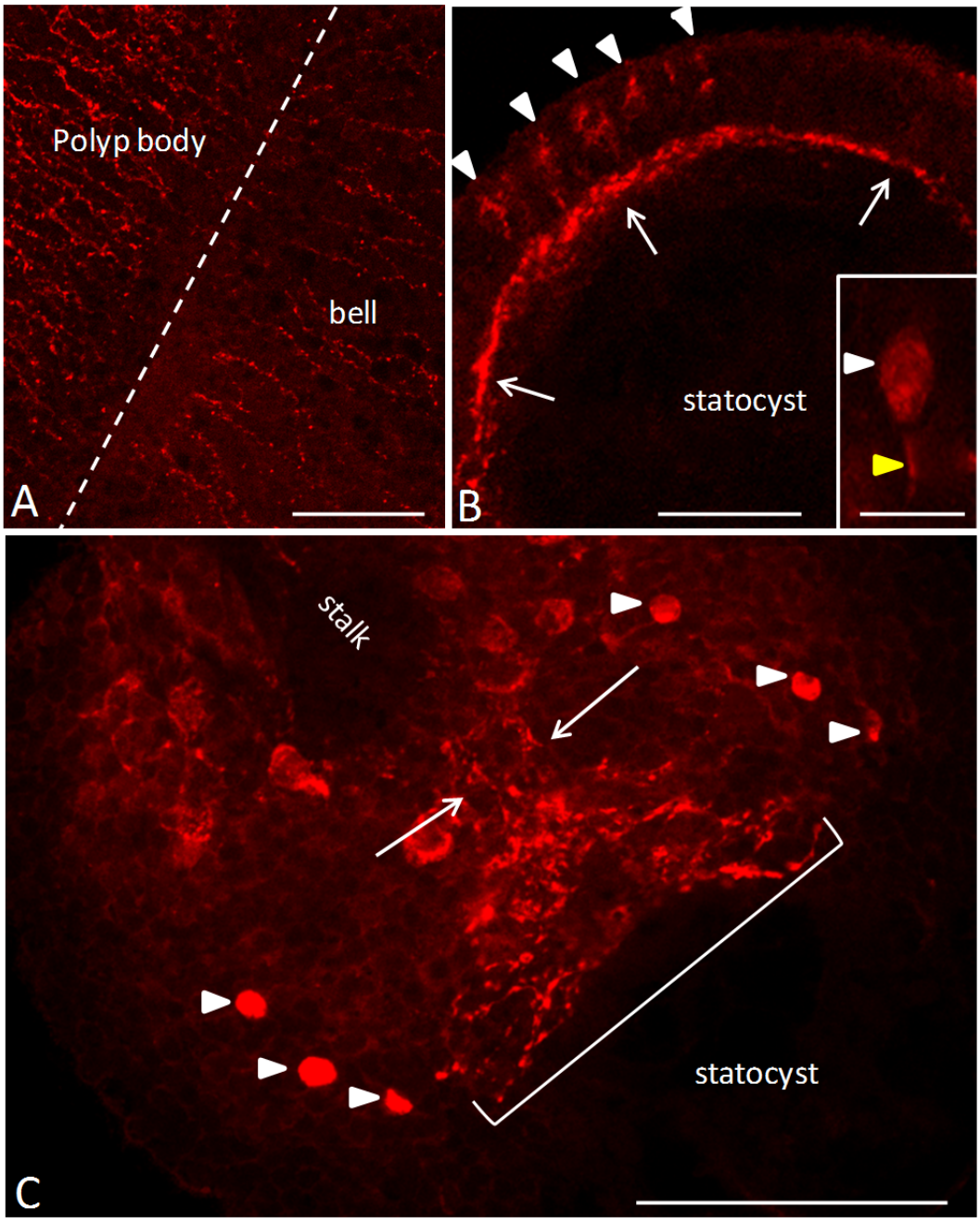

Figure 49. FMRFamide immunoreactivity in Stages 4-7 – Part 1. A. Nerve differences along body column. Fewer neurites are visible within the developing bell of a Stage 4 animal as compared to the polyp body, which still exhibits many. Even fewer neurites are visible across the bell and polyp body boundary (hashed line). Scale bar=100µm. B. Nerves encircling the statocyst. Although encircling the entire perimeter of the upper edge of the statocyst, a large cluster of nerves can be found along the back perimeter (white arrows) in a Stage 4 rhopalium. Stretching back from the statocyst base are often several oval-shaped structures (white arrowheads) resembling sensory neurons. Scale bar=50µm. An enlarged example of one of these structures is shown inset and demonstrates the oval-shaped cell body (white arrowhead) and thin neurite extension (yellow arrowhead). Scale bar=10µm. C. Nerves on the back of the rhopalium. Above the bottom edge of the statocyst on the back of a Stage 7 rhopalium, multiple intertwined neurites (white bracket), which are oriented perpendicular to the rhopalial length, are visible along with some fainter neurites (white arrows), which are parallel with the rhopalial length and located close to the stalk. Also visible are symmetrically-paired and brightly-stained structures often seen at either end of this region of nerves (white arrowheads). Scale bar=50µm.

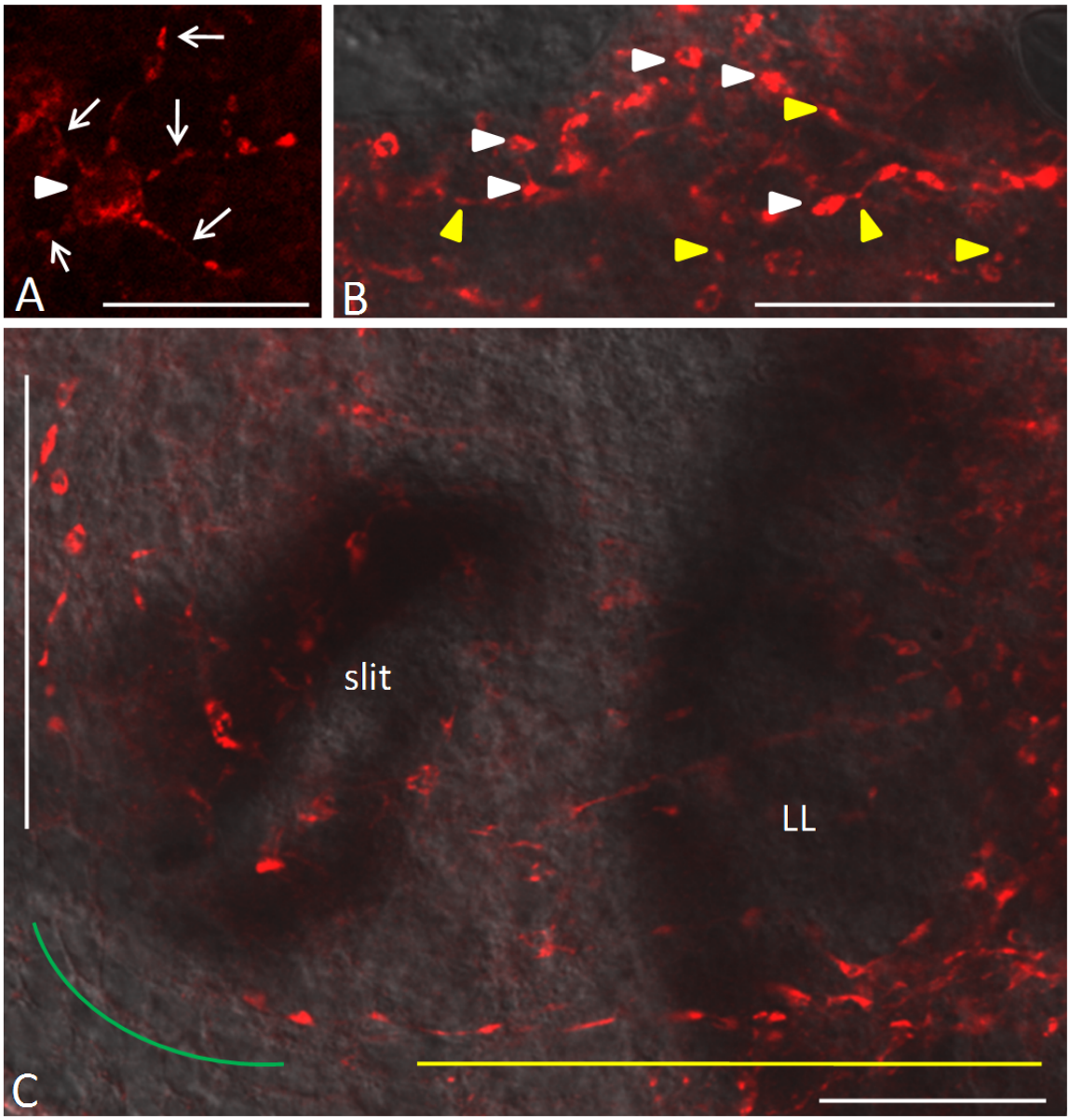

Figure 50. FMRFamide immunoreactivity in Stages 4-7 – Part 2. A. Large multipolar neuron. Often found close to the stalk origin on the back of the rhopalium are large multipolar ganglion cells (white arrowhead) with approximately 5 thin processes (white arrows). Scale bar=25µm. B. Nerves at the top of the rhopalium. A portion of a group of interconnected neurites, which are primarily oriented perpendicular to the rhopalial body and found near the top of the rhopalium, is shown. Several ganglion cell bodies are visible (white arrowheads) along with small vesicles (yellow arrowheads) along the length of the neurites. Scale bar=20µm. C. Nerve pattern on back of rhopalium. The group of ganglion nerves found just above the statocyst are primarily oriented perpendicular to the rhopalial length. Processes extending from this group of nerves curve out (yellow line) and upward (green line) forming a group of neurites behind the simple ocelli which are primarily oriented parallel (white line) with the rhopalial length. The large lensed eye (LL) and a slit ocellus (slit) are visible on the opposite side of the rhopalium. Scale bar=50µm. Differential interference contrast (DIC) imaging was used in B and C to provide structural context.

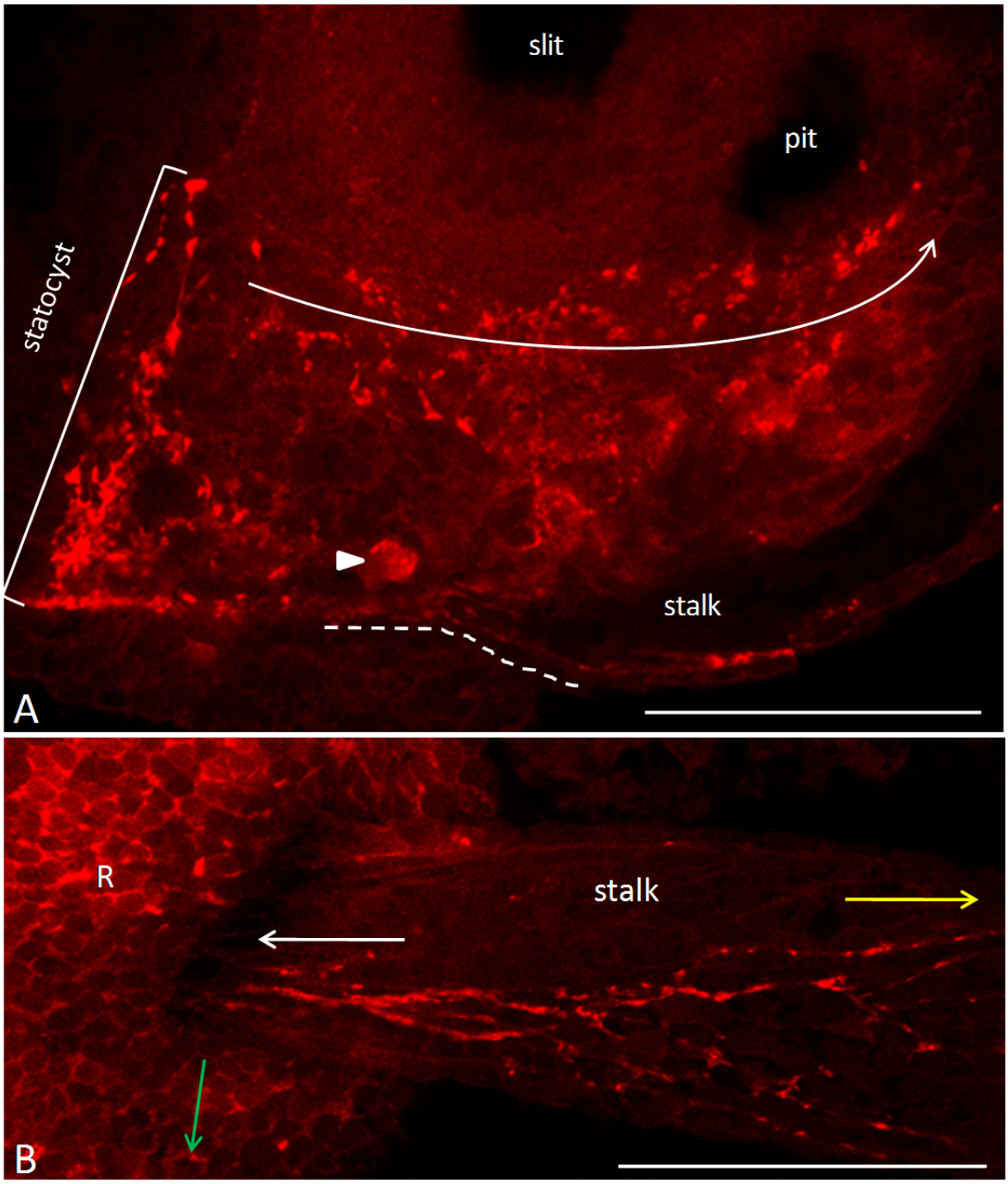

Figure 51. FMRFamide immunoreactivity in Stages 4-7 – Part 3. A. Profile view. In a Stage 7 rhopalium, the cluster of neurites located near the statocyst on the back of the rhopalium is primarily oriented perpendicular to the rhopalial length. Processes extend outward from this cluster (white bracket) and curve upward forming a group of nerves behind the simple ocelli that are primarily oriented parallel with the rhopalial length (white arrow). These nerves are found in closest association with the simple ocelli, particularly the pit ocelli (pit). Neurites are visible passing from the stalk into the rhopalial body (hashed line) along with an example of the large multipolar ganglion cells found near the stalk origin (white arrowhead). A slit ocellus (slit) can also be seen. B. Rhopalial stalk. A group of neurites spanning the rhopalial stalk length can be seen more spread out closest to the polyp body (yellow arrow) and can be seen converging together (white arrow) prior to entering the back of the rhopalium (R). The direction of the location of the basal statocyst is indicated with a green arrow. Scale bars=50μm.

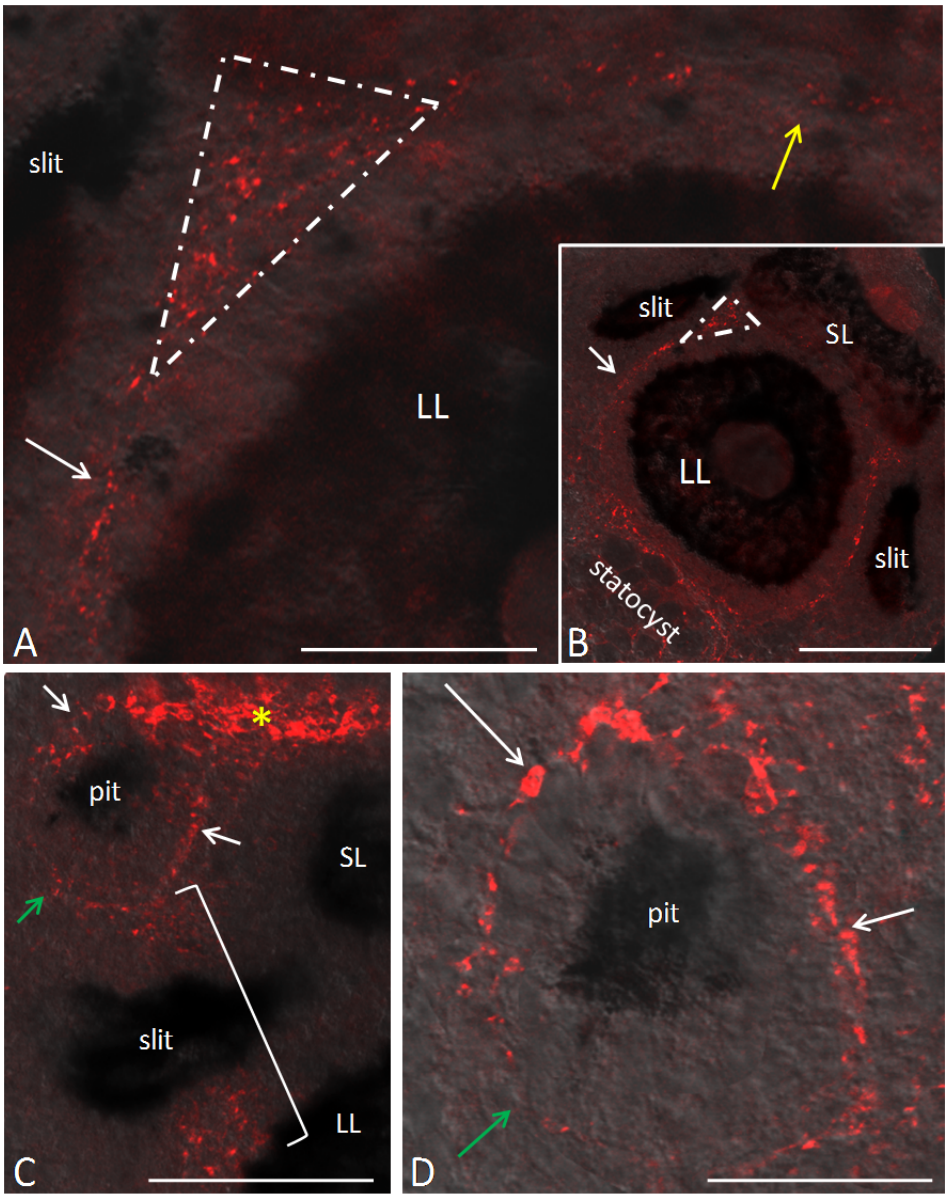

Figure 52. FMRFamide immunoreactivity in Stages 4-7 – Part 4. A. Large lensed eye. On the front of the rhopalium, small and faint ganglion nerves encircle the large lensed eye (LL) and form a triangular-shaped group of nerves (hashed line) just below the small lensed eye. One of the three nerve groups extending from this triangular region is visible (white arrow) coming from the bottom region of the large lensed eye and another faint group of nerves (yellow arrow) continues around the top of the eye. The third nerve extension (which is not visible) moves to the side in between the simple ocelli. Scale bar=20µm. B. Large lensed eye overview. The location of the triangular-shaped group of nerves (hashed line) can be seen in reference to the perimeter of nerves around the large lensed eye (LL). The neurites along the bottom of the eye are a part of the nerves lining the statocyst base. One of the three neurites coming off of the triangular region is visible (white arrow). Scale bar=50µm. C. Pit ocellus overview. The ring of nerves encircling the pit ocellus (pit) is thicker closer to the center of the rhopalium (white arrows) and thinner closer to the side of the rhopalium (green arrow). The nerves, which are primarily oriented parallel with the body column, behind the simple ocelli, are visible (white bracket) along with the brightly-stained nerves (asterisk) located between the pit ocelli and just above the small lensed eye (SL). The large lensed eye (LL) is also visible. Scale bar=50µm. D. Pit ocellus. The ring of nerves encircling the pit ocellus (pit) is thicker closer to the center of the rhopalium (white arrows) and thinner closer to the side of the rhopalium (green arrow). Scale bar=20µm. Differential interference contrast (DIC) imaging was used in all images to provide structural context.

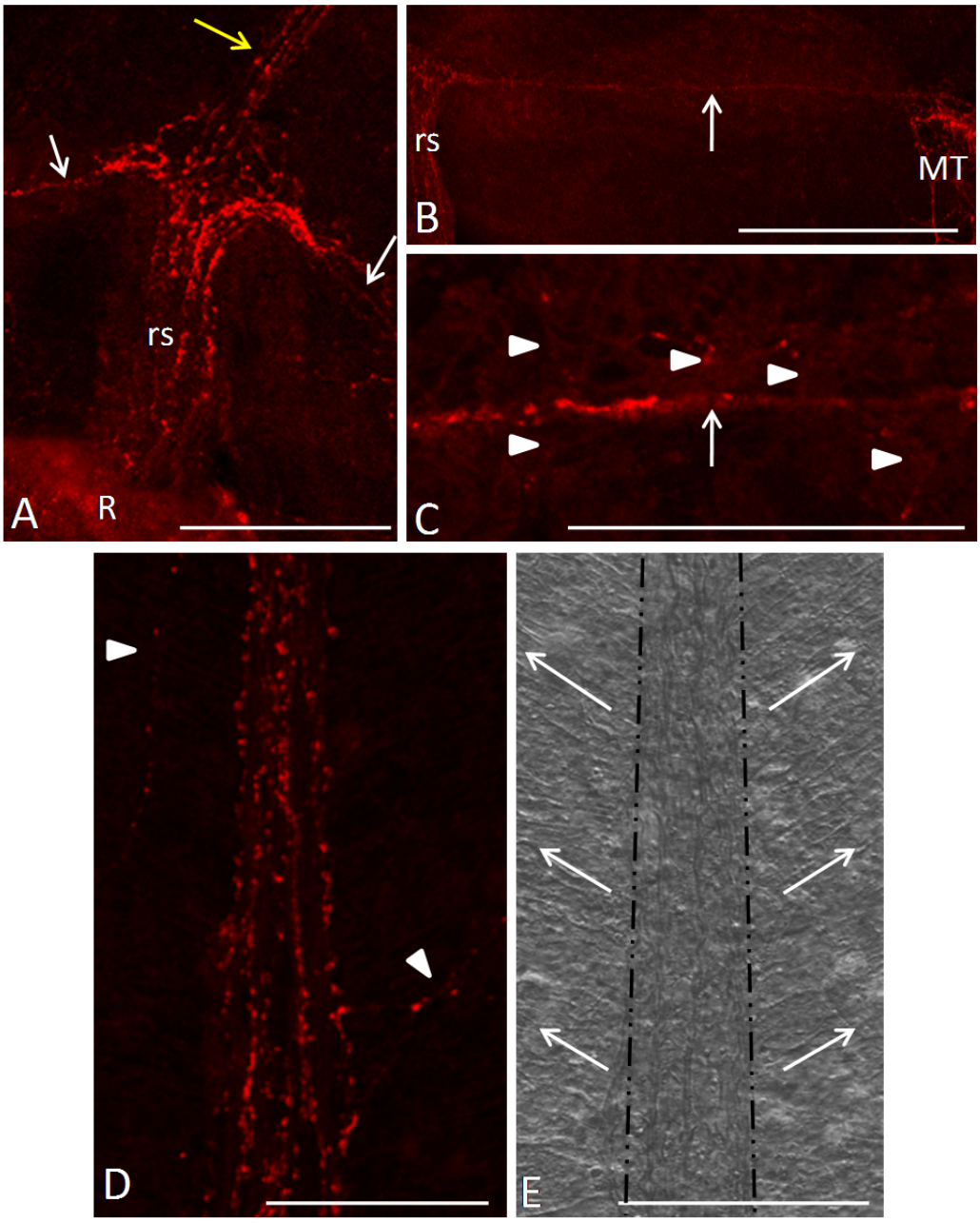

Figure 53. FMRFamide immunoreactivity in juvenile jellyfish – rhopalial nerve extensions. A. Three groups of nerves branch off from the base of the rhopalial stalk (rs); two branch off to the side (white arrows) and connect to an adjacent medusa tentacle or secondary medusa tentacle bud. The third, and thickest, one (yellow arrow) connects to a small cluster of nerves near the top of the bell and is parallel with the bell length. The rhopalial body (R) is also visible. Scale bar=100µm. B. Nerve ring. A portion of the forming nerve ring, consisting of a single thin neurite (white arrow), can be seen connecting from a rhopalial stalk (rs) to an adjacent medusa tentacle (MT). Scale bar=200µm. C. Nerve ring enlarged. An enlargement of a portion of the forming nerve ring (white arrow) is shown. Smaller neurites can be seen branching off the central neurite (white arrowheads). Scale bar=50µm. D. Thick group of neurites branching from base of the rhopalial stalk. The thickest group of nerves branching up from the base of the rhopalial stalk is shown enlarged. Thinner neurites can be seen branching off of the sides (white arrowheads). Scale bar=50µm. E. Differential interference contrast (DIC) image of thick group of neurites branching from the base of the rhopalial stalk. The DIC image shows how the group of neurites (hashed lines) directly follows the underlying band of smooth muscle which lies parallel with the bell length and is surrounded on each side by the circular swim musculature (white arrows). Scale bar=50µm.

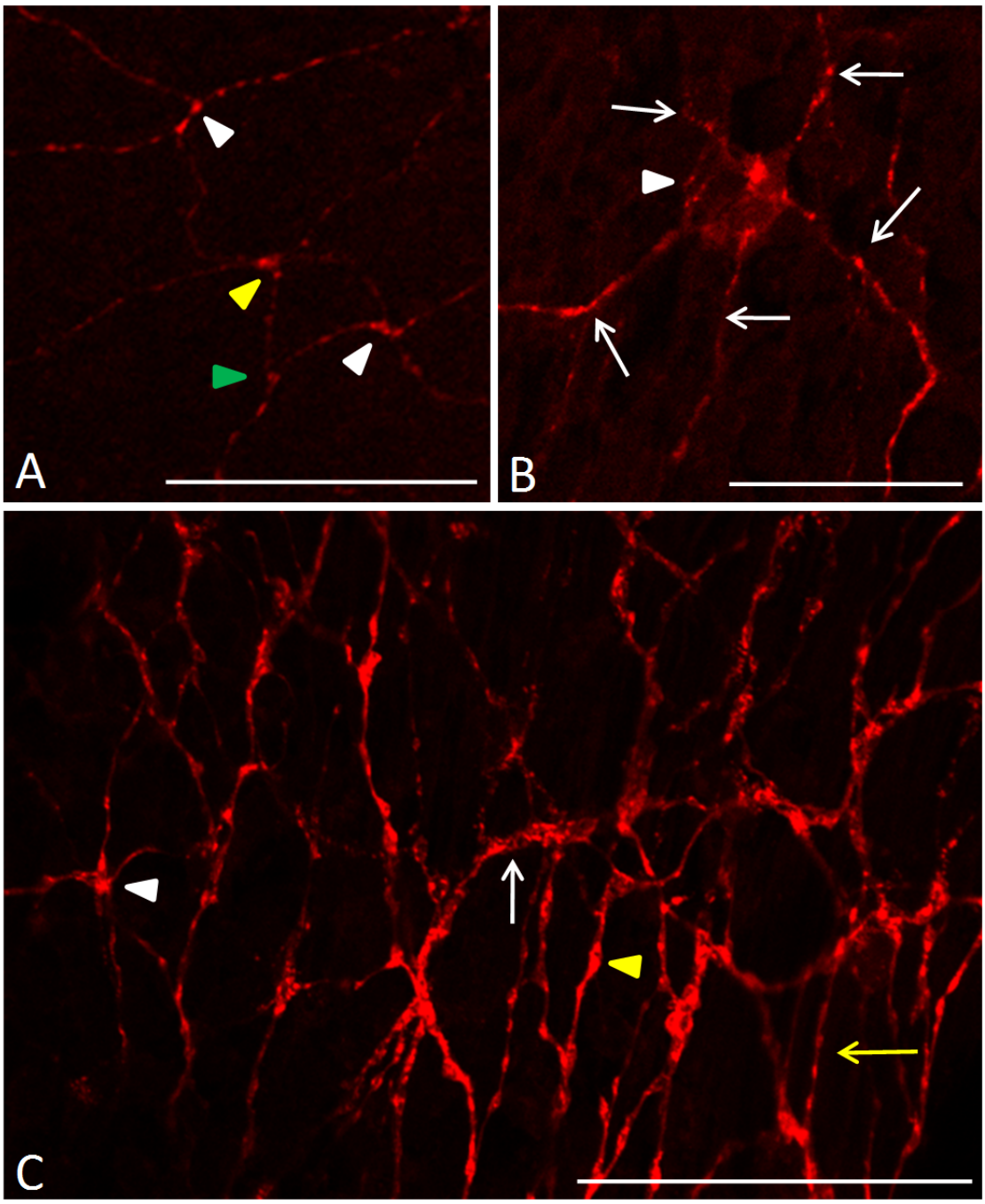

Figure 54. FMRFamide immunoreactivity in juvenile jellyfish – nerve net and tentacular nerves. A. Nerve net. The nerve net of a juvenile jellyfish is made up of both multipolar and bipolar ganglion nerves which interconnect via branching neurites. Several multipolar neurons are visible including one with three branching neurites (green arrowhead), two with four branching neurites (white arrowheads), and one with five branching neurites (yellow arrowhead). Scale bar=50µm. B. Large multipolar neuron from tentacle nerve net. The cell body (white arrowhead) of a large multipolar cell is visible along with its five branching neurites (white arrows). Scale bar=25µm. C. Tentacle nerve net. The brightly-stained tentacle nerve net is made up of both thick (white arrow) and thin (yellow arrow) neurites which branch from both multipolar (white arrowhead) and bipolar (yellow arrowhead) ganglion cells. Scale bar=50µm.

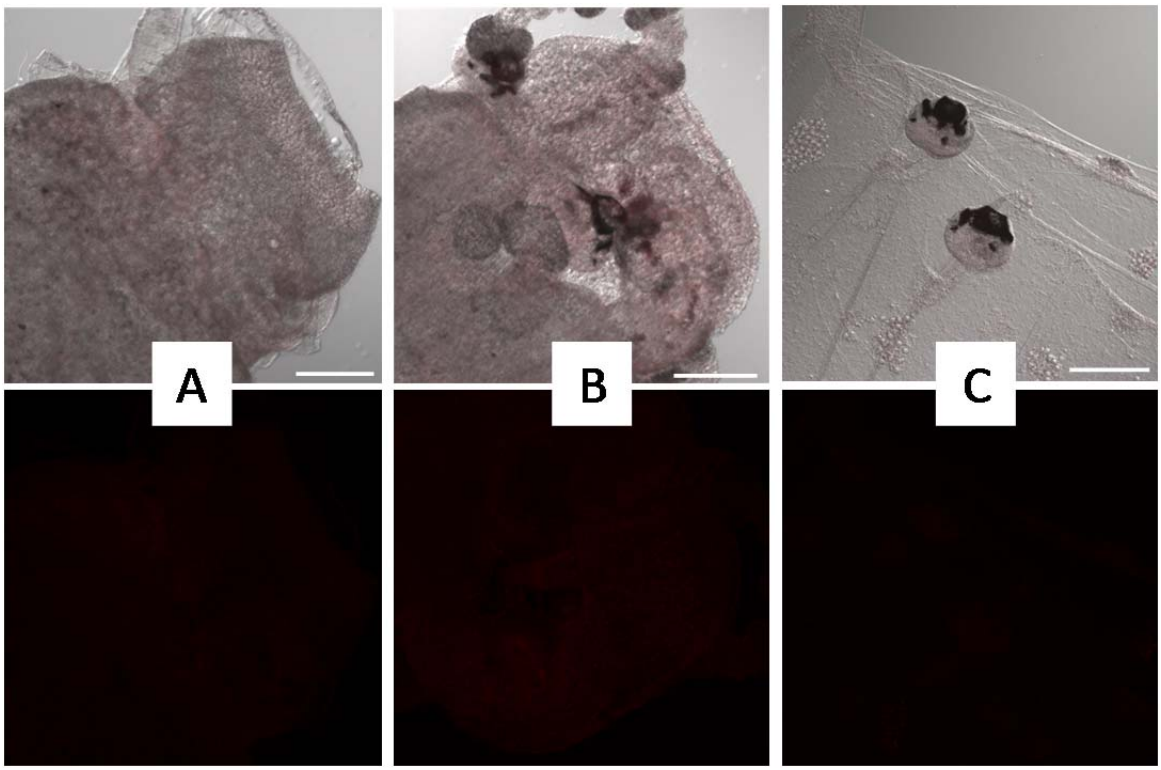

Figure 55. Selected FMRFamide controls. A. Steady-state polyp control. No staining was seen in samples not subjected to the primary antibody targeting the neuropeptide. The same control sample is shown with (top) and without (bottom) differential interference contrast (DIC) imaging to demonstrate the lack of staining while giving structural context. B. Stage 3 control. No staining was seen in samples not subjected to the primary antibody targeting the neuropeptide. The same control sample is shown with (top) and without (bottom) DIC imaging to demonstrate the lack of staining while giving structural context. C. Stage 7 control. No staining was seen in samples not subjected to the primary antibody targeting the neuropeptide. The same control sample is shown with (top) and without (bottom) DIC imaging to demonstrate the lack of staining while giving structural context. Scale bars=200μm.

Vita

Jenna Rose Valley was born in Chapel Hill, North Carolina, to parents Robert and Ellen. Ever since childhood, Jenna has had an avid interest in all things ocean, particularly the strange and unusual invertebrates. Jenna discovered jellyfish in elementary school and has had an obsessive fascination with them since. She graduated from East Chapel Hill High School in May of 2004 and attended Appalachian State University for one year before transferring to the University of North Carolina Wilmington where she was awarded the Bachelor of Science degree with a major of biology and minor in chemistry in May of 2008. Deciding to pursue her Master of Science in Biology and now ready for a break from the numerous coastal hurricanes and hot climate, Jenna was ecstatic to discover a jellyfish research lab situated back at Appalachian State University in the beautiful mountain town of Boone. During her first year at ASU, Jenna received an Alumni Fellowship followed by a Provost Fellowship the following year. Jenna discovered a love for teaching while working as a laboratory instructor in the biology department and received the Graduate Teaching Assistantship Award for Introductory Biology – Majors in 2010. Jenna is a member of Phi Kappa Phi in both the UNCW and ASU chapters. She is also a member of the prestigious Cratis D. Williams Society. After moving from the mountains to the coast and back to the mountains, Jenna will be returning to the coast to pursue her Doctorate at the Marine Biological Institue of the University of Oregon in coastal Charleston.